ATP Delivery Rates in Myocardial Hypertrophy

MARK ANDREW PETERZAN

St Catherine's College
Oxford Centre for Clinical Magnetic Resonance Research
John Radcliffe Hospital, University of Oxford



A thesis submitted in partial fulfilment of the requirements for the degree of Doctor of Philosophy in Medical Sciences

Trinity Term 2019

Declaration

This thesis is entirely my own work unless otherwise indicated. It has not been submitted, either wholly or substantially, for another degree at this university, or for a degree at any other institution. I have acknowledged assistance from colleagues and collaborators where relevant.

The word count, not including front matter, tables, figures, captions, appendices, or references, but including the Abstract, is 46,141.

Abstract

ATP Delivery Rates in Myocardial Hypertrophy

MARK ANDREW PETERZAN
St Catherine's College, University of Oxford

A thesis submitted in partial fulfilment of the requirements for the degree of Doctor of Philosophy in Medical Sciences, Trinity Term 2019

This thesis aims to better understand the metabolic dimension of cardiac adaptation to increased work by studying the creatine kinase (CK) system in participants with pathological hypertrophy secondary to severe aortic stenosis with preserved ejection fraction (SevAS-pEF) or secondary to severe primary mitral regurgitation (MR), participants with hearts adapted to exercise training, and participants with no hypertrophy (NH). It also aims to understand why some hearts transition to failure in the presence of pressure overload, by studying a group with severe aortic stenosis with reduced ejection fraction (SevAS-rEF).

Broadly speaking there are two pathways for ATP delivery from sites of production in mitochrondria to sites of use at the myofibrils: facilitated diffusion by the CK system and simple diffusion. This thesis aims to investigate both. Closely related to this, CK also has roles in the temporal buffering of adenine nucleotides and the control of respiratory flux over varying work rates, so more broadly represents a kind of metabolic reserve. CK activity can be assessed on freeze-and-extract biochemical assay.

Using ^{31}phosphorus-magnetic resonance spectroscopy (MRS) saturation transfer to estimate the CK rate constant (k_f) is the first step toward estimates of in vivo flux. Over 60 intra-operative left ventricular (LV) biopsies in participants with pre-operative ^{31}P-MRS are collected to validate the novel TRiST sequence against biochemically-assessed maximum CK rate. Ch. 3 describes non-invasive and invasive predictors of CK total activity and derives a three-variable linear regression model in 37 triplicate datasets to predict CK total activity from total creatine, k_f and LV end-systolic volume index.

Ch. 4 studies invasive and non-invasive measures of the CK system in participants with sevAS-pEF, sevAS-rEF, and NH. The chapter argues for the assessment of metabolic reserve as a way of identifying – and explaining – the recently described subset of patients whose ventricles deteriorate sooner in the face of pressure overload. A stepwise fall in median CK total activity is found when arranging groups in order of increasing LV mass index. Non-invasive measures are also assessed in participants with moderate AS, healthy volunteers, and sevAS-pEF participants late post-operatively.

The CK system is then studied in participants with severe primary MR and preserved systolic function pre- and post-operatively (Ch. 5), and in participants with physiological hypertrophy or normal, non-trained, hearts at rest and during dobutamine stress (Ch. 6). Ch. 7 relates CK activity with ATP diffusion distance using 3D models built from tomographic stacks of electron microscopy images in a subset of LV biopsies.

Publications

Some ideas and figures have appeared previously in the following publications:

- Peterzan, M. A., Lygate, C. A., Neubauer, S., and Rider, O. J. (2017). Metabolic remodeling in hypertrophied and failing myocardium: a review. *American Journal of Physiology-Heart and Circulatory Physiology*, 313(3):H597–H616.
- Clarke, W. T., Peterzan, M. A., Rayner, J. J., Sayeed, R. A., Petrou, M., Krasopoulos, G., Lake, H. A., Raman, B., Watson, W. D., Cox, P., Hundertmark, M. J., Apps, A. P., Lygate, C. A., Neubauer, S., Rider, O. J., and Rodgers, C. T. (2019). Localized rest and stress human cardiac creatine kinase reaction kinetics at 3 T. *NMR in Biomedicine*, 32(6):e4085.
- Peterzan, M. A., Clarke, W. T., Lygate, C. A., Lake, H. A., Lau, J. Y. C., Miller, J. J. J. J., Johnson, E., Rayner, J. J., Hundertmark, M. J., Sayeed, R. A., Petrou, M., Krasopoulos, G., Srivastava, V., Neubauer, S., Rodgers, C. T., Rider, O. J. (2019). Impaired cardiac energetics in severe human aortic stenosis: characterisation in preserved versus reduced ejection fraction. *Submitted; in revision.*

Contents

Declaration i

Abstract iii

Publications v

Contents vii

List of Figures x

List of Tables xiv

List of Abbreviations xxi

Acknowledgements xxiii

1 Introduction 1

1.1 Why investigate hypertrophy? . . . 1

Geometric patterns of hypertrophy . . . 3

Models of hypertrophy . . . 4

1.2 Overview of mechanisms of hypertrophy . . . 5

Mechanisms of physiological hypertrophy . . . 7

Mechanisms of pathological hypertrophy . . . 11

1.3 Metabolic remodelling in hypertrophy . . . 13

Concepts in cardiac metabolism . . . 14

Substrate utilization in hypertrophy and HF . . . 21

Phosphotransfer – a historical perspective . . . 28

Phosphotransfer today . . . 37

Phosphotransfer in hypertrophy and HF . . . 44

1.4 Research aims . . . 50

2 Methods and methods development 53

2.1 Participants included . . . 53

2.2 Measurements . . . 54

2.3 Ethical considerations . . . 55
2.4 Statistical analysis . . . 56
2.5 ^{31}P-MRS . . . 57
Estimation of PCr/ATP . . . 57
Estimation of CK rate constant . . . 61
2.6 ^{1}H-MRI . . . 70
Cardiac volumes and mass . . . 70
Aortic valve cine and through-plane flow . . . 71
Late gadolinium enhancement . . . 71
2.7 Measurements of creatine content and CK activity . . . 72
From biopsy to homogenate . . . 72
Analysis of CK activity . . . 73
Analysis of CK isoenzymes . . . 74
Citrate synthase assay . . . 75
Lowry protein assay . . . 76
Measurement of total creatine concentration . . . 77
2.8 Serial block-face scanning electron microscopy . . . 77
Sample fixation and imaging . . . 78
SBEM dataset analysis . . . 79
2.9 Echocardiography . . . 83
2.10 Cardiopulmonary exercise tests . . . 84

3 ATP delivery rates validated ex vivo 87
3.1 NMR studies of energy transfer rates by magnetisation transfer, 1977–present . . . 87
3.2 Methods . . . 92
Correlation . . . 92
Linear regression . . . 93
3.3 Results . . . 95
Correlation . . . 95
Linear regression . . . 99
3.4 Discussion . . . 104
CK total activity and CK k_f . . . 106
CK total activity and CS activity . . . 109
CK total activity and total creatine concentration . . . 111
CK total activity and LV volumes and mass . . . 114
Limitations . . . 114

4 ATP delivery rates in chronic pressure loading by aortic stenosis 117
4.1 Introduction . . . 117
The LVEF < 0.50 threshold for the definition of 'reduced LVEF' in severe AS is insensitive for the detection of LV dysfunction 120

Alternative markers of myocardial dysfunction in severe AS 126
The argument for metabolic reserve assessment 128
4.2 Results 129
Participants 129
LV mass and volumes 130
CK total activity, CS activity, total creatine, and CK capacity 134
CK isoform expression 141
Estimated ATP delivery rates 141
TAN pool 145
Late follow-up after AVR 145
Summary of results 148
4.3 Discussion 151
CK total activity 152
CK isozymes 154
CS activity 156
Total creatine concentration 157
Estimated CK flux and CK k_f 158
TAN pool 160
Late follow-up 161
Limitations 161
Outstanding questions 165

5 ATP delivery rates in chronic volume loading by primary mitral regurgitation 167
5.1 Introduction 167
5.2 Results 174
Participants 174
LV mass and volumes 175
Energetic measures 175
CK isoform expression 181
Late follow-up after MV repair 181
5.3 Discussion 183

6 ATP delivery rates in acute increases in work and physiological hypertrophy 189
6.1 Introduction 189
The athletic heart 189
The stressed heart 191
6.2 Results 194
Participants 194
LV mass and volumes, diastolic indices and CPET 197
Energetic measures at rest and stress 197

6.3 Discussion 203

7 Correlation of energy handling with ultrastructure 213
7.1 Introduction 213
7.2 Results 215
7.3 Discussion 216

8 Summary and future directions 223

A Appendix 229
A.1 CK equilibrium constant, rate equation and reserve 229
A.2 Basic principles underlying NMR magnetisation transfer experiments 231
A.3 Correlates of CK/CS activity ratio 235
A.4 RV dimensions in AS cohorts 237
A.5 CK isoforms in severe MR 239

Bibliography 241

List of Figures

1.1 Major substrate fates, energy fluxes, and carriers involved in the three stages of energy supply [A-D (first stage), E and F (second stage), and G (third stage)]. Bold arrows indicate major routes of electron donation to the electron transport chain (ETC). Highlighted subdivisions include glucose/pyruvate uptake (A), fatty acid (FA) uptake (B), pyruvate oxidation and FA oxidation cycle (C), tricarboxylic acid cycle (D), electron shuttle (E), ETC/oxidative phosphorylation (oxphos) (F), and phosphotransfer (G). 16
1.2 Major activators and downstream effects of AMPK in cardiomyocytes. 20
1.3 The CK reaction (from Wyss and Kaddurah-Daouk (2000)). 39
1.4 Schematic showing that ATP may be delivered to, and ADP removed from, myofibrils by diffusion and the CK system (facilitated diffusion). Alternate phosphotransfer and ATP-producing pathways not shown. . . 41

2.1 (a) Selection of cods (green crosses) and one fiducial (red cross); (b) saturation band placement (yellow), FID inversion recovery curve, and PCr/ATP ratio correction. 58

2.2 The most basal sepal voxel (b-d) is a half voxel-shift below the left ventricular outflow tract (a). 59
2.3 (a) The centre frequency for the PCr/ATP sequence is set at 49.859373 MHz (vertical line), 250 Hz negative of PCr, which resonates here at 49.859623 MHz. (b) The centre frequency for TRiST is found for the voxel of interest and set (in this case) at 49.859552 Mhz (vertical line). Typical offsets for selective γ-ATP (–63 Hz) and control (+189 Hz) saturation are shown. 60
2.4 Placement of the 1D 16-step adjust volume for TRiST. The saturation band is used only if the frequency-finding sequence (TR 330 ms) is run. 63
2.5 The 1D 16-step adjust volume was oriented to position the most apical unambiguously cardiac voxel (# 7) in line with the surface coil for (a–b) two participants. 64
2.6 Off-line analysis tool to calculate centre frequencies and expected offsets. As the input data was a full resting TRiST spectrum, PCr and γ-ATP appear in the +2 and –2 ppm range respectively; the fiducial appears around 20 ppm positive to PCr. 64
2.7 Generation of centre frequencies and expected offsets for each of 16 voxels. That for voxel 7 is used. 65
2.8 3D summary of spectra #1–4 from Table 2.3 for cardiac-depth voxels (participant _021) demonstrates signal fall-off with depth. 66
2.9 (A–D) 2D summary of spectra #1–4 from Table 2.3 for the VOI (voxel 7, participant _021). Labelled peaks in (A) are 2,3-diphosphoglycerate (2,3-DPG), PCr, and γ-, α- and β-ATP. Inorganic phosphate (P_i) is hidden by 2,3-DPG. 67
2.10 2D summary of spectra #1–6 from Table 2.3 for the VOI (voxel 7, participant _037). 68
2.11 The plane planned through the AV leaflet tips (middle of the three green lines in A–B) is used for capture of the AV cine (C). The through-plane flow (D) is planned just distal to the plane of (C). 72
2.12 CK isoenzymes separate by gel electrophoresis from top to bottom: mtCK, CK-MM, CK-MB, CK-BB. 76
2.13 (a–b) Before and after Perona-Malik filter. (c–d) Black and white thresholding applied to (a–b) respectively. (e) Inversion of (d). (f) After manual segmentation. 81
2.14 Histograms of 3D distances for one dataset generated using (a) 30 alternate slices, (b) 30 consecutive slices, (c–d) after removing the five largest modal spikes from (a–b). 83
2.15 Histogram of 3D distances for one dataset (_021) after interpolation of slices and model to achieve 20 nm isotropic voxels. 84

3.1 Scatter plots indicated no relationship between the time LV biopsies spent in the freezer until analysis and the results of the analysis. *r(df) is Pearson correlation coefficient r where the number of degrees of freedom (df) = number of datapoints – 2.* 96
3.2 Scatter plots for (A) CS activity, (B) TAN pool against CK total activity. 99
3.3 Scatter plots for (A) total creatine, (B) CK k_f, (C) CK flux estimated by k_f × estimated [PCr], and (D) CK flux estimated by total creatine × k_f against CK total activity. (Compare Figure A.2, p. 236.) 100
3.4 Scatter plots for (A) LVEDVi, (B) LVESVi, (C) LVEF, and (D) LVMi against CK total activity. 101
3.5 Plots of studentized residuals for model 8 (creatine + k_f + LVESVi) including all cases: (A) Histogram, (B) Quantile-quantile plot, (C) Observed vs predicted studentized residuals. 106
3.6 Predicted vs observed CK total activity (IU/mg protein) using (A) model 7 (creatine + k_f + LVEF), (B) model 8 (creatine + k_f + LVESVi) and (C) model 9 (creatine + k_f + k_f:LVESVi), all cases included. 107

4.1 LVMi, LVEF, and LV volumes in two control and three AS groups, in order of ascending LVMi. Post hoc tests were performed with the healthy volunteer group as reference (p-values marked with asterisks at top of each plot). *Each boxplot indicates 25th, 50th, and 75th centiles; the whiskers extend to the maximum value of the data that is within 1.5 times the IQR over the third quartile, and to the minimum value of the data that is within 1.5 times the IQR under the first quartile. Values outside the whiskers are depicted with circles. Beside each boxplot individual datapoints are shown with 50% transparency, with darker areas indicating areas of overlap.* 133
4.2 LVSVi and LVM/LVEDV ratio in two control and three AS groups. Post hoc tests performed with the healthy volunteer group as reference. . . . 136
4.3 (A) CK total activity, (B) citrate synthase activity in one control group and two AS groups. Post hoc one-sided pairwise Wilcoxon rank-sum tests significant versus NH are marked ∗, significant versus sevAS-pEF are marked †. 137
4.4 (A) Total creatine concentration, (B) CK capacity estimated by CK total activity × total creatine in one control group and two AS groups. Post hoc pairwise tests were not significant in (A–B). 138
4.5 CK isoform activity (IU/mg protein) in one control and two AS groups: (A) MtCK, (B) CK-MM, (C) CK-MB, (D) CK-BB. Post hoc pairwise tests significant versus NH are marked ∗, significant versus sevAS-pEF are marked †. 142

4.6 CK isoform expression relative to total CK activity (value = 1) in one control and two AS groups: (A) MtCK, (B) CK-MM, (C) CK-MB, (D) CK-BB. Post hoc pairwise tests significant versus NH are marked $*$. . . 143
4.7 (A) PCr/ATP ratio and (B) CK k_f in two control and three AS groups; (C–D) Panels A–B after combining the non-hypertrophied groups. Post hoc tests performed using the NH group as reference. 146
4.8 (A) CK flux (μmol/g wet weight/s) estimated by $k_f \times$ estimated [PCr], combining the NH groups; (B) CK flux (nmol/mg protein/s) estimated by $k_f \times$ [total creatine] in one control and two AS groups. 147
4.9 (A) Histogram of TAN pool values in NH, sevAS-pEF and sevAS-rEF; (B) TAN pool in one control and two AS groups. 148
4.10 Values for (A) LVMi, (B) PCr/ATP ratio, (C) CK k_f adj, (D) estimated CK flux in patients with sevAS-pEF group who were assessed pre- and post-op. 149

5.1 LVMi, LVEF, and LV volumes in primary MR and healthy volunteers. Conventions as for Figure 4.1. 177
5.2 LVSVi, RVSVi, and MR regurgitant volume calculated by two methods (LVSV–RVSV and LVSV–Aortic forward flow) in primary MR and healthy volunteers. 178
5.3 (A) PCr/ATP ratio, (B) CK k_f adj, and (C) $k_f \times$ estimated [PCr] in primary MR and healthy volunteers. 182
5.4 Scatter plot of MR regurgitant volume (LVSV–RVSV) against (A) PCr/ATP; (B) CK k_f in primary MR (circles) and healthy volunteers (triangles). . 182
5.5 Scatter plot of (A) LVEDVi, (B) LVESVi against PCr/ATP ratio in primary MR (circles) and healthy volunteers (triangles). 183

6.1 LVMi, LVEF, and LV volumes in athletes and controls. *Males shown as triangles, females as circles.* 198
6.2 LVSVi and LVM/LVEDV ratio in athletes and controls. 199
6.3 RV volumes and RVEF in athletes and controls. 199
6.4 Anaerobic threshold (AT), peak VO_2, and AT/peak VO_2 ratio in athletes and controls. *Males shown as triangles, females as circles.* 202
6.5 Response of k_f to dobutamine stress in (A) controls, (B) athletes, (C) both. 204
6.6 Response of k_f to dobutamine stress in (A) controls, (B) athletes, (C–D) both. *Males shown as triangles, females as circles. In (A–C) icon size is proportional to anaerobic threshold across all participants; in (D) icon size is proportional to -fold change in RPP. Dotted lines have intercept (b_0) = 0, slope (b_1) = 1; dashed lines follow the linear model $k_f^{stress} = b_0 + b_1\, k_f^{rest}$ (for coefficients see Table 6.8).* 205

7.1 Representative screenshots for SEM datasets (a) _021, (b) _035, (c) _033, (d) _081, (e) _041, and (f) _145. Subfigures (a–d), sevAS-pEF, (e–f), sevAS-rEF. 217
7.2 Representative screenshots for SEM datasets (a) _139, (b) _015, (c) _023, (d) _048, (e) _066, and (f) _092. Subfigures (a), sevAS-rEF, (b–c), sevMR, (d–f), NH. 218
7.3 TEM in (a) (_033) indicated holes in the resin; in (b) (_126) indicated ambiguous regions. 219
7.4 Scatterplots of median diffusion distance (A) against CK total activity, (B) against CK capacity estimated by CK total activity × total creatine. 219

A.1 The relationship between the fractional change in resonance intensity at A, $\Delta M_A/M_A^0$, and k_A/R_A, from Alger and Shulman (1984). 235
A.2 Scatter plots for (A) CK total activity, (B) CK k_f, (C) CK flux estimated by k_f × estimated [PCr], and (D) CK flux estimated by total creatine × k_f against CK/CS activity ratio. (Note that total creatine was not significantly correlated with CK/CS activity ratio. Compare Figure 3.3, p. 100.) . . . 236
A.3 RVSVi, RVEF, and RV volumes in two control and three AS groups. . . 237

List of Tables

2.1 Group definitions and recruitment 54
2.2 Measurements by group 55
2.3 TRiST acquisition parameters at rest (Steps 1–4) and stress (Steps 5–6) 69

3.1 Five number summaries for invasively obtained variables 97
3.2 Correlates of CK total activity 98
3.3 Correlates of CK k_f 98
3.4 Five number summaries for participants in the triplicate set 102
3.5 Coefficients for models including CS – excluding one case (1) 103
3.6 Coefficients for models including CS – excluding one case (2) 104
3.7 Coefficients for models excluding CS – all cases included 105

4.1 Participants recruited to AS or comparison groups 131
4.2 AS severity on clinical echocardiography 131
4.3 Participants' medical and drug history 132
4.3 Participants' medical and drug history (AS) 134

4.4 Chamber dimensions by cardiac MRI (CMR) in AS and comparison groups 135
4.5 Baseline energetic measures in AS and comparison groups (combined) . 139
4.5 Baseline energetic measures in AS and comparison groups (separated) . 140
4.6 CK isoform absolute activities and relative expression 144
4.7 LV mass and energetics after AVR in sevAS-pEF 150
4.8 Prior studies of CK k_f (/s) in pressure overload 160

5.1 Participants' medical and drug history (MR) 176
5.1 Participants' medical and drug history (MR) 179
5.2 Chamber dimensions by CMR in severe MR 180
5.3 Baseline energetic measures in MR 181
5.4 LV energetics and dimensions after MV repair 184

6.1 Prior studies of CK k_f and flux at different workloads (1) 195
6.1 Prior studies of CK k_f and flux at different workloads (2) 196
6.2 Chamber dimensions by CMR in controls and athletes 200
6.3 Diastolic parameters by echocardiography in controls and athletes . . . 201
6.4 Cardiopulmonary exercise test results in controls and athletes 202
6.5 Effect of dobutamine on haemodynamics in controls and athletes 206
6.6 Effect of dobutamine on CK system in controls and athletes 207
6.7 Effect of dobutamine on CK system (controls and athletes pooled) . . . 208
6.8 Coefficients for linear models (dependent variable: k_f^{stress}) 208

A.1 Correlates of CK/CS activity ratio 235
A.2 RV Chamber dimensions by CMR in AS 238
A.3 CK isoform activities (expanded from Tables 4.5 and 4.6) 240

List of Abbreviations

ΔG_{ATP}	free energy change of ATP hydrolysis
k_f	pseudo-first order CK rate constant in the forward or ATP-generating direction
2,3-DPG	2,3-diphosphoglycerate
ADP	adenosine-5'-diphosphate
AFib	atrial fibrillation
AGAT	arginine-glycine amidinotransferase
AHP	adiabatic half-passage
AIC	Akaike information criterion
AK	adenylate kinase
AMP	adenosine-5'-monophosphate
AMPK	AMP-activated protein kinase
ANP	atrial natriuretic peptide
ANT	adenine nucleotide translocase
AP5A	diadenosine pentaphosphate
AR	adrenergic receptor
AS	aortic stenosis
ASD	atrial septal defect
AT	anaerobic threshold
ATP	adenosine-5'-triphosphate
AV	aortic valve
AVA	aortic valve area
AVR	aortic valve replacement
BNP	natriuretic peptide B
BP	blood pressure
BSA	body surface area
C/EBPβ	CCAAT-enhancer binding protein β
CAC	citric acid cycle
CAD	coronary artery disease
CaMK	Ca^{2+}-calmodulin-dependent protein kinase
CITED4	Creb binding protein/p300-interacting transactivator with ED-rich carboxy-terminal domain-4

CK	creatine kinase
CK-B	brain-isoform CK
CK-M	muscle-isoform CK
CMR	cardiac MRI
CPET	cardiopulmonary exercise test
CPT-I	carnitine palmitoyltransferase 1
CrT	creatine transporter
CS	citrate synthase
CSI	chemical shift imaging
DANTE	Delays Alternating with Nutation for Tailored Excitation
DKO	double knockout
DTNB	5,5'-dithio-bis(2-nitrobenzoic acid)
DVI	dimensionless velocity index
ECG	electrocardiogram
ECV	extracellular volume
EF	ejection fraction
eGFR	estimated glomerular filtration rate
EM	electron microscopy
eNOS	endothelial NO synthase
EROA	effective regurgitant orifice area
ERR	estrogen-related receptor
ETC	electron transport chain
FA	fatty acids
$FADH_2$	reduced form of flavin adenine dinucleotide
FAO	fatty acid oxidation
FAST	four-angle saturation transfer
FDNB	the CK inhibitor fluorodinitrobenzene
FID	free induction decay
FOV	field-of-view
G6P	glucose-6-phosphate
G6PD	glucose-6-phosphate dehydrogenase
GAMT	guanidinoacetate methyltransferase
GDP	guanosine-5'-diphosphate
GLS	global longitudinal strain
GLUT4	glucose transporter type 4
GPA	β-guanidinopropionate
HCM	hypertrophic cardiomyopathy
HDAC	histone deacetylase
HF	heart failure
HFD	high-fat diet

HFpEF	heart failure with preserved ejection fraction
HFrEF	heart failure with reduced ejection fraction
HPLC	high-performance liquid chromatography
HR	heart rate
HV	healthy volunteers
IGF-1	insulin-like growth factor 1
IQR	interquartile range
IR	insulin receptor
IRS	insulin receptor substrate
K_m	Michaelis constant
KO	knockout
LA	left atrium
LBBB	left bundle-branch block
LDH	lactate dehydrogenase
LGE	late gadolinium enhancement
LV	left ventricle
LVAD	left ventricular assist device
LVEDP	left ventricular end-diastolic pressure
LVEDV	left ventricular end-diastolic volume
LVEF	left ventricular ejection fraction
LVESD	left ventricular end-systolic diameter
LVM	left ventricular mass
LVOT	left ventricular outflow tract
LVSV	left ventricular stroke volume
LVSVi	left ventricular stroke volume index
MAPK	mitogen activated protein kinase
MAPSE	mitral annular plane systolic excursion
MCD	malonyl-CoA decarboxylase
MHC	myosin heavy chain
MI	myocardial infarction
MIB	Microscopy Image Browser
miRNA	micro-ribonucleic acid
MR	mitral regurgitation
MRI	magnetic resonance imaging
MRS	magnetic resonance spectroscopy
MS	mitral stenosis
mtCK	mitochondrial-isoform CK
mTORC	mechanistic target of rapamycin complex
MV	mitral valve
MVO_2	myocardial oxygen consumption per minute
NAC	N-acetyl cysteine

NADH	reduced nicotinamide adenine dinucleotide
NDPK	nucleoside diphosphate kinase
NFAT	nuclear factor of activated T-cells
NH	non-hypertrophied
NICM	nonischemic cardiomyopathy
NMR	nuclear magnetic resonance
NO	nitric oxide
NR	nuclear receptor
NRF-1	nuclear respiratory factor-1
NYHA	New York Heart Association
OAC	oral anticoagulant
OCMR	Oxford Centre for Clinical Magnetic Resonance Research
oxphos	oxidative phosphorylation
P_i	inorganic phosphate
PCr	phosphocreatine
PDH	pyruvate dehydrogenase
PDK	pyruvate dehydrogenase kinase
PGC-1α	peroxisome proliferator-activated receptor-γ coactivator-1α
PI3K	phosphoinositide 3-kinase
PKA	protein kinase A
PKG	protein kinase G
PMS	phenazine methosulfate
PPA	phenylphosphonic acid
PPAR	peroxisome proliferator-activated receptor
ppm	parts per million
PPRE	PPAR response element
RCT	randomized controlled trial
RER	respiratory exchange ratio
RF	radiofrequency
RPP	rate-pressure product
RV	right ventricle
RWT	relative wall thickness
RXR	retinoid-X-receptor
SAR	specific absorption rate
SAVR	surgical aortic valve replacement
SBEM	serial block-face scanning electron microscopy
SCOT	succinyl-CoA-3-oxoacid-CoA-transferase
SD	standard deviation
SEM	scanning electron microscopy

SERCA2a	sarco/endoplasmic reticulum calcium-ATPase 2a
SevAS-pEF	severe aortic stenosis with preserved ejection fraction
SevAS-rEF	severe aortic stenosis with reduced ejection fraction
SHR	spontaneously hypertensive rat
SNR	signal-noise ratio
SSE	sum of squared errors
SSFP	steady-state free precession
StreST	'stressed' saturation transfer
STS-PROM	Society of Thoracic Surgeons Predicted Risk of Mortality
TAC	thoracic aortic constriction
TAG	triacylglycerol
TAN pool	total adenine nucleotide pool
TAVR	transcatheter aortic valve replacement
TE	echo time
TEM	transmission electron microscopy
Tfam	mitochondrial transcription factor A
TNB	5-thio-2-nitrobenzoate
TNBT	tetranitro blue tetrazolium
TR	repetition time
TRiST	triple repetition time saturation transfer
TwiST	two repetition time saturation transfer
UCP	uncoupling protein
VDAC	voltage-dependent anion channel
VHD	valvular heart disease
VO_2	oxygen consumption
VOI	voxel of interest
VTI	velocity time integral
WT	wild-type

Acknowledgements

I would like to thank the following:

The British Heart Foundation who provided me a Clinical Research Training Fellowship (No. FS/15/80/31803).

The patients and volunteers who took part.

My supervisors: Oliver J Rider, Christopher T Rodgers, Stefan Neubauer.

Spectroscopy: William T Clarke, Ladislav Valkovic, Ferenc E Mozes.

Cardiac surgeons: Rana A Sayeed, Mario Petrou, George Krasopoulos, David P Taggart, Vivek Srivastava.

Sample analysis: Craig Lygate, Hannah Lake.

Electron microscopy sample preparation, sectioning and imaging: Errin Johnson (Dunn School of Pathology, University of Oxford).

Electron microscopy image interpolation: Justin YC Lau.

Advice on statistical analysis: Jack JJJ Miller.

Researchers: Jenny J Rayner, Moritz J Hundertmark, William D Watson, Andrew P Apps, Svetlana Reilly, Pete Cox, David Dearlove.

Radiographers: Jane Francis, Fiona Mcmillan, Joana Leal-Pelado, Andrea Borghetto, Raj Soundarajan.

Research nurses: Roser Farras-Araya, Judith Delos Santos.

Patient administration: Karen Whatley, Nawal Osman, Ella May.

Research management and governance: Hanan Lamlum, Kathryn Lacey.

1 Introduction

1.1 WHY INVESTIGATE HYPERTROPHY?

When the heart is asked to do more work habitually, it adapts to the increased demand across multiple dimensions. A convenient shorthand for this adaptation is the term hypertrophy. The term has come to mean different things to different people. It is broadly defined as an increased mass of the organ to a degree more than would be expected for the size and sex of the animal, but the term is also used in situations of increased regional or global wall thickness, chamber dimension and chamber volume. Today one must be careful to nail down what one means: this is usually done by specifying the stimulus and the phenotype (physiological or pathological hypertrophy). Not all stimuli involve increases in work, and I will not discuss these (inherited mutations, cardiomyopathies, storage diseases) further.

Physiological hypertrophy occurs in the settings of endurance exercise training, pregnancy, and postnatal growth, and is considered benign. As the cardiomyocyte is terminally differentiated soon after birth, this largely depends on an increase in the size of individual cardiomyocytes by addition of sarcomeric units. Pathological hypertrophy may arise in settings of haemodynamic overload (hypertension, aortic stenosis (AS), mitral regurgitation (MR), aortic regurgitation), neurohormonal activation (post myocardial infarction (MI)), and obesity, and matters a great deal, because it predisposes to heart failure with preserved ejection fraction (HFpEF), heart failure with reduced ejection fraction (HFrEF), arrhythmias and death. But once the stimulus

is removed (or lessened), the degree of hypertrophy is to some extent reversible and an individual's trajectory (i.e. chance of transitioning to heart failure (HF) and premature death) may improve if something is done early enough but – in the case of valvular heart disease (VHD) – not too early. Unfortunately, we are poor at predicting the time course of such trajectories for any given individual case. Understanding what it is about these adaptive processes that predisposes to good or bad outcomes continues to be the subject of research efforts spanning multiple dimensions of adaptation. This thesis is one such effort framed around the question: can we understand better what is going on when the heart adapts to habitually increased work? Developing good answers to the questions why pathologial hypertrophy may progress to HF but physiological hypertrophy does not, and why some hearts with pathological hypertrophy progress faster than others, should allow us to identify key molecular mechanisms suggesting worrisome trajectories, time our existing interventions optimally and develop mechanistically targeted therapies.

To tackle this I will be asking a series of narrower, complementary questions looking at the metabolic dimension of adaptation to increased work, and within this at the energy transfer component, which intimately involves creatine kinase (CK) activity. I have designed these to build a picture of what is going on with the energy transfer component of metabolism in cardiac hypertrophy in the settings of chronic pressure overload, volume overload and exercise training, from the perspective of three conventionally nonoverlapping disciplines: from consenting participants I obtain biopsy samples of myocardium during open-heart surgery and measure maximal CK activity using freeze-and-extract biochemical techniques; I use a nuclear magnetic resonance (NMR) magnetisation saturation transfer method (recently implemented locally) to measure the pseudo-first order CK rate constant in the forward or ATP-generating direction (k_f); and I use electron microscopy in biopsy samples to estimate the distance across which the two CK compartments must transfer energy. The thesis

is therefore positioned at the intersection of two fields of research: understanding the significance of metabolic remodelling in the context of hypertrophy and HF and exploring this noninvasively in the human heart using NMR.

I will first review what is understood about the cardiac adaptation to increased work: in what dimensions can one think about this? Why and how should one take the metabolic dimension seriously? Ex vivo attempts at understanding energy transfer before NMR techniques were introduced are discussed in this chapter; the introduction to Chapter 3 outlines early investigations of energy transfer using NMR saturation transfer techniques. Later introductions then develop the story around specific stimuli, namely AS, MR, and endurance exercise.

Geometric patterns of hypertrophy

Acquired hypertrophic remodelling falls into three geometric patterns: concentric remodelling, where relative wall thickness (RWT) increases yet cardiac mass remains normal; concentric hypertrophy, where both RWT and cardiac mass increase, yet chamber volumes are normal or mildly reduced; and eccentric hypertrophy, where chamber volumes and cardiac mass increase, and RWT may be increased, normal, or decreased (Ganau et al., 1992). Typically, strength training and pressure overload result in concentric hypertrophy while endurance training and volume overload result in eccentric hypertrophy. In the setting of pressure overload, transition from concentric hypertrophy to a dilated thin-walled chamber with impaired contractility (i.e. to HFrEF) is considered a late stage of pathological hypertrophy. It is not well understood why some people's hearts follow certain geometric phenotypes more faithfully than others', nor why similar geometric phenotypes arising from the same stimulus may have diverse trajectories (Drazner, 2011). Morphology alone is thus insufficient to predict prognosis.

Models of hypertrophy

Significant progress in understanding has depended on animal models of hypertrophy and a brief outline is given here.

Animal models of physiological cardiac hypertrophy have focussed on the genetically modified mouse. Three exercise training protocols predominate: motorized treadmill running using either endurance protocols (fixed or progressively increasing difficulty) or interval protocols (varying intensities), swim training (protocols may vary duration and carried weight), and voluntary cage-wheel running. The former two types elicit increases in cardiac mass of up to 24% (endurance protocols), 30% (interval protocols) and 30-50% (swim training); voluntary running is considered to have no stressful element, i.e. no 'stress'-signalling contribution, and elicits increases of 5-20% (Vega et al., 2017). The degree of hypertrophy is modulated by sex, strain, diet and age.

Commonly used models of pathological hypertrophy include pressure overload induced by constriction of the ascending, transverse or abdominal aorta, or renovascular hypertension (nephrectomy, high-salt diet in a salt-sensitive strain), volume overload induced by aortocaval shunt, and continuous infusion of agonists of hypertrophic signalling pathways (e.g. angiotension II, isoproterenol) (Bernardo et al., 2010). A distinct pressure overload model is the spontaneously hypertensive rat (SHR), a complex genetic model which includes a CD36 loss-of-function mutation, impairing its ability to uptake and oxidize long-chain fatty acids (FA) (Aitman et al., 1999). The SHR develops cardiac hypertrophy and, after 18–24 months, HF, with hypertrophy attributable to both pressure overload and impaired fatty acid oxidation (FAO) (Hajri et al., 2001). Fifteen-week-old SHR hearts have reduced contractile reserve at high workloads which improve with provision of octanoate (Labarthe et al., 2005), suggesting that in the model at this time point, reduced FAO is sufficient to limit contractile reserve despite normal or increased glucose oxidation and efficiency.

1.2 OVERVIEW OF MECHANISMS OF HYPERTROPHY

Cardiac hypertrophy initially results in the addition of sarcomere units in parallel, which increases contractility and attenuates wall stress as per Laplace's law.[1] There are also qualitative changes in gene expression which drive changes in cardiomyocyte survival, contractility and metabolism. Physiological and pathological hypertrophy have distinct structural and functional, cellular, molecular, and metabolic characteristics.

Physiological hypertrophy is characterised by mild (10-20%) increases in cardiac mass and cardiomyocyte growth in length and width. It is reversible in the case of exercise- and pregnancy-induced hypertrophy. The molecular signature comprises activation of gene expression and signalling across the domains of haemodynamic load sensing, cell proliferation, growth and survival, protein synthesis, organisation of new sarcomeric units, angiogenesis, mitochondrial proliferation, and energy production and efficiency. Myosin ATPase activity, contractility and contractile reserve are preserved or increased. Structural remodelling in the fibrillar collagen network and in angiogenesis is proportional to growth, accomodating increases in cardiomyocyte size while preserving structural integrity and perfusion reserve. There is no interstitial or replacement fibrosis or cell death, aside from in the extremes of endurance training, where the relative contribution between stimulus dose and individual susceptibility is still debated. The trajectory is benign, with rare cases of progression to heart failure accepted as the unmasking of an individual susceptibility rather than a consequence of physiological hypertrophy itself.

Conversely, signalling pathways in pathological hypertrophy not only promote cell growth and protein synthesis through pathways distinct from those activated in physiological hypertrophy, but also drive impaired protein and mitochondrial quality control, sarcomeric disorganisation, insufficient angiogenesis, and metabolic remodelling.

[1] This states that chamber wall stress is proportional to PR/T, where P is intracavity pressure, R is chamber radius, and T is wall thickness.

Myosin ATPase activity and contractile reserve may be reduced. Structural remodelling comprises cardiomyocyte cell death, myofibroblast proliferation and activation, interstitial and replacement fibrosis, altered calcium handling and reduced capillary density, resulting in increased chamber stiffness, impaired intercellular electrical coupling, and reduced perfusion reserve. These contribute to increased end-diastolic pressure-volume slopes, increased filling pressures, ischaemia-reperfusion intolerance, and increased likelihood of transition to failure.

When comparing models of physiological and pathological hypertrophy (before and after transition to failure), distinct but overlapping profiles of gene expression are identified (Iemitsu et al., 2003, 2001; Kong et al., 2005; Lai et al., 2014; Strøm et al., 2005). In pathological (but not physiological) hypertrophy there is increased expression of genes such as atrial natriuretic peptide (ANP), natriuretic peptide B (BNP), skeletal α-actin (acta1) and myosin heavy chain (MHC)β (myh7), while other genes are downregulated: sarco/endoplasmic reticulum calcium-ATPase 2a (SERCA2a), cardiac α-actin, and MHCα (Bernardo et al., 2010). There is a similar divergence of metabolic gene expression, with pathological hypertrophy typically showing upregulation of muscle-isoform lactate dehydrogenase (LDH), brain-isoform CK (CK-B), carnitine palmitoyltransferase 1 (CPT-I)α (liver-isoform), and downregulation of heart-isoform LDH, mitochondrial-isoform CK (mtCK), CPT-Iβ (muscle-isoform) and glucose transporter type 4 (GLUT4). In certain areas, evidence from transcriptomic, metabolomic and flux observations corroborates: reduced FAO rates, downregulation of genes involved in FAO and mitochondrial oxidative capacity, increased acylcarnitine, and reduced phosphocreatine (PCr) pool size are all signatures of pathological hypertrophy (Aubert et al., 2013; Beisvag et al., 2009; Lai et al., 2014). After transition to failure, the heart develops insulin resistance and reduced glucose oxidative capacity. The physiologically hypertrophied heart in contrast maintains high capacity for FAO, mitochondrial biogenesis and adenosine-5'-triphosphate (ATP)

production, and increases CK efficacy (as defined by the Michaelis constant (K_m) for adenosine-5'-diphosphate (ADP)-stimulated respiration without creatine / K_m with creatine) (Rimbaud et al., 2009).

For the sake of simplicity the preceding overview has been kept relatively polar, but closer analysis of the molecular mechanisms responsible unearths some complexity. An important observation is that stimuli for physiological hypertrophy can antagonise molecular signalling in pathological hypertrophy and improve prognosis (McMullen et al., 2007; Tsujita et al., 2006). It is therefore reasonable to think of the combination of wall thickening or chamber enlargement with a molecular signature typical of physiological or pathological hypertrophy as prognostically adaptive or maladaptive respectively. It also means that signalling crosstalk (growth-growth, metabolic-metabolic, or growth-metabolic) between the two 'polar' signatures of physiological and pathological hypertrophy occurs and is worth exploring. But one should take care to distinguish 'compensated' pathological hypertrophy, i.e. before transition to failure, from the hypertrophied heart after transition to failure, when further divergent signalling pathway activation occurs (Haq et al., 2001). It is therefore challenging to understand the significance of any one component mediator or signalling pathway in isolation: first, interpreting the degree to which it is up- or downregulated in disease, second, deciding whether the observed phenotype is a cause or consequence of the process, and third, deciding what stage of disease is evoked by the disease model (or patient group) in question.

Mechanisms of physiological hypertrophy

The field of identified players in hypertrophic growth signalling is large, expanding and has extensive crosstalk[2] – here I will outline major pathways in exercise-induced and pathological hypertrophy, points of divergence between the two, and instances of

[2]Reviewed (Bernardo et al., 2018, 2010; Maillet et al., 2013; Nakamura and Sadoshima, 2018; Shimizu and Minamino, 2016; Vega et al., 2017; Wilson et al., 2015).

crosstalk with metabolic signalling.[3]

Several key classes of transcriptional regulators are involved in physiological hypertrophy: peroxisome proliferator-activated receptor-γ coactivator-1α (PGC-1α) and downstream transcription factors, CCAAT-enhancer binding protein β (C/EBPβ), Creb binding protein/p300-interacting transactivator with ED-rich carboxy-terminal domain-4 (CITED4), and non-coding RNAs.

PGC-1α, originally identified as a cold-inducible mediator of mitochondrial biogenesis in brown adipocytes (Puigserver et al., 1998), is induced by exercise in cardiac muscle (O'Neill et al., 2007; Riehle et al., 2014) and serves to mediate the adaptive response to exercise with respect to mitochondrial biogenesis and substrate oxidative capacity. PGC-1α, together with PGC-1β and PGC-1-related coactivator, coactivate multiple transcription factors to promote transcription at every level of oxidative metabolism, thus coordinating mitochondrial biogenesis, FAO and growth signalling (Rowe et al., 2010). Activated transcription factors include peroxisome proliferator-activated receptor (PPAR)-α, PPAR-δ, estrogen-related receptor (ERR)-α, ERR-γ, nuclear respiratory factors and mitochondrial transcription factor A (Tfam). In the heart, PGC-1α is required for normal FAO reserve (Lehman et al., 2008) and PGC-1β for normal expression of oxidative phosphorylation genes (Vianna et al., 2006). PPARα is the key positive regulator of cardiomyocyte FA uptake and oxidation (Finck et al., 2002) and is downregulated in pathological hypertrophy and HF (Aubert et al., 2013). PPARδ upregulates cardiomyocyte FAO but not FA uptake (Burkart et al., 2007; Gilde et al., 2003), improves insulin sensitivity (Barish et al., 2006), and attenuates hypertrophic agonist signalling (Planavila et al., 2005b). ERRα and ERRγ, like PGC-1α, are expressed in cardiac, slow-twitch oxidative skeletal muscle and brown fat and are induced by exercise, fasting, cold exposure and with the postnatal rise in FAO capacity. ERRα is required for maximal ATP synthesis capacity and the

[3] Reviewed (Abel and Doenst, 2011; Crawford and Schaffer, 2013; Gibb et al., 2017; Gibb and Hill, 2018; Hawley et al., 2014; Kolwicz, 2018; Platt et al., 2015).

adaptation to pressure overload (Huss et al., 2007) and ERRγ for postnatal substrate switching to FAO (Alaynick et al., 2007). Together, ERRα/ERRγ regulate genes involved in energy supply, transfer, transduction, sensing, mitochondrial biogenesis and fusion, and cardiac conduction (Alaynick et al., 2007; Dufour et al., 2007; Huss et al., 2015; Wang et al., 2015). The adaptive metabolic benefits of exercise are mimicked by transgenic overexpression of PGC-1α (Lin et al., 2002; Summermatter et al., 2013), PPARδ (Wang et al., 2004) and ERRγ (Narkar et al., 2008) in skeletal muscle and pharmacological PPARδ agonism (Narkar et al., 2008), but their precise roles in the cardiac response to exercise require further study.

C/EBPβ is a transcription factor identified on an unbiased RT-PCR screen which is repressed in the heart by exercise. RNA interference or heterozygosity results in a phenocopy of cardiac adaptation to endurance exercise – cardiomyocyte growth and proliferation, and resistance to failure upon pressure overload (Boström et al., 2010). At least part of this response is mediated by an increase in CITED4. Cardiomyocyte-specific overexpression of CITED4 induces a phenocopy of physiological hypertrophy and mitigates adverse remodelling after ischaemic injury (Bezzerides et al., 2016).

Micro-ribonucleic acids (miRNAs) are a class of non-coding RNAs with multiple members regulated in the heart by exercise and acting as necessary mediators of the normal response to exercise. MiRNA-222 is upregulated by exercise and is required for physiological hypertrophy; in mice transgenic for cardiomyocyte-specific overexpression of miR-222, cardiac dysfunction and fibrosis were mitigated after ischaemic injury (Liu et al., 2015). Clusters of miRNAs upregulated by exercise were found to promote growth, reduce fibrosis (miR-29), modulate renin-angiotensin, and increase angiogenesis (miR-126) (Fernandes et al., 2015).

Upstream of these transcriptional regulators, the most well established signalling pathway in physiological hypertrophy is the insulin-like growth factor 1 (IGF-1)—IGF1R—insulin receptor substrate (IRS)—phosphoinositide 3-kinase (PI3K) (class

1A)—phosphoinositide-dependent protein kinase-1—Akt1 axis. Serum and cardiac IGF1 are increased by exercise-training (Koziris et al., 1999; Neri Serneri et al., 2001; Scheinowitz et al., 2003). PI3K(p110α) is necessary for physiological postnatal growth and exercise-induced hypertrophy but not pressure overload-induced hypertrophy (McMullen et al., 2003): it is necessary for exercise-induced cardioprotection and when upregulated prolongs survival and attenuates pathological hypertrophy induced by pressure overload (McMullen et al., 2007; Weeks et al., 2012). Conversely, loss of PI3Kα results in dilated cardiomyopathy in response to pressure overload (McMullen et al., 2003; Patel et al., 2018). IGF1R is necessary for physiological hypertrophy and cardiomyocyte-specific overexpression of IGF1R induces physiological hypertrophy in a PI3K(p110α)-dependent manner, without activating pathways associated with pathological hypertrophy (Kim et al., 2008; McMullen et al., 2004). IRS-1 and -2 are necessary for the growth and metabolic components of physiological hypertrophy (Riehle et al., 2014). Akt1 is necessary for physiological hypertrophy and antagonises the growth response to pressure overload (DeBosch et al., 2006).

The PI3K—Akt pathway is also activated by insulin—insulin receptor (IR) and neuregulin-1—ErbB2/ErbB4 tyrosine kinase receptor signalling. IR knockout resulted in reduced inotropic reserve, reduced FA and pyruvate oxidative capacity, reduced expression of genes involved in FAO (including PPARα) and reduced mtCK expression (Boudina et al., 2009). Neuregulin is a growth factor upregulated with exercise (Waring et al., 2014) which stimulates cardiomyocyte dedifferentiation and developmental proliferation (Bersell et al., 2009; D'Uva et al., 2015). Its importance in physiological hypertrophy remains to be defined.

Nitric oxide (NO) is a mediator of exercise-induced hypertrophy. Exercise stimulates β_3-adrenergic receptors in endothelial cells, which result in activation of endothelial NO synthase (eNOS) and generation of NO. NO activates soluble guanylate cyclase, generating cGMP and activating protein kinase G (PKG). The NO—PKG

pathway has multiple cardioprotective effects (Rainer and Kass, 2016). Deficiency of eNOS or β_3-adrenergic receptors suppresses the cardioprotective effect of exercise after MI (Calvert et al., 2011; de Waard et al., 2010). PKG suppresses pathological hypertrophy at least partly by activating regulator of G protein signalling (RGS)2/RGS4, which inhibits G protein-coupled receptor signalling (see below) (Takimoto et al., 2009).

Other pathways activated in physiological hypertrophy (not further discussed) include: gp130—JAK—STAT, thyroid hormone receptor, heat shock transcription factor 1, protein synthesis (eIF4F, mTORC1, PABPC1), stretch sensing/mechanotransduction (integrins, melusin) and angiogenesis (vascular endothelial growth factor, hypoxia-inducible factor 1α, placental growth factor).

In summary, exercise-induced hypertrophy recruits a number of pathways which coordinate the signature structural and metabolic adaptations of physiological hypertrophy. Many of these antagonise pathological signalling and are cardioprotective in animal models of pathological hypertrophy or HF. Exploration of the potential of therapies that promote exercise signalling in human HF is ongoing.

Mechanisms of pathological hypertrophy

Key signalling pathways activated in pathological hypertrophy include: $G\alpha_{q/11}$ protein-coupled receptors, β-adrenergic receptor (AR)—$G\alpha_s$—cyclic adenosine monophosphate—protein kinase A (PKA), and Ca^{2+}-dependent signalling (calcineurin, Ca^{2+}-calmodulin-dependent protein kinase (CaMK)II). Other activated mediators/processes (not further discussed) include: PI3K(p110γ), small GTP-binding proteins, mitogen activated protein kinase (MAPK) cascades (extracellular signal-regulated kinases, c-Jun amino-terminal kinases, p38-MAPKs), protein kinase C and D, protein synthesis, angiogenesis, mechanotransduction, cell death signalling, natriuretic peptides, fibroblast signalling, IL-6 family cytokine signalling, pro- and anti- inflammatory

cytokine signalling, and endothelial cell paracrine signalling. There is also modulation by epigenetic modification (histone methylation) and non-coding RNAs (miRNAs).

G$\alpha_{q/11}$-coupled G protein receptors are activated by the binding of vasoactive peptides (angiogensin II, endothelin 1) and α_1-AR agonists to their respective receptors. This activates G$\alpha_{q/11}$ and downstream signalling pathways, which involve phospholipase C-catalysed hydrolysis of phosphatidylinositol 4,5-bisphosphate to inositol triphosphate, release of Ca^{2+} from intracellular stores, and activation of MAPKs, diacylglycerol-sensitive isoforms of PKC, and PKA. G$\alpha_{q/11}$ is required for the hypertrophic response to pressure overload (Akhter et al., 1998; Wettschureck et al., 2001) and when overexpressed is sufficient to cause pathological hypertrophy and premature HF (D 'Angelo et al., 1997; Mende et al., 1998).

Overexpression of Gα_s (Iwase et al., 1996) or its upstream β_1-AR (Bisognano et al., 2000; Engelhardt et al., 1999) recapitulates a pathological hypertrophy with interstitial fibrosis and premature HF. The β_1-AR is overstimulated, downregulated and desensitised in human HF, while the α_1-AR is upregulated (Bristow, 2000). This is at least partly mediated by β_1-AR kinase 1 (β_1-ARK1) and PI3K(p110γ) (Naga Prasad et al., 2001; Perrino et al., 2007). These observations also are seen in pressure overload hypertrophy of the mouse heart, whether the stimulus is intermittent or continuous (Perrino et al., 2006).

Calcineurin is a Ca^{2+}-calmodulin-activated phosphoprotein phosphatase which dephosphorylates nuclear factor of activated T-cells (NFAT) transcription factors, promoting their nuclear translocation and activation of gene expression alongside other transcription factors (GATA4, MEF2). Calcineurin is upregulated in pressure overload but not in physiological hypertrophy (Saito et al., 2003; Wilkins et al., 2004), and transgenic mice with constitutively active calcineurin or NFAT develop pathological hypertrophy and HF (Molkentin et al., 1998). Calcineurin activity is increased in human hypertensive hypertrophy and HF, but to a greater degree in

nonfailing hypertrophy (Haq et al., 2001).

CaMKII is a serine-threonine protein kinase with major roles in excitation-contraction coupling and transcriptional regulation. CaMKIIδ, the major cardiac isoform, is upregulated in pressure overload hypertrophy (Colomer et al., 2003; Hagemann et al., 2001) and human HF (Hoch et al., 1999; Kirchhefer et al., 1999) and when overexpressed causes pathological hypertrophy and HF (Zhang, 2002; Zhang et al., 2003). This is at least partly mediated by phosphorylation of class II histone deacetylase (HDAC) 4, which releases MEF2 from tonic inhibition. CaMKII inhibition and/or deletion is cardioprotective after MI, β_1-AR agonist exposure and pressure overload (Backs et al., 2009; Zhang et al., 2005), indicating that it is required (at least in these models) for transition to failure.

Even with this selective, simplified picture of the most well described pathways, we should appreciate that the mechanisms by which (and the conditions under which) these pathways promote pathological hypertrophy are complex, and it is unlikely that any pathway is solely responsible for the overall hypertrophic response.

1.3 METABOLIC REMODELLING IN HYPERTROPHY

Metabolic reprogramming is a well established part of the molecular signatures of pathological hypertrophy and HF. As such, examination of metabolic phenotype in hypertrophy – before and after transition to HF – can generate candidate answers to the question of why pathological hypertrophy may progress to HF while physiological hypertrophy may not. There is now a body of evidence collectively supporting the metabolic starvation hypothesis of HF, which states that altered myocardial metabolism antedates, initiates and maintains contractile dysfunction in HF.[4] This is variably true depending on the model or stimulus under question. There is growing evidence supporting the argument that metabolic reprogramming acts as a modifier

[4]Reviewed (Ingwall, 2009; Ingwall and Weiss, 2004; Neubauer, 2007; Taegtmeyer et al., 2004; Ventura-Clapier et al., 2011).

of hypertrophic growth signalling, although this remains poorly understood. The relative contribution of metabolic reprogramming in situations of transition from hypertrophy to failure remains a challenging question and likely depends on the setting under question. The challenges here parallel the challenges identified above: first, performing a comprehensive in vivo metabolic interpretation, i.e. one that interprets the transcriptome, proteome, enzyme activities and/or metabolome alongside a measurement of energy flux rates (Taegtmeyer et al., 2016), is experimentally demanding, second, the interactions between metabolic signalling and growth signalling pathways have not been systemically explored (see below), and third, few animal model studies identify (and confirm by haemodynamic LV studies) longitudinally distinct stages of hypertrophy before and after transition to failure.

Concepts in cardiac metabolism

Normal cardiomyocyte metabolism spans energy supply, transduction and sensing, and encompasses the concepts of metabolic flexibility, reserve (capacity), efficiency, beat-to-beat feedback control to match energy demand with supply, and longer term regulation.[5] Metabolic phenotype has been defined as "substrate preference" at a given mix of inputs (substrates, insulin, catecholamines, oxygen), haemodynamics (heart rate, preload, afterload, perfusion) and contractility (Stanley et al., 2005), but I would broaden this definition to include metabolic flexibility (ability to alter substrate preference depending on context), capacity (maximum oxidative and/or phosphotransfer flux reserve) and efficiency.

ENERGY SUPPLY

Energy supply can be divided into three stages (Figure 1.1). First, there is substrate selection, uptake and oxidation.[6] Substrates are catabolised to acetyl-CoA, which

[5] Some of this section, including Figures 1.1–1.2, is shortened from my previous review (Peterzan et al., 2017).

[6] Reviewed (Lopaschuk et al., 2010; Neely and Morgan, 1974; Stanley et al., 2005).

then enters the citric acid cycle (CAC). This effectively transfers energy in the form of electrons from substrates – non-esterified long-chain FA (60–90%) and pyruvate (10–40%, derived evenly from glucose and lactate) – to CAC intermediates to reduced nicotinamide adenine dinucleotide (NADH) and the reduced form of flavin adenine dinucleotide ($FADH_2$). At this stage there is substrate-level phosphorylation of ADP and guanosine-5'-diphosphate (GDP) (glycolysis, CAC).

Second, electrons are shuttled from cytosolic to mitochondrial reducing equivalents and from reducing equivalents to O_2 via electron transport chain (ETC) complexes. This is accompanied by the generation of an electrochemical proton gradient within the mitochondrial intermembrane space (by complexes I, III, and IV). F_0, F_1-ATPase (Complex V) releases this gradient and couples the energy obtained to the synthesis of ATP from ADP + inorganic phosphate (P_i). This is called oxidative phosphorylation (oxphos) and contributes >95% of myocardial ATP synthesis under aerobic conditions. Owing to this dependence on oxphos, rates of CAC flux, cardiac work and oxygen consumption are linearly correlated (De Sousa et al., 1999; Kapelko et al., 1988; Kobayashi and Neely, 1979; Saupe et al., 1998) and at high workloads approach 90% of mitochondrial oxidative capacity (Bittl et al., 1985; Cooney et al., 1981; Mootha et al., 1997). Besides a non-limiting oxygen supply, oxphos capacity requires normal mitochondrial number (mass, biogenesis), dynamics and unit activity (integrity).

The third stage, phosphotransfer, refers to delivery of ATP from mitochondria to sites of use. This involves ADP-ATP exchange across the inner mitochondrial membrane by the adenine nucleotide translocase (ANT) and transfer of adenine nucleotide equivalents (PCr, creatine) by the CK system, which represents a form of facilitated diffusion. Besides CK, there are minor contributions from adenylate kinase (AK), other phosphotransfer systems and direct adenine nucleotide "channeling" (Dzeja and Terzic, 2003).

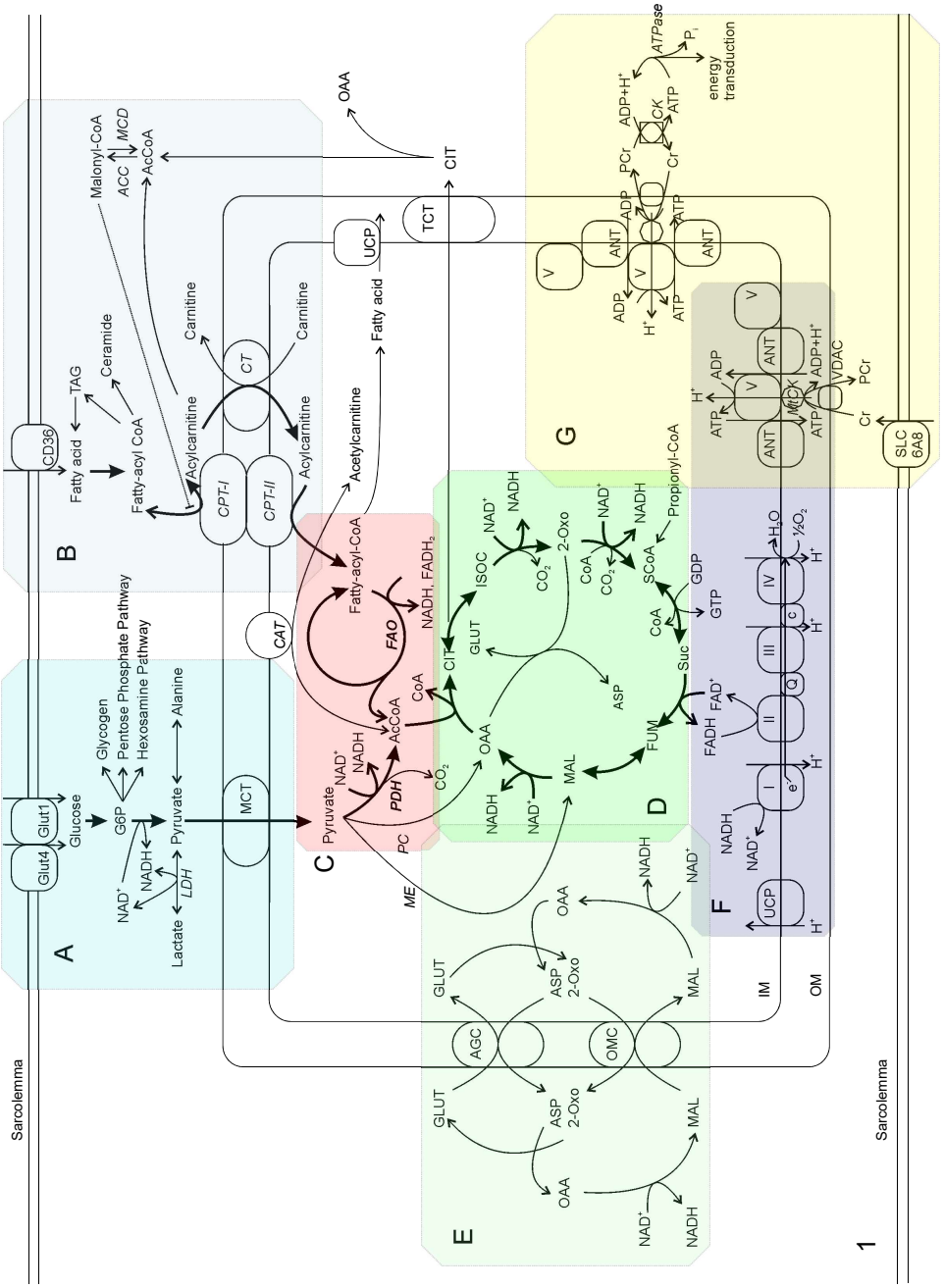


Figure 1.1: Major substrate fates, energy fluxes, and carriers involved in the three stages of energy supply [A-D (first stage), E and F (second stage), and G (third stage)]. Bold arrows indicate major routes of electron donation to the electron transport chain (ETC). Highlighted subdivisions include glucose/pyruvate uptake (A), fatty acid (FA) uptake (B), pyruvate oxidation and FA oxidation cycle (C), tricarboxylic acid cycle (D), electron shuttle (E), ETC/oxidative phosphorylation (oxphos) (F), and phosphotransfer (G).

ENERGY TRANSDUCTION

Cardiomyocyte work is not performed by ATP but by enzymes (myosin ATPase, SERCA2a and sarcolemmal Na^+-K^+-ATPase) that use the energy obtained from ATP hydrolysis to do work. The free energy change of ATP hydrolysis (ΔG_{ATP}):

$$\Delta G_{ATP} = \Delta G^0_{ATP} - RT \ln([ATP]/[ADP][P_i])$$

is the maximum energy that could be extracted were the sarcomere working at 100% thermodynamic efficiency. Were ATP demand to outstrip supply, phosphorylation potential ([ATP]/[ADP][AMP] ratio) would fall, and with it, ΔG_{ATP} (Gibbs, 1985). CK keeps the phosphorylation potential high at points of ATP hydrolysis and low at points of ATP synthesis, and so maximizes the ΔG_{ATP} available to energy transducing ATPases and minimises end-product inhibition of ATP synthase.

The ATPases most vulnerable to changes in ΔG_{ATP} are those with the highest required ΔG, i.e. the aforementioned three enzymes. ΔG_{ATP} tends to fall at increased workloads (Zhang et al., 1999) and for any given workload, ΔG_{ATP} falls as free [ADP] or [P_i] rise and CK reaction velocity falls (Tian and Ingwall, 1996). This relationship varies with different substrate fuels (Balschi et al., 1997; Ben Cheikh et al., 1994; From et al., 1990; Saupe et al., 2000).

METABOLIC FLEXIBILITY

The healthy heart is an omnivore: the proportional contribution of any substrate to ATP synthesis varies depending on prevailing conditions or activity.[7] Metabolic inflexibility, or relative bias for oxidation of certain substrates, is recognised in obesity and diabetes, hypertrophy, and HF (see below).

METABOLIC RESERVE

Regional contractile reserve upon inotropic challenge is used clinically as a surrogate of regional perfusion reserve, but also more fundamentally implies the concept of

[7] Reviewed (Goodpaster and Sparks, 2017; Muoio, 2014).

cellular energy flux reserve (Kassiotis et al., 2008). The previously described energy supply pathways can be thought of a series of metabolic cycles, each with conserved intermediates. When energy demands increase, energy fluxes increase and the rate of turnover of each cycle increases. However, the concentration of cycle intermediates remains stable over a wide range of flux. Crucially, one cannot predict cycle flux from the concentration of cycle intermediates. E.g., upon exercise, cardiac output and oxygen consumption may rise sixfold in healthy hearts, yet this is accompanied by no change in time-averaged [PCr], [ATP] and [NAD^+]/[NADH] (Balaban, 1990; Balaban et al., 1986). Cardiac stored ATP content is low – enough for only ten cardiac cycles – so the need for ATP turnover reserve is reflected in the high proportion (>30%) of cardiomyocyte volume occupied by mitochondria (Ingwall, 2002).

Of course, one can talk of metabolic reserve outside the context of flux reserve, e.g. 'PCr content is sufficient to replenish ATP content two-fold', but one should be careful to specify the sense in which this is meant.

METABOLIC EFFICIENCY

Organ-level metabolic efficiency refers to the relationship between myocardial oxygen consumption per minute (MVO_2) and cardiac work. It is very difficult to noninvasively estimate myocardial efficiency without making multiple assumptions about the numerator, work, and the denominator, MVO_2, and in the context of mitral regurgitation practically impossible (Knaapen et al., 2007). Total work is the sum of external work and elastic potential energy, with external work being defined by the area within a pressure-volume loop (Suga, 1990). Contractile efficiency, the reciprocal of the MVO_2:work ratio, depends on the product of two efficiencies: that of oxygen consumption (VO_2) to ATP synthesis [(P/O) ratio and thermodynamic efficiency (ΔG_{ATP})] and that of ATP hydrolysis to mechanical energy.[8]

[8] For a discussion of competing conceptions of efficiency see Han et al. (2012).

Oxphos efficiency is substrate-dependent. For each substrate there are theoretical stoichiometric relations between moles of substrate oxidized, ATP produced and O_2 reduced. Glucose oxidation is more oxygen-efficient than FAO yielding higher P/O ratios per mole, making unloaded MVO_2 lower (Burkhoff et al., 1991; How et al., 2005; Korvald et al., 2000; Mjøs, 1971; Simonsen and Kjekshus, 1978). However, glucose is less carbon-efficient (only two-thirds of its carbon is oxidized) and less energy-dense (more grams must be oxidized to yield the same quantity of ATP). P/O efficiency of FAO may also be lower than anticipated, as uncoupling proteins (UCPs) can leak protons from the mitochondrial inter-membrane space without them contributing to ADP phosphorylation (futile cycling).

BEAT-TO-BEAT METABOLIC CONTROL

Full understanding of beat-to-beat control of energy flux remains debated. Ca^{2+} is a key control mediator, regulating energy-transducing (myosin, SERCA2a) ATPases, energy-supplying mitochondrial dehydrogenases and F_0, F_1-ATPase (Kohlhaas and Maack, 2013). By linking mitochodrial Ca^{2+} cycling with ETC flux, energy supply-demand matching is achieved (Glancy and Balaban, 2012). A second metabolic control of oxphos flux is by ADP, P_i, creatine and mtCK (Saks et al., 2012). Here, ATP supply and utilization reactions are colocalized within "intracellular energetic units", or microdomains, and channeling of ATP/ADP between energy supplying and energy transducing ATPases depends on direct inter-organellar crosstalk rather than (CK-facilitated) diffusion (Kaasik et al., 2001).

METABOLIC REGULATION

Members of the nuclear receptor (NR) transcription factor superfamily are responsible for gene transcription programmes directing energy metabolism and mitochondrial biogenesis. PPAR subfamily members are activated by FA and eicosanoid ligands, particularly in fasting, starvation and diabetes, when circulating ligands are increased.

To be transcriptionally active they must also heterodimerize with retinoid-X-receptor (RXR) and recruit coactivators (e.g. histone acetyltransferases, PGC-1α, ERRα). Active PPARα-RXR-PGC-1α complexes bind to PPAR response elements (PPREs) within the promoter regions of genes encoding enzymes controlling FA and glucose uptake and oxidation (Barger and Kelly, 2000; Huss and Kelly, 2004).

ENERGY SENSING

AMP-activated protein kinase (AMPK) is an evolutionarily conserved energy sensing molecule that exerts both control and regulation by sensing metabolic stress (exercise, ischaemia, pressure-overload, glucose deprivation), and responding by stimulating ATP-supplying pathways and inhibiting anabolic pathways (Hardie, 2014; Zaha and Young, 2012). AMPK is a heterotrimer comprising a catalytic α subunit and regulatory β (glycogen-binding) and γ (adenine nucleotide-binding) subunits. AMPK is activated by raised adenosine-5'-monophosphate (AMP)/ATP ratio, phosphorylation (α-Thr-172), upstream AMP- and Ca^{2+}-dependent kinases (LKB1, CaMK kinase-β (CaMKKβ)) and other mechanisms (summarised in Figure 1.2).

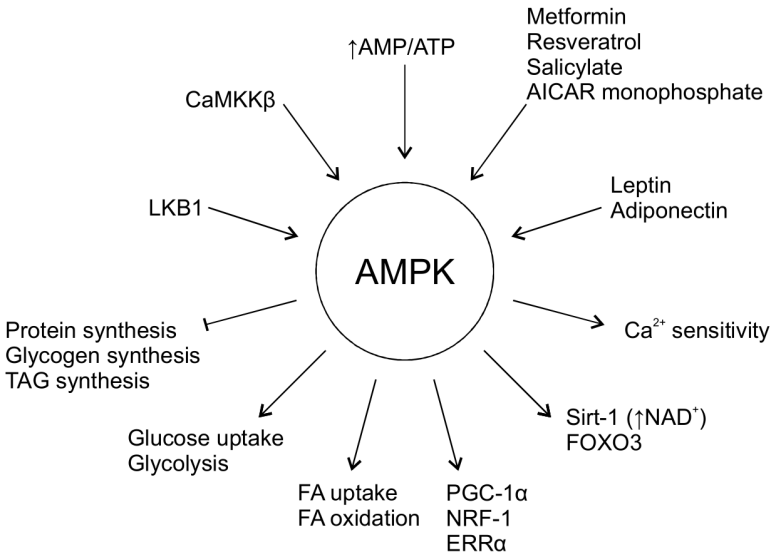


Figure 1.2: Major activators and downstream effects of AMPK in cardiomyocytes.

When activated, AMPK inhibits protein synthesis (mechanistic target of rapamycin complex (mTORC) 1-p70S6K axis) (Gwinn et al., 2008) and promotes mitochondrial biogenesis by enhancing PGC-1α activity, by activating nuclear respiratory factor-1 (NRF-1) (Bergeron et al., 2001), and (in the heart) by promoting the transcription of ERRα and its targets (Hu et al., 2011). In the heart, AMPK increases glucose uptake (via GLUT4 translocation), glycolysis, FA uptake, and FAO (by inhibitory phosphorylation of acetyl-CoA carboxylase) (Hardie, 1992). A recently described AMPK-mediated phosphorylation of troponin I (Ser-150) increases myofilament Ca^{2+} sensitivity, resulting in increased contractility (Oliveira et al., 2012).

Substrate utilization in hypertrophy and HF

FA METABOLISM IN HYPERTROPHY AND HF

Cardiac FA uptake is variably reported in animal models of nonfailing pressure overload hypertrophy as reduced, particularly subendocardially (Kagaya et al., 1990), or unchanged (in pigs (Massie et al., 1995) and rats (Kato et al., 2010)). Human hypertensive hypertrophy displays reduced uptake and oxidation of [^{11}C]palmitate, negative correlation between these and left ventricular mass (LVM), and reduced efficiency (de las Fuentes et al., 2003, 2006). In nonfailing hypertrophy models, FAO is most commonly found to be reduced (e.g., in aortic-banded rats (Doenst et al., 2010) and SHRs (Christe and Rodgers, 1994)) but has been reported as unchanged (Degens et al., 2006; Schönekess et al., 1995), which may in part reflect differences in hypertrophy severity, duration, and the level of cardiac work. The capacity to upregulate FAO at higher workloads was reduced in nonfailing pressure overload hypertrophy in rats (Doenst et al., 2001).

FA uptake progressively falls during the development of HF secondary to hypertension in rats (Kato et al., 2010) and pacing in dogs (Nikolaidis et al., 2004; Osorio et al., 2002; Recchia et al., 1998), with concomitant changes in the gene expression of

FA transporters. FA uptake is reduced in humans with nonischemic cardiomyopathy (NICM) where patients and control participants are matched for plasma [FA] and diabetes mellitus is excluded (Dávila-Román et al., 2002; de las Fuentes et al., 2003; Neglia et al., 2007; Tuunanen et al., 2006b). FA uptake correlates negatively with LV mass in human NICM (de las Fuentes et al., 2003) and also with left ventricular ejection fraction (LVEF), attributable to increased [FA] and insulin resistance in patients with lower LVEF (Tuunanen et al., 2006b).

Fractional oxidation of FA is reduced in human NICM (Neglia et al., 2007) and in most animal HF models: pressure overload in rats (Pound et al., 2009) and mice (Kolwicz et al., 2012), volume overload (el Alaoui-Talibi et al., 1992) and MI (Heather et al., 2006) in rats, and pacing in dogs (Lei et al., 2004). FAO downregulation preceded the onset of systolic dysfunction in pressure-overloaded rats (Doenst et al., 2010). However, several studies, some in HF with more moderate degrees of systolic dysfunction, found unchanged FAO at basal workloads. In this latter group, FAO reserve was reduced (O'Donnell et al., 2008).

Underlying the reduced FAO is a fall in nuclear receptor signalling. PPAR-α expression in reduced in nonfailing hypertrophy in rats (Young et al., 2001) and mice (Barger et al., 2000), with concomitant reduction in PPAR-α target gene expression. PPAR-δ activity is reduced in pressure overload hypertrophy in rats (Planavila et al., 2005a). PGC-1α is suppressed in rat cardiomyocytes by agonists of G$\alpha_{q/11}$-coupled receptors (Garnier et al., 2009) and in non-failing aortic-constricted mice (Lehman and Kelly, 2002). All of these observations run counter to findings in physiological hypertrophy, and all would be expected to impair FAO capacity.

In HF, reduced expression of PPAR-α and PPAR-α/PGC-1α target genes maintains the reduced FA uptake and oxidation, whether in late-stage human HF (ischemic and nonischemic) (Sihag et al., 2009), after pressure loading (Kato et al., 2010; Sack et al., 1996), pacing (Lei et al., 2004), or infarction (Rosenblatt-Velin et al., 2001).

Carnitine, initially thought to be a marker of mitochondrial import capacity for fatty acyl-CoA, is now understood to buffer intramitochondrial acetyl-CoA and thus increase metabolic flexibility (Schroeder et al., 2012). Myocardial total carnitine is reduced in nonfailing aortic-banded rats (Allard et al., 1994) and rabbits (Revis and Cameron, 1979), and in multiple animal HF models and late-stage human HF (Gupte et al., 2014; Martín et al., 2000). Increased long-chain acylcarnitines on metabolomic profiling of failing pressure-overloaded murine hearts indicates bottle-necked FAO (Lai et al., 2014), but in human HF, reports of long-chain acylcarnitine content are discordant, with reversibility demonstrated after unloading (Gupte et al., 2014). The inconsistency may partially be explained by differences in HF stage and rate of HF development.

CARBOHYDRATE METABOLISM IN HYPERTROPHY AND HF

Basal glucose uptake is increased in nonfailing pressure overload hypertrophy in rats (Nascimben et al., 2004) and dogs (Zhang et al., 1995). Glycolytic rates are generally increased in pressure overload, both before the development of hypertrophy in rabbits (Taegtmeyer and Overturf, 1988) and rats (Lewandowski et al., 2007) and in established hypertrophy (Labarthe et al., 2005; Nascimben et al., 2004). In contrast, unaltered glycolytic rates have been documented in pigs (Massie et al., 1995) and rats (Lewandowski et al., 2007) developing moderate pressure overload hypertrophy over 10 wk, indicating within-model longitudinal variation.

Basal glucose oxidation rates in hypertrophy models lack consensus. This likely reflects differences in genetic background, severity of the inciting stimulus, longitudinal variation, and FAO. Sequential assessments in pressure-overloaded rats found glucose oxidation to be reduced at 1 wk, increased at 2 wk, and progressively reduced at 6-10 wk (Doenst et al., 2001, 2010). Pyruvate dehydrogenase (PDH) flux is unchanged in aortic-constricted rats on normal diets (Seymour et al., 2015) but increased in 15-wk-old SHRs (Dodd et al., 2012). Glucose oxidative reserve is reduced in rats

pressure overloaded for 8 wk (Lydell et al., 2002).

Fractional oxidation of glucose, i.e., the fraction of glucose passing through glycolysis that is subsequently oxidized by PDH, is consistently reduced in nonfailing hypertrophy, despite reduced FAO and accelerated glycolysis, both in aortic-constricted and SHRs (Labarthe et al., 2005). CAC cycle flux is maintained by increased anaplerosis (Seymour et al., 2015), with concomitant upregulation of malic enzyme (Pound et al., 2009; Sorokina et al., 2007).

Glucose uptake reserve on insulin challenge is reduced (Friehs et al., 1999; Paternostro et al., 1995; Tian et al., 2001), and glycolysis and glucose oxidation decline on longitudinal assessments of nonfailing hypertrophy (Friehs et al., 1999; Zhang et al., 2013), implicating these as markers of transition to failure.

In HF, as in nonfailing hypertrophy, glucose uptake reserve is reduced (in human NICM (Neglia et al., 2007) and animal models (Murray et al., 2006; Nikolaidis et al., 2004)), glucose oxidative reserve is reduced (in infarcted rats (Amorim et al., 2010) and paced dogs (Lei et al., 2004)), and fractional oxidation of glucose is reduced and anaplerosis increased (in pressure-overloaded rats and mice (Kolwicz et al., 2012; Pound et al., 2009)).

The capacity to oxidize both FA and glucose reduces during transition to failure, so the "substrate switch" to glucose reflects greater and/or earlier downregulation of FAO rather than potentiation of glucose oxidation (Doenst et al., 2010; Lei et al., 2004). In late-stage human HF, the expression of both FA and glucose metabolism genes is repressed (Cordero-Reyes et al., 2014; Sebastiani et al., 2007). Metabolomic profiles indicate bottle-necked pyruvate metabolism (increased pyruvate and decreased CAC cycle intermediates excepting succinate) with reversibility post left ventricular assist device (LVAD) unloading (Gupte et al., 2014).

However, remodeling of glucose uptake, glycolysis, and oxidation in HF is variably reported. Of these, glucose uptake is the most inconsistent. Reasons for discordant

reports of glucose handling include the opposing effects of glucose transporter down-regulation and pyruvate dehydrogenase kinase (PDK) downregulation on oxidative glucose flux (Razeghi et al., 2001b), and variation in the stage of disease examined, which influences insulin resistance, adrenergic activation, FA availability, and FAO. Myocardial insulin resistance is permissive for the development of HF in patients without diabetes mellitus (Witteles and Fowler, 2008) and compounds the deficit in FAO capacity in HF by inhibiting glucose oxidation and increasing reliance on FAO.

KETONE BODY METABOLISM IN HYPERTROPHY AND HF

Increased ketone body oxidation with concomitant upregulation of β-hydroxybutyrate dehydrogenase and succinyl-CoA-3-oxoacid-CoA-transferase (SCOT) was recently observed in nonfailing hypertrophy and pressure overload/infarction-induced HF in mice (Aubert et al., 2016), advanced human NICM (Bedi et al., 2016), and nonfailing diabetic humans undergoing clinically-indicated cardiac catheterization (Mizuno et al., 2017). Whether this is adaptive or maladaptive is unknown (Cotter et al., 2013). Cardiac-specific knockout of SCOT, which is required for ketone body oxidation, exacerbates dysfunction after aortic constriction (Schugar et al., 2014).

Given the unexpected cardiovascular benefits of empaglifozin in diabetic humans (Zinman et al., 2015), some have hypothesised that these could in part derive from increased systemic fat oxidation and hepatic ketogenesis increasing the supply of ketone bodies to the heart (Ferrannini et al., 2016; Mudaliar et al., 2016). However, this hypothesis remains unproven (Kappel et al., 2017), and the relationship between fractional oxidation rates of ketones, FA, and glucose and cardiac function remains unclear (Crawford, 2018; Lopaschuk and Verma, 2016).

EFFICIENCY

Myocardial efficiency (work/MVO_2) is reduced in human NICM (Neglia et al., 2007; Tuunanen et al., 2006a,b) and correlates inversely with cavity size. Efficiency is also

reduced in HF models driven by pressure overload (O'Donnell et al., 2008), infarction (Neubauer et al., 1995), and pacing (Osorio et al., 2002) and is improved with β-blockade (Nikolaidis et al., 2006). Acute suppression of FA uptake reduces work but not efficiency in controls, but reduces work and efficiency in NICM, suggesting impaired flexibility to upregulate glucose metabolism (Tuunanen et al., 2006a). Similarly, pacing stress causes increased fractional FAO and reduced efficiency secondary to failure to upregulate glucose uptake (Neglia et al., 2007).

In summary, metabolic remodeling of substrate utilization capacity takes place during hypertrophic remodeling with consequences for flexibility and performance during metabolic stress. Further work is required to demonstrate these phenomena in humans and establish the conditions under which these most impair contractile function. Progressive metabolic remodeling occurs on transitioning from hypertrophy to failure and likely perpetuates the contractile dysfunction. Areas deserving exploration include the mechanisms underlying inefficiency and inflexibility and the potential for reversibility.

MODELS OF MANIPULATED SUBSTRATE HANDLING

Whether and which of the above alterations in substrate handling are maladaptive is a complex question. Some insight is provided by genetically modified models of altered substrate handling.[9]

First, basal substrate oxidative preference predicts neither metabolic flexibility nor oxidative reserve, while it is these latter phenomena that predict improved outcomes. For example, CPT-Iβ heterozygous mice have unaltered resting FAO but fail to upregulate FAO on pressure overload and die prematurely with HF (He et al., 2012). When resting FAO preference is reduced, cardiac tolerance of increased workload may be increased (Kienesberger et al., 2012) or reduced (Augustus et al., 2006); conversely,

[9] Reviewed (Ritterhoff and Tian, 2017).

increasing resting FAO preference can be cardioprotective during pressure overload (Kolwicz et al., 2012).

Second, failure to upregulate substrate oxidation under stress results in exacerbated hypertrophy and/or contractile dysfunction, whether the inflexibility is for FA (Yan et al., 2009) or glucose. Prevention of substrate switching from FA to glucose in aortic-constricted rats by pharmacological PPAR-α reactivation is not accompanied by matched increases in FAO, resulting in reduced cardiac power and efficiency (Young et al., 2001). In malonyl-CoA decarboxylase (MCD) knockout mice similarly, insufficient FAO reserve is not compensated for by increases in glucose oxidation, resulting in reduced cardiac performance, efficiency, and survival, a phenotype that improves as dietary fat reduces on weaning (Aksentijević et al., 2014).

Conversely, where increases in glucose oxidation are sufficient to match falls in FAO, models are protected from pressure overload and/or high-fat diet (HFD) (Kienesberger et al., 2012; Pulinilkunnil et al., 2014). Examples include GLUT1 overexpression in lipoprotein lipase knockout (Khan et al., 2013), PPAR-α knockout (Luptak et al., 2005), and aortic constriction (Liao et al., 2002) models.

Third, manipulations that improve the matching of oxidative and nonoxidative glucose metabolism improve efficiency and contractility. Examples include PDK-4 inhibition by dichloroacetate in pressure-overloaded rats (Pound et al., 2009) and MCD knockout in infarcted mice (Masoud et al., 2014). Cardiac-restricted PDK-4 overexpression constrains substrate flexibility (biased toward increased FAO), which counterintuitively improves matching in the setting of HFD and attenuates triacylglycerol (TAG) accumulation.

Conversely, manipulations that increase FA uptake and oxidation mismatch, despite increasing FAO, result in TAG accumulation and cardiac lipotoxicity. Examples include cardiac-specific PPAR-α overexpression (Finck et al., 2003) and cardiac-specific PPAR-δ knockout (Cheng et al., 2004). When this mismatch is relieved

(medium-chain FA diet (Finck et al., 2003), CD36 knockout (Yang et al., 2007), and lipoprotein lipase knockout (Duncan et al., 2010)), lipotoxic cardiomyopathy is prevented.

In summary, maladaptive metabolic remodeling may take multiple forms not specific to any one substrate preference or transcriptomic profile. Instead, lack of metabolic flexibility and reserve (both oxidative and phosphotransfer) represents a final common denominator underlying reduced efficiency and contractile reserve. The lessons learned from animal models indicate that metabolic modulation as a therapeutic strategy for HF, while promising, is unlikely to be straightforward or appropriate for all individuals or at all stages of the condition – at least some metabolic phenotyping will likely be required. This has been borne out by early clinical studies assessing metabolic modulation in human HF, which have identified improved matching of oxidative and nonoxidative glucose metabolism, and an increased contribution of glucose relative to fatty acid oxidation, as sensible strategies (not further discussed).[10]

Phosphotransfer – a historical perspective

Models of understanding of energy transport in muscle developed as the field was tackled by various disciplines. Initially (1927–1977), only biochemical analyses were possible; thereafter NMR measurements became possible (see Introduction to Ch. 3); most recently have emerged experiments manipulating the CK system (see Section 1.3 (p. 49). This section concentrates on the initial period, from which derives our contemporary model of phosphotransfer. From this historical perspective, we understand how the role of ATP delivery (or turnover) rates and CK activity in cardiac metabolism has changed, and the outstanding limitations of NMR measurements become clearer. The importance of high-energy phosphate turnover (or delivery) rate over content, initially not appreciated, is now understood to matter mostly in contexts

[10]For reviews see Fillmore and Lopaschuk (2013); Fillmore et al. (2014); Lopaschuk (2017); Maack et al. (2018); Mallet et al. (2017); Witteles and Fowler (2008).

of high metabolic stress.

PCR AS THE PRIMARY ENERGY SOURCE

The role of high-energy phosphates and CK in cardiac metabolism is of significant historical interest. In 1927 PCr was identified as the highly-labile phosphagen that breaks down during muscle contraction and is restored during recovery (Fiske and Subbarow, 1927). Its hydrolysis was accompanied by the release of base (Fiske and Subbarow, 1928). Contemporary work showed that the heat of hydrolysis was considerable, hence the later term 'high-energy' phosphate compound, that the phosphagen could be restored rapidly in the presence of oxygen, and that a large proportion could be restored in the absence of oxygen. Experiments by Lundsgaard showed that iodoacetate-poisoned muscle, which is unable to perform glycolysis or oxphos, can contract normally without forming lactate, but after repeated stimulation a phosphagen-deplete, inexcitable contracture develops, when the muscle does not recover even in the presence of oxygen (cited in Hill (1932)). These experiments showed that phosphagen alone could supply all the energy required for a normal contraction.

Shortly thereafter, ATP was identified (Lohman, 1931) and the reversibility of transfer of phosphate between PCr and ADP was established (Lehmann, 1935). Under this model, PCr was the prime energy supplier, with ATP given the role of regenerating PCr.

ISOLATION OF CK

CK was isolated in crystalline form from rabbit skeletal muscle by Kuby et al. (1954), who established conditions under which maximal enzyme activity may be determined. The first measurements of the equilibrium constant where equilibrium concentrations of all reactants were measured were made in rat skeletal muscle in 1979 (Lawson and Veech, 1979; Veech et al., 1979).[11]

[11] For the effect of Mg^{2+} on the CK equilibrium see Section A.1 (p. 229).

ATP AS THE PRIMARY ENERGY SOURCE

Although the discovery that myosin is an ATPase (Engelhardt and Ljubimowa, 1939) implicated ATP as the source of energy for muscular work, the proof did not come until the concentrations of adenine nucleotides, PCr, creatine and P_i were measured in isolated frog rectus abdominis with and without pretreatment with the CK inhibitor fluorodinitrobenzene (FDNB). In the presence of CK inhibition, the number of normal contractions that could be elicited was reduced from 30 to 3, while the PCr content did not change (Cain and Davies, 1962; Cain et al., 1962). These experiments demonstrated a direct relationship between ATP utilized and work done in the setting of CK inhibition, established ATP as the primary energy source in muscle and showed that ATP is reconstituted by transphosphorylation of ADP by PCr via CK (ADP + PCr $\longrightarrow$ ATP + creatine) or by AK.

Under this model, PCr functioned as an energy reservoir, maintaining ATP during periods of high energy demand. This model could not be complete however, as the FDNB experiments could not explain why the muscle became inexcitable before ATP content was exhausted. Furthermore, iodoacetate-poisoned frog sartorius stimulated to the point of inexcitable fatigue under anaerobic conditions did not contract when PCr was depleted, even though ATP content was not significantly changed (Seraydarian et al., 1961). By implication, CK-catalysed transphosphorylation was essential for contractility.

DISCOVERY OF MITOCHONDRIAL CK & PRIMACY OF HIGH-ENERGY PHOSPHATE TURNOVER OVER CONTENT

The discovery of mtCK, its localisation to mitochondria and its high organ-specific activity in muscle and brain (but not liver and kidney, where creatine is synthesised) (Jacobs et al., 1964) set the stage for three further hypotheses.

Adenylate energy charge. First, the energy charge hypothesis proposed that the adenylate "energy charge", as defined by $\frac{ATP+0.5ADP}{ATP+ADP+AMP}$, is a global metabolic regulator (Atkinson, 1968), such that at ratios <0.8, catabolic reactions (phosphofructokinase, pyruvate dehydrogenase) are stimulated and anabolic reactions inhibited, while at ratios >0.9, vice-versa. Homeostasis would then require the cell's energy charge to remain near 0.85. However, Atkinson admitted that this likely represented an oversimplification from the perspective of functional compartments at the subcellular level.

Two ATP compartments & primacy of turnover over content. The second hypothesis arose from experiments which failed to show a common CK equilibrium constant across resting and other muscle states and failed to correlate muscle contractility with tissue concentrations of ATP. There was also the conceptual problem that ATP and PCr could not be regenerated at each other's expense: regenerating ATP at the contractile site required PCr (and CK), but the restoration of PCr itself required ATP (and CK working in the opposite direction). In response, this hypothesis posited that there were two functionally distinct ATP pools (one at the contractile site and the other restoring PCr) and that ATP turnover (or delivery), but not content, best predicted muscle contractility. This is developed below.

A first line of evidence observed that when CK reactants were measured in rat rectus abdominis at rest and during tetanic stimulation, PCr/creatine levels underwent rapid, large changes while ATP/ADP levels varied only minimally, such that PCr/creatine and ATP/ADP ratios were independent. Whatever the apparent CK equilibrium constant in resting skeletal muscle was, it did not apply in tetanized muscle (Hohorst et al., 1962). To explain this, the authors proposed functional compartmentation of high-energy phosphates such that >85% of ATP and ADP is in a 'storage-ATP compartment' and does not react 'quickly' with CK (at a rate comparable to the breakdown of PCr), while a small proportion is present in a 'turnover-ATP

compartment' which is in equilibrium with PCr/creatine. Likewise, the differential rate of fall in PCr and ATP stores in the first minute of acute myocardial ischaemia implied no consistent equilibrium between the two (Gudbjarnason et al., 1970).

In a second line of evidence, several investigators found no clear-cut relation between high-energy phosphate content and contractility. Feinstein (1962) observed that the positive inotropic effect of ouabain in failing pressure-overloaded guinea pig hearts was accompanied by a fall in PCr content and no change in ATP. In a separate experiment, LV samples were taken at serial timepoints from anaesthetized normal guinea pigs before, during and after 8 min of acute anoxic myocardial depression. Within 2 min of anoxia, PCr had fallen to 20% of baseline and ATP to 80%. For the remaining anoxic time, PCr remained around 6-10% of baseline and ATP reduced progressively to 30%. After resumption of ventilation, contractile function recovered to normal within 20–90 sec, despite PCr not recovering to >30% baseline and ATP not increasing at all during this time. The authors concluded: "steady-state levels of high-energy phosphate compounds are not as important in determining the mechanical capacity of the heart as are their rates of synthesis".

Pool et al. (1966) took serial LV biopsies in anaesthetized dogs before and during acute hypoxic myocardial depression. After 16.1 min, when left ventricular end-diastolic pressure (LVEDP) had risen significantly yet stroke work was maintained, PCr content was either normal or depressed compared to baseline, with ATP unchanged; after 17.9 min, when LVEDP was increased and stroke work depressed, PCr content was reduced with ATP maintained.

Seraydarian et al. (1969) showed that when glycolysis and oxphos were inhibited in cultured neonatal rat cardiomyocytes (by 2-deoxyglucose and oligomycin respectively), high-energy phosphate content and cell beating rates progressively fell until cell beating stopped, at which time PCr content was one sixth of baseline and ATP 75%. In FDNB-pretreated cardiomyocytes, beating stopped when ATP fell to 80% of

baseline, despite no change in PCr (Seraydarian et al., 1970).

Gudbjarnason et al. (1970) took serial LV biopsies from ischaemic myocardium in anaesthetized dogs before and after coronary ligation. Contraction ceased 1–2 min after coronary occlusion, at which time PCr had fallen to 26% and ATP to only 81% of baseline. However, in biopsies from remote viable, contracting myocardium 1-10 days post infarction, ATP levels as low as 30% of baseline were recorded. Rates of lactate accumulation and PCr diminution correlated with each other but not with the rate of ATP diminution. To explain these observations the authors proposed "functional compartmentation" of ATP and PCr, such that

> a deficient transfer of energy rich phosphate from the site of synthesis to the site of utilization for muscle contraction may contribute to the early cessation of contractile activity,[12]

and sketched one of the first representations of the CK shuttle hypothesis. However, it took the findings of the next section to clinch the two ATP pool hypothesis.

TWO CK COMPARTMENTS, WITH THE PRODUCT OF ONE, CREATINE, STIMULATING ATP SYNTHESIS VIA THE OTHER

The third hypothesis built on the realisation that mtCK could work in the reverse direction to that assumed by hypothesis two, i.e. generating PCr + ADP from creatine + ATP. This direction was particularly favoured when oxphos was allowed to proceed:

1. When ^{32}P-labelled ATP was added to a mixture of creatine, P_i, α-ketoglutarate and mitochondria isolated from rabbit ventricles, mtCK formed both labelled and unlabelled PCr, but preferentially the latter (Yang et al., 1977). Labelled PCr had been formed by CK using labelled, exogenous ATP (creatine +

[12] They went onto posit acidosis-mediated inhibition of mtCK as the mechanism underlying the apparent inability to use ATP stores in acute ischaemia, with relative preservation of cytoplasmic CK activity underlying continued (proton-consuming) PCr hydrolysis. Later work confirmed the link between contractile activity and mtCK activity during ischaemia and in postischaemic recovery (Bittl et al., 1985) and with energy transfer flux during hypoxia (Bittl et al., 1987a).

ATP $\longrightarrow$ PCr + ADP); unlabelled PCr had been formed by CK using creatine and unlabelled ATP newly generated by oxphos ($ADP + P_i \longrightarrow ATP$). The preference was reversed in the presence of the oxphos uncoupler CCCP and the ANT inhibitor atractyloside. These findings showed that mitochondrially-generated ATP is a preferred substrate of mtCK compared with extramitochondrial ATP and supported the two ATP compartment hypothesis.

2. In isolated mitochondria, the rate of synthesis of PCr by mtCK was markedly accelerated when oxphos was allowed to proceed compared with when oxphos was inhibited. Even in the presence of high [PCr], the effect of allowing oxphos to proceed was sufficient to reverse the predicted direction of the CK reaction and result in net PCr production (Saks et al., 1975). This further emphasised the efficiency of mitochondrially-generated ATP as a substrate for mtCK over exogenous ATP.

However, the affinities (assessed using Michaelis constants) of mtCK for MgADP and PCr were around ten-fold higher than those for MgATP and creatine respectively, and maximal CK rate in the ATP-generating direction was 4 times that in the PCr-generating direction in rat mtCK (Saks et al., 1975).[13] In other words, the ATP-generating reaction direction was kinetically preferred. To explain why the PCr-generating direction should be dominant in mitochondria, the following observations were gathered.

1. For any given [Mg^{2+}], the ATP-generating direction is favoured by higher [PCr][ADP]/[creatine][ATP] ratios. For values of [Mg^{2+}] where overall CK reaction rate closely correlates with [Mg^{2+}], an isolated 1 mmol change in [MgADP] has a 100-fold greater effect on normalised CK reaction rate than a

[13] The V_{max}(ATP-generating):V_{max}(PCr-generating) ratio was later reported as 1 in beef heart mtCK (versus 4 in beef heart CK-MM) (Hall et al., 1979); 3 in human mtCK (Blum et al., 1983) and 1.4 in chicken mtCK (Van Dorsten et al., 1996).

1 mmol change in [MgATP] or [PCr] and a 1000-fold greater effect compared with the same change in [creatine].[14]

2. The K_m of mtCK for ADP of 20 µmol matches the known effective K_m of oxphos for ADP (Saks et al., 1975; Van Dorsten et al., 1996). Therefore [MgADP] is a likely regulator of CK activity in vivo.

3. The localisation of mtCK to the outer surface of the inner mitochondrial membrane, and its colocalisation with ANT, results in its 'seeing' a high local [ATP]/[ADP] ratio, enabling it to couple creatine phosphorylation to oxphos (Saks et al., 1975, 1980).

4. Mitochondria absorb protons during oxphos (combining them with O_2), alkalinizing the environment mtCK is exposed to. This shifts the CK equilibrium in the PCr-generating direction, and increases the V_{max} of the PCr-generating direction (Hall et al., 1979).

A second realisation was that creatine, rather than ADP, was the prime feedback regulator of respiratory control in muscle. Creatine was first reported to stimulate oxygen consumption in muscle in 1911 (cited by Jacobus (1985a)). A regulatory function for creatine was suggested by the observation that the addition of creatine to cultured cardiomyocytes resulted in large increases in PCr content (Seraydarian et al., 1974). As there was no depletion of ATP (not even transiently), cytoplasmic CK and cytoplasmic ATP were unlikely responsible – the PCr had to have come via mtCK and the ATP synthesis rate had to have increased. As ADP is a byproduct of CK working in the PCr-producing direction and itself stimulates oxphos, this implied control by creatine over oxphos rates. Conversely, inhibition of either glycolysis or oxphos (but not CK) resulted in marked drops in PCr content (Seraydarian and Artaza, 1976; Seraydarian et al., 1969).

[14] For the effect of $[Mg^{2+}]$ on the CK equilibrium see Section A.1 (p. 229).

Polarographic studies indicated that creatine does not affect state 3 (ADP-stimulated) respiration rates in isolated mitochondria but increases state 4 rates (post ADP rates in the presence of ATP) in a manner dependent on the concentrations of creatine, PCr, ADP, ATP, and Mg^{2+}. The mechanism involves mtCK trapping of ATP newly formed by oxphos (removing end-product inhibition) with simultaneous formation of PCr and ADP (stimulating respiration) (Bessman and Fonyo, 1966; Jacobus and Lehninger, 1973; Saks et al., 1975). (This effect is observed only in mitochondria with high mtCK expression (heart mitochondria but not liver mitochondria) and cannot be bestowed by adding cytoplasmic CK to isolated liver mitochondria, emphasising the importance of mtCK colocalisation with ANT (Jacobus and Lehninger, 1973).) Furthermore, this mechanism is kinetically preferred: ADP generated by mtCK phosphorylating creatine has a 4–5-fold higher efficacy (lower K_m) for stimulating respiration than ADP added in the absence of a phosphate acceptor (Jacobus, 1985a). But why would creatine-dependent respiratory stimulation matter in cells with high mtCK expression?

The much higher specificity of mtCK for ADP/ATP over other nucleoside diphosphates/triphosphates, its much higher activity compared with AK and nucleoside diphosphate kinase (NDPK) activities, and its much higher expression in heart than liver, indicated that cardiac mtCK has a much greater capacity to phosphorylate creatine than liver mtCK – enough in fact to transfer all the ATP generated during maximal respiration to creatine (Jacobus and Lehninger, 1973). If most of the ATP formed during oxphos was directed ('channelled') via mtCK to PCr before leaving the mitochondria, this trapping would result in a high steady-state ADP concentration at the mitochondria, which would in turn continuously stimulate respiration to above the state 4 rate, buffering any periodicity in contractile activity.[15]

The finding that CK-MM is localised to myosin myofilament M-lines (Turner et al., 1973) and that myosin ATPase preferentially uses CK-generated ATP over cytosolic

[15] Periodicity of cardiac [ATP] and [PCr] was first quantified by gating NMR excitation pulses to four different parts of the cardiac cycle (Fossel et al., 1980).

ATP (Bessman et al., 1980) completed the creatine-mediated feedback control and CK- and adenine nucleotide-compartmentation hypotheses.[16] In summary, the hydrolysis of ATP by myosin causes local acidification (produces ADP + H^+) and drives the cytosolic CK equilibrium in the ATP-generating direction. The ADP produced at the contractile site is almost completely phosphorylated by PCr (via cytosolic CK) or converted to ATP + AMP (by AK), allowing a high energy charge to be maintained locally but perhaps impairing the ability of ADP to function as an efficient feedback regulator to mitochondria. Under conditions of increased work, more creatine is generated by cytosolic CK which then (after diffusing to mitochondria) stimulates an increased rate of respiration, as mtCK is able to catalyse its transphosphorylation from endogenously generated ATP and the ADP so produced stimulates oxphos (Seraydarian and Abbott, 1976). Thus this hypothesis posits separate interdependent compartments of CK isozymes at the contractile site and mitochondria, each working in opposite directions on separate pools of ATP/ADP, with creatine, the end-product of muscle activity, regulating ATP synthesis.[17]

Phosphotransfer today

A CONTEMPORARY MODEL

A contemporary model of the CK system, or 'circuit', does not fundamentally change the two 'functionally coupled' compartment model that emerged by the late 1970s (cytosolic CK working to keep ATP/ADP ratios high and mtCK working in the opposite, PCr-producing direction), but expands the cytosolic CK compartment to

[16] It was later shown that portions of CK-MM specifically localise to the I-band (in fast-twitch muscle particularly), where it functionally couples with glycolytic enzymes, to the sarcoplasmic reticulum, where it functionally couples with SERCA2a, and to the sarcolemma, where it functionally couples with the Na^+/K^+-pump and K_{ATP} channel (Abraham et al., 2002; Wallimann et al., 1992).

[17] This hypothesis also allows us to understand why FDNB-treated muscle becomes inexcitable before ATP content is exhausted (Cain and Davies, 1962). In FDNB-poisoned cardiomyocytes, elicitable contractions use ATP but not PCr. Creatine cannot be made available to mtCK, so ATP cannot be generated as quickly at the mitochondria; at the contractile site, ATP cannot be reconstituted from PCr, so only a limited amount of ATP can be used (Seraydarian and Artaza, 1976).

include portions of CK localised to the sarcoplasmic reticulum, where it functionally couples with SERCA2a (de Groof et al., 2002; Steeghs et al., 1997a), and to the sarcolemma, where it functionally couples with the Na^+/K^+-pump and K_{ATP} channel (Abraham et al., 2002). Thus cytosolic CK helps maintain normal calcium kinetics and membrane stability. Two further compartments are added (Wallimann et al., 1992). The third is a portion of CK-MM specifically localised to the I-band (in fast-twitch muscle particularly), where it functionally couples with glycolytic enzymes and (under conditions where [ADP] is high and oxygen tension low) generates PCr while glycolysis removes ADP. The fourth is 'strictly-soluble' cytosolic CK, which acts to freely equilibrate bulk PCr/creatine and ATP/ADP pools. Each of the four compartments is understood to have its own equilibrium position.

PHOSPHOTRANSFER IN THE NORMAL HEART

Like any phosphagen system, the CK system comprises catalytic enzyme, phosphate acceptor (creatine), and phosphagen (PCr). CK catalyzes the reversible reaction

$$MgADP^- + PCr^{2-} + H^+ \rightleftharpoons MgATP^{2-} + \text{creatine}$$

(Figure 1.3). CK isozymes may be cytosolic, existing as dimers of M or B subunits (MM, MB, and BB), or mitochondrial, existing mostly as octamers (mtCK). The predominant isoform in cardiac and skeletal muscle is CK-MM, which is localized to ATP-utilizing microcompartments and partly to ATP-supplying glycolytic reactions. Octameric mtCK, the second most prevalent, comprises < 5% of CK in fast-twitch skeletal muscle but approx. 12% and 15-25% in slow oxidative skeletal muscle and cardiac muscle respectively (Bittl et al., 1987c; Scholte, 1973; Wallimann et al., 1992). CK-B-containing dimers are cytosolic, of low abundance after the neonatal period, and not thought to be compartmentalized. The functions of CK depend on whether the muscle is predominantly glycolytic or oxidative:

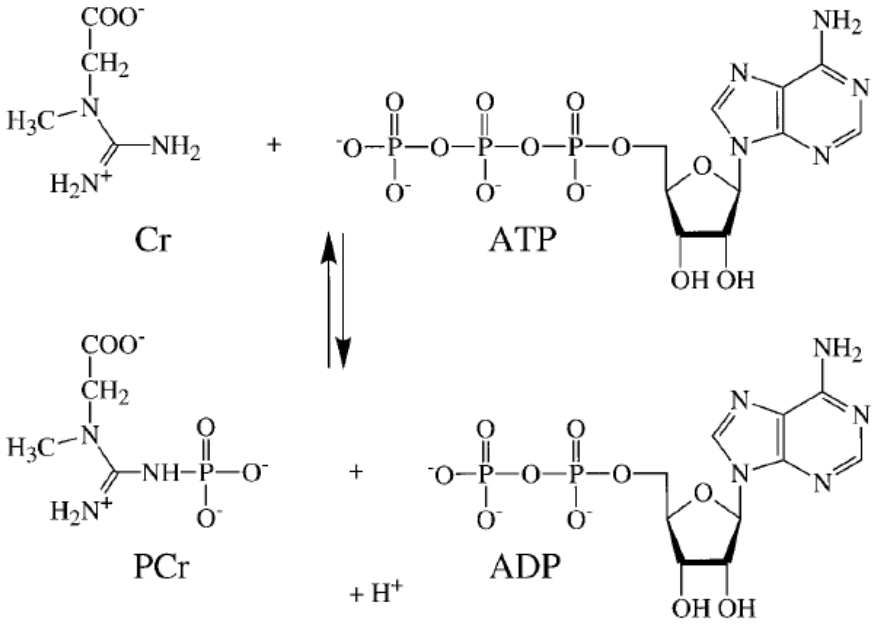


Figure 1.3: The CK reaction (from Wyss and Kaddurah-Daouk (2000)).

First, in oxidative and cardiac muscle, CK functions as a spatial energy buffer, energy transport system, or "energy shuttle" (Bessman and Geiger, 1981), between mitochondrial and cytosolic compartments.[18] MtCK spans the mitochondrial intermembrane space where it is functionally coupled to the inner membrane ANT and the outer membrane voltage-dependent anion channel (VDAC) (or porin). MtCK transphosphorylates newly synthesized ATP (transported into the intermembrane space by ANT) to PCr, whereupon PCr is exported to the cytosol via VDAC (Schlattner et al., 2006) (Figure 1.4). The ADP so produced by mtCK is transported back by ANT and stimulates oxphos, thus acting as a key controller of respiration. Because of restricted diffusion of ADP across the outer mitochondrial membrane (Kay et al., 2000; Saks et al., 2001), and the action of cytosolic CK and AK to keep cytosolic [ADP] low, ADP flux is below the maximal rate of ATP turnover, i.e. in the absence of another transport system, ADP diffusion could limit the rate of ATP turnover (Jacobus,

[18] Reviewed in more depth in Sections 1.3 (p. 29) and 7.1 (p. 213).

1985b). Creatine lowers the effective K_m for ADP-stimulated oxphos flux and, as a byproduct of cytosolic CK activity, allows the rate of ATP hydrolysis to feedback control over oxphos flux in mtCK-expressing tissues.

Second, CK is the major system for keeping cytosolic [ADP] low: virtually all ADP produced at the contractile site is transphosphorylated by CK (using PCr) to ATP. This allows ADP to participate in the control of oxphos.[19] Cytosolic CK activity keeps the [ATP]/[ADP] ratio high, maximizing the ΔG_{ATP} available to energy transducing ATPases.

Third, and probably more important in skeletal or hypoxic cardiac muscle, CK is the major short-term buffer of ATP: it supplies phosphate from PCr to ATP during bursts of ATP hydrolysis, and reconstitutes PCr from glycolytically- and oxphos-derived ATP. This dampens beat-to-beat fluctuations in adenine nucleotide concentrations (Hettling and van Beek, 2011). PCr can accumulate to much higher levels than ATP and is more diffusible, and the rate of ATP resynthesis from PCr by CK is an order of magnitude faster than that by oxphos (Saupe et al., 2000). Thus, rather than rely on diffusion of adenine nucleotides, the CK system represents "facilitated diffusion". Myosin ATPase and the ATP-producing portion of MM-CK are functionally coupled, i.e. myosin ATPase uses ATP supplied by CK in preference to cytosolic ATP (Bessman et al., 1980; Saks et al., 1984). Myosin ATPase produces ADP + H^+, driving the CK reaction in the ATP-producing direction. In the presence of oxidatively-derived PCr (normoxia), the action of CK to lower free [ADP] suppresses glycolytic flux (Kupriyanov et al., 1980). When ATP demands exceed oxidative supply, glycolysis removes ADP, driving the CK reaction in the PCr-producing direction (another functional couple).[20]

[19] In isolated mitochondria, half-maximal activation of oxphos is achieved by [ADP] in the 20-30 µmol range (Bygrave and Lehninger, 1967; Chance et al., 1986; Chance and Williams, 1955).

[20] A further function is proton buffering. This limits intracellular acidification in cells that start to perform a lot of work. An indirect consequence is that the CK system increases the amount and rate of P_i release from ATP hydrolysis at the start of burst work. This P_i stimulates glycolysis and glycogenolysis and, in the absence of PCr hydrolysis, can be rate limiting for glycogenolysis in muscles that depend

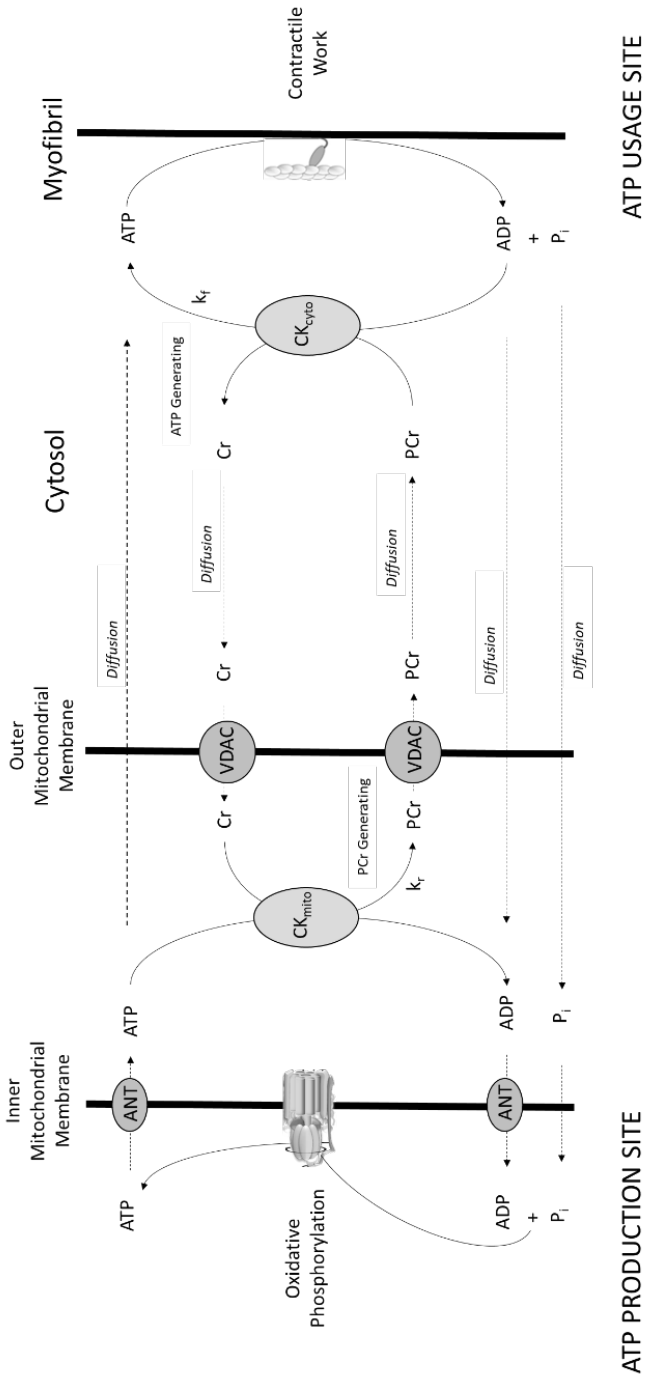


Figure 1.4: Schematic showing that ATP may be delivered to, and ADP removed from, myofibrils by diffusion and the CK system (facilitated diffusion). Alternate phosphotransfer and ATP-producing pathways not shown.

Why CK matters in cardiac muscle can thus be summarised:

1. CK activity predicts contractile reserve (Fossel and Hoefeler, 1987; Hamman et al., 1995; Harrison et al., 2003; Ingwall, 1993). This particularly matters at sustained high workloads. As CK activity is intimately linked to oxphos rates (through controlling [ADP] and [creatine]), oxphos rates to ATP demand, and ATP demand to external work, estimates of maximal CK activity (both CK total activity and in vivo CK capacity estimated by CK total activity $\times$ total creatine) closely correlate with isovolumic contractile reserve (Tian and Ingwall, 1996; Tian et al., 1996) and with post-ischaemic contractile function (Pucar et al., 2001; Saks et al., 2006). CK activity, not high-energy phosphate content, predicts return of function after reperfusion of jeopardized, inexcitable myocardium (Carvajal et al., 2007; Taegtmeyer et al., 1985).

2. CK activity keeps cytosolic [ADP] low. Falls in CK activity result in raised cytosolic [ADP], which raises the LV end diastolic pressure-volume slope (Harrison et al., 2003; Kapelko et al., 1996; Tian et al., 1997a,b). This is a key marker of diastolic dysfunction in pressure-overload hypertrophy and HFpEF.

3. CK activity reduces the energetic cost of accessing the myocardium's full metabolic capacity: during stress, cytosolic CK keeps ATP/ADP ratios near key ATPases high, preventing rises in LVEDP (myosin ATPase), blunting of calcium kinetics (SERCA2a) and action potential shortening by K_{ATP} channel opening, and releases creatine. MtCK traps newly synthesised ATP (minimizing the ΔG_{ATP} for ATP synthesis), replenishes PCr, and produces ADP, which stimulates oxphos.

on glycogenolysis. Conversely, creatine acts as a phosphate acceptor, permitting resting muscle after exercise to remove $P_i$to rate-limiting levels in order to control glycogenolysis and glycolysis (Davuluri et al., 1981).

Creatine is the essential phosphate acceptor for the CK system and a direct determinant of CK capacity (see below). While analogues such as β-guanidinopropionate (GPA) may compete with creatine for uptake and be phosphorylated by CK, phospho-GPA is an inefficient substrate for CK, with an in vitro V_{max} of $< 0.1\%$ that of PCr (Chevli and Fitch, 1979), and GPA is not a substrate of mtCK. Creatine is obtained from the diet or biosynthesized via arginine-glycine amidinotransferase (AGAT), which forms guanidinoacetate from arginine and glycine in the kidneys, and guanidinoacetate methyltransferase (GAMT), which methylates guanidinoacetate to form creatine, predominantly in the liver (Lygate and Neubauer, 2014). Cardiomyocytes cannot biosynthesize creatine and so import it against a large concentration gradient using a specific creatine transporter (CrT) (SLC6A8) that co-transports 2 Na^+, 1 Cl^- with each creatine molecule and normally operates at near-saturating levels of extracellular creatine. Creatine degradation to creatinine is slow, nonenzymatic, and unregulated; therefore, creatine content is determined by transporter activity. This is subject to substrate inhibition and negative regulation by thioredoxin-interacting protein (Zervou et al., 2013) (and other putative pathways (Zervou et al., 2016)).

The maximal capacity of the CK system is the product of CK "activity" under saturating conditions and total creatine concentration (Nascimben et al., 1996; Tian et al., 1996).[21] Although the term activity has been used loosely up until now, strictly one should distinguish CK activity, which can only be measured on freeze-and-extract biochemical assay and which refers to enzyme V_{max}, from CK flux, an in vivo estimate of enzyme-catalysed metabolite turnover rate. In vivo estimates of CK forward flux can be obtained using ^{31}P-NMR magnetization saturation transfer techniques and are reported as the product of the NMR-measured pseudo-first-order unidirectional forward rate constant k_f ($k_{PCr \longrightarrow ATP}$) and [PCr]. These do not discriminate between subcellular compartments and (in the case of k_f) represent a weighted-average of

[21] For the CK rate equation see Section A.1 (p. 229.)

all ATP-producing CK activity. The ratio of CK flux to oxphos flux is an index of "CK reserve" (Weiss et al., 2005). Although there are other enzymes with phosphotransfer activity (adenylate kinase (AK), 3-phosphoglycerate kinase, pyruvate kinase, NDPKs), none are specific for PCr, i.e. none are phosphagen kinases. AK catalyzes the reaction $2\,MgADP^{-} \rightleftharpoons MgATP^{2-} + AMP^{2-} + Mg^{2+}$. In the normal heart this is of minor importance; however, in ischemia, when energy demand exceeds supply, AK effectively doubles the energy available from ATP. The AMP can be converted to adenosine by 5'-nucleotidase, which diffuses across the plasma membrane to exert cardioprotective effects (Wallimann et al., 1992). However, this is at the cost of lost adenine nucleotides, which must be replenished.

Phosphotransfer in hypertrophy and HF

PHOSPHOTRANSFER IN HYPERTROPHY

Abnormal falls in myocardial [PCr], the PCr-to-ATP ratio, and CK flux at rest or on stress are seen in the absence of ischaemia in swine and canine models of pathological hypertrophy and failure (Bache et al., 1999; Murakami et al., 1999b). They reflect mismatch of ATP synthesis-demand fluxes and abnormal energy homeostasis. These abnormalities implicate problems with CK reserve itself and/or upstream flux control points, including mitochondrial ADP-ATP translocation, oxphos capacity, and substrate utilization.

Myocardial ATP and total adenine nucleotide (TAN) content are generally unaltered in pressure overload, whereas PCr/ATP is generally reduced (Ye et al., 2001b). In humans, PCr/ATP reduces with age (Esterhammer et al., 2014; Hollingsworth et al., 2012; Jakovljevic et al., 2015; Nathania et al., 2018; Schocke et al., 2003), chronic hypobaric hypoxia (Hochachka et al., 1996) and in aortic stenosis (Mahmod et al., 2014), particularly when there is concomitant dyspnoea or raised LV end-diastolic pressure (Conway et al., 1991; Neubauer et al., 1997b). In human hypertension,

normal and reduced ratios are found, the latter correlating with diastolic dysfunction (Lamb et al., 1999) and independent of coexistent HF (Smith et al., 2006).

Mean LV total creatine was not significantly reduced in nonfailing thoracic aortic constriction (TAC) dog models (32% increase in LV-body weight ratio) (Bache et al., 1994) or TAC mice (43% increase) (Lygate et al., 2007); the equivalent study has not been performed in humans. However, creatine decreased in other hypertrophy models: by 15% in TAC dogs (92% increase in LV-body mass ratio, 57% increase in LVEDP, but no overt evidence of HF) (Ye et al., 2001b), by 23% in TAC dogs (107% increase in LV-body mass ratio, 71% rise in LVEDP), and by 31% in TAC rats at 39-weeks (52% increase in heart-body mass ratio) (Tian et al., 1997b).

Total CK activity is generally preserved in nonfailing pressure overload models (Ingwall, 1984, 1993). CK-B is upregulated in pathological but not physiological hypertrophy (Ingwall, 1993), but as a percentage of total CK activity CK-B abundance remains very low.

MtCK activity is downregulated in nonfailing pressure-overloaded dogs (Ye et al., 2001b) and rats (Smith et al., 1990). mtCK is a transcriptional target of PGC-1α and ERRα/ERRγ, but mechanisms linking remodeling with mtCK downregulation are poorly understood.

Studies of CK flux in nonfailing hypertrophy are few: it is reduced in nonfailing pressure overload hypertrophy in dogs (Ye et al., 2001b) and human hypertension (Smith et al., 2006). Reversibility of initial k_f downregulation was observed in aortic-constricted pigs upon establishment of nonfailing hypertrophy (Xiong et al., 2015).

PHOSPHOTRANSFER IN HF

Total creatine pool size is consistently reduced in HF regardless of species or etiology. The underlying signaling mechanisms have not been elucidated, but CrT amount and/or activity is reduced (Neubauer et al., 1999b; ten Hove et al., 2005), leading to

progressive falls in creatine levels that predate any fall in [ATP] and parallel falls in [PCr] (Shen et al., 1999). Creatine content correlates with LVEF in human NICM (Nakae et al., 2003) and will limit CK capacity and flux. The fall in creatine may represent a compensatory adaptation that attenuates consequences of increased [ADP] (Tian et al., 1998, 1997b) to maintain ΔG_{ATP}.

Creatine loss also implies reduced PCr reserves, which are consistently reduced in failing hearts: in cardiomyopathic hamsters (Nascimben et al., 1995), postinfarction in rats (Murray et al., 2006; Neubauer et al., 1999b) and pigs (Liu et al., 2001; Murakami et al., 1999a), TAC pigs (Ye et al., 2001a), TAC mice (Lygate et al., 2007) and human NICM (Kalsi et al., 1999; Nascimben et al., 1996; Weiss et al., 2005). Because of the difficulty of obtaining absolute [PCr] values, this is more commonly expressed as PCr/ATP ratio. Correspondingly, PCr/ATP ratios are also generally reduced.

PCr/ATP below the median carries prognostic value in human NICM on prospective followup (Neubauer et al., 1997a). After pressure loading (Ye et al., 2001a) and infarction (Liu et al., 2001), progressive and more transmural reductions in PCr/ATP are seen in surviving pigs developing decompensated HF rather than compensated remodeling. Longitudinal decrements in PCr/ATP are seen in rat HF models (Kato et al., 2010), and improvements are seen in humans post-HF therapy for NICM (Neubauer et al., 1992) and aortic valve replacement (AVR) for severe aortic stenosis (Mahmod et al., 2014). On balance, the evidence suggests that reduced PCr/ATP may predate contractile dysfunction and exacerbates prognosis in HF but is neither a specific marker nor a necessary player in the transition to failure.

Myocardial ATP levels are protected by PCr but eventually fall in late-stage HF by 25-30% because of loss of the TAN pool across the sarcolemma. In pacing-induced HF in dogs, TAN pool and CK activities correlate (R^2 0.52) (Cha et al., 2006). Longitudinal studies in paced dogs have shown that ATP loss is slow and progressive (Shen et al., 1999), but de novo purine synthesis to replenish adenine nucleotides is

slower still. The fall in [ATP] can result in pseudonormalization of PCr/ATP ratios (Bottomley et al., 2013a, 2009), which limits the power to detect differences, disease stage, or mitigating effects of treatment.

Total CK activity is also reduced in NICM models (Liao et al., 1996), aortic constriction-induced HF in rats (De Sousa et al., 1999), mice (Gupta et al., 2011) and pigs (Ye et al., 2001a), human NICM (Nakae et al., 2003), and human HF of mixed etiology (Garnier et al., 2009). In cardiomyopathic hamsters, the fall in CK capacity correlated with reduced contractile reserve and predated contractile dysfunction (Tian et al., 1996). Impaired CK capacity predicts systolic dysfunction in aortic-constricted mice, but systolic dysfunction can occur with normal CK capacity (Lygate et al., 2007).

Downregulation of mtCK protein expression and activity is a consistent feature of HF, e.g., in paced dogs (Shen et al., 2005), SHRs (Ingwall et al., 1990), cardiomyopathic hamsters (Saks et al., 1991), rat (Neubauer et al., 1998) and pig (Hu et al., 2006) infarction, human NICM (Nascimben et al., 1996), and after aortic constriction (Lygate et al., 2007). mtCK efficacy may be assessed by comparing the increase in state 3 respiration in the absence and presence of creatine. It is reduced in late-stage human HF (Stride et al., 2013) and incrementally reduced in line with symptom severity in human NICM (Saks et al., 1991). Downregulation of mtCK and total CK activity is reversible after 4 mo of LVAD support in human HF (Park et al., 2002), with postinfarction HF therapy and exercise training in rats (Hügel et al., 1999; Kemi et al., 2007), and after unpaced recovery in paced dogs (Shen et al., 2005).

The consequences of mtCK downregulation and reduced creatine content include increases in steady-state free ADP and the K_m for ADP- and creatine-stimulated F_0, F_1–ATPase activity. This would exacerbate the effects of all other factors influencing mitochondrial oxphos flux, including the observed falls in ANT capacity in human NICM (Dörner et al., 1997), F_0, F_1–ATPase activity (Moe et al., 2004; Unverferth

et al., 1988), and F_0, F_1–ATPase expression in failing postinfarct pigs (Liu et al., 2001).

CK flux is a more sensitive indicator of abnormal energy homeostasis than PCr/ATP, since it incorporates input from both substrate (PCr) and enzyme (k_f). For example, decreased k_f, but not decreased PCr/ATP, is a specific marker for coexistent HF in human hypertensive hypertrophy (Smith et al., 2006) and pigs with pressure overload (Ye et al., 2001a) and postinfarction (Murakami et al., 1999a) remodeling. Depressed CK flux has prognostic value in human NICM (Bottomley et al., 2013a) and has thus emerged as a candidate marker of transition to failure. Progressive falls in CK flux, initially seen at high workload only (Osbakken et al., 1992), are observed in HF secondary to pressure loading in mice (Gupta et al., 2011), pigs (Ye et al., 2001a), and human hypertension (Smith et al., 2006), infarction in rats (Neubauer et al., 1995) and pigs (Murakami et al., 1999a), SHRs transitioning to failure (Ingwall, 1984), NICM models (Liao et al., 1996), and human NICM (Bottomley et al., 2013a; Weiss et al., 2005), but not post MI in humans (Bottomley et al., 2009).

Reduced CK flux has kinetic and thermodynamic consequences, i.e. blunting the kinetics of ADP- and creatine-stimulated oxphos flux (De Sousa et al., 1999) and ΔG_{ATP}. This slows the kinetics of Ca^{2+} release (Crozatier et al., 2002) and increases diastolic sarcoplasmic reticular Ca^{2+} leak (Kuum et al., 2009). As these effects are magnified at higher workloads, there is blunted contractile reserve and increased ischaemia-intolerance.

There is some capacity for compensatory upregulation of other phosphotransfer networks (Saks et al., 2006) or of direct channeling of ATP/ADP (Vendelin et al., 2010), but their significance is likely to be limited. Direct channelling of ATP/ADP was impaired in failing aortic-constricted rats (Barclay, 2008; Joubert et al., 2008) and SHRs transitioning to failure (Power et al., 2016) because of cytoarchitectural disorganization and increased diffusion distances; upregulation of AK only partially

compensated for reduced CK flux in pacing-induced HF (Dzeja et al., 1999).

MODELS OF MANIPULATED PHOSPHOTRANSFER

CK fluxes in failing hearts, although reduced, remain greater than ATP synthesis rates (Ning et al., 2000), so the question remains whether these are sufficient per se to cause chronic resting systolic dysfunction. This question has been addressed in multiple loss of function models.

Earlier studies using acute pharmacological CK inhibition and partial creatine depletion (Oudman et al., 2013) showed correlations between CK capacity and contractile reserve, thermodynamic efficiency (Tian and Ingwall, 1996; Tian et al., 1997b), diastolic function (Tian et al., 1997a), and tolerance of hypoxia and infarction (Horn et al., 2001). In contrast, muscle-isoform CK (CK-M) knockout (KO) (Saupe et al., 1998), mtCK KO (Spindler et al., 2002), and CK-M/mtCK double knockout (DKO) mice exhibit an unexpectedly normal contractile phenotype, despite a high degree of energetic abnormality revealed at increased workloads. It seems that creatine must be substantially (>80%) depleted to affect resting contractile function (Kapelko et al., 1988) and CK activity substantially suppressed (>74%) (Tian and Ingwall, 1996) before impacting on contractile reserve and ΔG_{ATP}. These represent much greater deficits than occur in the failing heart and demonstrate significant redundancy in CK system capacity.[22]

Notably, creatine depletion started postinfarction does not further impair resting function (Horn et al., 2001). Furthermore, whereas creatine-deficient GAMT KO and CK DKO mice have reduced contractile reserve and intolerance to ischemia-reperfusion (ten Hove et al., 2005), both models have unexpectedly normal baseline function, and postinfarct remodeling and function is not exacerbated (Lygate et al.,

[22] Importantly, this does not mean that smaller falls in CK activity are meaningless, as accompanying deficits across multiple domains (substrate handling, Ca^{2+}-handling, signalling (Mudd and Kass, 2008), fibrosis, LV geometry) could magnify the effects on contractile reserve of relatively modest changes in CK activity.

2013; Nahrendorf et al., 2005). The most recently characterised creatine deficiency model (creatine-naive AGAT KO) displayed normal baseline LVEF but reduced contractility (Faller et al., 2018). Different compensatory mechanisms may apply in each model, and between cardiac and skeletal muscle. DKO myocardium displayed mitochondrial reorganization and evidence of enhanced CK-independent phosphotransfer (Kaasik et al., 2001, 2003), but creatine-deficient GAMT KO myocardium did not (Branovets et al., 2013). Genetic modifiers may also explain variable phenotypes in CK knockout mice, since dysfunction is highly dependent on genetic background, sex, and age (Lygate et al., 2012b).

Nevertheless, gain of function models show therapeutic potential – besides supporting the energy starvation hypothesis. CK-M overexpression increased CK flux (increased k_f and PCr/ATP), systolic function, and survival in aortic-banding- (Gupta et al., 2012) and doxorubicin (Gupta et al., 2013)-induced HF and mitigated ischemia-reperfusion injury (Akki et al., 2012). mtCK overexpression protected against hypoxia-reoxygenation injury in vitro (Zervou et al., 2017) and ischaemia-reperfusion in mice (Whittington et al., 2018), associated with delayed opening of the mitochondrial permeability transition pore. Elevation of myocardial creatine by CrT overexpression protected against ischemia-reperfusion injury in young healthy hearts (Lygate et al., 2012a), aged hearts and hearts with nonfailing pressure overload hypertrophy (Whittington et al., 2016). Cardiac ANT-1 overexpression improved mtCK activity and survival in hypertensive hypertrophy (Walther et al., 2007).

1.4 RESEARCH AIMS

It should be clear that to what extent impaired metabolic reserve may be a necessary or sufficient driver of HF, and to what extent it may be merely a symptom of HF, is a complex question and unresolved for every situation, individual and metabolic pathway. But the metabolic starvation hypothesis of HF, to which the above review

of models of hypertrophy, failure and manipulated metabolism contributes evidence, also implies two further hypotheses. First, the metabolic biomarker hypothesis – that an effective biomarker of impaired metabolic reserve can be identified – and second, the metabolic therapy hypothesis – that metabolic therapies targeted to hearts with impaired metabolic reserve may help prevent HF. To be in a better position to tackle these hypotheses, I designed this thesis to build a picture of what happens to the myocardial CK system (i.e. to ATP delivery rates) when the heart adapts to conditions of increased work. One might then become better placed to comment on the importance of this system to hypertrophic remodelling.

Chapter 3 aims to:

- Validate the noninvasive estimate of unidirectional CK rate constant k_f using the novel ^{31}P TRiST sequence against a tissue-based measurement of maximum CK rate.
- Investigate the main predictors of myocardial CK velocity and the importance of LV mass.

Chapter 4 aims to:

- Relate in the non-failing heart the stage of adaptation to pressure overload (AS) with estimated myocardial ATP delivery rate.
- Investigate whether myocardial ATP delivery rate falls after transition to failure in pressure overload.
- Investigate the effect of AVR on myocardial energetics.
- Establish to what degree do invasively measured CK maximum velocity, creatine and CK isozyme distribution vary between patients with AS with preserved or impaired LVEF.

Chapter 5 aims to investigate:

- ATP delivery rates in severe primary MR with preserved systolic function, and
- Whether late after repair of severe primary MR there is normalisation of PCr/ATP.

Chapter 6 aims to investigate:

- Whether in physiological hypertrophy ATP delivery rates through CK are normal and unrelated to LV mass.
- Whether CK k_f and ATP delivery rate increase in normal and athletically-remodelled hearts subject to acute increases in work driven by catecholamine stress.

Chapter 7 attempts to relate ultrastructure with energetics, and aims to:

- Estimate the distribution of ATP diffusion distances between mitochondrial and sarcomeric compartments using a 3D tomographic model.
- Investigate whether changes in this distribution reflect changes in CK activity such that distances will reduce to compensate for significant falls in CK activity.

2 *Methods and methods development*

2.1 PARTICIPANTS INCLUDED

Participants had to be aged 18–85 and meet group descriptions as described in Table 2.1. Potential participants were identified from surgical waiting lists, clinically obtained echocardiography, and from poster advertisement. Group assignment (sevAS-pEF versus sevAS-rEF) was confirmed after MRI scans. Valve disease was defined according to European recommendations for the assessment of native valve disease (Baumgartner et al., 2009; Lancellotti et al., 2013).

Exclusion criteria were: impaired LV systolic function (excepting the severe AS with reduced LVEF (sevAS-rEF) group), known previous MI, flow-limiting coronary artery disease (CAD), more than mild 'bystander' valve disease, significant renal impairment (estimated glomerular filtration rate (eGFR) <30 $\mathrm{ml\,min^{-1}}$), pregnancy, or any other contraindication to MR scanning.

Recruitment targets were set as per Table 2.1. Overall recruitment target was 135 with an extension to sevAS-pEF for bringing this to 145 to test a ^{1}H-MRS creatine estimation sequence.[1]

[1]The methods and early results for this technique are described in an ISMRM abstract (Ding et al., 2019) and not further discussed.

Table 2.1: Group definitions and recruitment

Abbreviation	Description	Recruited
SevAS-pEF	Severe AS, preserved LV systolic function, clinically indicated AVR	30[a]
SevAS-rEF	Severe AS, impaired LV systolic function, clinically indicated AVR	15
SevMR	Severe primary MR, preserved LV systolic function, clinically indicated MV repair	20
HV	Healthy volunteers	20
ModAS	Moderate AS	14
Athlete	Participant with athletic heart remodelling	20
NH	Participants undergoing heart or aorta surgery with non-hypertrophied hearts, no more than mild pressure or volume-loading heart valve disease, and willing to donate LV biopsy contingent on surgeon agreement[b]	8

[a] Target extended from 25 to 35 to allow a series of participants to undergo ^{1}H-MRS for creatine estimation instead of TRiST.
[b] Mitral stenosis with indication for MV replacement; ascending aortic aneurysm with indication for repair; atrial myxoma with indication for excision. Biopsy was contingent on surgeon agreement.

2.2 MEASUREMENTS

In participants not receiving dobutamine, late gadolinium imaging to exclude MI was undertaken at baseline only. In participants receiving dobutamine, wall-motion abnormalities at stress were excluded before proceeding with spectroscopy.

Groups undergoing surgery were offered the opportunity to donate intra-operative LV biopsies. Initially, I recalled the sevAS-pEF participants one week post-op for baseline measures excepting PCr/ATP ratio and at 6 month for all baseline measures, but after several months I abandoned the one week timepoint as it was proving

Table 2.2: Measurements by group

Measure	Group[a]						
	1	2	3	4	5	6	7
Cardiac volumes and mass by ^{1}H-MRI	·	·	·	·	·	·	·
AV through-plane flow by ^{1}H-MRI	·	·	·	·	·	·	·
PCr/ATP ratio by ^{31}P-MRS	·	·	·	·	·	·	·
CK k_f by ^{31}P-MRS	·	·	·	·	·	·	·
Optional LV biopsy[b]	·	·	·				·
6 min walk test	·	·	·	·	·		·
Baseline measures repeated six months post-op[c]	·		·				
CK k_f during dobutamine stress				·		·	
Cardiopulmonary exercise test (CPET)				·		·	
Echocardiography				·		·	

[a] Groups 1–7: SevAS-pEF, SevAS-rEF, SevMR, HV, ModAS, Athlete, NH respectively, as defined in Table 2.1.
[b] Both patient and surgeon had to agree.
[c] CK k_f was not repeated in sevMR at late follow-up.

infeasible: most patients were either too uncomfortable to consent to repeat NMR or were discharged before time could be confirmed on the magnet. SevMR participants were recalled at 6 months for baseline measures excepting CK k_f.

2.3 ETHICAL CONSIDERATIONS

All work was approved by the South Central – Oxford C Research Ethics Committee (reference 16/SC/0323, IRAS project ID 197866) and Oxford University Hospitals Research & Development Department (R&D Ref 11977) and carried out in accordance with institutional procedures and the principles of the Declaration of Helsinki (World Medical Association, 2013).

All data was recorded in anonymized fashion with the cipher code file stored on a high-compliance server off-site. Written confidential data was kept in locked filing cabinets on-site.

2.4 STATISTICAL ANALYSIS

Data were reported as means with 95% confidence intervals or standard deviation (SD) for continuous variables passing the Shapiro-Wilk test of normality and medians with interquartile range (IQR) if not passing normality testing.

Boxplots indicate median, IQR, and whiskers, with individual datapoints superimposed to the right-hand side (see Figure 4.1, p. 133 for explanation of whiskers). Asterisks in figures denote statistical significance, with one denoting $p < 0.05$, two denoting $p < 0.01$, and three denoting $p < 0.001$.

Continuous variables meeting normality testing were compared with Student-t test with Welch's correction (two groups) or one-way ANOVA (more than two groups) if the Levene test of between-group homogeneity of variance was passed. Welch's correction was used for unequal sample sizes or if the assumption of homogeneity of variance was violated. If normality assumptions were not met, nonparametric tests (Wilcox rank-sum for differences between two independent groups, Kruskal-Wallis for differences between more than two groups, and Jonckheere-Terpstra for ordering of medians across more than two groups) were used. P-values were adjusted on post hoc pairwise t-tests or Wilcoxon rank sum tests with the Benjamini & Hochberg method to control the false discovery rate.[2] Categorical variables were compared by chi-square or (if expected cell counts were under five) by Fisher exact test. Analyses were performed using IBM SPSS version 24 and R (R Core Team, 2018).

[2] In tables where space was limited, ae–n was used as shorthand for $a \times 10^{-n}$.

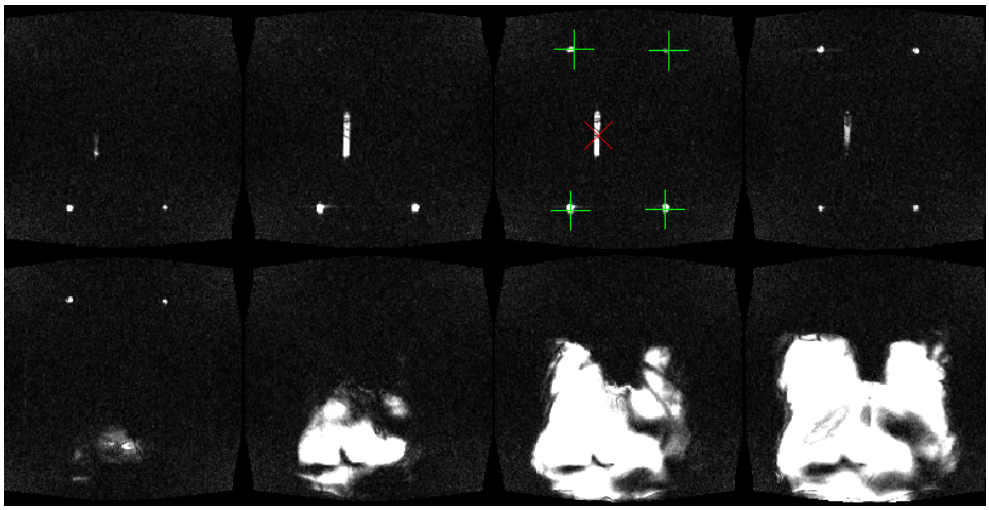
2.5 ^{31}P-MRS

Spectra were obtained on a multinuclear 3T MRI scanner (Trio; Siemens Healthcare, Erlangen, Germany). A dedicated three-element 'heart-liver' radiofrequency (RF) coil (Siemens) was used for PCr/ATP estimation. One element (28 × 26 cm) is dual-tuned to ^{1}H (127.7 MHz) and ^{31}P (49.8 MHz) and acts as a surface ^{1}H transmit-receive and ^{31}P transmit coil. ^{31}P signal is received by loop (12 × 15 cm) and butterfly (23 × 12 cm) elements. Saturation transfer experiments were performed using a local ^{31}P transmit-receive circular RF coil (10 cm diameter, PulseTeq Ltd, Chobham, UK).

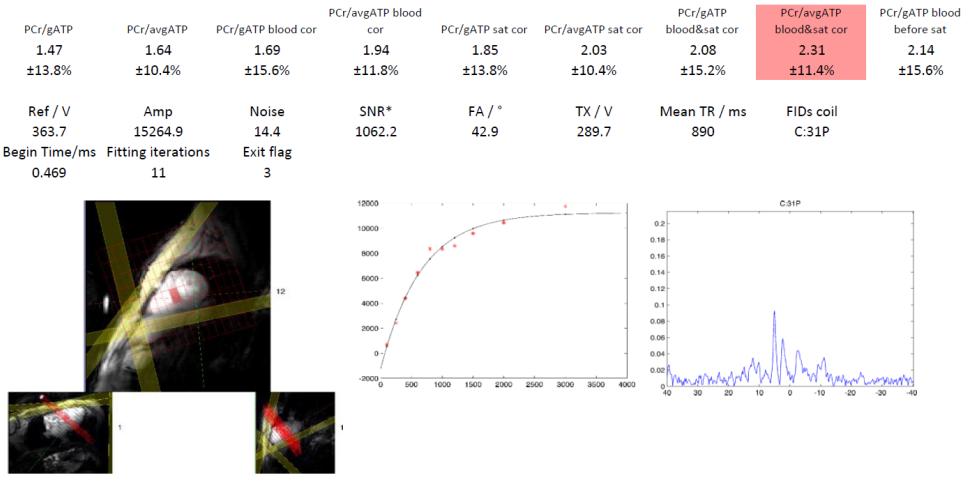
Estimation of PCr/ATP

After the participant is positioned prone over the coil centre and moved to the isocentre of the MR system, free induction decay (FID) inversion recovery curves (ten 1000 µs hard inversion pulses, inversion delay 100–3000 ms) and locations of phenylphosphonic acid (PPA) fiducial and cod liver oil phantoms are aquired (Figure 2.1a) together with a 3D stack of short axis localizers. Next, three saturation bands are positioned over liver and skeletal muscle (Figure 2.1b) while the middle of the acquisition matrix is placed over the basal-mid interventricular septum (Figures 2.2a–2.2d). Our non-gated 3D acquisition-weighted ultra-short echo time (TE) chemical shift imaging (CSI) sequence takes about 11 min. The centre frequency is set 250 Hz left of (lower than the resonant frequency of) PCr (Figure 2.3a), i.e. between γ- and α-ATP, so that the excitation bandwith covers from β-ATP on one side to phospho-monoesters on the other. Sequence parameters included: acquisition matrix size 16 × 16 × 8, field of view 240 × 240 × 200 mm^3, nominal voxel size 5.6 ml, 10 averages at the centre of k-space, repetition time (TR) = fixed with some inter-participant variability (910–1010 ms) dependent on specific absorption rate (SAR).

Selecting the three most basal septal voxels in turn, in-house code running on MATLAB R2015b (MATLAB compiler runtime version 8.3, copyright Chris Rodgers

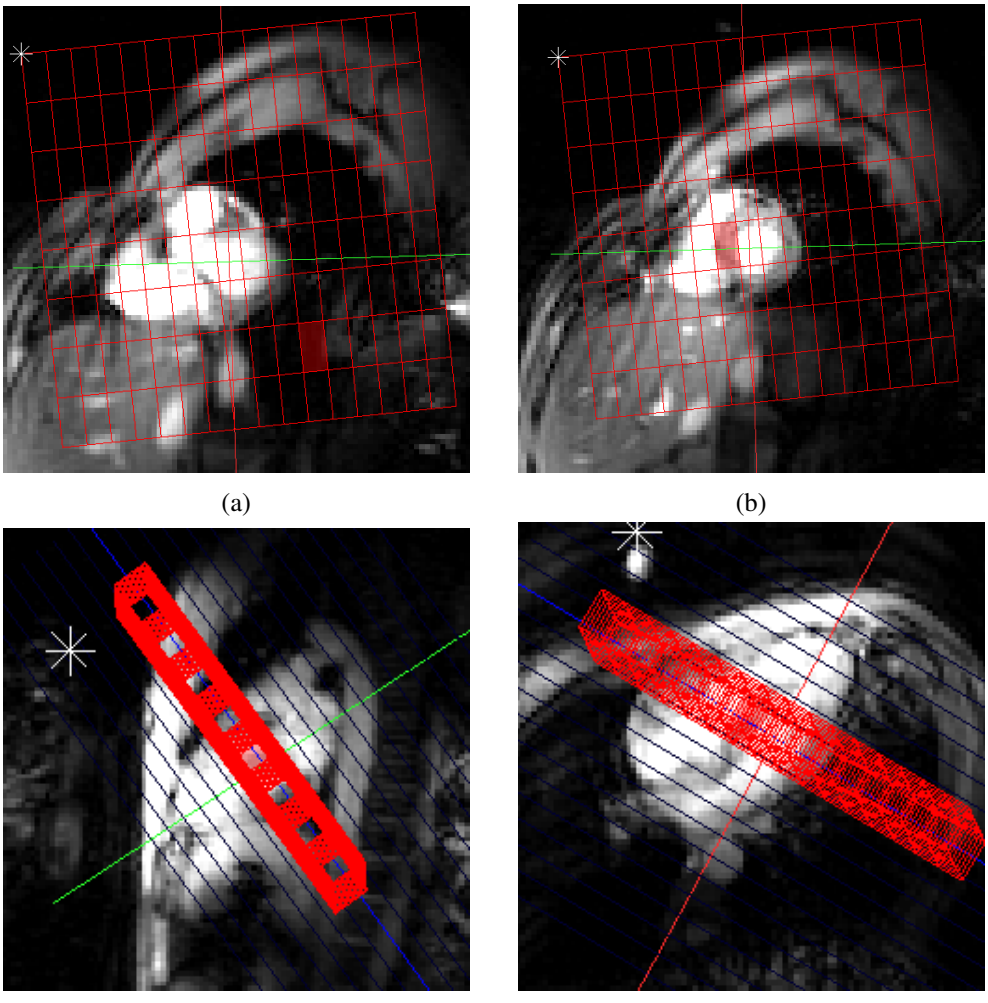


(a)



(b)

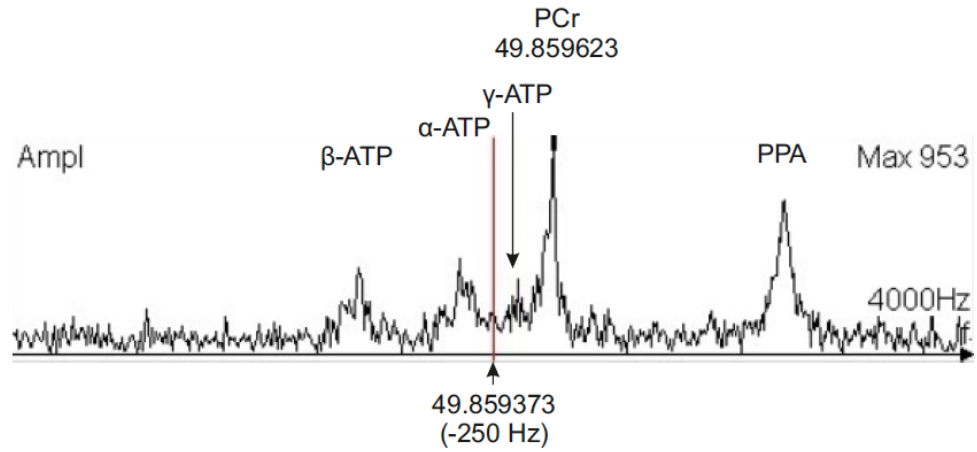
Figure 2.1: (a) Selection of cods (green crosses) and one fiducial (red cross); (b) saturation band placement (yellow), FID inversion recovery curve, and PCr/ATP ratio correction.



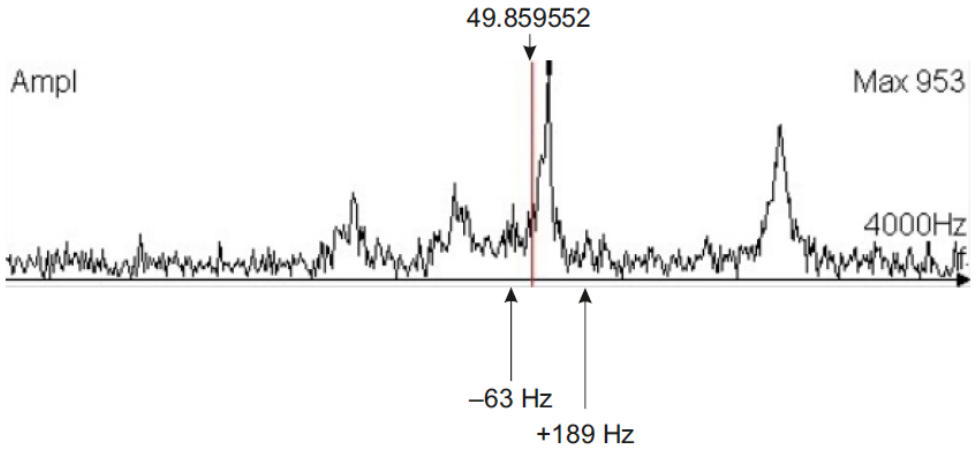
(a) (b)

(c) (d)

Figure 2.2: The most basal sepal voxel (b-d) is a half voxel-shift below the left ventricular outflow tract (a).



(a)



(b)

Figure 2.3: (a) The centre frequency for the PCr/ATP sequence is set at 49.859373 MHz (vertical line), 250 Hz negative of PCr, which resonates here at 49.859623 MHz. (b) The centre frequency for TRiST is found for the voxel of interest and set (in this case) at 49.859552 Mhz (vertical line). Typical offsets for selective γ-ATP (–63 Hz) and control (+189 Hz) saturation are shown.

2014, now available online (Purvis et al., 2017)) was used to fit the raw time-domain signal with the AMARES algorithm, taking into account prior knowledge (expected frequency shifts, j-coupling constants for ATP, metabolite-specific T_1 values) and experimental acquisition parameters (central frequency, bandwith, TR, and calculated flip-angles achieved across the field of view i.e. the B_1 field distribution of the transmit coil). Analysis also required correction for partial saturation (exciting nuclei while not waiting for full relaxation), blood contamination (reducing the ATP peak areas by a proportion of the 2,3-diphosphoglycerate peak area), nuclear Overhauser enhancement and spectral overlap of the α-ATP peak by NADH.

The resulting PCr/ATP ratio presented here is the blood- and saturation-corrected PCr/average ATP ratio, averaged over the two most basal septal voxels (each separated by a half-voxel shift) (Figure 2.2b). Measures of data quality include the signal-noise ratio (SNR) of the PCr peak and the coefficient of variation in the measured PCr/ATP ratio (Tyler et al., 2008). Apart from selection of voxels on anatomic criteria and visual confirmation of correct peak fitting, analysis is fully automated.

Estimation of CK rate constant

From the perspective of a two site steady state magnetisation transfer experiment,[3] the CK equilibrium expression may be reduced to a two site exchange:

$$\mathrm{MgADP^- + PCr^{2-} + H^+ \underset{k_{-1}}{\overset{k_1}{\rightleftharpoons}} MgATP^{2-} + Cr}$$

$$\mathrm{PCr \underset{k_r}{\overset{k_f}{\rightleftharpoons}} \gamma\text{-ATP},}$$

where k_f and k_r are the unidirectional pseudo-first-order rate constants in the forward (ATP-producing) and reverse (PCr-producing) directions.[4] Saturating the γ-ATP resonance and observing the fall in the height of the exchange partner (PCr) resonance

[3] The general case is discussed in Section A.2 (p. 231).

[4] The older biochemical literature refers to forward as the PCr-producing direction. In this thesis I refer to it only as the ATP-producing direction.

to a new equilibrium allows the calculation of k_f as

$$k_f = \frac{1}{T'_{1,PCr}} \cdot \left(1 - \frac{M'_{0,PCr}}{M_{0,PCr}}\right),$$

where $M'_{0,PCr}$ is the (fully relaxed, equilibrated) magnetisation of PCr during γ-ATP saturation, $M_{0,PCr}$ is the magnetisation of PCr without γ-ATP saturation, and $T'_{1,PCr}$ is the apparent T_1 of PCr during γ-ATP saturation.

The CK equilibrium is an example of 'slow' exchange as the exchange rate constant $k \approx 0.2$ s^{-1}, while the metabolites are separated by about 2.47 parts per million (ppm)[5] (123 Hz at 3T). In vivo estimates of (total, not net) CK forward flux are calculated as $k_f \times$ [PCr] and do not discriminate between subcellular compartments. At steady-state, forward and reverse fluxes are equal, i.e. $k_f \times$ [PCr] $= k_r \times$ [ATP].

Four saturation transfer techniques for measuring k_f in the human heart have been developed: four-angle saturation transfer (FAST) (Bottomley et al., 2002) at 1.5T, triple repetition time saturation transfer (TRiST) (Clarke, 2016; Clarke et al., 2019; Schär et al., 2010) and two repetition time saturation transfer (TwiST) (Schar et al., 2015) at 3T, and Bloch-Siegert four-angle saturation transfer (Clarke et al., 2017) at 7T. In this thesis, k_f was estimated using an implementation of TRiST, adapted from the original protocol by William Clarke to suit the 10 cm loop coil and 3T Trio system available in the Oxford Centre for Clinical Magnetic Resonance Research (OCMR), and extended to find k_f during dobutamine stress (Clarke, 2016). Unlike FAST, which uses 15° and 60° excitation angles for PCr and repeats each excitation at each angle with and without selective γ-ATP saturation, TRiST aims to achieve 90° excitation for PCr and repeats this for two different TRs, with only the long TR step repeated with and without selective γ-ATP saturation. TRiST is further described below.

Using TRiST, resting k_f requires about 60 min and four acquisition steps; k_f during 'stressed' saturation transfer (StreST) requires a further two steps over 18 min

[5] Parts per million is a magnetic field-strength-independent unit of chemical shift.

once target heart rate is achieved with dobutamine (5–10 min) (Clarke et al., 2019). After transaxial and sagittal ^{1}H localisers to confirm coil position over the LV and at magnet isocentre, acquiring FID inversion recovery curves, PPA cod locations and a transaxial slice at the level of the coil centre, the 1D-CSI matrix (200 × 200 × 160 mm) is oriented with voxels parallel to the chest wall, aiming to place two voxels outside the body and the voxel of interest (VOI) over the most apical unambiguously cardiac voxel.

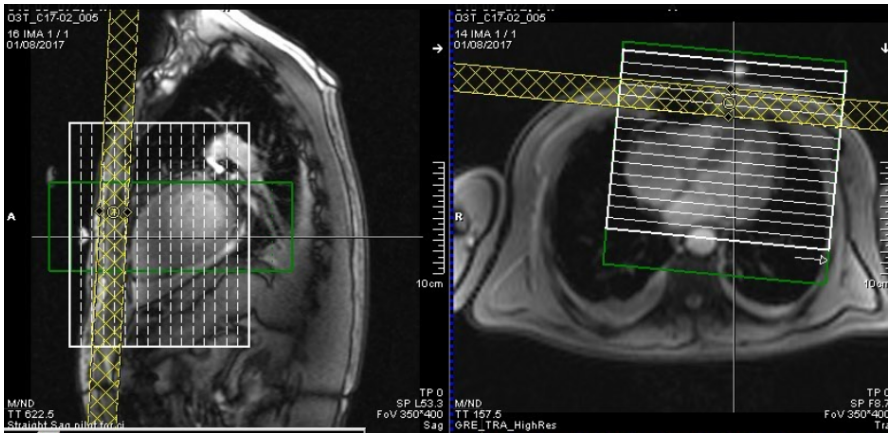
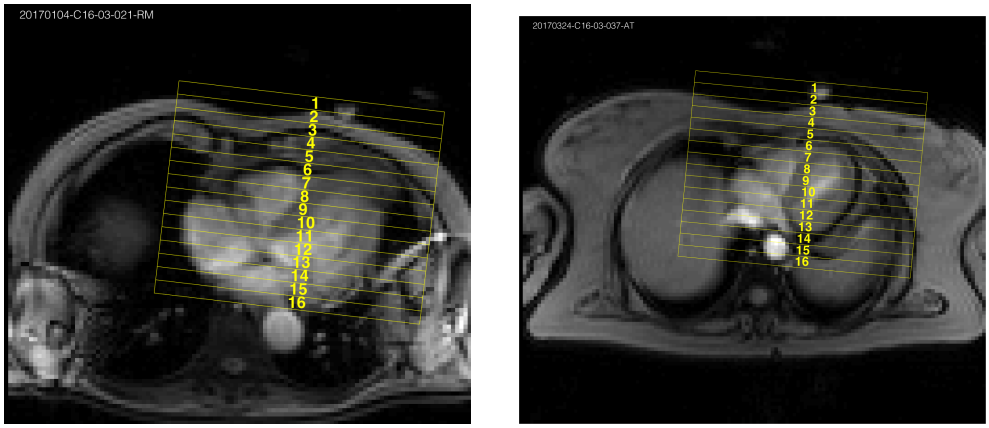


Figure 2.4: Placement of the 1D 16-step adjust volume for TRiST. The saturation band is used only if the frequency-finding sequence (TR 330 ms) is run.

A five min frequency-finding sequence (1D-CSI, 16 phase encode steps for depth selectivity, TR 330 ms, TE 2.3 ms, flip-angle 35°, 125 averages, centre frequency 250 Hz negative to PCr) is run with a 25 mm saturation band placed over skeletal muscle (Figure 2.4) and the adjust volume (200 × 200 × 80 mm) oriented as shown (Figures 2.5a, 2.5b). This is analysed off-line (Figures 2.6–2.7) to generate expected centre frequencies and frequency offsets for each of the 16 voxels. Those from the VOI are programmed for the next four–six steps. The centre frequency for TRiST should lie midway between γ-ATP and PCr (Figure 2.3b and Figure 2.7, grey line), the negative offset (Figure 2.7, blue line) should target γ-ATP, and the positive offset (Figure 2.7, light green line) should target a control region mirroring the negative offset around



(a) (b)

Figure 2.5: The 1D 16-step adjust volume was oriented to position the most apical unambiguously cardiac voxel (# 7) in line with the surface coil for (a–b) two participants.

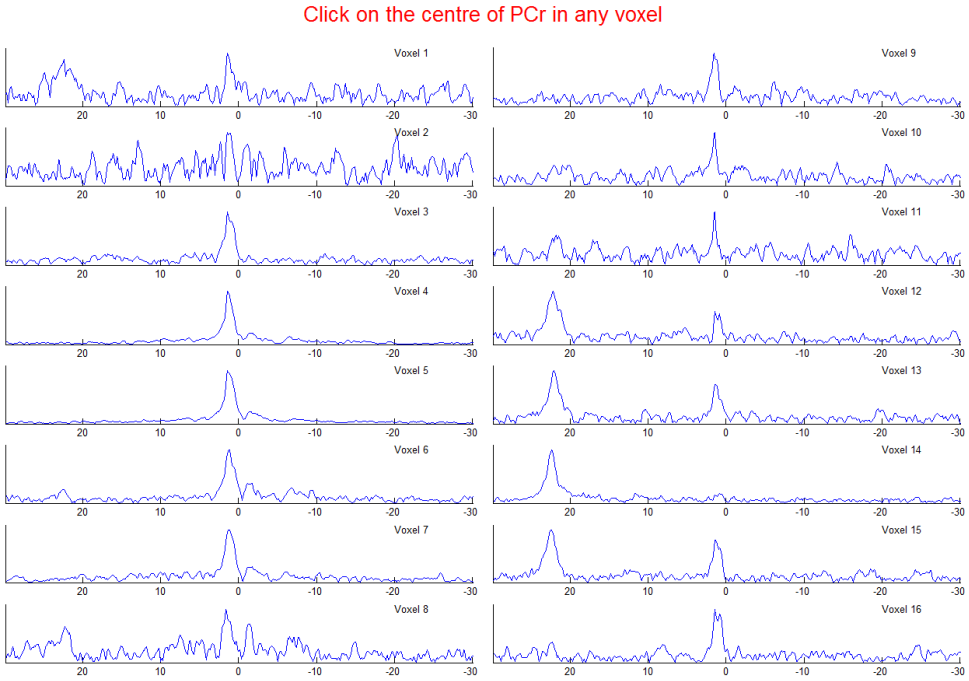


Figure 2.6: Off-line analysis tool to calculate centre frequencies and expected offsets. As the input data was a full resting TRiST spectrum, PCr and γ-ATP appear in the +2 and –2 ppm range respectively; the fiducial appears around 20 ppm positive to PCr.

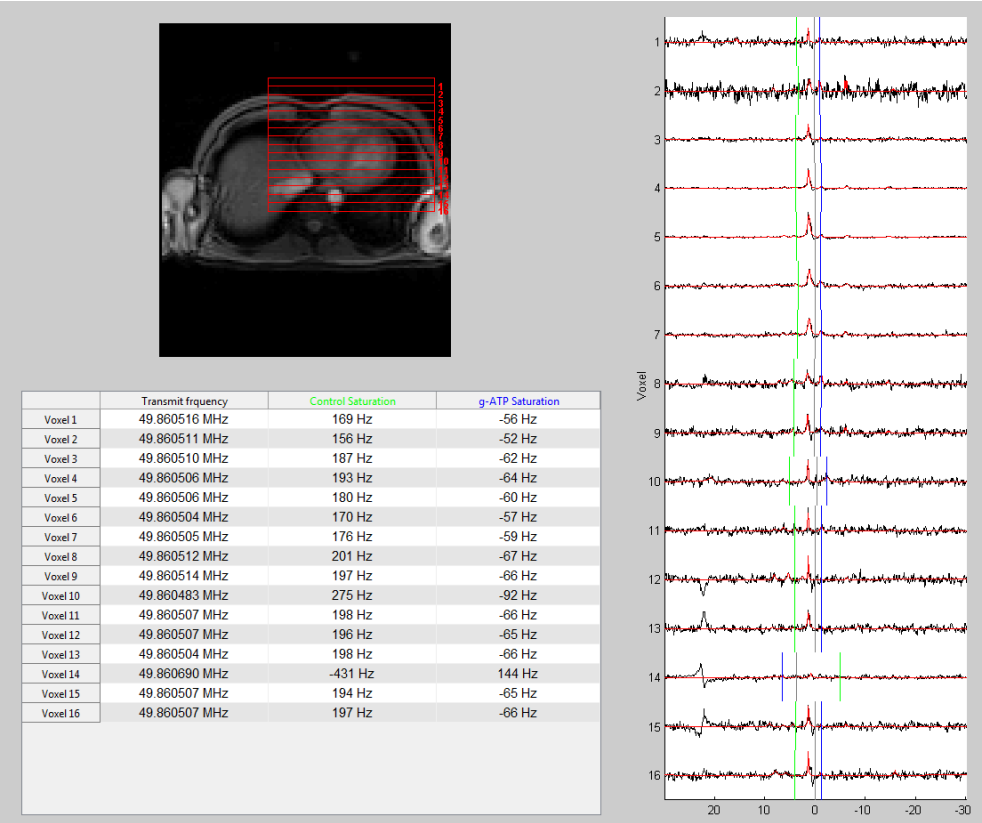


Figure 2.7: Generation of centre frequencies and expected offsets for each of 16 voxels. That for voxel 7 is used.

PCr (Table 2.3). I have found this depth-selective frequency-finding step to be more reliable than taking the centre frequency as 70 Hz left of PCr on the non-localised spectrum (Figure 2.3b), as the chemical shift of the PCr peak often becomes about 30 Hz more negative as one moves from skeletal to cardiac muscle depths, and the non-localised spectrum is biased toward the skeletal signal. Examples of resting and resting-then-stress TRiST scans are shown (Figures 2.8, 2.9, 2.10 – see Figure 2.9 Panel A for identification of peaks and Panels B–D for centre frequencies of Dante pulses).[6]

[6] If the five min frequency-finding sequence generates insufficient signal to be confident of the PCr peak location at the depth desired, the non-localised spectrum is used to run Step 1 of TRiST and the spectra resulting from Step 1 can be analysed off-line in a similar fashion to programme the following steps.

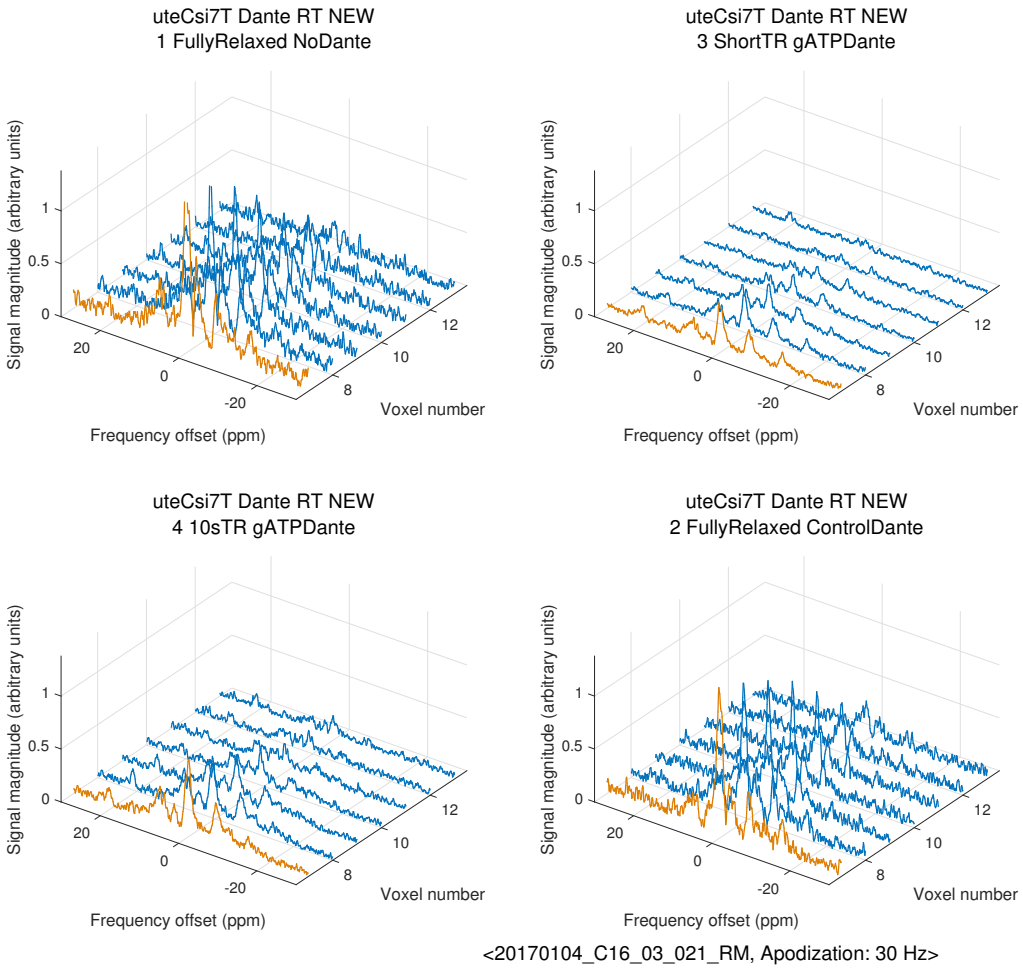


Figure 2.8: 3D summary of spectra #1–4 from Table 2.3 for cardiac-depth voxels (participant _021) demonstrates signal fall-off with depth.

Resting TRiST comprises four acquisitions localised with 1D-CSI, with uniform k-space sampling and 16 phase-encode steps. Steps 2–3 allow calculation of $T'_{1,PCr}$ using the two-TR partial saturation method (El-Sharkawy et al., 2009). This requires a lookup table for the ratio $M'_{9.5s,PCr} : M'_{1.5s,PCr}$. M^{Ctrl}_{PCr} is substituted for $M_{0,PCr}$ and $M'_{0,PCr}$ is calculated as

$$M'_{0,PCr} = \frac{M'_{1.5s,PCr}}{1 - e^{-1.5s/T'_1}}.$$

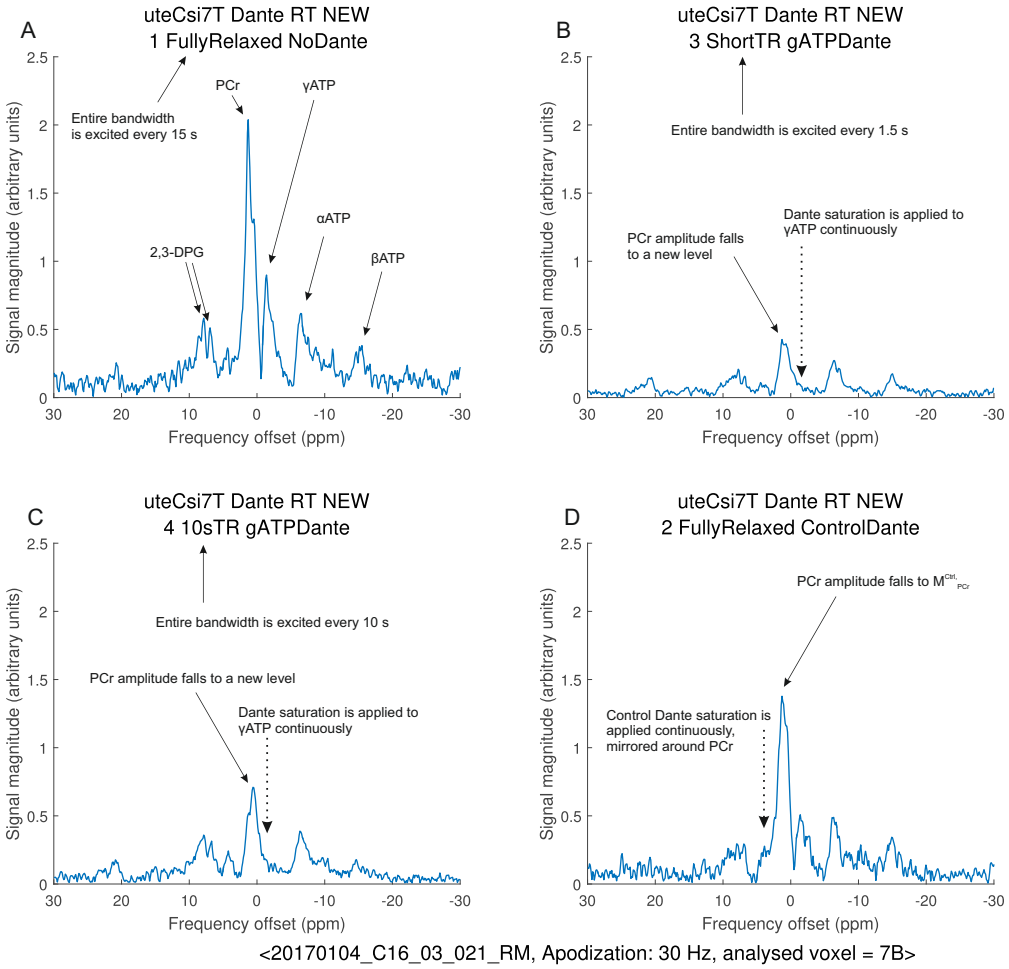


Figure 2.9: (A–D) 2D summary of spectra #1–4 from Table 2.3 for the VOI (voxel 7, participant _021). Labelled peaks in (A) are 2,3-DPG, PCr, and γ-, α- and β-ATP. Inorganic phosphate (P_i) is hidden by 2,3-DPG.

Thus k_f is calculated as

$$k_f = \frac{1}{T'_{1,PCr}} \cdot \left(1 - \frac{M'_{0,PCr}}{M^{Ctrl}_{0,PCr}}\right).$$

TRiST achieves 90° excitation for PCr and γ-ATP using frequency-cycled adiabatic half-passage (AHP) pulses. Adiabatic pulses are a family of pulses able to achieve 90° excitation irrespective of the fall in B_1 transmit strength with increasing distance from the coil, provided the adiabatic threshold is reached.[7] In practice, I

[7] For the 10 cm coil, the threshold is reached across the required 200 Hz bandwidth when γB_1^+

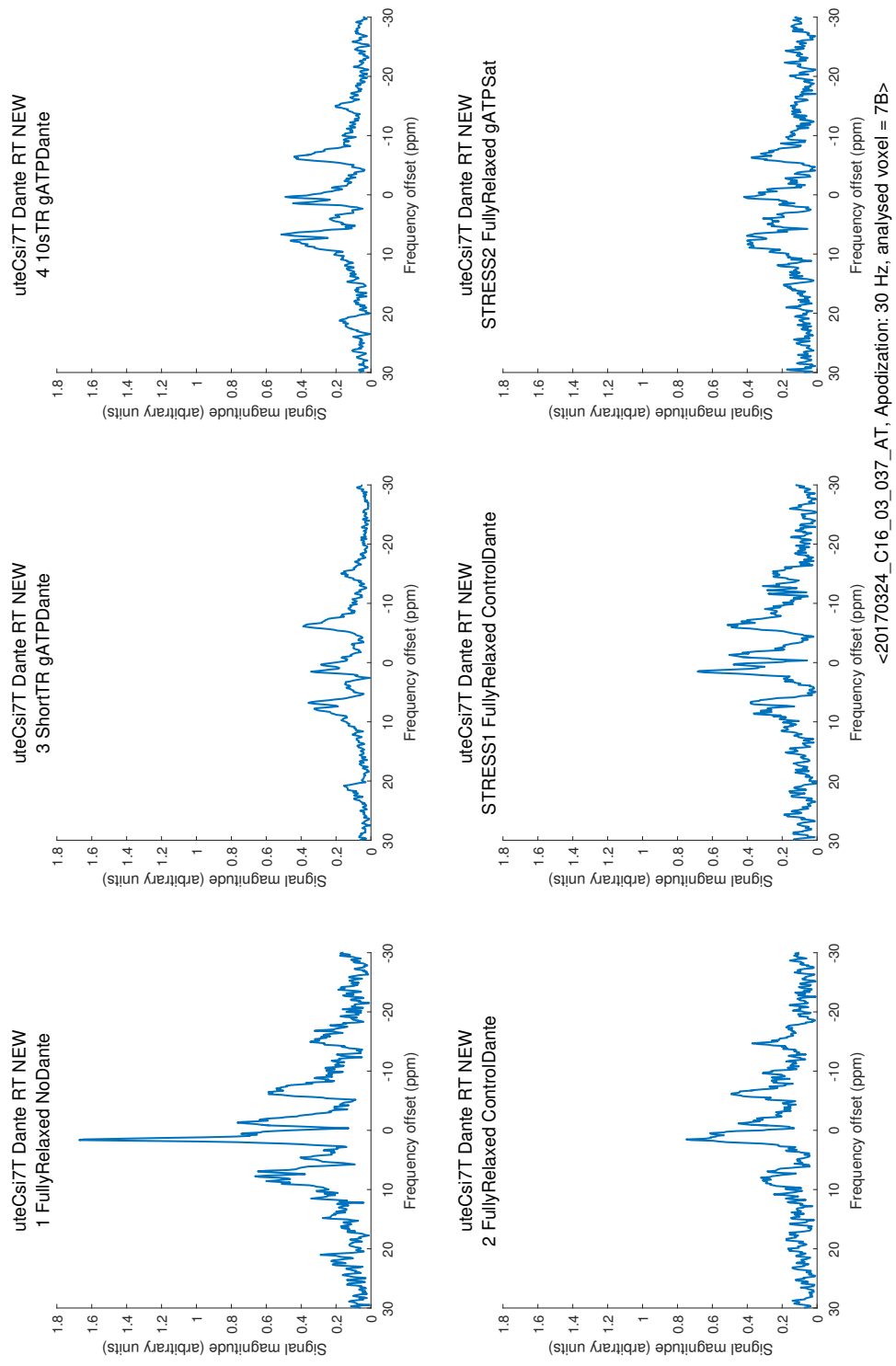


Figure 2.10: 2D summary of spectra #1–6 from Table 2.3 for the VOI (voxel 7, participant _037).

Table 2.3: TRiST acquisition parameters at rest (Steps 1–4) and stress (Steps 5–6)[a]

Condition	Step	TR (s)	Selective saturation	No. averages	Duration (min)	Measured parameters
Rest	1	15	Nil	2	9	$M_{0,PCr}$, $M_{0,\gamma ATP}$
Rest	2	1.5	γATP	18	11	$M'_{1.5s,PCr}$
Rest	3	9.5	γATP	8	21	$M'_{9.5s,PCr}$
Rest	4	15	Control	2	9	M^{Ctrl}_{PCr}, $M^{Ctrl}_{\gamma ATP}$
Dobutamine	5	15	Control	2	9	M^{Ctrl}_{PCr}, $M^{Ctrl}_{\gamma ATP}$
Dobutamine	6	15	γATP	2	9	$M'_{15s,PCr}$

[a] TR_{short} is 1.5 s and TR_{long} 9.5 s.

programmed the maximum allowed transmit voltage (220V) for the AHP pulses and reduced the coil-VOI distance by analysing (only) the most apical unambiguously cardiac voxel.

In TRiST steps where selective saturation is applied to γ-ATP, the exchange partner of PCr, selective, full and steady-state saturation of the intended peak with minimal off-target resonance ('spillover') saturation is desired before each 90° excitation, to avoid underestimating k_f. Selective saturation is achieved with an amplitude modulated Delays Alternating with Nutation for Tailored Excitation (DANTE) pulse train (pulse duration 100 µs, inter-pulse delay 250 µs). The control saturation step in part accounts for the confounding effect of spillover saturation. Incomplete saturation of γ-ATP (when DANTE is used with $\gamma B_1^+ < 50$ Hz) can introduce underestimation of k_f. In practice, I programmed the maximum possible transmit voltage (33–48V) for the DANTE train that SAR restrictions allowed and minimised the coil-VOI distance.

Several limitations remain, mainly reflecting difficulties inherent with human

> 250 Hz (Clarke, 2016). For each phase-encoding step, AHP pulses (transmit 220V, duration 10 ms, bandwidth 6 kHz) with alternating frequency sweep directions are used to reduce off-resonance asymmetry when averaged upon reconstruction.

cardiac ^{31}P-MRS experiments (long T_1s, short T_2s, low concentrations, and low SNR of the metabolites of interest). These include the participant breathing during the scan (superior-inferior translation of the heart causing dynamic B_0 inhomogeneity, see Fig. 3 in Clarke et al. (2019)), static B_0 inhomogeneity at the VOI, and the coil's sensitivity to two CK system compartments (skeletal and cardiac muscle). A further general limitation of steady-state saturation transfer experiments is that the slower the exchange rate relative to the relaxation rate, the smaller the relative change in magnetisation that must be detected and the higher the SNR required. To adjust for supine scanning with this coil and to improve comparability with prior (prone, FAST-sequence) measurements of k_f, k_f values were multiplied by 1.333 and presented as "k_f adj" (Clarke et al., 2019) (recommended by Prof. Paul Bottomley).

2.6 ^{1}H-MRI

Cardiac volumes and mass

Scans were performed supine in end-expiration on a 3T system (Siemens). A 24 channel spine matrix and 6 channel body matrix were used. Typical steady-state free precession (SSFP) sequence parameters were slice thickness 8 mm, gap 2 mm, retrospective gating, TE 1.5 ms, TR 46 ms, flip-angle 50°, field-of-view (FOV) 400 mm, matrix size 256 in frequency encode direction. LV endocardial and epicardial contours in end-diastole and end-systole were contoured using cvi42 version 5.3.4 (Circle Cardiovascular Imaging Inc, Calgary, Alberta, Canada).

In participants with primary mitral regurgitation, mitral regurgitant volume was estimated by subtracting forward stroke volume, measured by breath-hold and free-breathing through-plane phase contrast sequences at the aortic sinus level (aliaising velocity 200–250 cm/s), from mitral inflow stroke volume, measured by subtracting LVESV from LVEDV using the SSFP short-axis stack. Phase contrast and SSFP

sequences were gated prospectively when the participant was in atrial fibrillation; otherwise retrospective gating was used.

LV mass was calculated from the difference between epicardial and endocardial volumes multiplied by myocardial density (1.05 $\mathrm{g\,cm^{-3}}$). LV mass index was normalised to body surface area (BSA) using the Mosteller formula: BSA = (height $\times$ weight / 3600)$^{0.5}$.

Aortic valve cine and through-plane flow

Planning a plane perpendicular to both the left ventricular outflow tract (LVOT) long-axis LV cine and the coronal LVOT cine, aortic valve (AV) anatomy and AV area in mid-systole were captured at the AV leaflet tips using a breath-hold radial readout sequence (slice thickness 5 mm, TR 45 ms) (Figure 2.11). Through-plane flow sequences (both breath-hold and free-breathing) were planned just distal to the AV leaflet tips. Typical parameters for breath-hold sequences were TE 2.3 ms TR 50 ms, flip angle 30, slice thickness 5.5 mm, FOV 450 mm in frequency encode direction, and aliasing velocity set (in severe aortic stenosis) at 450 $\mathrm{cm\,s^{-1}}$ and increased in increments until no aliasing was seen, or (in cases without aortic stenosis) at 200 $\mathrm{cm\,s^{-1}}$.

Late gadolinium enhancement

A standard dose (0.1 $\mathrm{mmol\,kg^{-1}}$) of 0.5 $\mathrm{mmol\,ml^{-1}}$ gadoterate meglumine (Dotarem, Guerbet Laboratories, France) was given by slow intravenous injection, followed by a 10 ml saline flush. After a three min delay, electrocardiogram (ECG)-gated images were acquired in long- and short-axis planes using a free-breathing single-shot inversion-recovery sequence. Further breath-hold images were taken where the participant was able and willing to tolerate further scan time.



Figure 2.11: The plane planned through the AV leaflet tips (middle of the three green lines in A–B) is used for capture of the AV cine (C). The through-plane flow (D) is planned just distal to the plane of (C).

2.7 MEASUREMENTS OF CREATINE CONTENT AND CK ACTIVITY

I am grateful to Hannah Lake and Craig Lygate for their help with the following analyses (high-performance liquid chromatography (HPLC), CK isoenzymes, CK activity).

From biopsy to homogenate

10–20 min after going on cardiopulmonary bypass, surgical myocardial biopsies were obtained from left ventricular endocardium and immediately divided into two parts. The larger part was frozen in liquid nitrogen within twenty seconds of excision and the smaller, a thin sample (roughly 0.5 $\times$ 1 mm), was bathed in primary fixative and further divided into parts three times smaller for electron microscopy (see below).

The larger part was stored at –80°C until batch analyses on ice. Samples were crushed into powder using a metal pulveriser precooled with dry ice. A heaped spatula-full of frozen, crushed powdered LV (5–10 mg) was reconstituted in a droplet of ice-cold homogenizing buffer,[8] excess liquid chased off and the weight of tissue recorded. The sample was placed in a glass homogenising vessel with additional ice-cold homogenisation buffer, with the buffer volume adjusted to achieve a tissue concentration in buffer of 5 $\mathrm{mg\,ml^{-1}}$. The sample was then homogenised using a stirrer at 1300 rpm for 30 sec.

A 200 µl aliquot of the homogenate was mixed with 200 µl of 4% NaOH to create a solution for the Lowry assay. This solution was heated in a water bath at 60°C for two hours then stored at 4°C until analysis. The remainder was settled for 30 min at 4°C with 0.1% Triton-X 100 to permeablize membranes. The resulting supernatant was used for subsequent measurements.

Analysis of CK activity

Supernatant from Section 2.7 was diluted 1:5 in ice-cold homogenization buffer and kept on ice. CK-N-acetyl cysteine (NAC) reagent[9] (catalogue code TR14010, Thermo Fisher Scientific) was warmed to 30°C in a water bath. At the point of measurement, 20 µl of diluted supernatant was placed in a cuvette and 1 ml CK-NAC was added. The rate of increase of absorbance of NADPH at 340 nm and 37°C, which is proportional to CK activity, was then monitored over ten min using a spectrophotometer. CK velocity (IU/ml) was calculated from the rate of change in absorbance of NADPH, corrected for reaction volume and an assay-specific correction factor, averaged over three runs and normalised to Lowry protein (mg/ml). Results were presented as CK

[8] Ingredients: K_2HPO_4 0.08 M, KH_2PO_4 0.02 M, β-mercaptoethanol 1 mM, EGTA 1 mM, pH 7.4.

[9] Active ingredients: 100 $\mathrm{mmol\,l^{-1}}$ bis/tris buffer, PCr 31.5 $\mathrm{mmol\,l^{-1}}$, AMP 5.3 $\mathrm{mmol\,l^{-1}}$, NADP 2.2 $\mathrm{mmol\,l^{-1}}$, EDTA 2.1 $\mathrm{mmol\,l^{-1}}$, P_1P_5-Di(adenosine-5'-)pentaphosphate 10.3 $\mathrm{\mu mol\,l^{-1}}$, Mg^{2+} 10.5 $\mathrm{mmol\,l^{-1}}$, ADP 2.7 $\mathrm{mmol\,l^{-1}}$, D-glucose 21 $\mathrm{mmol\,l^{-1}}$, NAC 21 $\mathrm{mmol\,l^{-1}}$, hexokinase >3000 $\mathrm{IU\,l^{-1}}$, glucose-6-phosphate dehydrogenase (G6PD) >2000 $\mathrm{IU\,l^{-1}}$.

velocity (IU/mg protein). This method, first developed in 1955 (Oliver, 1955; Rosalki, 1967; Szasz et al., 1976, 1979), relies on the following series of reactions:

- $\text{Inactivated CK} \xrightarrow{\text{NAC}} \text{Reactivated CK}$
- $\text{PCr} + \text{MgADP} \xrightarrow{\text{Reactivated CK}} \text{creatine} + \text{ATP}$
- $\text{ATP} + \text{glucose} \xrightarrow{\text{hexokinase}} \text{ADP} + \text{glucose-6-phosphate}$
- $\text{G-6-P} + \text{NADP}^+ \xrightarrow{\text{G6PD}} \text{6-phosphogluconate} + \text{NADPH} + \text{H}^+$
- $2\,\text{ADP} \xrightarrow[\text{inhibited by AP5A and AMP}]{\text{AK}} \text{AMP} + \text{ATP}.$

Ex vivo CK becomes inactivated by oxidation of sulfhydryl groups at its active site. NAC reduces these oxidized groups and reactivates the sample CK. Reactivated CK generates ATP from the substrates provided, which is then used by hexokinase to transphosphorylate glucose to glucose-6-phosphate (G6P). G6P is used by G6PD to reduce NADP^+ to $\text{NADPH} + \text{H}^+$. The rate of this reaction is monitored by the rate of change in absorbance at 340 nm. Diadenosine pentaphosphate (AP5A) and AMP are included to prevent any AK activity generating ATP and confounding the observation of CK activity.

Analysis of CK isoenzymes

5 µl of supernatant from Section 2.7 was diluted 1:20 with ice-cold homogenization buffer and incubated with SPIFE CK vis activator[10] (SAS-1+ kit, cat. no. 3332, 3333, Helena Biosciences) at room temperature for 10 min. The mixed CK isoenzyme reagent underwent agarose gel electrophoresis using SAS-1+ kits to separate CK isoenzymes based on electrophoretic mobility. The separated isoenzyme bands were

[10] 114 mM β-mercaptoethanol in tris base.

visualised (Figure 2.12) by adding isoenzyme reagent[11] and isoenzyme chromogen[12] to the gel after 30 min. The gel was then incubated (60°C, 20 min), destained (0.3% acetic acid, 10 min), washed, dried (60°C, 30 min) and scanned (ChemiDoc MP Imager, Bio-Rad). The relative concentration of bands was quantified by densitometry.

The method relies on the following reactions:

- $\mathrm{PCr} + \mathrm{ADP} \xrightarrow{\mathrm{CK}} \mathrm{creatine} + \mathrm{ATP}$
- $\mathrm{ATP} + \mathrm{glucose} \xrightarrow{\mathrm{hexokinase}} \mathrm{glucose\text{-}6\text{-}phosphate} + \mathrm{ADP}$
- $\mathrm{G\text{-}6\text{-}P} + \mathrm{NAD} \xrightarrow{\mathrm{G6PD}} \mathrm{6\text{-}phosphogluconate} + \mathrm{NADH} + \mathrm{H^+}$
- $\mathrm{NADH} + \mathrm{H^+} + \mathrm{TNBT} \xrightarrow{\mathrm{PMS}} \mathrm{NAD} + \mathrm{formazan}\cdot$

Ex vivo CK generates ATP from PCr and ADP supplied in the CK isoenzyme reagent. This is used to generate G6P, which is used to reduce NAD to NADH + H^+. The latter then reduces TNBT to formazan in the presence of PMS. Formazan produces a dark band which is quantified by densitometry.

Citrate synthase assay

Citrate synthase (CS) catalyses the entry of carbon into the tricarboxylic acid cycle. Its activity correlates with mitochondrial content (Larsen et al., 2012; Park et al., 2014). 50 µl of supernatant from Section 2.7 was incubated with 850 µl of reagent[13] for 3 min at room temperature. 100 µl of 10 mM oxaloacetate was added and absorbance at 412 nm monitored over 1 min. The method relies on the following reactions:

- $\mathrm{acetyl-CoA} + \mathrm{oxaloacetate} \xleftrightarrow{\mathrm{CS}} \mathrm{CoA\text{-}SH} + \mathrm{citrate}$

[11] Ingredients: ADP 12 mM, PCr 90 mM, AMP 15 mM, magnesium acetate 60 mM, diadenosine pentaphosphate 0.1 mM, NAD 10 mM, D-glucose 60 mM, G6PD 7500 $\mathrm{IUl^{-1}}$, hexokinase 9000 $\mathrm{IUl^{-1}}$, phenazine methosulfate (PMS) 0.15 mM, bovine serum albumin 4.5 $\mathrm{gl^{-1}}$.

[12] Ingredients: tetranitro blue tetrazolium (TNBT) 0.023 $\mathrm{g\,ml^{-1}}$ dimethylformamide.

[13] Acetyl-CoA 0.35 mM, 5,5'-dithio-bis(2-nitrobenzoic acid) (DTNB) 0.12 mM; all solutions made up in Tris base adjusted to pH 8.1.

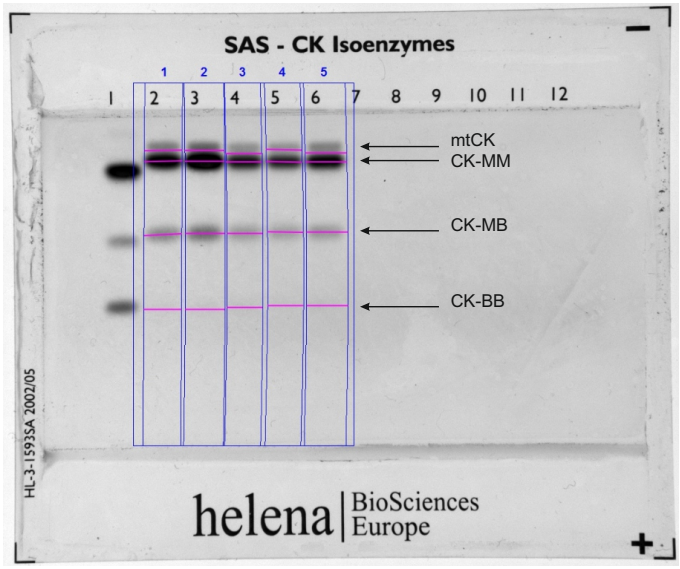


Figure 2.12: CK isoenzymes separate by gel electrophoresis from top to bottom: mtCK, CK-MM, CK-MB, CK-BB.

- CoA-SH + DTNB $\longleftrightarrow$

  CoA-S-S-5-thio-2-nitrobenzoate + TNB,

where 5-thio-2-nitrobenzoate (TNB) is measured by spectrophotometry at 412 nm. Mean activity over 40 sec and two runs was reported in IU/mg protein.

Lowry protein assay

The solution for the Lowry assay was diluted in triplicate in water (1:10 for CK and CS assays, 1:50 for creatine assays). Duplicate control 'standards' were made using known concentrations of bovine serum albumin 0-80 $\mu g\,ml^{-1}$. Samples and standards were mixed with 1 ml Lowry reagent, vortexed and incubated at room temperature for 20 min. 500 µl Folin and Ciocalteu's phenol reagent was added and samples were vortexed and incubated at room temperature for 30 min. Samples were then filtered into cuvettes (3 ml syringe, 0.45 µm filter) and protein concentration quantified by measuring absorbance at 750 nm.

Measurement of total creatine concentration

'Standards' containing known standard concentrations of creatinine, creatine, PCr, AMP, ADP and ATP were run through the HPLC column (SupelcosilTM LC-18-T, 5 µmol, cat. no. 58971, Sigma Supelco) at three dilution strengths and their concentrations plotted against peak area under the chromatogram to generate calibration curves for each molecule. (Runs with an adenosine standard were unreliable and this was abandoned for a majority of samples.)

Frozen crushed LV was homogenised in perchloric acid, neutralised with potassium hydroxide, adjusted to pH 7, centrifuged at 4°C and filtered. All preparation was done on ice.

10 µl of homogenate was loaded onto the HPLC column under standard conditions (28°C, flow rate 0.7 mL/min, detection wavelength 206 nm, mobile phase 3.5% acetonitrile, 215 mM potassium dihydrogen orthophosphate, 2.3 mM tetrabutylammonium bisulphate). Concentrations ($\mathrm{nmol\,ml^{-1}}$) were normalised to Lowry protein ($\mathrm{mg\,ml^{-1}}$) and presented as $\mathrm{nmol\,mg^{-1}}$ protein.

2.8 SERIAL BLOCK-FACE SCANNING ELECTRON MICROSCOPY

I am grateful to Dr Errin Johnson (Dunn School of Pathology, University of Oxford) for the serial fixation, mounting and image acquisition steps below.

The purpose of the serial block-face scanning electron microscopy (SBEM) was to generate 3D sarcomere-mitochondrion distance maps for each dataset, which would represent diffusion distance distributions for high-energy phosphates. This influenced the choices and compromises made below, in particular: resolution was not optimised for mitochondrial number or health; alternate slices were analysed rather than single slices to maximise 3D coverage.

Sample fixation and imaging

Primary fixative (2 ml) was made on the day by mixing sodium cacodylate buffer (1000 µl of 0.2 M), paraformaldehyde (500 µl of 16%), milli-Q water (300 µl) and glutaraldehyde (200 µl of 25%). Samples were stored at 4°C for up to four weeks before further batch processing.

Samples were washed and underwent secondary fixation A with osmium ferricyanide (1.5% potassium ferricyanide, 2% osmium tetroxide). Samples then underwent further washing and staining cycles with thiocarbohydrazide, 2% osmium tetroxide (secondary fixation B), 1% uranyl acetate (overnight tertiary fixation), and lead aspartate, followed by dehydration cycles with increasing concentrations of anhydrous ethanol (30–100%) and 100% acetone (day 2). After dehydration, samples were infiltrated with durcupan resin acetone solution overnight and incubated in increasing concentrations of resin over days 3–5, before curing at 60°C for three days.

The resin-embedded sample was sectioned and checked for quality with transmission electron microscopy (TEM) (Tecnai12) before proceeding. The sample was mounted onto an aluminium pin with conductive epoxy glue and a smooth block face was prepared with a microtome and diamond knife. The pin was then coated with gold to enhance conductivity and mounted in a Zeiss Merlin Compact Field Emission Gun-Scanning Electron Microscope with Variable Pressure and a Gatan 3View System. Serial sectioning involves cycling through: imaging of the top surface of the sample, upward translation of the block by the microscope, and sectioning of the top surface by a diamond knife.

Acqusition parameters were found by experimentation, aiming to achieve sufficient resolution to identify mitochondrial outlines but balancing this against achieving a wide field of view and acceptably short time per slice. Pressure was tuned to reduce charging of the sample surface. Typical acquisition parameters (magnification 6100×, voltage 3 kV, dwell time 6 ms, pressure 0.3 Torr, field of view 40 µm square or 4000

$\times$ 4000 pixels, slice thickness 100 nm, pixel pitch 10 $\times$ 10 nm) resulted in approx. 220 slices serially sectioned and imaged over 24 hours for each dataset.

SBEM dataset analysis

DOWNSAMPLE FROM RAW TO 8-BIT .TIFF AND COMBINE AS A STACK

The following workflow was found by experimentation. Raw datasets were converted from raw .dm3 format to 16-bit .tiff (Gatan DigitalMicrograph version 3.21.1374.0), batch processed for inter- and intra-slice contrast normalisation with an in-house Matlab script to correct for drift in image intensity and combined as a single stack (.am format) with Microscopy Image Browser (MIB) version 2.0.1 for Matlab (Belevich et al., 2016). After contrast stretching and downsampling to 8-bit, acquisition parameters (normally saved in separate .hdr text files) were copied to the clipboard and imported to the dataset before the stack was saved for future use.

SAVE A SHARP STACK OF 80 SLICES AS A .AM FILE

To reduce working memory requirements, the stack was screened for 80 contiguous slices for analysis, and a further subsample was saved after repeating the previous procedures.

FIND A BLUR SETTING AND A BLACK AND WHITE THRESHOLD AND APPLY THESE IN 3D TO GENERATE A SEMI-AUTOMATIC 'MODEL'

Using the 80-slice stack and experimenting on a single slice at a time, a blur setting was found by varying the number of iterations (30, 45, 60...) applied by the perona malik anisotropic diffusion filter on each of 4 contiguous slices. Typical settings were iterations 45, K 4%, lambda 0.25. The filter was recommended by Dr Ilya Belevich[14]. For each blurred slice, a black and white threshold filter was applied, aiming to separate the mitochondrial and ex-mitochondrial compartments. A typical value

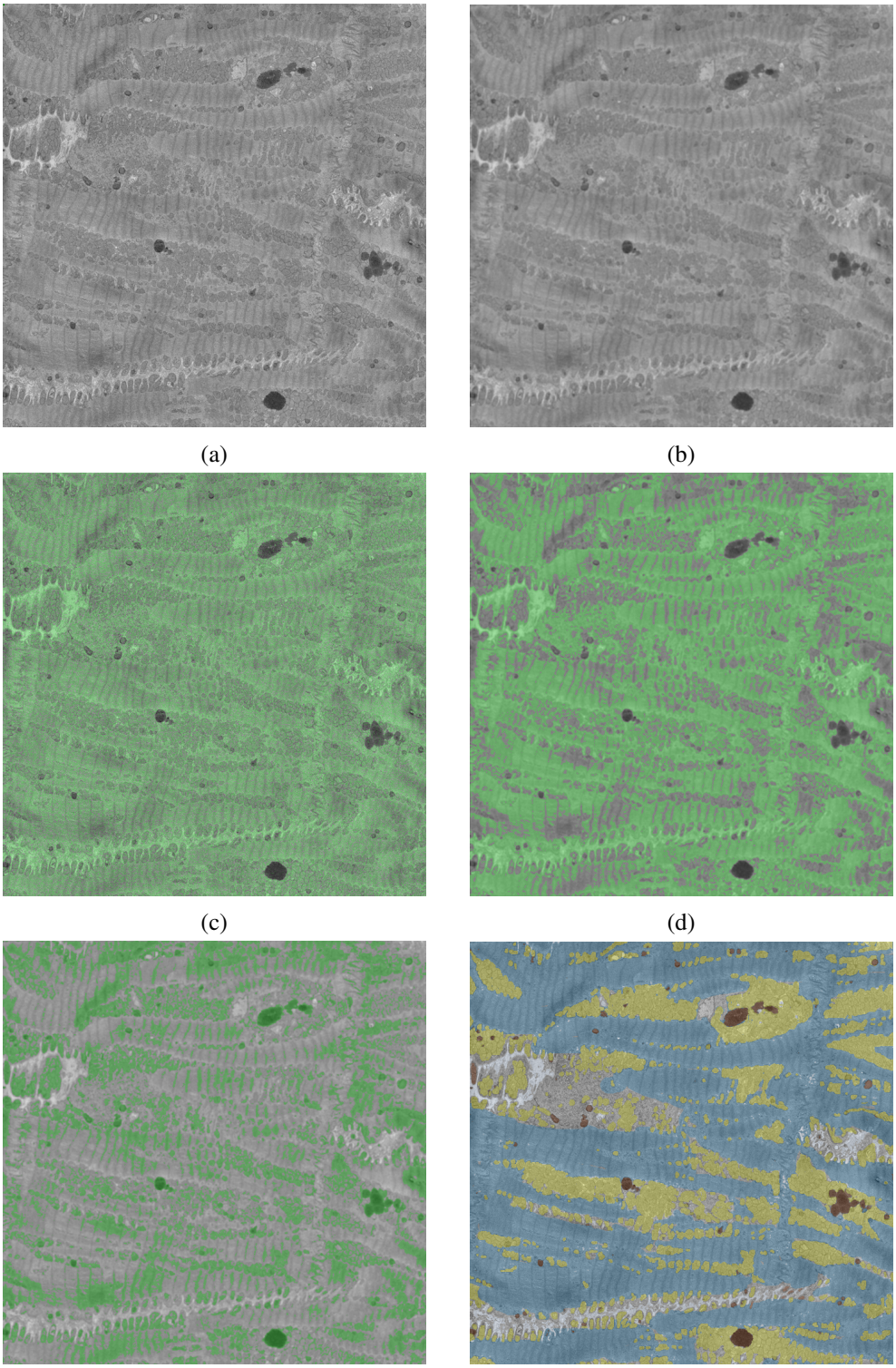
[14]Post-doctoral researcher, chief developer of MIB, Electron Microscopy Unit, Institute of Biotechnology, University of Helsinki, Finland, personal communication

settled on would be approx. 136 (out of 255 brightness levels). With too few iterations of the anisotropic diffusion filter, no black and white threshold could differentiate these two compartments, but with an optimal number of iterations, reasonable separation could be achieved (e.g. see SEM dataset _021(sevAS-pEF), slice 1 of 80, Figures 2.13a–2.13d). Having decided on the number of iterations required, the 80-slice stack was loaded afresh (to reset the iteration-finding experiment) and the anisotropic diffusion filter applied in 3D. The resulting stack was saved.

To this blurred 80-slice stack, a black and white filter with the settled value (approx. 136) was applied in 3D. The selection, comprising all pixels brighter than this threshold, was inverted so that all pixels darker than the threshold would be highlighted, dilated and eroded (by 3 within-slice pixels and 2 cycles), and then assigned as the first label, or 'material' of a semi-automatic segmentation 'model' (Figure 2.13e). Second and third black and white threshold filters were applied, aiming to separate darker organelles (approx. 103 of 255) and lighter, sarcolemmal and extracellular spaces (approx. 163 of 255). By similar procedures, these were used to save further materials within the 'model'. The resulting model was saved as a .model file.

IMPORT THE MODEL GENERATED FROM THE BLURRY STACK ONTO THE SHARP STACK

The sharp 80-slice stack was reloaded and on top of this the model generated from blurry stack was imported. Four 'materials' were defined: 1, mitochondria, 2, sarcomere, 3, darker organelles, 4, lighter sarcolemmal and extracellular spaces. The mitochondria material was analysed for all slices (R-click, get statistics, by 2D area, 4/6 connectivity) by diminishing area magnitude. Islands of pixels labelled mitochondria with areas <200 pixels squared were assigned as no material ('Exterior'). These are areas much smaller than a typical-sized mitochondrion and represent an artefact of the black and white threshold filter. At this point the model was ready for manual



(a) (b) (c) (d) (e) (f)

Figure 2.13: (a–b) Before and after Perona-Malik filter. (c–d) Black and white thresholding applied to (a–b) respectively. (e) Inversion of (d). (f) After manual segmentation.

segmentation.

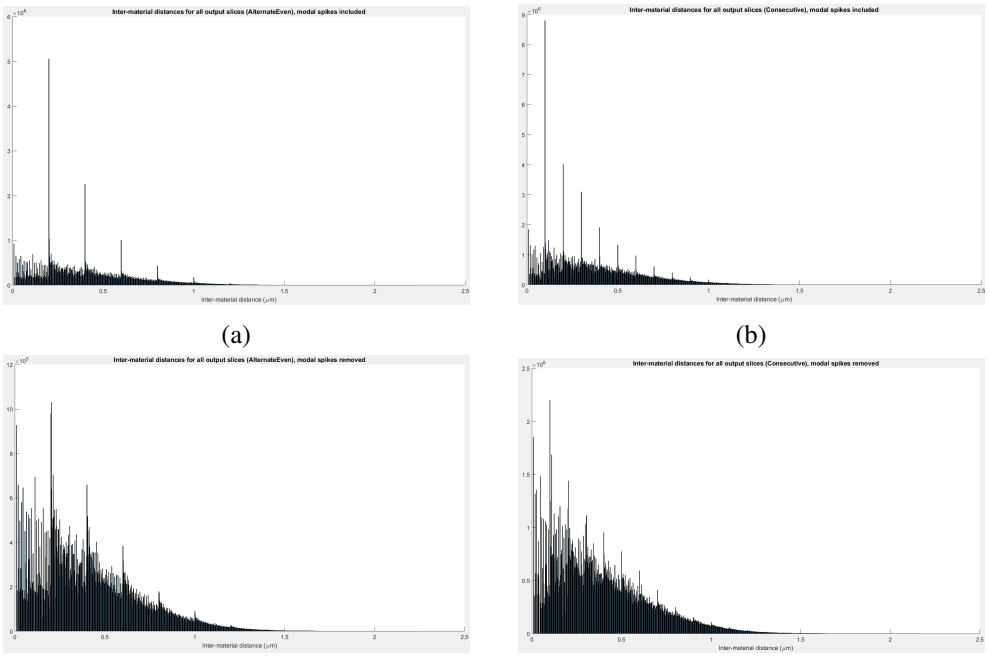
MANUAL SEGMENTATION OVER 30 ALTERNATE SLICES

Manual segmentation was performed to improve the existing model, aiming to define areas as either mitochondria, sarcomere or neither (Figure 2.13f).

GENERATION OF 3D INTER-MATERIAL DISTANCE DISTRIBUTION

Dr Ilya Belevich (Chief Developer of MIB, University of Helsinki, Finland) kindly supplied a Matlab script that calculated the shortest distance between two materials across a 3D dataset. Specifically this would calculate, for each pixel labelled 'material 2', the shortest distance to the nearest pixel labelled 'material 1', where material 2 = sarcomere and material 1 = mitochondrion. I am also grateful to Dr Ferenc Mozes (post-doctoral researcher, OCMR), who helped me customise this script to generate a matrix of non-zero distances for material 2. Due to the time-intensive nature of segmentation (7–21 working days for 30 slices) I compared the results of a consecutive-slice and alternate-slice approach. Histograms of the raw inter-material distance distribution displayed modal spikes (more frequently occuring distances) at multiples of the slice thickness (Figures 2.14a, 2.14b). When these distances were removed (Figures 2.14c, 2.14d), the problem remained yet much of the data had been discarded. I also attempted to fit lognormal distributions to both strategies and found little meaningful difference between the parameters, so decided to proceed with a 30 slice, alternate-slice approach for each dataset to achieve greater coverage.

To tackle the impact of the modal spikes (an artefact of acquisition) on the summary statistics I used the following strategy (I am indebted to Dr Justin Lau (post-doctoral researcher, OCMR) for his help with coding and for assigning the processing to a remote supercomputer). A linear interpolation script (MatlabR2016b::interpmask) was run on both the stack of 8-bit tiffs and the manually segmented model, such that four imaginary slices were interpolated between each pair of consecutive slices



(a) (b)

(c) (d)

Figure 2.14: Histograms of 3D distances for one dataset generated using (a) 30 alternate slices, (b) 30 consecutive slices, (c–d) after removing the five largest modal spikes from (a–b).

(tiffs). This reduced the inter-slice gap from 100 nm to 20 nm (5-fold). Similarly, 10-fold interpolation was run on the model in the z-direction and 0.5-fold interpolation was run in the xy plane, resulting in isotropic 20 nm voxels. The matrix size was thus reduced from $4000 \times 4000 \times 61$ to $2000 \times 2000 \times 301$. Running the distance distribution script on this stack resulted in a smoothened output (Figure 2.15). As no common or simple distribution could fit the data, the median distance was taken as a summary statistic.

2.9 ECHOCARDIOGRAPHY

Data for participants with valve disease was acquired from routine clinical scans. In healthy volunteers and athletes, transthoracic echocardiography (Philips EPIQ, CX50) was performed to acquire standard markers of diastolic function (pulse-wave Doppler

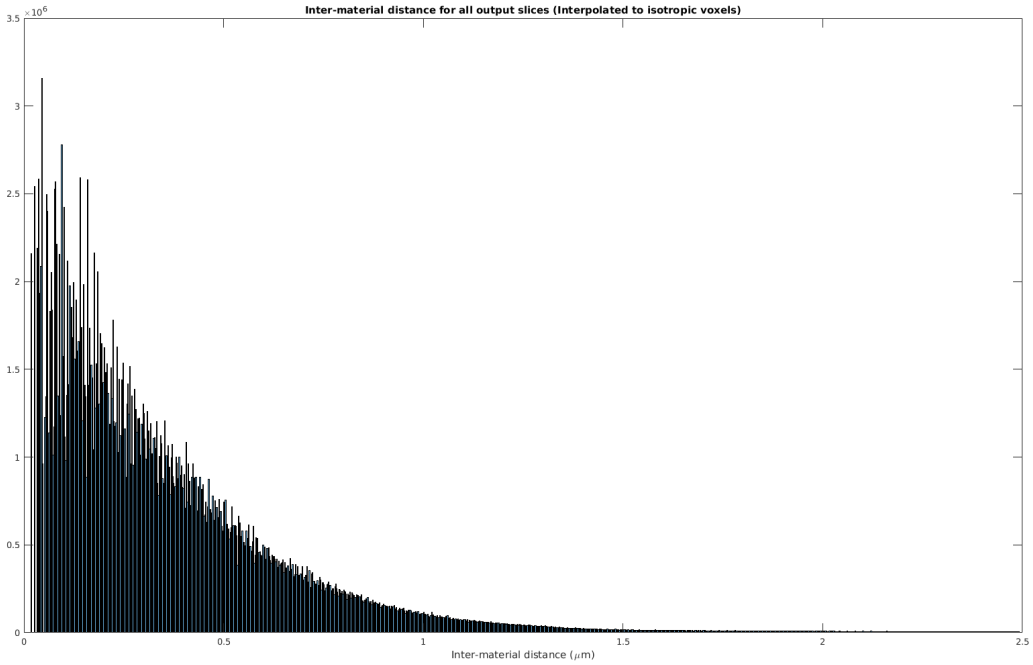


Figure 2.15: Histogram of 3D distances for one dataset (_021) after interpolation of slices and model to achieve 20 nm isotropic voxels.

at mitral valve (MV) leaflet tips and mitral annular tissue Doppler E').

2.10 CARDIOPULMONARY EXERCISE TESTS

Participants underwent bicycle CPETs with individualised protocols and breath-by-breath respiratory gas measurement. Protocols aimed to achieve peak oxygen consumption at 10-12 mins. Typical parameters were: resting 2 min, unloaded 2 min, starting work rate 25 W, continuous ramp increase of 15-20 W/min, recovery 3 min. Criteria for ending the test were achievement of maximum heart rate and respiratory exchange ratio (RER) >1.1 and inability to maintain increasing work. Measured or derived parameters included work rate, minute CO_2 production (VCO_2), minute O_2 consumption (VO_2), heart rate, breathing frequency, tidal volume, minute ventilation (VE), anaerobic threshold (AT), and peak VO_2.

A subset of athletes were co-recruited for a concurrent study; I am grateful to

David Dearlove (DPhil student, Department of Physiology Anatomy & Genetics, Univeristy of Oxford) for performing their CPETs.

3 *ATP delivery rates validated ex vivo*

This chapter aims to:

1. Validate the noninvasive estimate of unidirectional CK rate constant k_f using the novel ^{31}P TRiST sequence against a tissue-based measurement of maximum CK rate.

2. Investigate the main predictors of myocardial CK activity, and the importance of LV mass.

3.1 NMR STUDIES OF ENERGY TRANSFER RATES BY MAGNETISATION TRANSFER, 1977–PRESENT

Contemporaneous with the first hypotheses that high-energy phosphates are functionally compartmented, the first use of magnetic resonance spectroscopy (MRS) to observe phosphorus-containing metabolites was in excised rat skeletal muscle (Hoult et al., 1974): integration of resonances gave metabolite concentrations, and backward extrapolation from measurements at serial timepoints after death gave estimates of concentrations at time of death. NMR-visible resonances included sugar phosphates, P_i, PCr, and the three ATP resonances. Observations in perfused rat or rabbit working hearts subject to ischaemia (Garlick et al., 1977; Hollis et al., 1978; Jacobus et al.,

1977) found that (from relative positions of the ATP resonances) almost all ATP is complexed with Mg^{2+}, while the resonant frequency of P_i is strongly pH-dependent around pH 7.[1]

The first validation of metabolite measurements in living muscle was in oxygenated, resting frog sartorius, where concentrations of PCr and ATP obtained by MRS and by freeze-clamping and chemical extraction were similar (Gadian et al., 1977). Later studies confirmed that PCr and ATP measurements agreed well between the two modalities, but that P_i measurements did not (Meyer et al., 1982). The reason for this discrepancy was that freeze-and-extract chemical methods estimate total extractable metabolite content, which may change if there is delay in freezing, while MRS is sensitive only to the mobile portion of a metabolite (immobile metabolites have shorter T_2s and give broad peaks) and to metabolites present in concentrations > 0.6 mM or $0.3\ \mu mol\,g^{-1}$ wet weight (assuming a ten min limit to record) (Ingwall, 1982).[2] The observation that the ATP/P_i ratio was closer to 10 (by ^{31}P-MRS) rather than 1 (by chemical extraction) meant that the calculated cytosolic phosphorylation potential became ten-fold higher and many biochemical reactions previously thought saturated by P_i could now be considered controlled by P_i, in particular oxphos (Balaban, 1984). Despite ^{31}P-NMR's low sensitivity[3] and low time resolution,[4] the advantage of ^{31}P-NMR over the alternatives (analysis of coronary arterial-venous differences and freeze-clamped tissue) was that information obtained about intracellular metabolites could be repeated in a single organ non-destructively, allowing correlation

[1] This is because the pK of P_i is 6.9; that of PCr is 4.6. The two predominant exchanging species of P_i have different chemical shifts and are in fast exchange with each other, so that only a single peak is seen (Valkovič et al., 2017).

[2] For all these reasons (ADP-binding to actin, rapid hydrolysis of ATP, very low concentration of free ADP at 1–1.5% of ATP (Steenbergen et al., 1978)) and resonance overlap between β-ADP/γ-ATP at available field strengths, free [ADP] cannot be visualised with MRS, and values calculated from the CK equilibrium are 25-fold lower than values found with extraction methods.

[3] Signal is reduced by around 10^5-fold compared with proton NMR owing to the 15-fold reduced magnetic susceptibility and reduced concentrations of the molecules of interest.

[4] Low sensitivity mandates many averages to improve SNR; long T_1 times mandate longer TRs to minimise saturation and short T_2s mandate short pulse and read-out durations (Bogner et al., 2009; Rodgers et al., 2014).

with mechanical function. The time course of relatively slow metabolic events such as ischaemia-reperfusion or changes in workload or substrate availability could thus be followed in living muscle.

Shortly afterward came the first studies of NMR magnetisation transfer to study cardiac CK rates, and these were able to confirm the previously generated hypotheses. All assume steady-state conditions and reduce the CK system to a two-site reaction, where $k_f \times [\text{PCr}] = k_r \times [\text{ATP}]$, as outlined in Sections 2.5 (p. 61) and A.2 (p. 231). Studies were made in the perfused hearts of rats (Bittl et al., 1987a,b,c; Bittl and Ingwall, 1985, 1986; Brown et al., 1978; Koretsky et al., 1986; Kupriyanov et al., 1984; Matthews et al., 1981, 1982; Ugurbil et al., 1986; Zahler et al., 1987), rabbits (Bittl et al., 1985; Nunnally and Hollis, 1979; Perry et al., 1988), and ferrets (Neubauer et al., 1988). Most of these tested CK activity under different physiological conditions and are summarised later (Section 6.1, p. 191). Here I note a key contradiction identified by these studies, that is still limiting today: forward flux from PCr to γ-ATP was greater than the (measured) backward flux from γ-ATP to PCr, contradicting the assumption that the concentrations of PCr and γ-ATP are at steady-state during the experiments. Why did this discrepancy arise?

There are at least two explanations. The first posits two pools of ATP and PCr which, although both NMR-visible, are not equally available to react with CK. Consistent with the recently described compartmentation of CK-M and mtCK (Section 1.3, p. 37) would be a model where under normal conditions, k_f reflects cytosolic, ATP-producing CK activity and k_r mitochondrial, PCr-producing CK activity. Cited in support of this were NMR measurements of k_f, k_r, and the T_1 of γ-ATP and PCr in isolated working rabbit hearts under control conditions and after recovery from 25 min no-flow ischaemia (Nunnally and Hollis, 1979). Measured k_f was 0.70 and 0.74 /s under the two respective conditions; calculated k_f (by measured $k_r \times$ [ATP]/[PCr]) was 0.43 and 0.72 /s; and the T_1 of γ-ATP was 1.2 and 0.6 s respectively. Mismatch

in the control condition between measured and calculated k_f due to underestimation of k_r was interpreted as indicating that not all ATP is equally available to react with mitochondrial CK. Furthermore, the change in γ-ATP T_1 and match between measured and calculated k_f in the reperfused ischaemic heart was interpreted as reflecting preferential loss of ATP from one compartment. The remaining pool of ATP was hypothesised to be the less mobile, mitochondrial compartment, hence the fall in γ-ATP T_1.[5]

A variation on this explanation posits two pools of ATP and PCr, not equally available to react with CK, where some organellar-bound reactions are not as NMR-visible because of saturation effects (i.e. one pool of one metabolite has a much longer T_1 than another pool of the same metabolite) or immobilization of a significant fraction of the reactants (i.e. linewidth broadening) (Ingwall, 1982). A complicating factor is the cardiac- and species-specific CK isoform breakdown, which in rats and rabbits comprises 30% mtCK, 55% CK-MM, and 15% CK-MB. With all this in mind, we can appreciate that k_f reflects a weighted average for all ATP-producing CK activity and k_r a weighted average for all PCr-producing CK activity (Figure 1.4).

The second explanation is that saturation of γ-ATP (reducing the CK system to a two site system) works for estimation of k_f because PCr is a substrate solely of CK, but saturation of PCr will result in underestimation of k_r if ATP is converted to products other than PCr at appreciable rates. Thus the mismatch between measured and calculated k_f is "small or nonexistent" when hearts are perfused with glucose alone – where the CAC cycle is substrate-limited, PCr/ATP ratio low, calculated [ADP] high and CK activity high – but increases when hearts are perfused with glucose-pyruvate and CK rates fall (Ugurbil, 1985a).

[5] Further unpublished support for compartmentation comes from NMR experiments measuring obliteration of ^{31}P resonances as a function of time after administration of Mn^{2+} in the perfusate (referenced in Nunnally and Hollis (1979)). There was a rapid initial loss of nearly all PCr and part of the ATP resonances, but a proportion of the ATP took 2-3 times longer to disappear. This could be an ATP pool which is not as accessible to Mn^{2+} as the cytosolic pool.

As ATP is indeed hydrolysed by multiple ATPases whose summed reaction rates are not dwarfed by k_r (and can be estimated under aerobic conditions from the rate of oxygen consumption), ATP hydrolysis to P_i cannot be ignored and a three site system incorporating ATP hydrolysis/synthesis can be recommended: PCr $\underset{k_r}{\overset{k_f}{\rightleftarrows}}$ γ-ATP $\underset{k_{-2}}{\overset{k_2}{\rightleftarrows}}$ P_i. Here, in the presence of continuous P_i saturation, the problem reduces to a two site system, ensuring k_r will not be underestimated. Although infeasible in the normoxic human heart owing to difficulty visualising P_i, measurements in the isolated perfused working rat heart did confirm that $k_f \times$ [PCr] = $k_r \times$ [ATP], as expected under steady-state conditions (Ugurbil, 1985a,b).[6]

Whatever the in vivo situation is regarding the mobility of CK substrate pools, NMR saturation transfer-measured flux in both directions has been validated for both MtCK and CK-MM in vitro using two-site assumptions and ATPase-free solutions. As predicted by the rate equation, a linear relationship between NMR-measured CK flux and CK V_{max} was found for both isozymes (Van Dorsten et al., 1996), confirming that when enzymes and substrates are free in solution (and there is no contamination from ATPases), all CK fluxes are visible to the two-site saturation transfer experiment.

Subsequently, saturation transfer (limited for the above reasons to the ATP-producing direction) was extended to the human heart. There remains however a gap. All published noninvasive estimates of myocardial CK flux in humans measured k_f using FAST (Abraham et al., 2013; Bottomley et al., 2013a, 2009; Smith et al., 2006; Weiss et al., 2005) and estimated [PCr] noninvasively using techniques limited to a single centre. None attempted to measure creatine content by ^{1}H-MRS nor sample myocardium by extraction methods. Separately, ^{1}H-MRS estimates of myocardial

[6] Even this is a simplification – but a reasonable one. A four-site model adds further exchange sites γ-ATP $\rightleftarrows$ other, where 'other' sites include β-ADP (catalysed by adenylate kinase), 1,3-DPG (3-phosphoglycerate kinase), glucose-6-phosphate (hexokinase), and phosphoenolpyruvate (pyruvate kinase) (Kupriyanov et al., 1984; Matthews et al., 1982). The three-site model thus assumes that fluxes through these 'other' sites are neglible relative to CK and ATP hydrolysis/synthesis. Another approach treats ATP local to cytosolic CK, mtCK and MM-bound CK, and $PCr_{cytosolic}$ and PCr_{mito} as separate pools (Joubert et al., 2001, 2002b). This approach has the potential to assess subcellular fluxes between compartments.

creatine content in humans,[7] although validated against extraction methods at autopsy in dogs (Bottomley and Weiss, 1998, 2001), have neither assessed k_f nor sampled myocardium. There remains a need therefore to estimate k_f and total creatine in the same human heart, and compare these with total CK activity obtained by extraction methods. This chapter is intended to address this gap.

3.2 METHODS

Correlation

To explore the relation between components of the energy transfer system, oxidative capacity and LV volumes and mass, I first looked for correlations between these variables, irrespective of whether they were invasively or noninvasively obtained, and irrespective of participant group membership.

Variables examined were CK total activity, CS absolute activity, CK/CS activity ratio, total creatine, total adenine nucleotide pool (TAN pool), CK k_f, PCr/ATP ratio, and LV mass and volumes. Derived variables were volumes indexed for BSA, estimated forward CK flux calculated by k_f adj $\times$ estimated [PCr] (where k_f adj = raw k_f $\times$ 1.333 to correct for supine position, and estimated [PCr] is derived from PCr/ATP ratio $\times$ literature values for [ATP] of 5.7 or 5.2 μmol/g/wet weight (Weiss et al., 2005)), and estimated CK flux calculated by k_f adj $\times$ total creatine.

Each variable pair was independent, i.e. came from a different participant. For those participants with two pairs separated in time, e.g. k_f and volumes before and late post surgery, only the first pair was used. Absolute PCr or free creatine concentrations were not measured invasively, as the former is labile enough that between-sample differences in the delays between aortic crossclamp, surgical biopsy and freezing

[7] Creatine can be identified on ^{1}H-MRS by its N-methyl resonance at 3.0 ppm. It is not possible to distinguish between PCr and creatine noninvasively. Creatine content has been estimated in chronic MI (Bottomley and Weiss, 1998; Nakae et al., 2004b), NICM (Nakae et al., 2005, 2004a, 2003) and hypertrophic cardiomyopathy (HCM) (Nakae et al., 2005, 2003).

would confound the true value, and non-invasive PCr quantification was not possible. For clarity I excluded: correlation pairs with p-values > .05, non-indexed volumes when these showed similar findings to indexed volumes, and variable pairs that were internally aliased, e.g. creatine against $k_f \times$ creatine. As an exception I kept the CK/CS activity ratio (see below).

Linear regression

To further investigate predictors of myocardial CK activity I then explored whether variation in the outcome (dependent) variable, CK total activity, could be predicted by a combination of two of more predictor (independent) variables (parameters) better than a single predictor alone. I was interested whether the amount of variance that could be explained by combining the variables total creatine and CK k_f could improve on either alone, as these are key to the CK rate equation (notwithstanding the inherent assumption that total creatine was being used in place of PCr or free creatine), and whether better models than this could be found from the correlating variables identified, excluding CK/CS ratio as this assumes knowledge of the dependent variable.[8]

Criteria for preferring a model were: explanatory variables that had biological, mechanistic relevance to the outcome variable, fewer parameters, high explanatory value given the number of parameters (higher values of adjusted R^2 and F-statistic, lower values of AIC), inclusion of parameters that were feasible to measure nonin-

[8] For the reader not familiar with multiple linear regression, the idea is to model a function $y = b_0 + b_1x_1 + b_2x_2 + \varepsilon$ where y is the outcome variable, x_1, x_2 etc. are predictor variables (parameters), ε is residual error, and values for the coefficients b_1, b_2 are chosen to minimise the residual error, or difference between predicted and observed values for y (or the sum of squared errors (SSE)). The model coefficient of determination, or multiple R^2, is the square of the correlation between predicted and observed values. R^2 falls as the ratio of SSE to the total sum of squares rises. For each parameter, the standardized coefficient β gives the number of standard deviations the outcome variable is expected to change for a one standard deviation change in the parameter. A t test is performed to check the likelihood of the observed value of b for any parameter having occurred, given the assumption that the population value of $b = 0$. The F-ratio divides the variance explained by the model by the residual unexplained variance; numbers > 1 are preferred. The Akaike information criterion (AIC), a parsimony adjusted measure of model fit, penalises a model for increasing SSE (like R^2), but also for increasing the number of parameters. A smaller AIC is preferred. Generally speaking there is no single right model (all models are wrong), but some are better than others and the simplest, minimal adequate model is preferred.

vasively, larger number of observations, linearity, and every parameter contributing independently i.e. having a non-zero β coefficient. It follows that explanatory variables should correlate with the outcome variable but not with each other.

Models were tested by stepwise deletion of parameters from the maximal model (Crawley, 2015). The maximal model contained all covariates that could be of interest. The least significant terms were removed first, starting with higher-order interactions, with each deletion step accepted if it did not significantly increase model deviance. The minimal adequate model was defined as that remaining when the model contained only significant terms.

Patients included in the maximal model had to have all variables recorded independently by MRI, ^{31}P-MRS and biopsy-extraction methods, so completing 'triplicate' datasets.

Maximal models were tested systematically without starting with excess numbers of parameters. I aimed to test no more than n/3 parameters at once, where n was the number of triplicate datasets (n =37). The first maximal model contained seven variables (CS activity, creatine, CK k_f, LVEDVi, LVESVi, LVEF, LVMi). LVEDVi was dropped, owing to its lower explanatory power over LVESVi. This left six variables remaining and fifteen two-way interactions between them. The interactions were numbered[9] and maximal models containing six variables and a random sample of five two-way interactions (eleven parameters) were tested until it was clear that interactions 3–6 and 12–15 should be dropped. Of the remaining eight interactions, maximal models starting with random samples of four interactions added to the six variables (ten parameters) were tested repeatedly until certain minimal adequate models kept being found. The four strongest two-way interactions were k_f:CS, k_f:LVESVi, k_f:LVMi, and creatine:CS.[10] By way of further exploration, the six single

[9]The fifteen interactions are (1) CS:k_f, CS:creatine, CS:LVESVi, CS:LVEF, CS:LVMi, (6) k_f:Cr, k_f:LVESVi, k_f:LVEF, k_f:LVMi, creatine:LVESVi, (11) creatine:LVEF, creatine:LVMi, LVESVi:LVEF, LVESVi:LVMi, LVEF:LVMi.

[10]k_f:CS is shorthand for $k_f \times$ CS.

variables and four strongest two-way interactions were tested.

As minimal adequate models consistently included CS activity, which is not feasible to measure noninvasively, this process was repeated, dropping CS activity and starting with the five remaining variables and a random sample of five of the ten possible two-way interactions. Of numbers 6–15 of the original 15, numbers 13–15 were dropped and random samples of five of the remaining seven interactions were added to the five variables.

For each minimal adequate model, diagnostic parameters and plots were examined in order to identify influential cases.[11]

3.3 RESULTS

Correlation

There was no general relation between the time a sample spent in the freezer before analysis and the results of the analysis (Figure 3.1). Median (IQR) storage times for CK total activity and CS activity were 5.2 (1.5, 7.6) months; for total creatine and TAN pool 4.1 (1.2, 6.9) months.

Five number summaries for the first five variables, which were obtained from LV biopsy, are provided in Table 3.1. One participant had outlier values for total creatine (297, z-score +5.40) and TAN (273, z-score +4.33), which I omitted from analyses.

CK total activity correlated strongly with citrate synthase activity (pearson r = .84, p = 1×10^{-13}) and well with TAN pool (r = .52, p = .006) (Figure 3.2, Table 3.2). There were also good correlations with total creatine concentration and CK flux estimated by $k_f \times$ total creatine (r = .56 and .65 respectively, p < 10^{-4} for both),[12] and

[11] There are several ways of measuring whether a case is disproportionately influential: studentized residuals indicate the influence of a case on the ability of the model to predict that case and can identify homogeneity of error variance; cooks distance indicates the influence of a case on the model's ability to predict all cases; dfbeta indicates the influence of a case on the coefficients of the model parameters.

[12] The correlation with $k_f \times$ total creatine may not be linear.

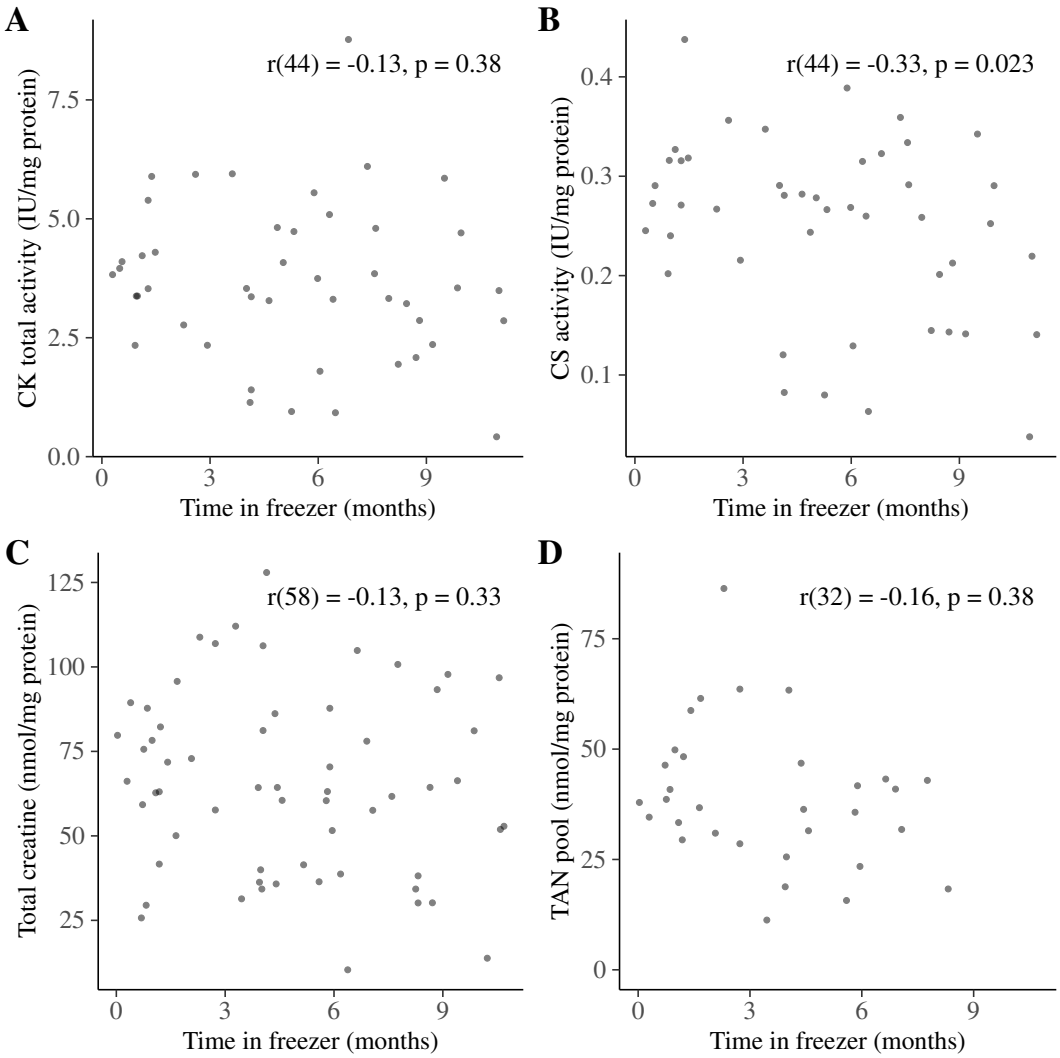


Figure 3.1: Scatter plots indicated no relationship between the time LV biopsies spent in the freezer until analysis and the results of the analysis. *r(df) is Pearson correlation coefficient r where the number of degrees of freedom (df) = number of datapoints – 2.*

Table 3.1: Five number summaries for invasively obtained variables[a]

Parameter	n	Min	Q1	Q2	Q3	Max
CK total activity (IU/mg protein)	47	0.42	2.63	3.53	4.73	8.77
CS activity (IU/mg protein)	47	0.038	0.202	0.267	0.316	0.438
CK/CS activity ratio (IU/IU)	47	9.5	12.0	14.1	16.5	27.2
Total creatine (nmol/mg protein)	61	10.4	41.4	64.3	82.2	127.9
TAN pool (nmol/mg protein)	35	11.3	31.0	38.6	48.3	136.7

[a] For each variable, the number of participants contributing (n), minimum (min), first quartile, median (Q2), third quartile and maximum (max) values recorded are given.

moderate correlations with k_f and CK flux estimated by $k_f \times$ estimated [PCr] (r = .44 and .35 respectively, p = .007 and .037 respectively) (Figure 3.3).

There was also a moderate positive correlation between CK total activity and LVEF, and moderate negative correlations with LV volumes and LVMi (Figure 3.4).[13] This evidence of an association between CK activity and systolic performance agreed with the theoretically expected coupling of metabolic and contractile reserve.

As scatter plots of these correlations were largely linear and interpretation of these correlations (as strong, good, and moderate) was essentially unaltered by the use of the Spearman rank correlation coefficient, both coefficients were tabulated (Tables 3.2–3.3 and A.1).

There were only two correlates of CK k_f: CK total activity and CK/CS activity ratio (p = .44 and .52 respectively, p = .007, and .001) (Table 3.3, Figure 3.3 Panel B, Figure A.2 Panel B). As CK/CS activity can be thought of as an index of CK activity normalised to mitochondrial volume, or of extra-mitochondrial CK activity, and CK k_f is specific for ATP-producing (and typically extra-mitochondrial) CK activity, it was reassuring that k_f should correlate more tightly with CK/CS activity ratio than with CK total activity. The correlations between CK total activity and the two estimates of

[13] Correlations with LV mass and volumes non-indexed for BSA were very similar.

CK flux were also maintained with CK/CS activity ratio (Table A.1, p. 235, Figure A.2 Panels C–D, p. 236).

Table 3.2: Correlates of CK total activity[a]

Parameter	n	r[b]	p-value[b]	rho[c]	p-value[c]
CS activity (IU/mg protein)	47	.84	1e–13	.86	2e–16
CK/CS activity ratio (IU/IU)	47	.62	3e–6	.53	1e–4
TAN pool (nmol/mg protein)	27	.52	.006	.51	.007
Total creatine (nmol/mg protein)	47	.56	4e–5	.58	3e–5
CK k_f adj (/s)	37	.44	.007	.32	.05
k_f adj $\times$ est [PCr] (μmol/g/s)	35	.35	.037	.36	.034
k_f adj $\times$ total creatine (nmol/mg/s)	37	.65	1e–5	.63	5e–5
LVEDVi (ml/m^2)	46	–.41	.005	–.45	.002
LVESVi (ml/m^2)	46	–.49	5e–4	–.45	.002
LVEF (%)	46	.44	.002	.38	.010
LVMi (g)	46	–.43	.003	–.45	.002

[a] Only those correlates meeting p $\leq$ .05 are included. LVEDV, LVESV, and LVM were significantly correlated to similar extents to their indexed counterparts.
[b] Pearson r correlation coefficient.
[c] Spearman rho correlation coefficient.

Table 3.3: Correlates of CK k_f[a]

Parameter	n	r[b]	p-value[b]	rho[c]	p-value[c]
CK total activity (IU/mg protein)	37	.44	.007	.32	.05
CK/CS activity ratio (IU/IU)	37	.52	.001	.39	.018

[a] Only those correlates meeting p $\leq$ .05 are included.
[b] Pearson r correlation coefficient.
[c] Spearman rho correlation coefficient.

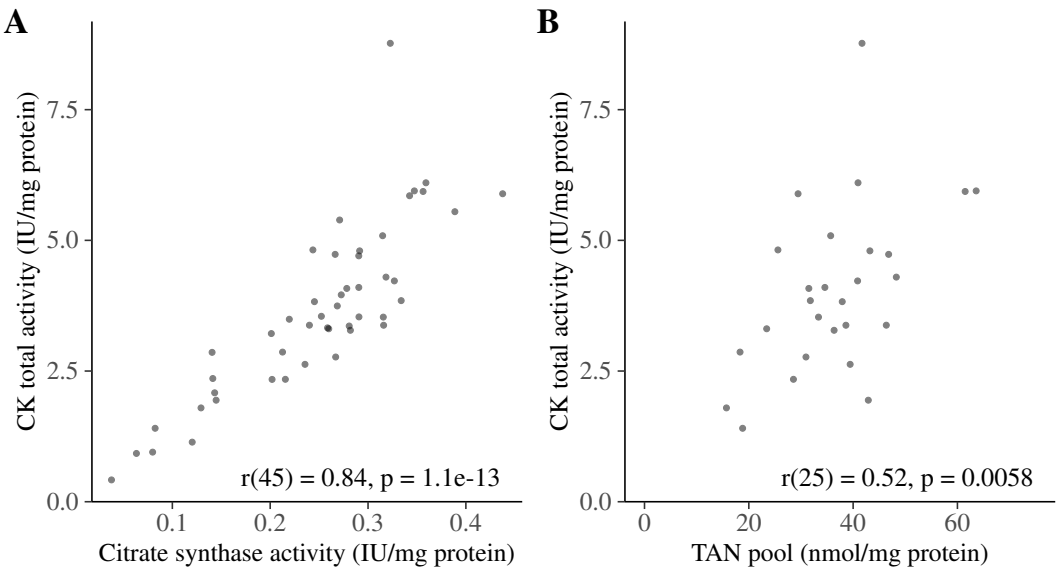


Figure 3.2: Scatter plots for (A) CS activity, (B) TAN pool against CK total activity.

Linear regression

37 participants contributed triplicate datasets (Table 3.4): 27 had severe AS (8 with impaired LVEF); 2 had severe primary MR and preserved LVEF; 5 had mitral stenosis (2 with impaired LVEF); 2 had ascending aortic aneurysms with preserved LVEF; 1 had a left atrial mass. 10 were scanned in atrial fibrillation.

Minimal adequate models found (listed here in order of descending simplicity) either:

1. Included CS activity (Tables 3.5, 3.6):
    - CS + k_f
    - CS + CS:k_f
    - k_f + k_f:CS
    - creatine + creatine:CS + k_f + LVESVi
    - creatine + creatine:CS + k_f:CS + LVESVi, or

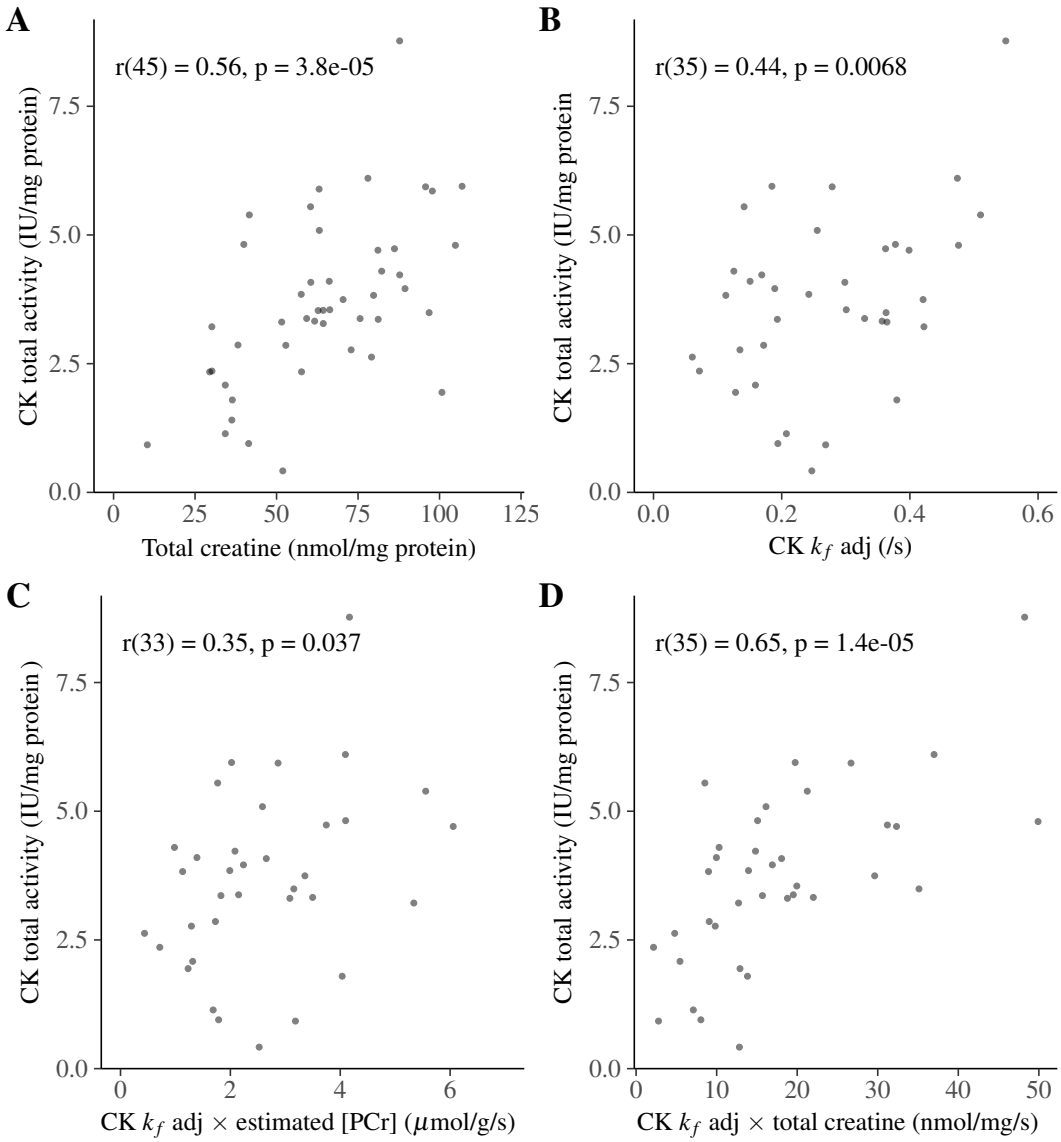


Figure 3.3: Scatter plots for (A) total creatine, (B) CK k_f, (C) CK flux estimated by k_f × estimated [PCr], and (D) CK flux estimated by total creatine × k_f against CK total activity. (Compare Figure A.2, p. 236.)

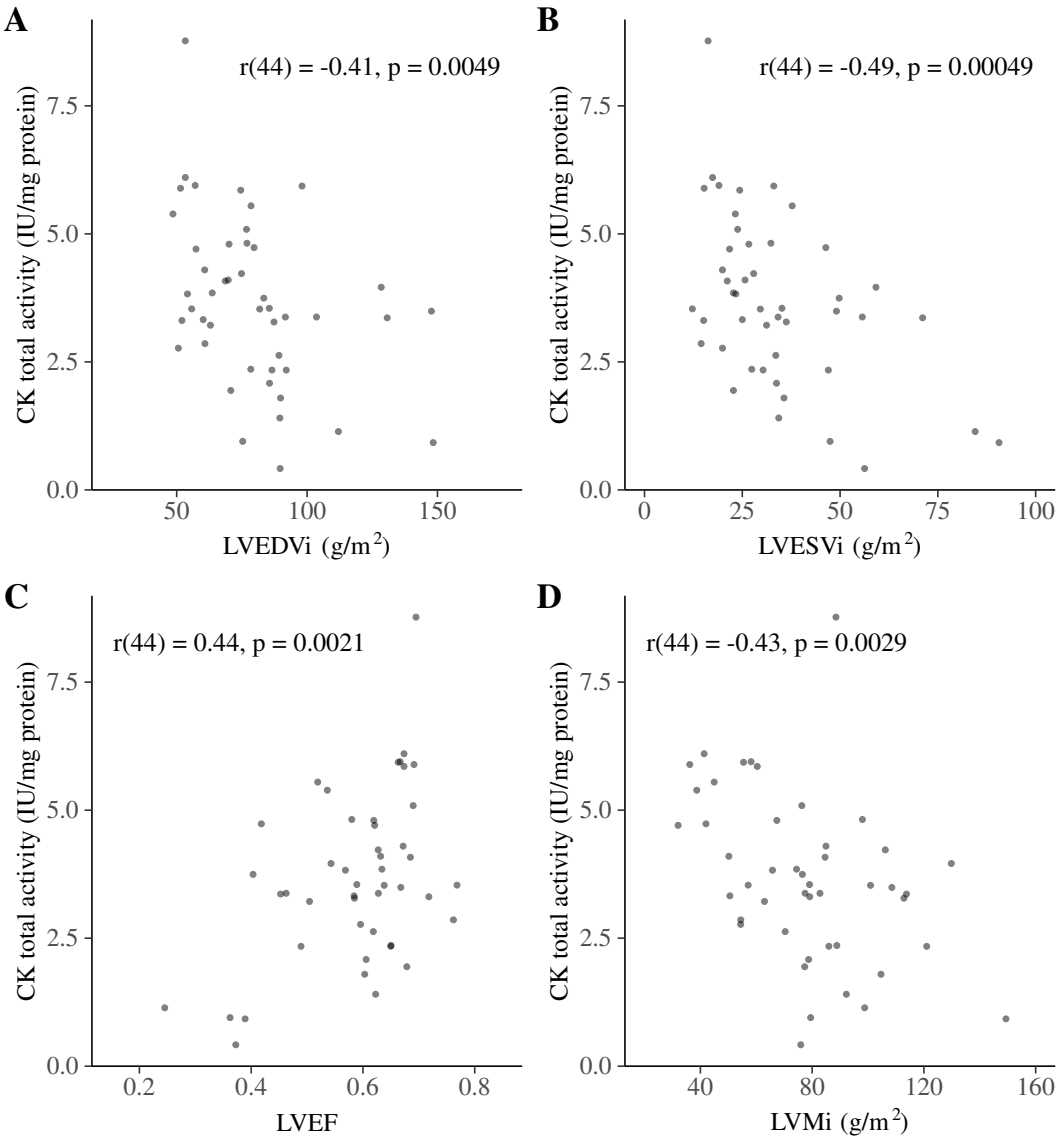


Figure 3.4: Scatter plots for (A) LVEDVi, (B) LVESVi, (C) LVEF, and (D) LVMi against CK total activity.

Table 3.4: Five number summaries for participants in the triplicate set[a]

Parameter	n	Min	Q1	Q2	Q3	Max
CK total activity (IU/mg protein)	37	0.42	2.77	3.75	4.73	8.77
CS activity (IU/mg protein)	37	0.038	0.201	0.266	0.291	0.389
Total creatine (nmol/mg protein)	37	10.4	51.6	66.2	82.2	106.9
CK k_f adj (/s)	37	0.06	0.17	0.26	0.36	0.55
LVESVi (ml/m^2)	37	14	23	28	46	91
LVEF (%)	37	25	52	61	67	76
LVMi (g/m^2)	37	32	55	76	89	149
Age (years)	37	43	65	71	75	84

[a] Conventions as for Table 3.1.

2. Excluded CS activity (Table 3.7, Figure 3.6):

   - creatine + k_f + LVEF
   - creatine + k_f + LVESVi
   - creatine + k_f + k_f:LVESVi.

Coefficients for models including CS activity were presented using a triplicate dataset of n = 36, as for these models, diagnostic statistics and plots indicated that the case with the maximum CK total activity was a relative outlier with a high studentized residual.[14] These models, although statistically different from each other (adjusted R^2 0.81–0.87), were visually very similar to the simple correlation between CK total activity and CS activity. Importantly, adding k_f or $k_f \times$ CS activity were the only simple ways to improve upon the predictive power of CS activity alone (Models 1 and 2 respectively, Table 3.5), although it should be said that CS activity remained the dominant predictor.

[14] This case was removed, model coefficients were reassessed against the remaining 36 datasets, and repeat diagnostics on the model (CS + k_f) found no highly problematic cases.

CS-excluding models were presented with the full triplicate dataset (n = 37) as there were no problematic cases on model diagnostics (e.g. for Model 8 see Figure 3.5). Each of the three minimal adequate models included three factors: creatine, k_f, and a third indicative of systolic performance: one of LVEF, LVESVi or $k_f \times$ LVESVi. These models achieved adjusted R^2 values of 0.52–0.56 and provided visually similar plots of predicted versus observed CK total activity (Figure 3.6).

Table 3.5: Coefficients for models including CS – excluding one case (1)[a]

			Unstandardized				
Model	R^2	Parameter	b	SE	β	t	p-value
0[b]	.827	(Intercept)	–0.12	0.30		–0.41	.685
		CS activity	15.33	1.18	0.912	12.97	1e–14
1[c]	.860	(Intercept)	–0.63	0.32		–1.96	.059
		CS activity	14.88	1.07	0.885	13.85	3e–15
		CK k_f	2.45	1.06	0.142	2.30	.028
2[d]	.867	(Intercept)	–0.10	0.27		–0.37	.715
		CS activity	12.65	1.31	0.752	9.69	4e–11
		CS:k_f	10.48	3.89	0.606	2.70	.011
3[e]	.812	(Intercept)	3.08	0.26		11.86	2e–13
		k_f	–16.62	2.21	–1.036	–7.53	1e–8
		k_f:CS	77.40	6.67	4.604	11.61	3e–13

[a] Dependent variable: CK total activity. n = 36 after the case with the maximum CK activity was excluded. Note that the coefficients for k_f refer to unadjusted k_f.
[b] Residual SE: 0.6143 on 34 DF. F-statistic: 168.1 on 1 and 34 DF, p-value: 1.025e–14. AIC 71.0.
[c] Residual SE: 0.5525 on 33 DF. F-statistic: 108.5 on 2 and 33 DF, p-value: 3.107e–15. AIC 64.3.
[d] Residual SE: 0.5377 on 33 DF. F-statistic: 115.4 on 2 and 33 DF, p-value: 1.267e–15. AIC 62.4.
[e] Residual SE: 0.6394 on 33 DF. F-statistic: 76.78 on 2 and 33 DF, p-value: 3.867e–13. AIC 74.8.

Table 3.6: Coefficients for models including CS – excluding one case (2)[a]

			Unstandardized				
Model	R^2	Parameter	b	SE	β	t	p-value
4[b]	.843	(Intercept)	2.67	0.48		5.58	4e–6
		creatine	–0.04	0.01	–0.630	–4.48	9e–5
		creatine:CS	0.20	0.02	2.510	8.84	6e–10
		k_f	3.70	1.09	0.220	3.38	.002
		LVESVi	–0.02	0.01	–0.001	–3.24	.003
5[c]	.861	(Intercept)	2.71	0.43		–6.29	5e–7
		creatine	–0.03	0.01	–0.534	–3.87	5e–4
		creatine:CS	0.16	0.02	0.010	6.98	8e–8
		k_f:CS	15.20	3.72	193.1	4.09	3e–4
		LVESVi	–0.01	0.01	–0.001	–2.77	.009

[a] Dependent variable: CK total activity. n = 36 after the case with the maximum CK activity was excluded. Note that the coefficients for k_f refer to unadjusted k_f.
[b] Residual SE: 0.5843 on 31 DF. F-statistic: 48.11 on 4 and 31 DF, p-value: 7.254e–13. AIC 70.1.
[c] Residual SE: 0.5509 on 31 DF. F-statistic: 55.07 on 4 and 31 DF, p-value: 1.196e–13. AIC 65.9.

3.4 DISCUSSION

In summary, maximal CK activity correlated strongly with CS activity, well with total creatine concentration and CK flux estimated by $k_f \times$ total creatine, and moderately with k_f and CK flux estimated by $k_f \times$ estimated [PCr]. The analysis was not biased by differences in freezer storage time. Models comprising combinations of predictor variables (outcome variable: CK total activity) were tested against the 37 available triplicate datasets. CS-containing models shared 81–86% of the variance in total CK activity and were dominated by CS activity, while CS-excluding models shared 52–

Table 3.7: Coefficients for models excluding CS – all cases included[a]

			Unstandardized				
Model	R^2	Parameter	b	SE	β	t	p-value
7[b]	.518	(Intercept)	–2.38	1.08		–2.20	.035
		Creatine	0.03	0.01	0.406	3.24	.003
		CK k_f	7.66	2.01	0.442	3.82	6e–4
		LVEF	4.60	1.80	0.320	2.55	.016
8[c]	.531	(Intercept)	1.34	0.91		1.47	.151
		Creatine	0.03	0.01	0.427	3.56	.001
		k_f	7.11	1.99	0.410	3.58	.001
		LVESVi	–0.03	0.01	–0.333	–2.76	.009
9[d]	.564	(Intercept)	0.57	0.72		0.80	.433
		Creatine	0.03	0.01	0.420	3.65	9e–4
		k_f	11.74	2.29	0.677	5.13	1e–5
		k_f:LVESVi	–0.17	0.05	–1.902	–3.28	.002

[a] Dependent variable: CK total activity. Independent variable excluded: CS activity. All cases included. Note that the coefficients for k_f refer to unadjusted k_f.
[b] Residual SE: 1.172 on 33 DF. F-statistic: 13.87 on 3 and 33 DF, p-value: 5.089e–06. AIC 122.5.
[c] Residual SE: 1.156 on 33 DF. F-statistic: 14.59 on 3 and 33 DF, p-value: 3.22e–06. AIC 121.5.
[d] Residual SE: 1.114 on 33 DF. F-statistic: 16.55 on 3 and 33 DF, p-value: 9.76e–07. AIC 118.8.

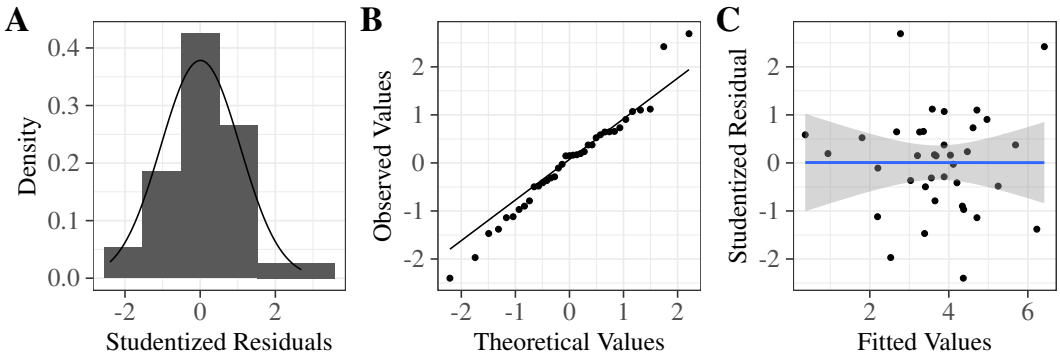


Figure 3.5: Plots of studentized residuals for model 8 (creatine + k_f + LVESVi) including all cases: (A) Histogram, (B) Quantile-quantile plot, (C) Observed vs predicted studentized residuals.

56% of the variance and incorporated variables (total creatine, k_f and either LVESVi or LVEF) that do not co-correlate, are all feasible to measure noninvasively and are biologically relevant to the outcome variable.

Furthermore, the moderate inverse correlation between CK total activity and markers of LV dysfunction, and the finding that a model predicting total CK activity from k_f and creatine content can be improved upon by adding a marker of LV dilation or dysfunction, imply a relationship between CK activity and the process of transition to failure (see next chapter for further discussion).

CK total activity and CK k_f

The above results collectively constitute the first evidence of agreement in human myocardium between CK activity measurements by freeze-and-extract chemical methods and CK flux estimates in human myocardium by MRS (the TRiST sequence), i.e. the first tissue validation of non-invasively-assessed CK kinetics. The findings that k_f correlates with total CK activity and CK/CS activity ratio (Panel B in Figures 3.3 and A.2) and that k_f adds value to the CS measurement in regression models indicates that k_f is able to reflect myocardial CK activity, and more specifically

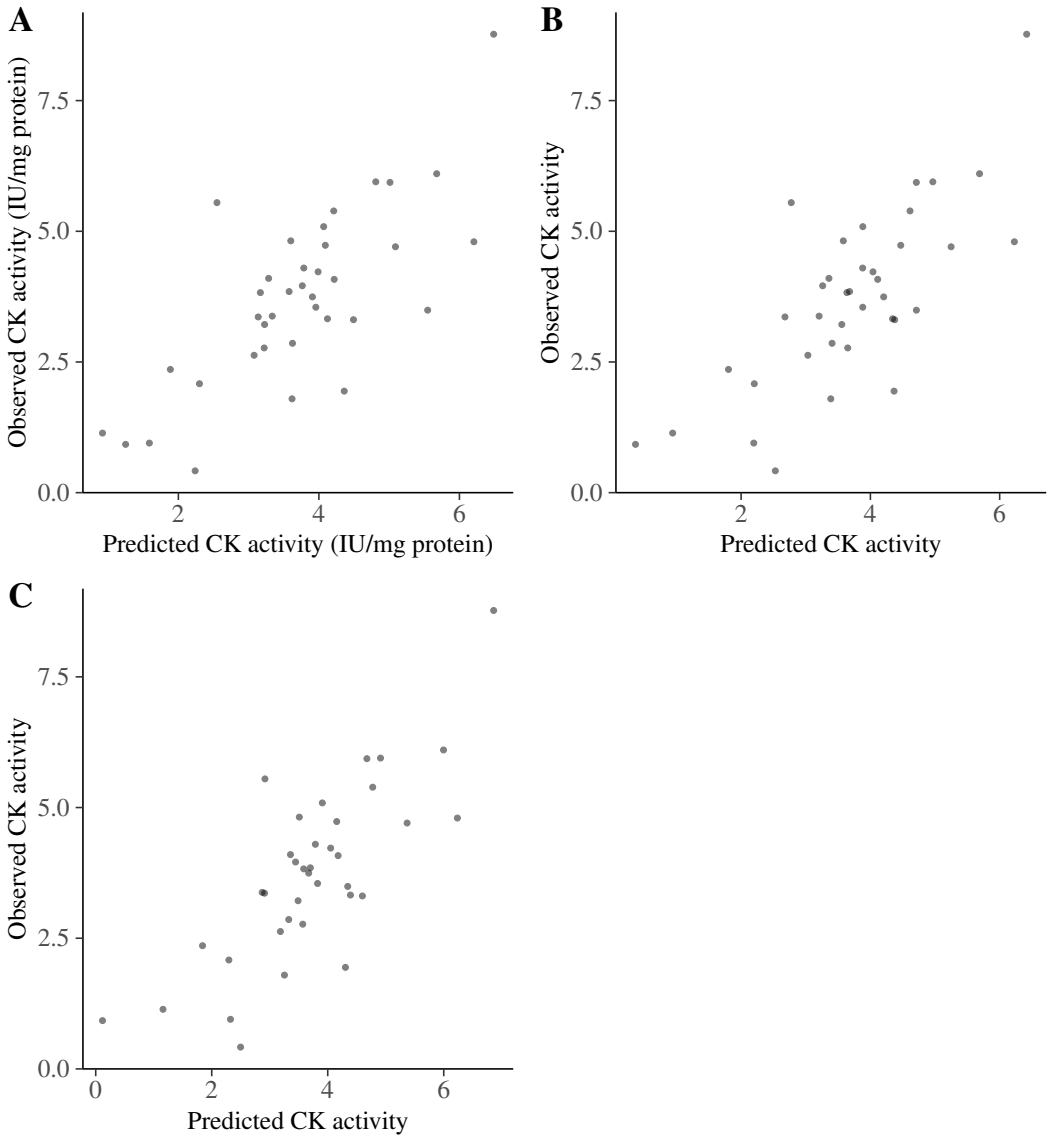


Figure 3.6: Predicted vs observed CK total activity (IU/mg protein) using (A) model 7 (creatine + k_f + LVEF), (B) model 8 (creatine + k_f + LVESVi) and (C) model 9 (creatine + k_f + k_f:LVESVi), all cases included.

extramitochondrial CK activity in the ATP-generating direction (i.e. that it measures what it is intended to measure). Collectively, these findings are an important step in developing non-invasive approaches to the CK system that represent an effective metabolic biomarker.

These observations are important because, as discussed above, ^{31}P-MRS is an inherently insensitive technique. One might be tempted to attribute any variance observed in k_f as reflecting the imprecision of the technique, but knowing that total CK activity also displays substantial variance, a proportion of which is explained by k_f, reassures us that the technique is at least specific to what it intends to measure. A second possible worry might be that this implementation of TRiST uses only a 10 cm surface coil which is more sensitive to nearby tissues: could the signal be contaminated by skeletal muscle? One response would be that contamination was minimal given that there was a clear fall in PCr/ATP ratios from 5–6 to 1–2 when comparing skeletal voxels with the voxel analysed. (The voxel analysed was the closest unambiguously cardiac voxel to the coil.) Another response would be that the resonant frequencies of PCr and ATP became more negative when moving from skeletal to cardiac muscle. As frequencies were planned to optimise for the cardiac depth, the assumption of continuous γ-ATP saturation was best met at this depth, so making any contamination from skeletal depths less meaningful. These arguments are now supported by the tissue analysis.

These results also go further, and demonstrate the first correlations in human myocardium between CK total activity (and CK/CS activity ratio) and two estimates of CK flux: $k_f \times$ estimated [PCr], and $k_f \times$ total creatine (Panels C–D in Figures 3.3 and A.2). While it is possible that enzyme flux could be modulated predominantly by changes in CK reactant concentrations and enzyme activity, and not by changes in rate constant (see Section A.1, p. 229), given that part of CK's role is to minimise fluctuations in reactant concentrations (see Section 1.3, p. 37), it is reassuring to see

these relationships with k_f and k_f-containing variables.

CK total activity and CS activity

THIS STUDY

The finding that CS activity correlates strongly with CK activity indicates that myocardial oxidative capacity (ATP synthesis capacity) is strongly correlated with phosphotransfer capacity (ATP turnover capacity). This argues for the role of CK in myocardium to be primarily tied up with oxidative energy production rather than acting in the mode of fast-twitch skeletal muscle CK. Given that mtCK constitutes not more than 30% of myocardial CK (the IQR on my participants was 15–19%, see next chapter), the strength of this correlation is surprising. The underlying mechanism is unrevealed from this data: either there is an intrinsic (perhaps genetically determined) factor that controls the expression of both CK and CS, and/or there is some factor arising from pathological hypertrophy which suppresses both concordantly.

PRIOR LITERATURE

The relationship between total CK activity and CS activity is known to depend on whether the muscle is adapted for oxidative metabolism.[15] It is likely that the two are closely related in health but less so in disease. Mean incorporation rates of ^{18}O into PCr in healthy mouse and dog hearts were 90% and 89% respectively of that into γ-ATP, with the remainder made up by adenylate kinase, indicating tight synchronisation between CK flux and ATP synthesis (Abraham et al., 2002; Dzeja et al., 1999).[16]

[15] In humans, myocardium has 2.9–3.0-fold lower total CK activity and 1.9–3.3-fold higher CS activity than vastus lateralis (unpaired samples) (Sylvén et al., 1983). In mice, myocardium has 5.3–6.9-fold lower total CK activity than hind-limb muscle, and 5.6–6.2-fold higher CS activity (Saupe et al., 1998; Veksler et al., 1995).

[16] ^{18}O-assisted ^{31}P-MRS, in combination with ex vivo mass spectrometry, can be used to infer net reaction rates by following the rate of incorporation of ^{18}O (provided from ^{18}O-labelled water) from ^{18}O-water to P_i (ATP hydrolysis), from ^{18}O-P_i to γ-ATP (ATP synthesis), and from ^{18}O-γ-ATP to either PCr (CK) or β-ADP and β-ATP (AK) or G6P (hexokinase) (Dzeja et al., 2011; Pucar et al., 2001; Zeleznikar and Goldberg, 1991).

Six freeze-extraction studies previously measured total CK and CS activities in human LV in at least two groups (Ingwall et al., 1990; Nascimben et al., 1996; Sylvén et al., 1988, 1983, 1993, 1991): only one plotted an inter-heart individual-level correlation (Sylvén et al., 1983); one plotted a within-heart correlation for ten different sampling sites between MtCK and CS activity ($r = .94$, $p < .001$) (Sylvén et al., 1991); and two of the remaining four gave group-level data.[17]

In the first (Sylvén et al., 1983), strong correlation was found between total CK and CS activities ($r = .84$, $p < .001$) in LV apical biopsies from seven participants with AV disease (mean (SD) age 63 (8)) and papillary muscle from five participants with MV disease (mean (SD) age 56 (5)).[18] Also supporting this finding, neither CK nor CS activites were reduced in papillary muscles taken from participants with MR (mean (SD) LVEF 0.50 (0.10)) when compared with donor hearts, while both were depressed in end-stage NICM hearts (LVEF 0.23 (0.05)) (Sylvén et al., 1993, 1991). However, a second group did not replicate this correlation between CK and CS activities, finding that although CK activity and creatine content were reduced in human NICM hearts compared to donor hearts, CS activity was unchanged (Nascimben et al., 1996).[19] In the failing SHR heart also, total CK and mtCK fell by 45% and 66%, yet mtCK/CS ratio fell only by 33% (Ingwall et al., 1990), suggesting that CK and CS activities are regulated differently in disease.

Further evidence of differential regulation comes from mouse models of CK deficiency, where CS activity was raised or unaltered. Relative to wild-type (WT), ventricular CS activity:

[17] Single-group studies (Bendz et al., 1980; Haralambie and Uy, 1980; Urdal et al., 1983) are not discussed here.

[18] The nature of the valve disease and the myocardial performance were unspecified. Myocardial biopsies were taken during open-heart surgery, flash-frozen in liquid nitrogen, and analysed for CK, CK-MB, CS and protein. Skeletal muscle biopsies from 11 elite athletes and 11 untrained subjects also showed correlation between CK and CS activities ($r = .68$, $p < .05$ and $r = .60$, $p < .10$ respectively).

[19] Ingwall's group later found reduced CK activity in right ventricular samples from human NICM hearts, but no correlation between CS activity and LVEF (Ingwall et al., 1990).

- in M-CK knockout (total CK activity 30% of WT) was unaltered (Saupe et al., 1998; van Deursen et al., 1993);
- in MtCK knockout (total CK activity 60–68% of WT) was raised to 111–118% of WT (Lygate et al., 2009; Steeghs et al., 1997b) or unchanged (Spindler et al., 2002);
- in M-CK/MtCK DKO (total CK activity 0.3–4% of WT) was raised to 111–122% of WT (Dzeja et al., 2011; Momken et al., 2005; Steeghs et al., 1997a, 1998) or unchanged (Saupe et al., 1998).

Likewise, models of partial creatine depletion (β-guanidinopropionic acid feeding) (Oudman et al., 2013) and total creatine depletion (GAMT knockout and creatine-free diet) (Schmidt et al., 2004; Ten Hove et al., 2005) did not change CS or CK activities. Thus either CK and CS are not straightforwardly related, or CS upgregulation is part of the way the murine heart adapts to CK isoform knockout to maintain oxidative capacity. (Indeed, in skeletal muscle there can be a marked increase in CS activity.)

Thus, if one expects CS activity to increase to compensate for falls in CK activity, as is most markedly seen in murine skeletal muscle, then the tight correlation found here may be unexpected. If however one believes that the two are so closely related in health that this relation is not much altered in pathological hypertrophy, or that both are concordantly depressed in pathological hypertrophy, the correlation found here would be unsurprising.

CK total activity and total creatine concentration

THIS STUDY

The finding that total creatine correlates with total CK activity indicates that creatine is not present in excess of amounts that would saturate CK system requirements. It is also an original observation in human myocardium which holds even when participants

with impaired LVEF are excluded.[20] The finding that total creatine correlates with CS activity supports its role as a phosphate-acceptor at the mitochondrion. The lack of correlation between CK/CS ratio and total creatine reflects the strong co-correlation between creatine and CS activity.[21]Cardiomyocyte creatine content is known to be regulated by the activity of the Na-creatine cotransporter (Ten Hove et al., 2005). But the correlations found here would indicate that (as for CS and CK) either there is some other, intrinsic, factor that controls both CS activity and creatine pool size concordantly in the absence of hypertrophy and HF, and/or there is some factor arising from the process of pathology hypertrophy that suppresses both concordantly.

These results also indicate the relative range over which each variable is spread. Given the 3-fold variation in each of CK total activity and total creatine, and their correlation, creatine content could be limiting at least some hearts. As modest (1.3-fold) increases in MtCK activity are cardioprotective in ischaemia-reperfused mouse hearts (Whittington et al., 2018), any future potential therapeutic augmentation of creatine or CK activity in the heart could be applicable to a substantial minority of participants undergoing cardiopulmonary bypass. This should also help guide efforts at improving the ^{1}H-MRS estimation of total creatine, as it indicates the range of sensitivity to which any noninvasive protocol should be tailored. Current ^{1}H-MRS protocols tend to be optimized for myocardial lipid quantification, and none of the published noninvasive estimates of creatine content have included series of participants with VHD.

PRIOR LITERATURE

The correlation between total CK activity and total creatine is unsurprising. Correlation between $\log_{10}$ total CK activity and cellular PCr was observed across multiple cell types, e.g. between fast and slow muscles from the same species (flounder, mouse)

[20]Pearson r(35) = 0.53, p = 8e–4 (triplicate dataset); r(33) = 0.44, p = .008 (after removing participants with impaired LVEF).

[21]Pearson r(45) = .59, p = 1e–5.

(Iyengar, 1984). There were paired increases in CK and PCr in human, rabbit and bovine myometrium in response to oestrogen or pregnancy. There was good correlation (R^2 = 0.91) between total CK activity and total creatine when plotting paired values from rat brain, heart and skeletal muscle (Bittl et al., 1987c). Paired measurements in human LV showed correlation between creatine and CK-MM activity (r = .80) in samples from accident victims' LV and atria and ventricles of organ donors or NICM patients (Nascimben et al., 1996). Paired falls in CK activity and creatine content have also been widely observed (Section 1.3), for instance in residual viable myocardium after infarction in rats (prevented by early bisoprolol treatment) (Laser et al., 1996) and in failing SHR hearts, where falls in creatine preceded falls in CK activity (Ingwall et al., 1990).

However, the mechanism underlying this correlation within myocardium remains unclear. Cardiomyocyte creatine content depends on CrT amount and activity. The strongest regulator of CrT activity is substrate inhibition by creatine; transcriptional regulation is likely to play a minor role compared with post-transcriptional and post-translational mechanisms (ten Hove et al., 2008; Zervou et al., 2016). Although CrT activity reduced in post-infarction HF in rats (ten Hove et al., 2005), the degree to which CrT expression changes in HF is unclear, as previously used anti-CrT antibodies crossreact with PDH (Speer et al., 2004). No study assessing CrT activity (by uptake of [^{14}C]creatine) has also assessed CK or CS activity. The relationship between creatine content and CK expression is not straightforward: partial creatine depletion by creatine analogue feeding reduced CK flux, but not total CK activity (Oudman et al., 2013); cardiac creatine content was unchanged in M-CK knockout (Saupe et al., 1998; Van Dorsten et al., 1998), MtCK knockout (Spindler et al., 2002) and CK DKO (Saupe et al., 1998; Steeghs et al., 1997a). One argument suggests that reduced creatine represents an adaptive change: that falls in creatine, despite reducing CK flux, attenuate the rises in ADP (and fall in ΔG_{ATP}) that would occur (via the

CK equilibrium expression) were PCr, ATP and PCr/ATP to fall yet total creatine remain unchanged (Shen et al., 1999, 2010). There could also be an unidentified factor associated with pathological hypertrophy that suppresses both CK expression and CrT activity.

CK total activity and LV volumes and mass

The relationship between total CK activity and LV volumes and mass is likely indirect. Prior to 2009, studies of DKO mice noted increased heart weight/body weight ratio (120–160% of WT) without hypertension, yet were on a mixed genetic background (Boehm et al., 2000; Gustafson and Van Beek, 2002; Kaasik et al., 2001; Momken et al., 2005; Nahrendorf et al., 2005, 2006). However, there was no hypertrophy in M-CK knockout (Nahrendorf et al., 2005), and MtCK knockout mice on a pure genetic background when compared with an unrelated strain had normal cardiac volumes, mass and function at rest and stress, with no upregulation of hypertrophic markers (β-MHC, ANP, BNP, p-skeletal actin) (Lygate et al., 2009). The story is complicated by the younger ages (all under one year) and lower work rates achieved in perfused heart models. More recently, a study of DKO hearts assessed in vivo was able to show that CK deficiency does ultimately result in hypertrophy and HF, but that the severity of dysfunction is influenced by sex, age and genetic modifiers (Lygate et al., 2012b). Thus, the correlation found here is supported by the animal data and implies a relationship between CK activity and the transition to failure in human pathological hypertrophy.

Limitations

There were not sufficient datapoints to establish the validity of the models on a fresh set of participants. This limitation probably applies more to the model coefficients than to the significance of the explanatory variables themselves. Given the modest number of samples, the coefficients should not be considered generalizable to a

wider population. However, the parameters proving significant provide insight into underlying mechanisms and should be considered hypothesis-generating.

A convenience sampling strategy was used, focussing on participants with LV dysfunction listed for surgical aortic valve replacement (SAVR) rather than transcatheter aortic valve replacement (TAVR), in order to maximise the chance of obtaining triplicate MRI, MRS and chemical extraction data. The dataset is thus more representative of participants considered fit enough to undergo SAVR. Two participants with AS and LV dysfunction were claustrophobic and did not undergo MRI or MRS but did contribute biopsy samples. As participants with LV dysfunction were in a minority this reduces the power of the relationships that might have been observed. Furthermore, most, but not all, participants had severe pressure- or volume-loading valve disease, which is a form of chronic metabolic stress. If these disease states 'recruit' a higher k_f then the inclusion of participants with mitral stenosis might have weakened the correlations observed. Had k_f been recorded during acute metabolic stress (elicited by inotropic stimulus), higher k_f may have been observed and correlations with CK V_{max} may have been stronger, but this was contraindicated by the valve disease.

Only linear models were used, as the focus was on exploring what the most likely explanatory variables were (rather than perfecting model coefficients or shapes). However the true relation with some variables is likely to be curved: it is unlikely that a plot of CK activity against LVEF or LVESVi will reach the x-axis (where CK activity is zero). Limited exploration showed that $e^{-\text{LVESVi}}$ was more powerful than LVESVi, but there was no added value for the purposes of this chapter from this kind of complication. Similarly, some prefer to divide numeric regression inputs by the standard deviation or by two standard deviations (Gelman, 2008) before assessing coefficients, but the added value here was limited.

The majority of participants included here had isolated severe AS; the aetiology of LV dysfunction was predominantly pressure overload. As no ischaemic myocardial

dysfunction group was included, the contribution of infarction to CK kinetics independent of reduced LVEF or raised LVESVi is unknown. Likewise, the meaningfulness of k_f and k_f-containing variables in hearts with LV dysfunction secondary to MI was not tested here. Given the limited numbers, it was also not possible to quantify the independent contributions of atrial fibrillation and LBBB to the LV dysfunction observed.

In the triplicate dataset (n = 37), two participants had severe primary MR and five were neither pressure nor volume loaded. As LVEF reflects both loading conditions and contractility, the coefficient for LVEF loses explanatory power; however, the finding that LVEF and LVESVi both predict CK activity independent of creatine and k_f implies a relationship between CK velocity and impaired contractility, predominantly in pressure-loaded conditions.

4 ATP delivery rates in chronic pressure loading by aortic stenosis

This chapter aims to:

- Relate in the non-failing heart the stage of adaptation to pressure overload (AS) with estimated myocardial ATP delivery rate.
- Investigate whether myocardial ATP delivery rate falls after transition to failure in pressure overload.
- Investigate the effect of AVR on myocardial energetics.
- Establish to what degree do invasively measured CK maximum velocity, creatine and CK isozyme distribution vary between patients with AS with preserved or impaired LVEF.

4.1 INTRODUCTION

AS is the second commonest VHD in participants aged > 65, when VHD is defined as at least moderately severe valve disease (Nkomo et al., 2006), and the most commonly intervened upon VHD in Europe and North America (Baumgartner et al., 2017; Iung et al., 2003). In a UK community population aged >18 and referred for echo for suspected HF, the prevalence of at least moderate AS was 3.2% (Marciniak et al.,

2017). Untreated severe symptomatic AS can be rapidly fatal, with well-timed intervention (AVR) able to restore much of the life expectancy at risk. Concordant with the idea of AS as a disease of both the AV and the left ventricle (LV), guidelines suggest that AVR is indicated in severe AS when there are concomitant symptoms (exertional dyspnoea, angina or syncope) (class IB) or LV dysfunction (LVEF < 0.50) not due to another cause (class IC) (Baumgartner et al., 2017; Nishimura et al., 2014). To warrant AVR in moderate AS, one must also require coronary bypass or surgery of the ascending aorta or another valve (class IIaC). Risk-benefit decisions about AVR timing must balance the risks of intervening with SAVR or TAVR against the risks of not intervening (active surveillance, medical therapy, or palliation). This has become a complex decision, with the evidence-base evolving on both sides.

Since the first human TAVR case (Cribier et al., 2002), the pool of patients eligible for AVR has expanded, with participants previously considered at prohibitive (extreme) surgical risk[1] shown to benefit from TAVR in the first randomized controlled trial (RCT) (Kapadia et al., 2015; Leon et al., 2010; Popma et al., 2014). With improvements in valve sizing, deliverability, positioning, procedural mortality, and major complication rates, the threshold risk at which TAVR can be recommended has since fallen, with at least non-inferiority of TAVR for mortality compared with SAVR shown in prospective RCTs in participants with symptomatic severe AS and high (Adams et al., 2014; Deeb et al., 2016; Gleason et al., 2018; Mack et al., 2015; Smith et al., 2011), intermediate (Leon et al., 2016; Reardon et al., 2017), and intermediate-

[1] "High", "intermediate" and "low" surgical risk are terms that reference conventional surgical risk scores, such as Society of Thoracic Surgeons Predicted Risk of Mortality (STS-PROM) (O'Brien et al., 2018, 2009), EuroSCORE II (Nashef et al., 2012), and EuroSCORE (Nashef et al., 1999; Roques et al., 1999). These have been used to judge eligibility for trials of SAVR versus TAVR in severe symptomatic AS. Intermediate and low risk refer to STS scores of 4–10% and <4% respectively (Kappetein et al., 2012). However, annual reestimation of STS coefficients would result in participants judged high-risk in 2009 being reclassified as intermediate risk in 2015 (Rogers et al., 2017). Furthermore, these scores were not originally designed for the TAVR population, and do not incorporate factors relevant to TAVR such as favourable transfemoral access, porcelain aorta, frailty, and functional disability (Hermiller et al., 2016).

low (Thyregod et al., 2019, 2015) surgical risk.[2] These findings are supported by the SAPIEN 3 observational study of intermediate-risk patients (Thourani et al., 2016). At the time of writing, the first trials indicating at least non-inferiority of TAVR versus SAVR in low-risk patients at two years were published (Mack et al., 2019; Popma et al., 2019). Current trials in this field[3] are either assessing the role of TAVR in participants with symptomatic severe AS and low surgical risk (NOTION-2 (NCT02825134)), or unconventional indications for AVR: moderate AS with impaired LV function (TAVR UNLOAD (NCT02661451)), asymptomatic severe AS with a negative treadmill stress test (EarlyTAVR (NCT03042104)), and asymptomatic severe AS with mid-wall fibrosis on MRI (EvoLVeD (NCT03094143)).

In parallel with the shift in focus to lower-risk participants with severe symptomatic AS has been a growing appreciation of the inadequacy of the LVEF < 0.50 threshold to capture all participants at increased risk. VHD guidelines have added further recommendations for intervention in asymptomatic severe AS – symptoms revealed on exercise testing (class IC), abnormal falls in blood pressure (BP) on exercise testing, AV peak velocity (V_{max}) > 5.5 m/s, severe AV calcification with V_{max} progression > 0.3 m/s/year, BNP levels > 3-fold age- and sex-corrected upper limit of normal without other explanation, and systolic pulmonary artery pressure > 60 mmHg at rest without other explanation (all class IIaC). Although all reasonable markers of an increased risk of not intervening, the search for an early and accurate marker of LV dysfunction continues. The rest of this section is thus structured around: why the LVEF < 0.50 threshold for the definition of 'reduced LVEF' in severe AS is more specific than sensitive for the detection of LV dysfunction; what newer markers of myocardial dysfunction (global longitudinal strain (GLS), mid-wall fibrosis) can and cannot add; and whether metabolic reserve assessment (e.g. a non-invasive estimate of CK capacity) could play a role in risk assessment.

[2]Reviewed (Al-Azizi et al., 2019; Siontis et al., 2016).
[3]Reviewed (Cahill et al., 2018).

The LVEF < 0.50 threshold for the definition of 'reduced LVEF' in severe AS is insensitive for the detection of LV dysfunction

LVEF, the proportion of left ventricular end-diastolic volume (LVEDV) ejected during systole, is a continuous variable dichotomized into values that we accept connote higher risk and values we may falsely feel reassured about (Baicu et al., 2005; Carabello, 2002). For the detection of contractile dysfunction, any threshold LVEF represents a trade-off: lower thresholds are more specific, but less sensitive. The most appropriate threshold depends on the substrate in question (acute and chronic haemodynamic loading conditions, contractility and inotropic status, heart rhythm and rate), the participant's age and sex, the measured parameter (e.g. ejection fraction (EF), fractional shortening, GLS, mitral annular plane systolic excursion (MAPSE), stroke work), and imaging modality. The problem in AS is that reduced LVEF may indicate increased afterload with or without depressed contractility. This can be difficult to judge. In borderline cases or where there is mixed VHD, serial measurements, ideally with a single modality (Pellikka et al., 2018), can be particularly helpful.

LVEF has become the most widely used indicator of systolic function, partly because of its ease of understandability (across specialties) and applicability (across vendors and modalities). Reference ranges (mean $\pm$ 2 SD) for normal LVEF by Simpson's biplane 2D echocardiography were recently updated from $\geq$ 0.55 (Lang et al., 2005) to 0.52–0.72 (men), 0.54–0.74 (women) (Lang et al., 2015), and $\geq$ 0.52 (men), $\geq$ 0.54 (women) (Galderisi et al., 2017). By comparison, normal LVEF ranges (mean $\pm$ 2 SD) are higher by SSFP magnetic resonance imaging (MRI) at 1.5T: 0.57–0.75 (men, age < 60), 0.59–0.77 (men, age $\geq$ 60), 0.58–0.76 (women, age <60), and 0.60–0.78 (women, age $\geq$ 60) (Kawel-Boehm et al., 2015). Despite marginally higher reference LVEFs at 3T, a consistent finding is that LV volumes tend to decrease with age (Gandy et al., 2016). Disease-specific LVEF thresholds already take haemodynamic loading into account: the cut-off LVEF warranting intervention is

0.50 in asymptomatic severe AS (class IC) and asymptomatic severe chronic aortic regurgitation (class IB), but in asymptomatic severe chronic primary MR, an LVEF $\leq$ 0.60 and/or left ventricular end-systolic diameter (LVESD) $\geq$ 45 mm predict worse post-operative outcome independent of symptom status and indicate intervention (class IB) (Baumgartner et al., 2017). Considering that increased afterload and systolic wall stress tend to depress LVEF and that reduced afterload and increased preload tend to flatter LVEF – all other factors fixed – these seem reasonable. However, these thresholds do not take into account (1) the effect of concentric remodelling, which reduces left ventricular stroke volume (LVSV), mandates higher LVEFs to preserve LVSV, and results in higher LVEFs for similar extents of sarcomere shortening (Aurigemma et al., 1995; Dumesnil and Shoucri, 1991); (2) the impact of any myocardial vulnerability on the response to abnormal haemodynamic loading.

Participants with low-flow low-gradient severe AS (aortic valve area (AVA) < 1.0 cm^2, mean gradient < 40 mmHg, left ventricular stroke volume index (LVSVi) < 35 ml/m^2) with LVEF $\leq$ 0.40 are uncommon, comprising 5–10% of participants with severe AS (Pibarot and Dumesnil, 2012). Low-flow low-gradient severe AS with LVEF < 0.50, or ACC/AHA Stage D2, was seen in 15% of 971 patients with evaluable echos in the PARTNER 1A (high-risk) and 1B (prohibitive-risk) trials (Herrmann et al., 2013). These patients carry a poor prognosis (Brogan et al., 1993; Connolly et al., 2000; Herrmann et al., 2013; Monin et al., 2003). Participants with severe AS and LVEF < 0.50 constituted 15% of patients undergoing SAVR in one cohort of 2017 participants (Dahl et al., 2015), of which asymptomatic participants are even more uncommon, with one study of 9940 adults $\geq$ age 40 with severe AS documenting a prevalence of 0.4% and five-year mortality of 48% (Henkel et al., 2012). At odds with current guideline definitions of LV dysfunction in severe AS as LVEF < 0.50, several recent observational studies dating from 2015 and all using Simpson's biplane echocardiography support the contention that this threshold is too conservative if one

wants to detect myocardial dysfunction. A substantial minority – 17% of participants with severe AS undergoing SAVR (Dahl et al., 2015), and 31% of participants with asymptomatic severe AS (Lancellotti et al., 2018) – have an LVEF in the range 0.50–0.59, a range I will call 'borderline'. These studies document increased mid-term overall mortality in this borderline group, as compared with participants with LVEF $\geq$ 0.60:

1. In 928 participants (mean age 78) diagnosed with severe AS (time zero) at Mayo Clinic, Rochester, Minnesota, LVEF < 0.50 (n = 196) predicted higher all-cause mortality than LVEF $\geq$ 0.50 (n = 732), and LVEF in the range 0.50–0.59 (n = 151) predicted higher all-cause mortality than LVEF $\geq$ 0.60 (n = 581) – both comparisons over a median follow-up of 3.3 years (Ito et al., 2018). The best cut-off LVEF at the –3 year timepoint to predict LVEF < 0.50 at time of diagnosis of severe AS was 0.60.

2. In 1678 participants (mean age 76) with asymptomatic or minimally symptomatic severe AS, an LVEF of 0.50–0.54 (n = 239) at time of diagnosis of severe AS predicted increased all-cause mortality compared with LVEF $\geq$ 0.55 (n = 1439) over a median follow-up of 3.6 years, irrespective of conservative or surgical management (Bohbot et al., 2019).

3. In 1375 participants with asymptomatic moderate or severe AS and LVEF $\geq$ 0.50 at entry to the Heart Valve Clinic International Database, an LVEF of 0.50–0.59 at time of diagnosis of severe AS predicted increased all-cause mortality compared with LVEF $\geq$ 0.60 over a mean follow-up of 27 months (Lancellotti et al., 2018). The best cut-off LVEF to predict overall mortality was 0.60 in severe AS (n = 861).

4. 3794 patients with severe AS (mean gradient > 40 mmHg) enrolled in the CURRENT AS registry across 27 Japanese centres were stratified by LVEF

(< 0.50, 0.50–0.59, 0.60–0.69, ≥ 0.70) and strategy (initial AVR or conservative) (Taniguchi et al., 2018). Given an initial conservative strategy, all-cause mortality (adjusted for confounders in the lower LVEF strata such as higher STS scores and higher incidences of previous MI, CAD and renal disease) over a median 3.7 year follow-up progressively increased with decreasing LVEF stratum, relative to LVEF ≥ 0.70. The primary outcome (AV-related death or HF hospitalisation) was increased in the two lowest LVEF strata.

5. In 1065 patients with at least mild AS at baseline (severe AS, n = 565) followed for a median 5.7 years, independent predictors of mortality after multivariable adjustment were LVEF and LVSVi (Capoulade et al., 2016). The best cut-offs to predict 1-year all-cause mortality were 0.56 for LVEF and 34 ml/m^2 for LVSVi (flow). Stratified by LVEF and flow, all-cause mortality decreased across strata: low flow, low LVEF > normal flow, low LVEF > low flow, normal LVEF > normal flow, normal LVEF. In the subset with baseline asymptomatic status (n = 212), LVSVi but not LVEF independently predicted all-cause mortality after multivariable adjustment.

6. In 2017 participants with symptomatic or asymptomatic severe AS who underwent SAVR from 1995–2009 at Mayo Clinic, preoperative LVEF 0.50–0.59 (n = 331) predicted increased mortality compared with LVEF ≥ 0.60 (n = 1386) over a mean follow-up of 5.3 years, irrespective of the presence of symptoms or need for coronary revascularization (Dahl et al., 2015).

The above evidence however has not carried over to the 2018 STS risk calculator (O'Brien et al., 2018), which (like the previous STS score and 1999 EuroSCORE) still maps LVEF values > 0.50 to 0.50 irrespective of operation type (Table 3, O'Brien et al. (2009)). This may be because of a historical emphasis on stratifying LVEF as < 0.30, 0.30–0.50 and > 0.50. Multiple studies have assessed outcomes with respect

to a group with LVEF > 0.50 but not explored higher LVEF strata[4]; prior to these, no study explicitly supported the guideline cut-off of LVEF < 0.50 for intervention in asymptomatic severe AS, as studies were either single-arm in design or lacked comparison groups with LVEF > 0.50.[5] Thus current guidelines fail to recognise that a substantial minority of participants with asymptomatic AS, previously regarded as unremarkable, in fact carry a worse prognosis than conventionally appreciated.

It is also becoming recognised that there is a subset of participants whose LVs, in the face of pressure overload, develop more marked LVEF depression and are more likely to be diagnosed with LVEF < 0.50 (frank LV dysfunction) at the time of diagnosis of severe AS. In 928 patients (mean age 78) with a median three serial echocardiograms prior to their first diagnosis of severe AS (time zero), participants with LVEF < 0.50 at time zero (n = 196) were more likely to have atrial fibrillation (AFib) or flutter, left bundle-branch block (LBBB), CAD, prior MI, and higher NT-proBNP, while AVAs were similar (Ito et al., 2018). LVEF in these participants was already on a declining trajectory while the AS was moderate in degree. An LVEF of 0.50–0.59 in the presence of moderate AS identified increased risk of having LVEF < 0.50 at the time of diagnosis of severe AS. (Other predictors included LBBB and low log medial e'.) However, if we assume LVEFs were normally distributed at timepoint –3 years, a timepoint where AS was moderate, 26% of the group with severe AS and LVEF < 0.50 at timepoint zero had LVEF 0.50–0.59, and 23% had LVEF > 0.60. Clearly a single timepoint identification of borderline LVEF cannot clinch the diagnosis of deteriorating LVEF in any given individual.

The important observation here is not only that a minority of participants' ventricles appear to be more intolerant of pressure overload, but that their LVEF is deteriorating before the development of severe AS. Notwithstanding the inclusion

[4]Not reviewed here (Baron et al., 2016; Clavel et al., 2015; Goldberg et al., 2013; Herrmann et al., 2013; Mihaljevic et al., 2008; O'Toole et al., 1978; Pellikka et al., 1990).

[5]Reviewed (Généreux et al., 2016).

of participants with concomitant moderate MR, we can infer that in some ventricles with LVEF 0.50-0.59, even moderate AS poses enough of an afterload challenge to be associated with LVEF deterioration. This supports the argument that 'normal LVEF' in moderate or severe AS be defined as "at least" 0.60 (Ito et al., 2018).[6]

We should also question the paradigm of the natural history of LV decompensation in the face of chronic pressure overload. Classically this describes the development of concentric hypertrophy which minimizes wall stress at the expense of raising filling pressures.[7] Given fixed intrinsic contractility, LVs experiencing higher wall stress have lower LVEF (Carabello et al., 1980). Cavity dilation is considered a late complication, where 'late' conventionally refers to 'after the development of severe AS'. However, the observation that some ventricles dilate (transition to failure) earlier, when the pressure overload is moderate, implies some intrinsic (unspecified) myocardial vulnerability in a subset of patients. Such ventricles would have a lower than expected LVEF for any given wall stress. While the reasons for this pressure overload-intolerance are unclear, whether reduced CK (or metabolic) reserve could be contributing is an intriguing question.

These studies challenge us to reconsider what we mean by normal LVEF in the presence of moderate or severe pressure overload. To my mind there are four options:

1. The LVEF is normal if it falls within expected normal ranges for age, sex, BSA and measurement technique in the absence of VHD.

2. The LVEF is normal if today's measurement compares well with serial prior

[6] It also raises the prospect of prospective trials randomizing patients with moderate AS and LVEF < 0.60 to early intervention. There are at least three provisos here. (1) No RCT evidence of benefit of intervention in asymptomatic severe AS exists. (2) If these ventricles are intrinsically more pressure overload intolerant, they would fare worse in the case of patient-prosthesis mismatch. (3) Any raising of the LVEF threshold would significantly increase the numbers of asymptomatic patients warranting AVR: although < 1% of all participants with severe AS were asymptomatic with LVEF < 0.50 (Henkel et al., 2012), 14% of asymptomatic or minimally sympomatic participants with severe AS and LVEF $\geq$ 0.50 had LVEF 0.50–0.54 (Bohbot et al., 2019) and 31% of asymptomatic participants with severe AS and LVEF $\geq$ 0.50 had LVEF 0.50–0.59 (Lancellotti et al., 2018). More specificity would likely be required.

[7] Wall stress is proportional to pressure $\times$ radius / wall thickness (Grossman et al., 1975).

(normal) measurements in the same individual prior to the development of pressure overload.

3. The LVEF is normal if after relief of pressure overload and wall stress by AVR there is an expected increase in LVEF indicating normal contractility (without which one would suspect permanent injury in a pressure-intolerant myocardium).

4. The LVEF is normal if (in the asymptomatic patient and all other things fixed) it is not associated with worse mid-term survival.

With the first three options, the difficulty is that we need an expected afterload (or wall stress) adjustment factor for LVEF, which is unfortunately not well established in large numbers of participants (Carabello et al., 1980). Further provisos regarding the AS population include: participants > age 70 and/or with hypertension are in the majority in severe AS, yet are poorly (if at all) represented in the reference range studies available; some participants remodel with more pronounced concentricity, which would be expected to flatter LVEF, while others develop LBBB or AFib, which would be expected to depress LVEF. Even with the observational studies mentioned here bolstering the fourth option, the problem remains of significant overlap between groups when separated solely by LVEF. Future mortality risk models in asymptomatic severe AS will therefore need to incorporate LVEF as a continuous variable alongside other independent predictors.

Alternative markers of myocardial dysfunction in severe AS

Presenting with symptomatic severe AS and an LVEF < 0.50 is not uncommon (15% in a recent large SAVR cohort (Dahl et al., 2015)), but as this is arguably a stage where irreversible myocardial injury has been sustained, an earlier detection of myocardial

dysfunction would be desirable. To this effect, several non-invasive markers (not included in current guidelines) have been shown to have prognostic value.

Enlargement of the interstitial space by diffuse reactive fibrosis, and later, cell death and replacement fibrosis, is an established part of pathological hypertrophy. This mechanism is linked to myocardial stiffening, transition to HF, arrhythmias and mortality, with excess risk persisting after AVR in participants with residual hypertrophy and higher collagen volume fractions (Gavina et al., 2016). Midwall fibrosis on late gadolinium enhancement (LGE) MRI (Barone-Rochette et al., 2014; Dweck et al., 2011; Musa et al., 2018; Vassiliou et al., 2017; Weidemann et al., 2009), extracellular volume expansion on MRI (Chin et al., 2017; Treibel et al., 2018), and histological fibrosis (Azevedo et al., 2010; Herrmann et al., 2011) capture overlapping but not identical pictures of collagen remodelling, and are independent prognostic markers. Low LV GLS, a marker that reflects the susceptibility of longitudinal subendocardial fibres to interstitial fibrosis, identifies systolic dysfunction earlier than falls in LVEF, and predicted all-cause mortality in asymptomatic moderate or severe AS with LVEF > 0.50 on individual patient-data meta-analysis (Magne et al., 2019).[8]

Low flow, first proposed by Hachicha et al. (2007) as a distinct phenotype in AS and usually defined as LVSVi < 35 ml/m^2 by echocardiography, is a predictor of all-cause mortality independent of LVEF and mean gradient (Capoulade et al., 2016; Dayan et al., 2015; Herrmann et al., 2013; Le Ven et al., 2013; Rusinaru et al., 2018). Factors reducing LVSVi may include not only impaired contractility, higher global afterload, prior MI, AFib and LBBB (as with low LVEF), but also higher degrees of concentric remodelling, subendocardial fibrosis and LV stiffening, smaller LV cavity size, and larger BSA.

[8] Reviewed (Dahl and Carter-Storch, 2019; Galli et al., 2014).

The argument for metabolic reserve assessment

There are several reasons why a non-invasive estimate of CK activity might be relevant in severe AS.

1. Given the coupling of metabolism and contractile function, it would be reasonable to consider a test of metabolic reserve as the lower-risk, complementary face of contractile reserve testing. Participants may be minimally symptomatic because they have learnt to not exert themselves. Controlled exercise testing to elicit symptoms or abnormal BP responses can be helpful and safe in the right hands, but these are older participants with relative contra-indications to exercise and dobutamine stress: fixed stroke-volume reserve and high intra-cavity developed pressures.

2. As observed above, some but not all pressure overloaded ventricles with LVEF 0.50–0.59 are on a downward trajectory and more specificity than LVEF or LVEF trajectory is needed to identify higher risk patients. Future risk models will likely need to incorporate multiple independent mortality predictors, including LVSVi, GLS, and markers of pathological hypertrophic remodelling (midwall fibrosis, ECV) (see refs above). However, these do not completely explain why some but not all patients with severe AS develop otherwise unexplained reduced LVEF. Reduced metabolic reserve could represent an early and specific marker of myocardial dysfunction or vulnerability in the face of pressure overload.

3. It may provide a mechanistic explanation of why some LVs are more likely to transition to failure given similar degrees of pressure overload, and hence a therapeutic target. Besides comorbidities, all currently proposed risk parameters detect the degree of stenosis severity (degree of calcification; AVA; V_{max}; mean gradient; global LV afterload) or the LV response to pressure overload

(hypertrophy; EF; SVi; GLS; BNP) or both (valvulo-arterial impedance). In the absence of a clear reason for LV dysfunction (prior MI), any LV dysfunction found is currently considered 'otherwise unexplained' and attributed to pressure overload. The contribution of any myocardial vulnerability predating the pressure overload is unexplored. Our ignorance of what mechanisms constitute this vulnerability is reflected in the silence of guidelines on participants with moderate AS and unexplained LV dysfunction, or asymptomatic severe AS and unexplained borderline LV function (LVEF 0.50–0.59). Medical therapy for pressure overload amounts to standard heart failure therapy originally designed for post-infarct or nonischaemic cardiomyopathy in the absence of VHD. What metabolic reserve testing promises is an idea of not just whether a ventricle is intrinsically more intolerant of pressure overload, but why.

4.2 RESULTS

Participants

As per Table 2.1 (p. 54), I recruited participants for this chapter to three AS groups and two non-hypertrophied (NH) comparison groups (healthy volunteers (HV) and a NH group undergoing surgery) (Table 4.1). The AS groups were used as models of pressure overload-induced pathological hypertrophy, while the operated NH group represented a non-hypertrophied comparison group for biopsy-derived measures. Baseline echocardiography (Table 4.2) was used to provisionally assign group membership and was not repeated for research purposes. Group assignment was confirmed after MRI.[9] Given the preceding discussion, the cut-off LVEF for impaired function in severe AS was set to 0.55.

[9]More participants were finally assigned to sevAS-pEF than originally planned, and two participants with mitral stenosis dropped out of the NH group into a MS-rEF group.

For participants' ages, BMI, sex, New York Heart Association (NYHA) functional class, BP, 6 minute walk test distance, serum creatinine, medical and drug history, and ECG findings, see Table 4.3. Details for the HV group are provided in Table 5.1 (p. 176). Mean (SD) ages were 75 (8) in modAS, 72 (8) in sevAS-pEF, 72 (9) in sevAS-rEF, 45 (19) in HV, 67 (10) in NH and 62 in MS-rEF. As healthy volunteers were recruited for the primary purpose of comparison with athletic remodelling (Chapter 6), they were not all age-matched. Comparing NH (operated) and the three AS groups, mean age, median BMI, and proportion male did not significantly differ, but systolic BP, 6 min walk distance, serum creatinine, prevalence of LBBB, ECG strain pattern or anterolateral T-wave inversion and proportion using spironolactone or oral anticoagulation did. Participants with modAS were asymptomatic.

Some participants with sevAS-pEF (not included in Tables 4.1–4.4) underwent ^{1}H-MRS for creatine estimation instead of TRiST as part of a separate study; their LV biopsies were analysed in the same way as participants undergoing TRiST.

I have included results of biopsy measures of participants with severe MR (sevMR) or MS-rEF where this aids comparison in the Appendix.

LV mass and volumes

LVMi increased moving from healthy volunteers (HV) across the three AS groups to peak in sevAS-rEF, as might be expected given that these were modelling progressively later stages of pathological hypertrophy (Figure 4.1, Panel A; Table 4.4). By design, LVEF was preserved in the control groups and two AS groups (Figure 4.1, Panel B). As expected, LVEDVi and LVESVi were reduced in sevAS-pEF and increased in sevAS-rEF. LVSVi was reduced in sevAS-rEF (Figure 4.2). LVM/LVEDV ratio were increased in all AS groups, with the greatest increase in sevAS-pEF.

RV dimensions are charted in the Appendix (Figure A.3, Table A.2).

Table 4.1: Participants recruited to AS or comparison groups

Abbreviation	Description	Recruited	Biopsied
ModAS	Moderate AS	14	n/a
SevAS-pEF	Severe AS, LVEF ≥ 0.55	30	26
SevAS-rEF	Severe AS, LVEF < 0.55	15[a]	11[b]
HV	Healthy volunteers	20	n/a
NH	Non-hypertrophied with mitral stenosis, ascending aortic aneurysm or left atrial mass	8[d]	7[e]
MS-rEF	Mitral stenosis but found to have LVEF $\leq$ 0.50 at MRI	2	2

[a] 13 underwent MRI; 2 were claustrophobic.
[b] 11 of 15 underwent SAVR; 4 of 14 underwent TAVR and could not be biopsied. 11 were analysed for total creatine; 10 were sufficient to also measure CK total activity.
[d] 5 had mitral stenosis, 1 ascending aortic aneurysm, and 2 left atrial mass.
[e] 7 were biopsied; one was missed due to emergency operation rescheduling. 6 of 7 biopsies were analysed; one was ruined by premature fixation for EM before freezing.

Table 4.2: AS severity on clinical echocardiography[a]

Parameter	ModAS	SevAS-pEF	SevAS-rEF
Peak gradient	45 (40, 50)	81 (73, 89)	66 (49, 82)
Mean gradient	24 (21, 27)	46 (41, 51)	38 (28, 48)
Peak velocity	3.4 (3.2, 3.5)	4.4 (4.1, 4.7)	4.1 (3.6, 4.5)
DVI[b]	0.32 (0.25, 0.38)	0.24 (0.21, 0.27)	0.18 (0.15, 0.21)
AVA (by VTI)[c]	1.10 (0.92, 1.27)	0.87 (0.70, 1.05)	0.65 (0.50, 0.81)

[a] Mean (95% CI) values for 14 patients with modAS, 30 patients with sevAS-pEF, and 13 of 15 patients with sevAS-rEF who underwent MRI. Gradients given in mmHg, velocity in m/s, and AVA in cm^2.
[b] Dimensionless velocity index.
[c] Velocity time integral.

Table 4.3: Participants' medical and drug history[a]

Parameter	NH	modAS	sevAS-pEF	sevAS-rEF
n	8	14	30	15
Age (years)	67 (10)	75 (8)	72 (8)	72 (9)
BMI (kg/m^2)	23 (21, 30)	26 (24, 32)	28 (25, 33)	29 (26, 31)
Male (%)	1 (13)	8 (57)	15 (50)	10 (67)
NYHA 1 (%)	3 (38)		8 (27)	2 (13)
NYHA 2 (%)	3 (38)		13 (43)	8 (53)
NYHA 3 (%)	2 (25)		9 (30)	5 (33)
HR (/min)	76 (69, 90)	61 (53, 89)	65 (58, 71)	69 (62, 98)
SBP (mmHg) $*$	120 (23)	143 (25)	145 (20)	129 (14)
DBP (mmHg)	70 (13)	72 (16)	74 (11)	73 (8)
MAP (mmHg)	87 (15)	96 (18)	98 (12)	92 (8)
6mwt (m) $*$	389 (147)	465 (144)	425 (118)	310 (155)
Serum Cr (µmol/l) $*$	60 (10)	84 (19)	78 (20)	89 (21)
History:				
DM (%)	2 (25)	1 (7)	3 (10)	1 (7)
Hypertension (%)	3 (38)	7 (50)	18 (60)	7 (47)
VTE (%)	1 (13)	0 (0)	2 (7)	1 (7)
TIA/stroke (%)	1 (13)	2 (14)	4 (13)	1 (7)
Smoker (%)	0 (0)	1 (7)	3 (10)	1 (7)
Prior smoker (%)	3 (38)	2 (14)	15 (50)	4 (27)

[a] Counts given as number (%); continuous variables as mean (SD) or median (IQR). Parameters differing between the four groups at $p < .05$ level are marked $*$. NYHA, New York Heart Association symptom class; HR, heart rate; SBP, systolic BP; DBP, diastolic BP; MAP, mean arterial pressure; 6mwt, 6 minute walk distance; Serum Cr, serum creatinine; DM, diabetes mellitus; VTE, venous thromboembolism; TIA, transient ischaemic attack.

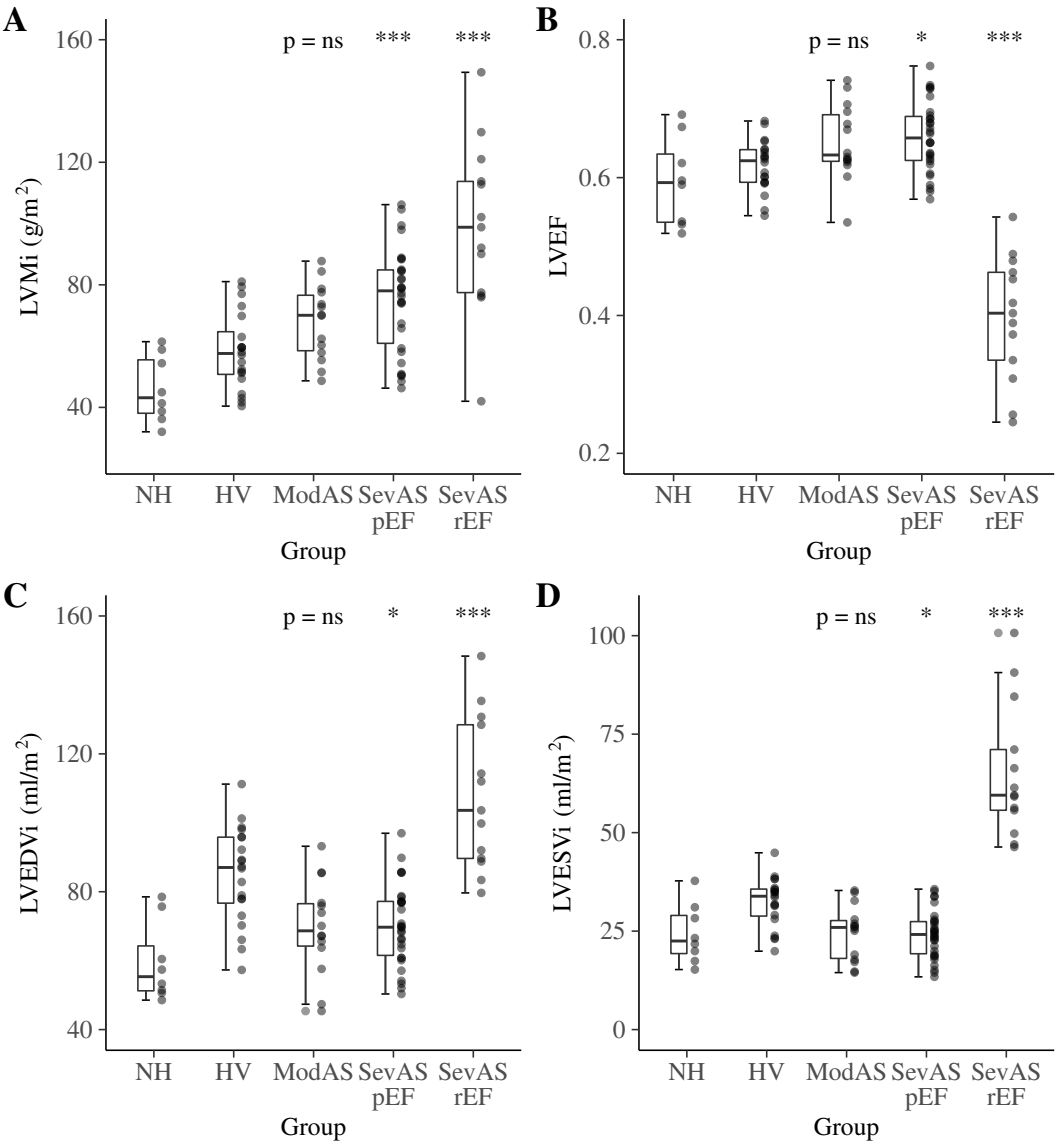


Figure 4.1: LVMi, LVEF, and LV volumes in two control and three AS groups, in order of ascending LVMi. Post hoc tests were performed with the healthy volunteer group as reference (p-values marked with asterisks at top of each plot). *Each boxplot indicates 25th, 50th, and 75th centiles; the whiskers extend to the maximum value of the data that is within 1.5 times the IQR over the third quartile, and to the minimum value of the data that is within 1.5 times the IQR under the first quartile. Values outside the whiskers are depicted with circles. Beside each boxplot individual datapoints are shown with 50% transparency, with darker areas indicating areas of overlap.*

Table 4.3: Participants' medical and drug history (AS)[a] (continued)

Parameter	NH	modAS	sevAS-pEF	sevAS-rEF
ECG:				
AFib (%)	4 (50)	3 (21)	5 (17)	3 (20)
LBBB (%) ∗	0 (0)	0 (0)	1 (3)	5 (33)
TWI/strain (%) ∗	0 (0)	2 (15)	12 (40)	10 (67)
QRS width (ms) ∗	78 (74, 83)	97 (83, 110)	94 (84, 100)	102 (96, 150)
Drugs:				
Beta-blocker (%)	4 (50)	5 (36)	11 (37)	7 (47)
ACE-I/ARB (%)	3 (38)	7 (50)	13 (43)	7 (47)
MRA (%) ∗	0 (0)	0 (0)	0 (0)	6 (40)
Loop diuretic (%)	1 (13)	1 (7)	7 (23)	5 (33)
Antiplatelet (%)	0 (0)	4 (29)	13 (43)	3 (20)
OAC (%) ∗	5 (63)	2 (14)	4 (13)	3 (20)

[a] LBBB, left bundle branch block; TWI/strain, anterolateral T-wave inversion or LV strain pattern; ACE-I, angiotensin-converting enzyme inhibitor; ARB, angiotension receptor blocker; MRA, mineralocorticoid receptor antagonist; OAC, oral anticoagulant.

CK total activity, CS activity, total creatine, and CK capacity

Compared with NH hearts, median total CK activity was significantly lower both in sevAS-rEF (by 43%, post-hoc one-sided p=0.016) and sevAS-pEF (by 35%, post-hoc one-sided p = 0.028), resulting in a decreasing trend in median values as one moved from non-hypertrophied to sevAS-pEF to sevAS-rEF hearts (NH > AS-pEF > AS-rEF, p = .002, Figure 4.3 Panel A, Table 4.5). Median values were also 12% lower in sevAS-rEF compared with sevAS-pEF (post-hoc one-sided p = .047).

There was also a significant stepwise fall in median CS activity as one moved across the groups in order of increasing LV mass index (p = .001) (Figure 4.3 Panel B): median CS activity in sevAS-rEF was 19% lower than in sevAS-pEF (post hoc

Table 4.4: Chamber dimensions by CMR in AS and comparison groups[a]

Parameter	NH	HV	ModAS	SevAS-pEF	SevAS-rEF	MS-rEF
n =	8	20	14	30	13	2
BSA (m^2)	1.66 (1.56, 1.85)	1.82 (1.70, 2.07)	1.97 (1.87, 2.04)	1.94 (1.82, 2.12)	2.00 (1.85, 2.17)	1.76
LVMi (g/m^2)	46.0 (36.8, 55.2)	58.3 (52.5, 64.1)	68.0 (60.9, 75.0)	75.2 (68.9, 81.6)	98.6 (81.8, 115.4)	71.2
LVEF (%)	59.5 (54.1, 64.9)	61.8 (60.0, 63.5)	65.1 (61.9, 68.3)	65.9 (64.0, 67.8)	39.7 (34.1, 45.2)	43.3
LVEDVi (ml/m^2)	59.5 (49.9, 69.1)	84.6 (78.1, 91.2)	69.6 (61.7, 77.6)	70.3 (66.0, 74.7)	108.2 (94.9, 121.5)	69.1
LVESVi (ml/m^2)	24.3 (18.0, 30.6)	32.3 (29.4, 35.3)	24.6 (20.5, 28.6)	24.2 (21.9, 26.4)	65.3 (55.0, 75.6)	39.3
LVSVi (ml/m^2)	35.1 (30.2, 40.0)	52.2 (48.0, 56.5)	45.1 (40.1, 50.0)	46.2 (43.5, 48.9)	42.9 (34.6, 51.2)	29.5
LVM/LVEDV (g/ml)	0.78 (0.63, 0.94)	0.69 (0.64, 0.75)	1.00 (0.88, 1.12)	1.08 (0.99, 1.17)	0.91 (0.80, 1.02)	1.03

[a] Mean (95% CI) values given, except for BSA (median (IQR)).
[b] BSA given as median (IQR).

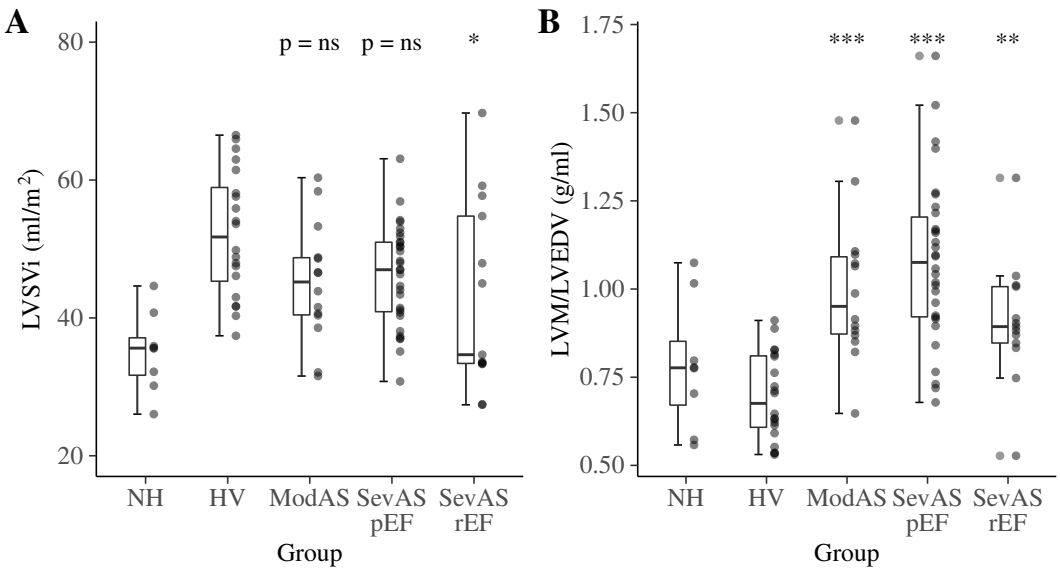


Figure 4.2: LVSVi and LVM/LVEDV ratio in two control and three AS groups. Post hoc tests performed with the healthy volunteer group as reference.

one-sided p = .02) and 30% lower than in NH (post hoc one-sided p = .007). In sevAS-pEF, median CS activity was 14% lower than in NH (post hoc one-sided p = .03).

Comparing total creatine concentration across the groups, there were no significant between-group differences (p = 0.6) and no stepwise fall in median values (p = 0.2) (Figure 4.4, Panel A). However, there was a stepwise fall in median CK capacity[10] across the groups (p = 0.016) (Figure 4.4, Panel B). Pairwise tests were not statistically significant.

Overall these findings show that associated with the development of pathological pressure overload hypertrophy and failure there was a downward gradient in CK activity, CK capacity and CS activity, such that in sevAS-rEF, both CK activity and CS activity were significantly reduced. Furthermore there was significant overlap between the sevAS-pEF and sevAS-rEF groups, the implications of which I will discuss below.

[10]Calculated by CK total activity × total creatine (Nascimben et al., 1996; Tian et al., 1996).

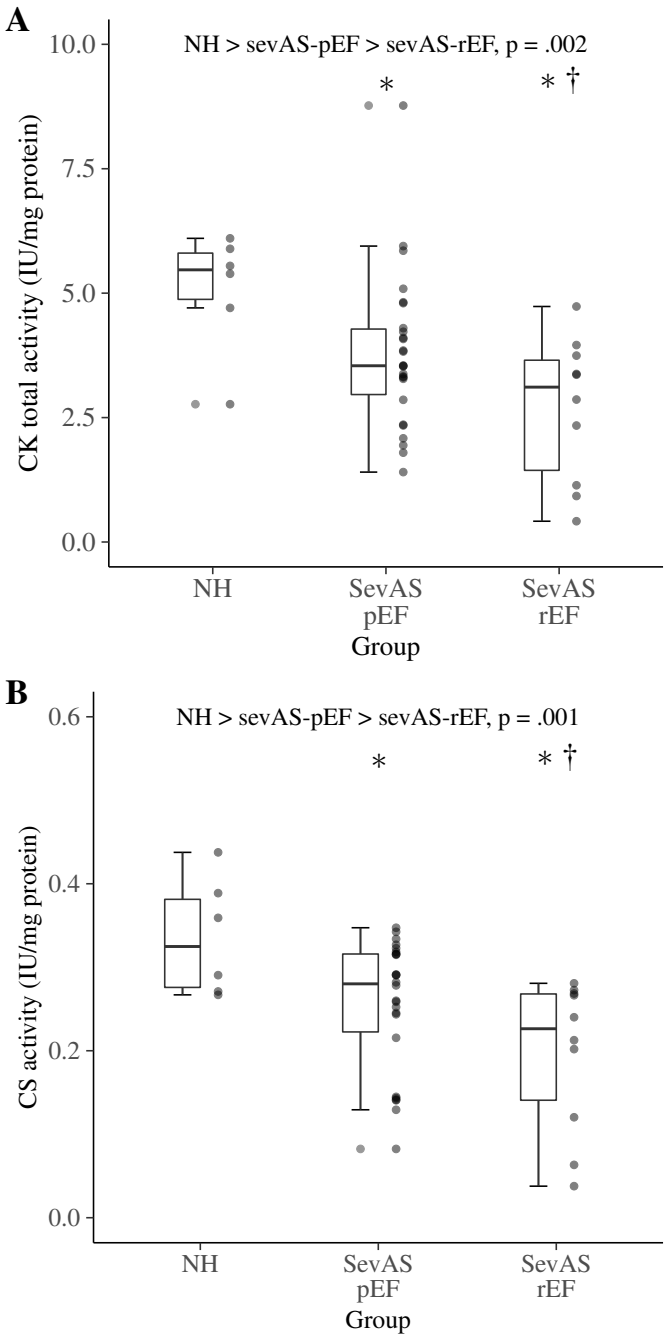


Figure 4.3: (A) CK total activity, (B) citrate synthase activity in one control group and two AS groups. Post hoc one-sided pairwise Wilcoxon rank-sum tests significant versus NH are marked $*$, significant versus sevAS-pEF are marked †.

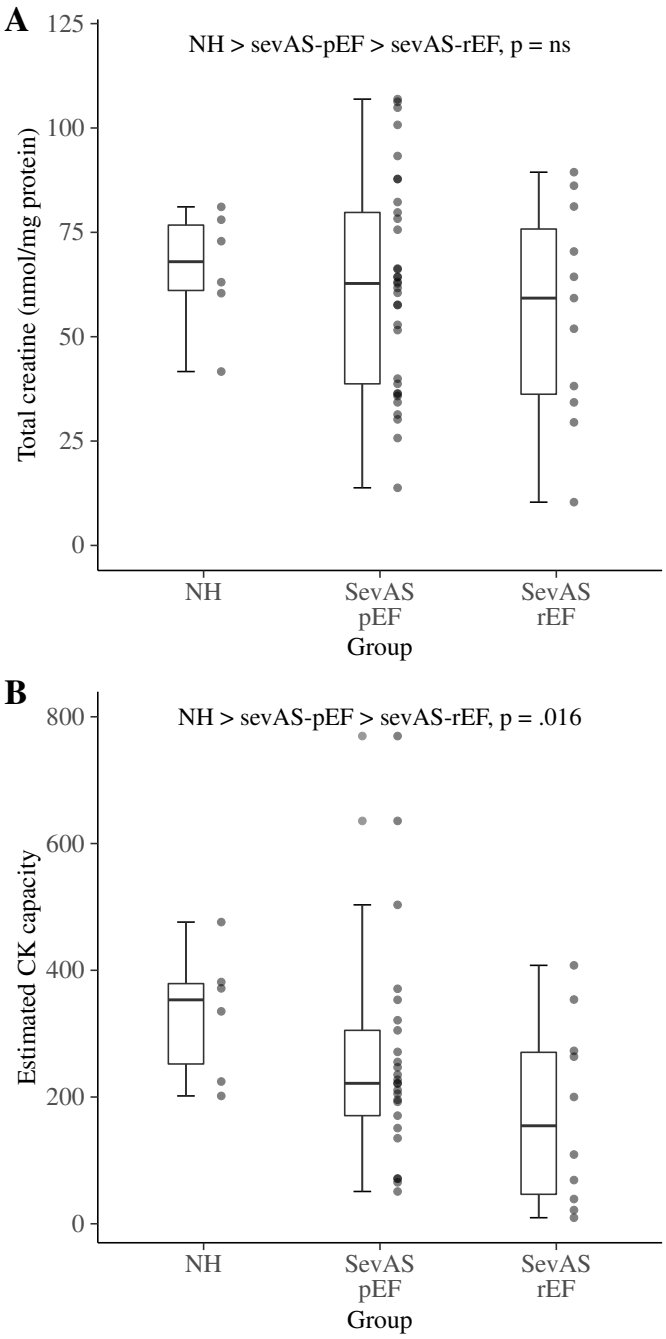


Figure 4.4: (A) Total creatine concentration, (B) CK capacity estimated by CK total activity × total creatine in one control group and two AS groups. Post hoc pairwise tests were not significant in (A–B).

Table 4.5: Baseline energetic measures in AS and comparison groups (combined)[a]

Parameter	Sig.	NH (combined)	SevAS-pEF	SevAS-rEF
n =		6	26	10
CK activity (IU/mg protein) ∗†	∗.017, †.002	5.47 (4.70, 5.89)	3.54 (2.86, 4.30)∗	3.11 (1.14, 3.75)∗†
CS activity (IU/mg protein) ∗†	∗.009, †.001	0.325 (0.271, 0.389)	0.280 (0.215, 0.316)∗	0.226 (0.120, 0.269)∗†
Estimated CK capacity †	†.016	353 (224, 381)	222 (171, 321)	155 (39, 273)
n =		6	34	11
Total creatine (nmol/mg protein)		66.2 (14.5)	63.3 (25.6)	55.9 (25.6)
n =		28	27	13
PCr/ATP ∗	∗4e–4	2.03 (0.38)	1.67 (0.25)∗	1.72 (0.38)∗
Est. [PCr] (μmol/g wet wt) ∗	∗4e–5	11.6 (2.2)	9.5 (1.4)∗	9.1 (1.9)∗
n =		27	30	12
CK k_f adj (/s)		0.25 (0.13, 0.38)	0.24 (0.15, 0.36)	0.20 (0.16, 0.30)
n =		27	27	12
Flux (k_f adj × est. [PCr]) †	†.031	2.9 (1.7, 4.1)	2.1 (1.3, 3.6)	2.0 (1.2, 2.9)

[a] Median (IQR) or mean (SD) values reported). Est. [PCr] derived from PCr/ATP × literature value for [ATP]. CK capacity estimated by CK total activity (IU/mg) × total creatine (nmol/mg). *Left column*: parameters differing significantly between NH, sevAS-pEF and sevAS-rEF (null hypothesis NH = sevAS-pEF = sevAS-rEF) are marked ∗; parameters significant for an ordered trend in medians (null hypothesis NH > sevAS-pEF > sevAS-rEF) are marked †. *Sig. column* indicates *p*-value(s) for left column. *Group columns*: post hoc pairwise tests significant versus NH are marked ∗, significant versus sevAS-pEF are marked †.

Table 4.5: Baseline energetic measures in AS and comparison groups (separated)[a] (continued)

Parameter	Sig.	NH	HV	ModAS	SevAS-pEF	SevAS-rEF
n =		8	20	14	27	13
PCr/ATP ∗	[b]	1.91 (0.37)	2.08 (0.38)	1.61 (0.36)∗	1.67 (0.25)∗	1.72 (0.38)∗
n =		7	20	14	30	12
CK k_f adj (/s)		0.40 (0.14, 0.51)	0.25 (0.12, 0.33)	0.23 (0.10, 0.36)	0.24 (0.15, 0.36)	0.20 (0.16, 0.30)
n =		7	20	14	27	12
Flux (k_f adj × est. [PCr]) †	.037	4.1 (1.8, 6.1)	2.7 (1.6, 3.8)	1.6 (0.9, 4.4)	2.1 (1.3, 3.6)	2.0 (1.2, 2.9)
n =		5			26	8
k_f adj × total creatine		21.3 (9.8, 32.3)			15.0 (9.1, 19.7)	16.3 (10.0, 24.6)
n =		3			17	3
TAN pool (nmol/mg protein)		31.0 (29.4, 40.9)			37.9 (31.5, 43.2)	46.4 (18.3, 46.8)

[a] Conventions as for Table 4.5, except here using the healthy volunteer group as reference.
[b] Null hypothesis NH = sevAS-pEF = sevAS-rEF, p = 0.175; null hypothesis HV = sevAS-pEF = sevAS-rEF, p = 2×10^{-4}.

CK isoform expression

Underlying the observed falls in total CK activity were reducing trends in median absolute activities of MtCK, CK-MM and CK-MB (p = .003, .001, .007 respectively) when moving from NH to sevAS-pEF to sevAS-rEF (Table 4.6, Figure 4.5), with post hoc tests significant at each step for MtCK (NH > sevAS-pEF, p = .05; sevAS-pEF > sevAS-rEF, p = .04) and CK-MM (NH > sevAS-pEF, p = .03; sevAS-pEF > sevAS-rEF, p = .01). Absolute activities of CK-MB were also reduced in both sevAS groups compared to NH hearts, but activities of CK-MB and CK-BB did not significantly differ between the sevAS groups. There were no differences in the relative expression of any isoforms except CK-BB, whose relative expression was increased in sevAS-rEF compared with NH (p = .02) (Figure 4.6). Between-group differences in mtCK/CS activity ratio were not statistically significant.

Biopsies from two participants with severe MR were large enough to analyse for CK isoforms and their values are tabulated for comparison (Table A.3, p. 240).

Estimated ATP delivery rates

Mean PCr/ATP ratios in modAS (1.61), sevAS-pEF (1.67), and sevAS-rEF (1.72) were reduced compared to non-hypertrophied hearts (all p < .01, Figure 4.7 Panels A and C, Table 4.5), in line with prior studies (see refs in Section 1.3). Mean values did not significantly differ between any AS group. Estimated [PCr] was derived from PCr/ATP ratio $\times$ literature values for [ATP] of 5.7 or 5.2 μmol/g/wet weight (Weiss et al., 2005), depending on HF status, and followed a similar pattern to PCr/ATP, being lower in all three AS groups than in NH hearts (all p < .001, Table 4.5) but similar between the AS groups. In contrast, there were no significant between-group differences in CK k_f (Figure 4.7 Panels B and D, Table 4.5).[11]

[11] The two participants with MS-rEF had mean PCr/ATP ratio = 1.92 and k_f adj = 0.31 /s (biopsy variables tabulated in Appendix Table A.3).

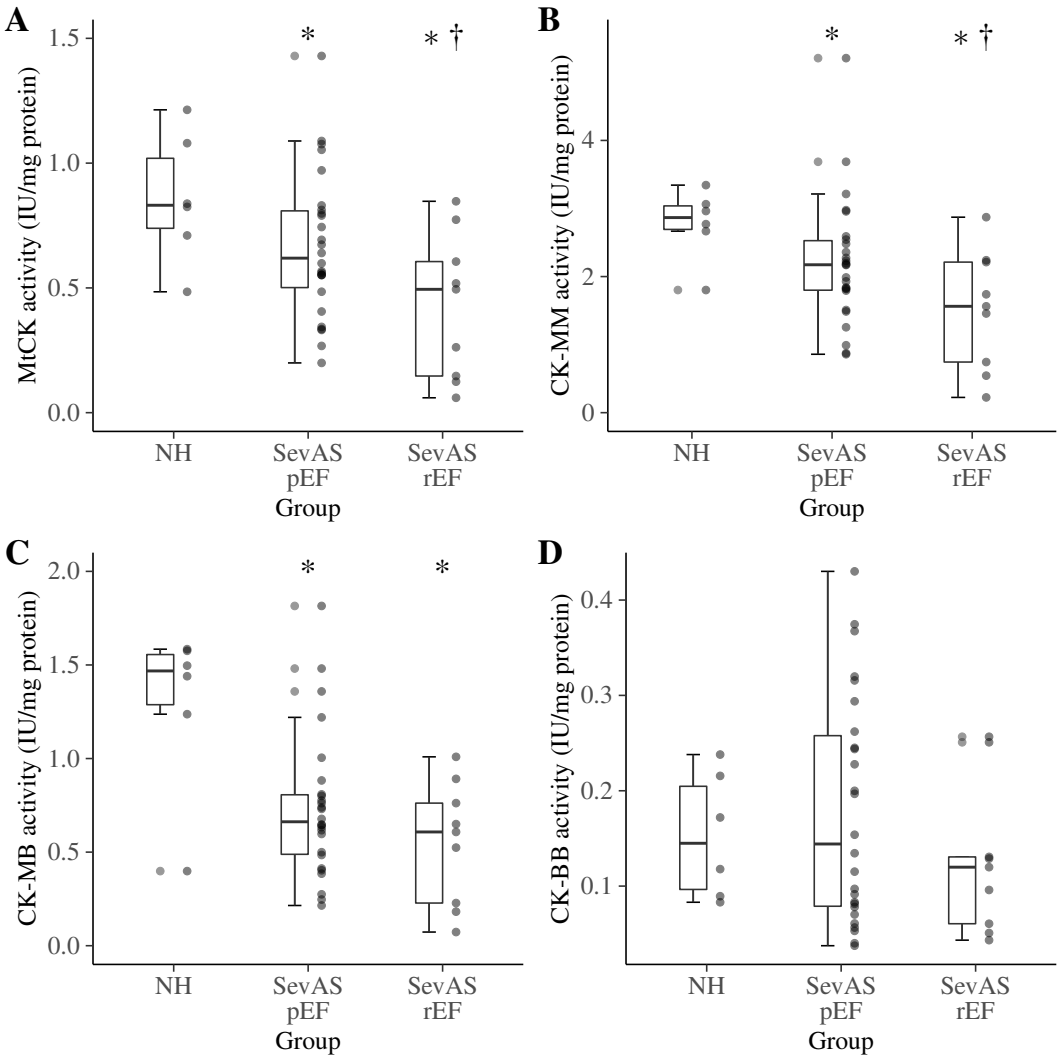


Figure 4.5: CK isoform activity (IU/mg protein) in one control and two AS groups: (A) MtCK, (B) CK-MM, (C) CK-MB, (D) CK-BB. Post hoc pairwise tests significant versus NH are marked $*$, significant versus sevAS-pEF are marked †.

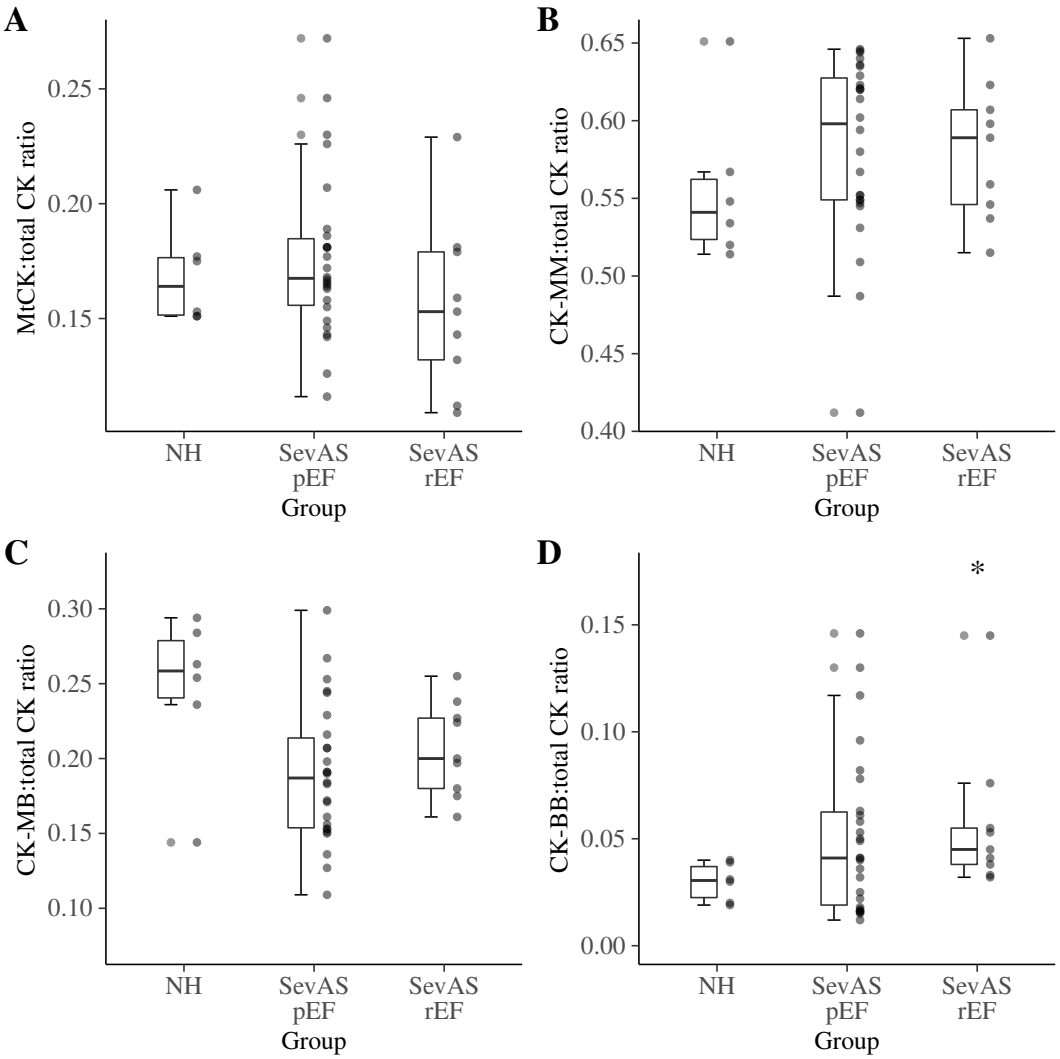


Figure 4.6: CK isoform expression relative to total CK activity (value = 1) in one control and two AS groups: (A) MtCK, (B) CK-MM, (C) CK-MB, (D) CK-BB. Post hoc pairwise tests significant versus NH are marked $*$.

Table 4.6: CK isoform absolute activities and relative expression

Parameter	Sig.	NH	SevAS-pEF	SevAS-rEF
n =		6	26	9
MtCK (IU/mg protein)∗†	∗.032, †.003	0.83 (0.71, 1.08)	0.62 (0.48, 0.81)∗	0.49 (0.15, 0.61)∗†
CK-MM (IU/mg protein)∗†	∗.015, †.001	2.87 (2.67, 3.06)	2.17 (1.79, 2.54)∗	1.56 (0.74, 2.21)∗†
CK-MB (IU/mg protein)∗†	∗.025, †.006	1.47 (1.24, 1.58)	0.66 (0.48, 0.81)∗	0.61 (0.23, 0.76)∗
CK-BB (IU/mg protein)		0.14 (0.09, 0.22)	0.14 (0.08, 0.26)	0.12 (0.06, 0.13)
MtCK (% of total CK)		16.4 (15.1, 17.7)	16.8 (15.5, 18.6)	15.3 (13.2, 17.9)
CK-MM (% of total CK)		54.1 (52.0, 56.7)	59.8 (54.9, 62.9)	58.9 (54.6, 60.7)
CK-MB (% of total CK)		25.8 (23.6, 28.4)	18.7 (15.3, 21.6)	20.0 (18.0, 22.7)
CK-BB (% of total CK)		3.0 (2.0, 3.9)	4.1 (1.8, 6.3)	4.5 (3.8, 5.5)∗
MtCK (% of CS activity, IU/IU)		2.54 (0.49)	2.60 (0.68)	2.13 (0.77)

[a] Median (IQR) or mean (SD) values are given. Conventions as for Table 4.5, p. 139. CK-B can be calculated as CK-BB + 0.5 × CK-MB.

Estimated forward CK flux was derived from estimated [PCr] $\times$ k_f adj. There was a downward trend in median resting estimated forward flux values when moving from NH to sevAS-pEF to sevAS-rEF (2.9 (1.7–4.1) > 2.1 (1.3–3.6) > 2.0 (1.2–2.9) μmol/g/s, p = .031, Figure 4.8 Panel A), but no significant differences between groups on post hoc pairwise testing. Similarly, there were no significant between-group differences in ATP delivery rates estimated by total creatine $\times$ k_f adj (Figure 4.8 Panel B).

Overall, the lack of difference in median estimated flux between SevAS-pEF and SevAS-rEF and the large overlap between all groups shows that although CK flux values became more homogenous in the SevAS-rEF group, reduced flux was not a prerequisite for having sevAS-rEF.

TAN pool

Although absolute [ATP] could not be measured noninvasively, median values for TAN pool, which comprises 85% of ATP in vivo, were not significantly different between NH, sevAS-pEF and sevAS-rEF hearts (n = 3, 17, 3 respectively) Table 4.5, Figure 4.9). This picture is likely incomplete and more complicated than presented, as the assay was unreliable and discarded for two of the four batch analyses, and as TAN pool correlated with CK total activity (Pearson r(25) = 0.52, p = .006, Figure 3.2).

Late follow-up after AVR

19 of 30 sevAS-pEF participants returned for late post-operative measurement of k_f, of whom 17 had adequate TRiST spectral quality pre- and late post-op. Participants not returning either never expected to return as they had been recruited under the AS-rEF consent form (which does not require follow-up tests) (n = 2), declined (n = 5) or had become ineligible due to pacemaker insertion (n = 3) or cognitive decline (n = 1).

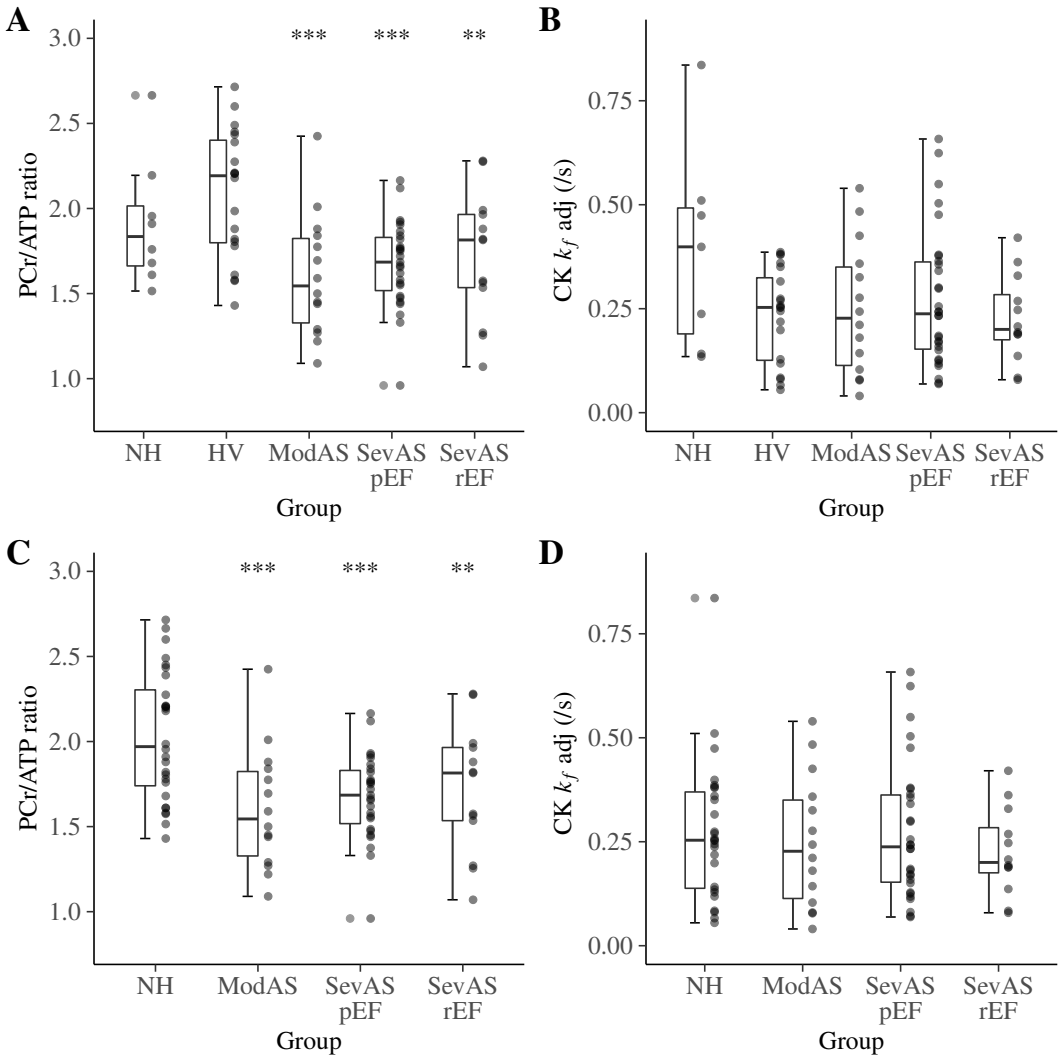


Figure 4.7: (A) PCr/ATP ratio and (B) CK k_f in two control and three AS groups; (C–D) Panels A–B after combining the non-hypertrophied groups. Post hoc tests performed using the NH group as reference.

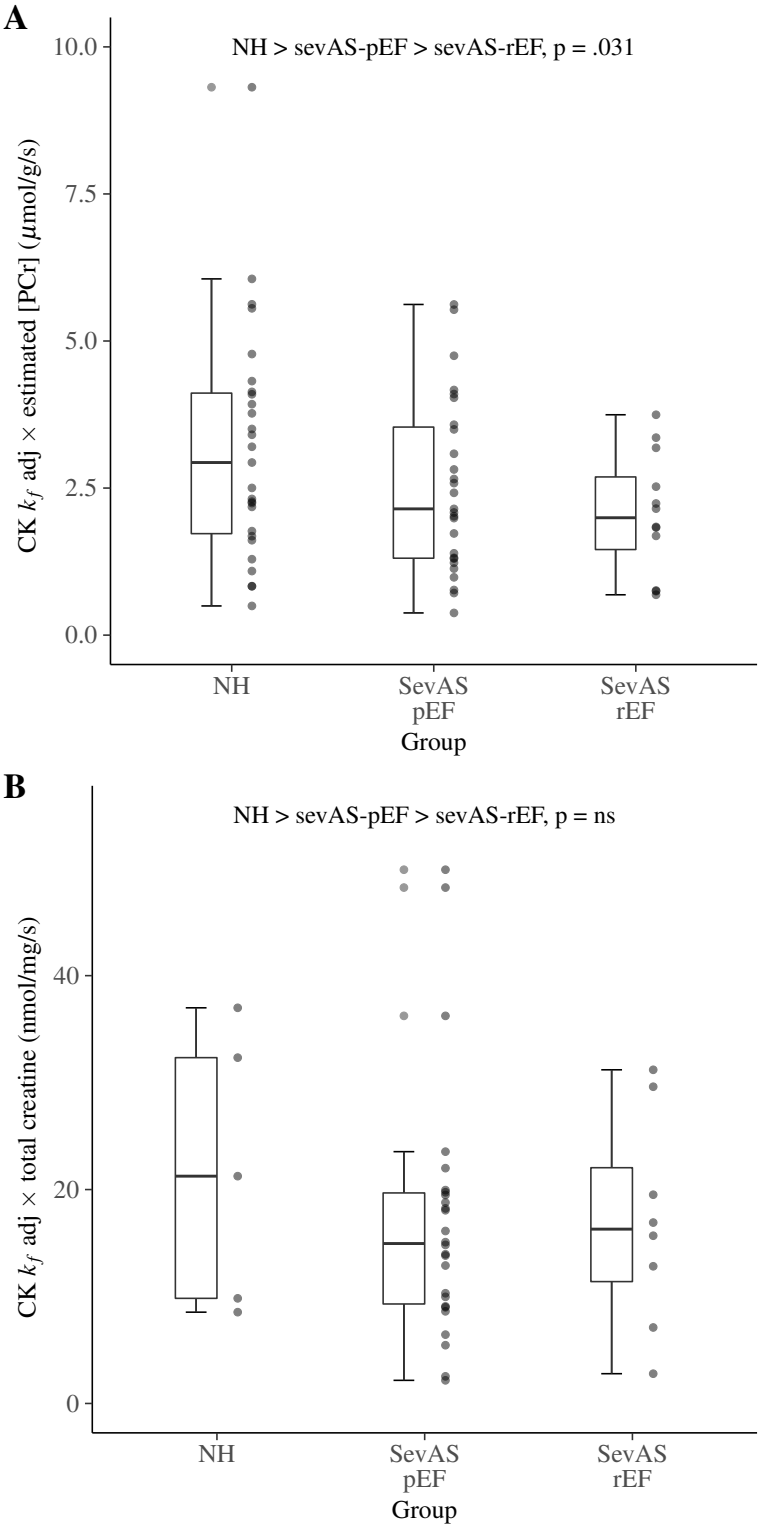


Figure 4.8: (A) CK flux (μmol/g wet weight/s) estimated by k_f × estimated [PCr], combining the NH groups; (B) CK flux (nmol/mg protein/s) estimated by k_f × [total creatine] in one control and two AS groups.

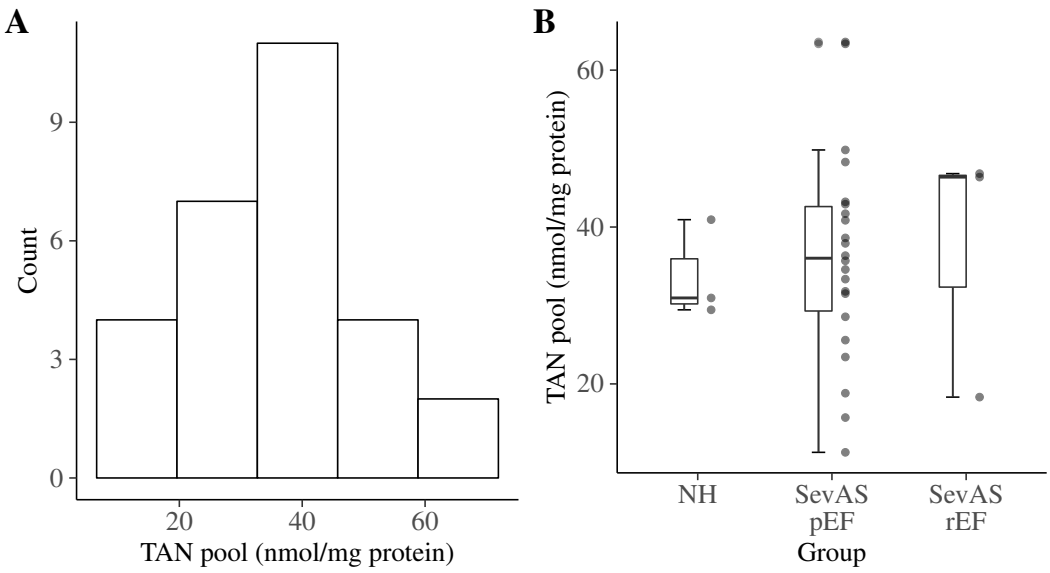


Figure 4.9: (A) Histogram of TAN pool values in NH, sevAS-pEF and sevAS-rEF; (B) TAN pool in one control and two AS groups.

In the paired dataset, follow-up scans were a median (IQR) 7.2 (6.1, 8.4) months post-op and 8.3 (7.6, 11.0) months post initial scan. Mean LVMi and LVM/LVEDV ratios reduced post-op (by 15% and 13% respectively), while LV volumes were unchanged, as expected (Table 4.7). Comparing the two timepoints, there were no significant changes in median k_f (0.17 /s pre- and 0.22 /s post, two-sided p = .07), nor in mean PCr/ATP ratio (1.67 pre- and 1.61 post, two-sided p = .53). As a result, estimated resting flux values were similar at both timepoints (Figure 4.10 Panels B–D).

Summary of results

In summary, the main original findings in this chapter (Figures 4.3–4.10) were that in human AS:

1. Median total CK activity trended downward as one moved from NH to sevAS-pEF to sevAS-rEF hearts (NH > sevAS-pEF > sevAS-rEF, post hoc pairwise

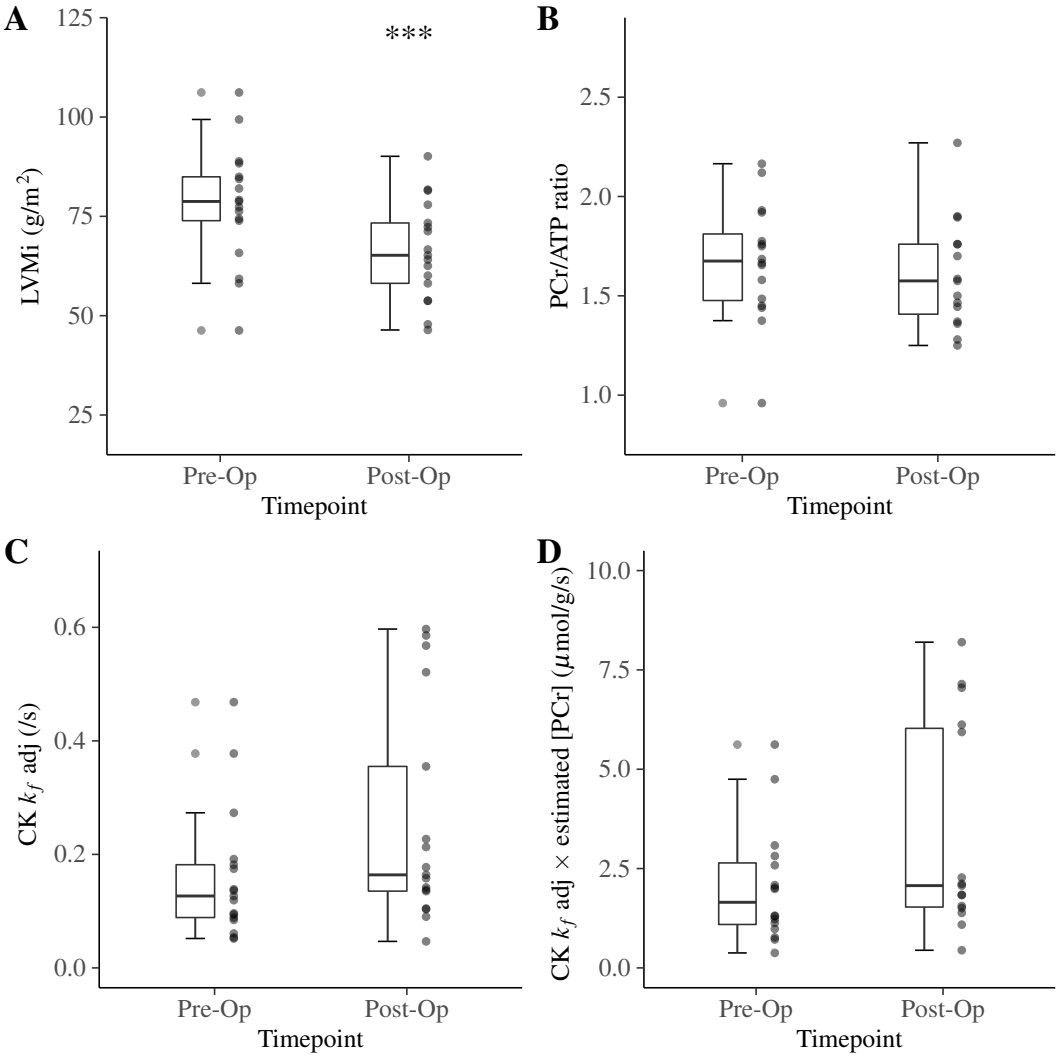


Figure 4.10: Values for (A) LVMi, (B) PCr/ATP ratio, (C) CK k_f adj, (D) estimated CK flux in patients with sevAS-pEF group who were assessed pre- and post-op.

Table 4.7: LV mass and energetics after AVR in sevAS-pEF[a]

Parameter (n pre, n post)	Pre-op	Late f/u	p-value
PCr/ATP ratio (n = 16, 15)	1.67 (0.30)	1.61 (0.28)	.53
CK k_f adj (/s) (n = 17, 17)	0.17 (0.12, 0.24)	0.22 (0.18, 0.47)	.07
Flux (μmol/g/s) (n = 16, 15)	1.7 (1.1, 2.7)	2.1 (1.5, 6.1)	.12
LVMi (g/m^2) (n = 17, 17) $*$	77.9 (14.8)	66.3 (12.4)	2e–4
LVEF (%)	66.9 (4.5)	65.4 (7.0)	.40
LVEDVi (ml/m^2)	69.7 (10.2)	68.2 (9.6)	.55
LVESVi (ml/m^2)	23.1 (4.7)	23.7 (6.1)	.72
LVM/LVEDV (g/ml) $*$	1.13 (0.21)	0.98 (0.18)	.002

[a] Summary data for 17 patients with sevAS-pEF with analysable k_f at late follow-up. All p-values given as two-sided. Values given as mean (SD) or median (IQR).

tests significant at each step).

2. There was a similar downward trend in median CS activity, and by implication mitochondrial density and oxidative capacity (post hoc pairwise tests significant at each step).

3. Median total creatine did not trend downward across the groups.

4. There was a downward trend in CK capacity estimated by CK total activity $\times$ total creatine (post hoc pairwise tests not statistically significant).

5. There was substantial overlap between the sevAS groups in CK total activity, CK capacity, and CS activity when dividing by the LVEF cutpoint of 0.55.

6. Downward trends in absolute activities of MtCK and CK-MM (NH > sevAS-pEF > sevAS-rEF, post hoc pairwise tests significant at each step) underpinned the downward trend in median total CK activity. Absolute activities of CK-MB

were reduced in both sevAS groups compared with NH hearts, but not different between sevAS-pEF and sevAS-rEF.

7. There was relative isoform redistribution towards CK-MM and CK-BB in sevAS, with significantly increased relative CK-BB expression in sevAS-rEF.

8. Moderate AS had similar PCr/ATP and k_f values compared with sevAS-pEF and sevAS-rEF.

9. CK k_f did not distinguish between failing hypertrophy, non-failing hypertrophy and non-hypertrophied hearts.

10. CK flux estimated first by k_f $\times$ estimated [PCr] and second by k_f $\times$ total creatine did not discriminate between NH, sevAS-pEF and sevAS-rEF hearts, but for the former estimate, median values did trend downard significantly and the distribution became more homogenous in sevAS-rEF hearts.

11. In sevAS-pEF at late post-operative follow-up, within-participant median CK k_f and mean PCr/ATP ratios did not significantly differ compared with the pre-operative timepoint, despite falls in LVMi and LVM/LVEDV ratio.

4.3 DISCUSSION

Transition to systolic failure in AS increases mortality and operative risk. It has not previously been assessed whether markers of metabolic reserve associate with and have explanatory power in human AS with reduced LVEF. This chapter found that stepping from NH to sevAS-pEF to sevAS-rEF resulted in stepwise falls in total CK, MtCK, CK-MM, and CS activities (post hoc tests significant at each step), and relative redistribution toward CK-MM and CK-BB. There were falls in median CK capacity and CK flux across the groups (post hoc tests not significant) but not in CK k_f or total creatine. Thus enzyme activity and PCr pool size are the main factors reducing

ATP delivery in sevAS, with much impairment already present at the sevAS-pEF stage. Furthermore, the significant overlap between the sevAS groups has several possible implications: first, there is likely significant intrinsic biological variation in CK activity before one developes a fall in LVEF; second, reduced CK activity or capacity is not a prerequisite for LVEF decline; and third, it is possible that reduced CK activity or capacity contributes to LVEF decline in at least some people, but perhaps (as it is not a prerequisite) only in the setting of other permissive factors.

CK total activity

Although two studies have measured total CK activity in pressure overloaded human LV (Ingwall et al., 1985; Sylvén et al., 1983), no distinction was previously made between hearts with or without preserved LVEF. Sylvén et al. (1988) found a similar degree of correlation to this study ($r = .45$, $p < .05$, compare Figure 3.4, p. 101) between LV or papillary muscle CK activity and LVEF determined by single-plane angiography in 21 patients with mixed aortic or mixed mitral valve disease, but 1-way ANOVA comparing patients with LVEF strata > 58%, 36-58% and ≤ 35% was not statistically significant. Here, total CK activity followed a stepwise pattern (NH > sevAS-pEF > sevAS-rEF), in line with previous animal pressure overload studies (De Sousa et al., 1999; Gupta et al., 2011; Ye et al., 2001a). The observed falls in total CK activity (35% and 43% in sevAS-pEF and sevAS-rEF respectively) were comparable in size to those observed in the single prior controlled human study: Ingwall et al. (1985) found that hypertrophied pressure overloaded hearts (n = 11) had 33% lower total CK activity, 46% lower CK-MM activity, unchanged CS activity, and 45% lower total creatine content compared with non-hypertrophied control hearts (n = 9).[12] Furthermore, human NICM hearts undergoing transplantation (n = 23, mean

[12]The non-hypertrophied group had ages 24–53, normal LV systolic function, and included seven organ donors, one patient with mitral stenosis and one with an atrial septal defect (ASD); the AS group had ages 39–83, mean LVEF 0.63, LVEF range 0.3–0.84; neither group had CAD. LV biopsies were taken before cardioplegic arrest.

age 34 ± 16) had 34% lower total CK activity and 50% lower creatine content than controls (n = 15, mean age 30 ± 10), and similar CS activities (Nascimben et al., 1996); a second group found that NICM hearts undergoing transplantation (n = 6, age 40 ± 11, LVEF 23 ± 5%) had 43% lower total CK activity and 28% lower CS activity than donor heart controls (n = 6, age range 14–42) (Sylvén et al., 1993). Thus, the relative falls seen here in sevAS are also comparable with those seen in end-stage NICM.

The observed variability in CK activity in sevAS may reflect an effect of LV decompensation on CK activity, and/or may indicate that those participants with inherently lower CK activity are more predisposed to LVEF decline. If the latter is true, then this index of metabolic reserve represents a potential future therapeutic and diagnostic target. However, I cannot separate these possibilities here. Given the large between-group overlap in total CK activity, and observations from CK knockout studies of relatively mild effects of CK deficiency on contractile reserve (Saupe et al., 1998; Spindler et al., 2002), and that substantial degrees of acute pharmacological inhibition of CK are required to depress contractile performance (Tian and Ingwall, 1996), this suggests that the fall in CK activity is not (in isolation) a necessary or central driver of contractile dysfunction. However, changes in the CK system during the transition to failure do not occur in isolation but are accompanied by changes in substrate metabolism, oxidative capacity, Ca^{2+}-handling, signalling pathways, and LV geometry, all of which collectively are likely to amplify the effects on contractile reserve of relatively modest changes in CK activity. Contractile dysfunction arising from CK deficiency in mice is also highly dependent on genetic modifiers, gender and age (Lygate et al., 2012b). Most knockout studies date from in utero, such that adaptations have time to mitigate the resulting phenotype; in human VHD, the timescale for adaptation is relatively shorter. Thus, reduced CK activity could nevertheless be an important contributor to contractile decline in AS.

CK isozymes

Left ventricular failure has generally been associated with reduced myocardial total CK activity and a foetal shift in CK isoform expression secondary to increases in the cytosolic CK-B isoform and decreases of the cytosolic CK-M and mitochondrial MtCK isoforms. Congruent with this expectation, I observed stepwise falls in absolute activities of MtCK and CK-MM, a fall in CK-MB absolute activity and a 50% increase in relative CK-BB expression. The mechanism underlying this isoform shift is unknown, but as it is: not observed in physiological hypertrophy, is not potentiated by MtCK- or CK-M KO (Saupe et al., 2000), is more marked subendocardially in the overloaded ventricle (Smith et al., 1990), is found in multiple HF models (ischaemia, pacing, NICM, haemodynamic overload), and reverses on unloading (Park et al., 2002), it is thought to relate to chronic wall stress and the foetal isoform shift seen across many genes in pathological hypertrophy.

Most animal models of pressure overload before or during transition to failure have found falls in MtCK and CK-M and rises in CK-B (i.e. rises in CK-MB and CK-BB) in rats (Ingwall, 1984; Ingwall et al., 1990; Smith et al., 1990; Vatner and Ingwall, 1984) and dogs (Ingwall, 1984; Ye et al., 2001b), though there are exceptions: the baboon, for which no consistent rise in CK-MB could be demonstrated (Ingwall, 1984), the TAC mouse before transition to failure (Lygate et al., 2007), and the TAC rat (Fontanet et al., 1991). In line with the former group of studies, there was a relative redistribution toward CK-MM and CK-BB in sevAS here. This could be construed as a compensatory adaptation, as CK-MM can functionally couple to various cytosolic ATPases and CK-BB has greater affinity for PCr and ADP: the K_m of CK-BB for PCr and ADP is 20-30% and 50-70% respectively that of CK-MM (Bittl et al., 1987c; Szasz and Gruber, 1978); the K_m of CK-MB for creatine is double that of CK-MM (Scholte, 1973; Wong and Smith, 1976). Thus for CK-B containing dimers, as compared with CK-M, the ATP-producing direction is kinetically favoured

especially at low PCr levels; for CK-M on the other hand the PCr-producing direction is kinetically favoured.[13]

The mtCK/CS ratio has been used to assess whether falls in MtCK activity surpass falls in mitochondrial volume. Here, there were no significant differences across NH, sevAS-pEF, and sevAS-rEF, because both mtCK and CS absolute activities were reduced. In contrast, the ratio was reduced in prior studies in human NICM (Nascimben et al., 1996), human MR (n = 6, LVEF unspecified) (Sylvén et al., 1991), TAC mouse, (Lygate et al., 2007), TAC rat (De Sousa et al., 1999), aging SHR (Ingwall, 1984), rat infarction (Neubauer et al., 1995), mouse infarction (Lygate et al., 2007), and pig infarction (Hu et al., 2006). This is at least partly because prior studies observed smaller or no falls in CS activity than here.

Three groups have previously studied CK isozyme expression relative to total CK activity in human LV, with only one controlled study in human AS. Prior literature values in organ donor controls are inconsistent (particularly for MtCK relative expression):

- In two uncontrolled studies, CK-MB relative expression was 19.5 $\pm$ 5.0 % in LV from 12 participants with AV or MV disease (valve disease and LVEF unspecified, no CAD) (Sylvén et al., 1983) and 18–20% in LV apex from 15 participants with AV disease (5 AS, 1 aortic regurgitation, 7 mixed) and LV papillary muscle from 6 with MV disease (4 mixed, 1 MS, 1 MR) (Sylvén et al., 1988). Means were 17.7, 19.9, 19.6 across three LVEF strata (> 0.58, 0.35–0.58, $\leq$ 0.35) respectively. Sylvén et al. (1991) found median relative isoform expression of 34:67:0.7 % (MtCK:CK-M:CK-B) in LV subendocardium and 33:60:0.5 % in anterior papillary muscle in organ donors (n = 9); values were

[13] The functional significance of this is difficult to predict, as CK-MM and CK-BB had similar CK forward flux/V_{max} ratios in mouse KO models (Saupe et al., 2000), and rat skeletal muscle with CK-BB substituted for CK-MM did not display impaired 5 Hz isometric twitch force, unlike CK-M KO muscle (Roman et al., 1997).

19:65:14 % in anterior papillary muscle in mitral regurgitation (n = 6). Mean CK-B relative expression was 2.0 ± 1.7 % of CK-B in donor hearts (n = 6), 6.0 ± 0.9 % in sevMR (n = 7), and 2.9 ± 0.8 % in end-stage NICM (n = 6) (Sylvén et al., 1993).

- Ingwall et al. (1985) found proportional expression of 10:89:1 % (MtCK:CK-MM:CK-MB) in controls (n = 2 of 9) and 13:72:15 % in AS with a range of EF (n = 4 of 11). Nascimben et al. (1996) reported relative expression of 7:73:20 (MtCK:CK-MM:CK-MB) in donor hearts (n = 36, on life support for 24–120 before heart harvesting), 9:63:27 % in end-stage NICM (n = 23), and 10:88:2 % in controls (n = 15, 13 accident victims, 1 MS, 1 ASD).

- Park et al. (2002) reported relative expression of 29:26:45 % (MtCK:CK-M:CK-B, normalised to β-actin) in failing LV during LVAD implantation (n = 11, 6 NICM, 5 ischaemic) and 33:30:37 % at 4.1 months post-LVAD (n = 7).

Nevertheless, this study is the largest controlled study in human pressure loading disease and the changes in isoform relative and absolute activities are congruent with expectations from most animal models.

CS activity

As with CK total activity, mtCK and CK-MM, I observed here a stepwise fall in CS activity moving from NH to sevAS-pEF to sevAS-rEF. Although only one marker of oxidative capacity, this suggests mitochondrial oxidative capacity is reduced in the failing AS heart. In contrast, prior animal studies found no change in CS activity in nonfailing pressure overload hypertrophy: in canine LV (Matlib et al., 1983), rats (Smith et al., 1990) and mice (Lygate et al., 2007). The 30% fall in median CS activity in sevAS-rEF compared with NH has no strictly comparable prior human studies, with no significant relationship with LVEF observed in human mixed aortic or mixed

mitral valve disease (n = 21) (Sylvén et al., 1988), but reduced activity or expression were observed in human NICM (Kalsi et al., 1999; Razeghi et al., 2001a; Sylvén et al., 1993),[14] failing TAC rats (De Sousa et al., 1999), aging SHRs (Ingwall et al., 1990; Power et al., 2016), pacing HF in dogs (Lei et al., 2004), and expression increased after LVAD implantation (Gupte et al., 2014). Conversely, unchanged activity or expression have also been observed in human NICM (Nascimben et al., 1996) and animal HF models: TAC mouse (Lygate et al., 2007), rat infarction (Neubauer et al., 1995), pig infarction (Hu et al., 2006), cardiomyopathic hamsters (Tian et al., 1996), NICM (Liao et al., 1996). Given the large between-group overlaps observed in this study and the literature inconsistency, reduced oxidative capacity is likely to an important consideration in the transition to failure in at least some, but not all, hearts with sevAS.

Total creatine concentration

Contrary to expectation, there was no downward trend in total creatine in sevAS-pEF. Although consistent with rat, dog and mouse TAC models of non-failing pressure overload (Bache et al., 1994; Ingwall, 1993; Lygate et al., 2007), prior studies in non-failing and failing hypertrophy have found reduced total creatine concentration: in TAC dogs (Ye et al., 2001b) and rats (Tian et al., 1997b), in human AS (Ingwall et al., 1985) and NICM (Kalsi et al., 1999; Nascimben et al., 1996; Neubauer et al., 1999b), in ^{1}H-MRS studies targeting creatine in human NICM (Nakae et al., 2004a, 2003), and in multiple animal HF models (see Section 1.3). As with CK and CS activities, there was significant overlap between the sevAS groups, and possible reasons for this are discussed in the Limitations sections below.

[14] CS activity was reduced by 53% and total creatine by 63% in NICM hearts undergoing transplantation (n = 14, mean age 39.1 $\pm$ 5.5, LVEF 19 $\pm$ 9%) compared with donor hearts (n = 4) (Kalsi et al., 1999).

Estimated CK flux and CK k_f

This study showed a statistically significant trend to reduced ATP delivery through CK, measured non-invasively (NH > sevAS-pEF > sevAS-rEF), but no significant between-group differences. This admits several possible interpretations. As ATP delivery (whether by facilitated diffusion or diffusion) is essential for normal contractile function, reduced ATP delivery may limit contractile reserve and contribute to the transition to failure. Given that failing pressure overloaded hearts are more dilated and so under greater wall stress per gram myocardium, even the 'normal' resting ATP delivery rates observed here may be inappropriately low (interpretation 1), as the increased ATP turnover must be accounted for by CK-independent means.

Although some failing hearts did show reduced ATP delivery rates through CK, the overlap indicates that reduced resting CK flux is not a prerequisite for having sevAS-rEF (interpretation 2). This result is in discrepancy with the previous report in human hypertensive hypertrophy (Smith et al., 2006), where PCr/ATP was reduced in hypertensive hypertrophy irrespective of HF status, while CK k_f was reduced only in the failing hypertrophy group. In that study, which used a surface coil, prone positioning, and the FAST protocol at 1.5T, the HF group (n = 10, mean age 50 $\pm$ 10, mean LVEF 46 $\pm$ 18%) was defined on clinical symptoms and signs with a modified Framingham system (McKee et al., 1971), and split equally by a LVEF cutpoint of 0.50. The implied aetiology was hypertension, yet prior MI or regional wall motion abnormalities were not excluded in the HFrEF group (as reported), and the HFpEF group may not have met current criteria for HFpEF: unlike in this study, the HF group was younger than its comparison group, did not have increased LVMi over the LVH group, and only 10% had AFib. But if the fall in k_f in the HF group was attributable to HF status, it cannot have been prior MI or LVEF that were contributory, as the same group later reported that k_f was normal in participants post anterior MI (LVEF 30 $\pm$ 9%) (Bottomley et al., 2009). And if the HF status was pressure overload-related, it is

unclear how to reconcile the fall in k_f in that HF group with the lack of fall of k_f in this chapter's sevAS-rEF hearts, which were subject to higher LV afterloads.

Given the variability in CK total activity and CK k_f observed here, it is likely that in AS, the trend (NH > sevAS-pEF > sevAS-rEF) to reduced ATP delivery through CK (and reduced CK capacity) is driven primarily by a combination of PCr pool depletion and total enzyme activity rather than a fall in k_f (the 20% fall in k_f in sevAS-rEF (p = ns) may also contribute in some participants). Indeed, falls in PCr but not k_f were previously observed in human failing myocardium post myocardial infarction (Bottomley et al., 2009) and in thoracic aortic constriction (TAC) models in swine at the nonfailing hypertrophy stage (Xiong et al., 2015; Ye et al., 2001a). On the other hand, TAC models of heart failure did show falls in k_f of 28–37% in swine and mice (Gupta et al., 2011; Ye et al., 2001a), but there, the failure phenotype was of gross decompensation within 8 weeks, unlike in this study (see Table 4.8 for refs).[15] It is also possible that the animal studies acquired cleaner spectra, as the large animal studies sutured the surface coil to the anterior LV pericardium, and all the animal studies used anaesthesia, so avoiding noise introduced by respiratory artefact. In comparison, any human study would be expected to be characterised by noisier data.

In any case, if (as the current data suggest) estimated ATP delivery rates are not significantly different in sevAS-rEF, despite a fall in CK total activity, it is also possible that it is not reduced resting CK flux that influences the transition to failure, but rather increased resting ATP delivery rate / CK total activity ratio (interpretation 3). This is another way of thinking about CK reserve, which was previously conceptualized as the difference between CK capacity and oxphos flux at high workloads. If ATP delivery rates through CK increase at higher workloads (I test this hypothesis in Chapter 6),

[15] The mechanism underlying previously seen changes in k_f in HF is unknown, but likely does not relate to reduced [PCr]. GPA feeding is known to induce large falls in PCr and forward CK flux; CK total activity is unchanged. In this (creatine-deficiency) model, both reduced (Horn et al., 2001), unchanged (Neubauer et al., 1999a) and increased (Kapelko et al., 1988; Shoubridge et al., 1985; Zweier et al., 1991) CK k_f has been observed.

Table 4.8: Prior studies of CK k_f (/s) in pressure overload[a]

Model	Control	LVH	HF
This study	0.25 (0.13, 0.38)	0.24 (0.15, 0.36)	0.20 (0.16, 0.30)
Human hypertension[b]	0.32 (0.06)	0.36 (0.04)	0.17 (0.06)
Canine TAC[c]	0.57	0.57	n/a
Swine TAC[d]	0.49 (0.22)	0.41 (0.09)	0.31 (0.08)
Murine TAC[e]	0.32 (0.03)		0.23 (0.03)
Swine TAC[f]	0.33 (0.05)	0.31 (0.05)	
Swine MI[g]	0.41 (0.09)	0.38 (0.14)	0.21 (0.07)
Human MI[h]	0.34 (0.07)		0.31 (0.08)

[a] Values given as mean (SD) or median (IQR).
[b] Smith et al. (2006). n = 14, 10, 10.
[c] Ye et al. (2001b). Duration 1 year. n = 10, 14. LVH animals had a 98% increase in heart-body mass ratio and rise in LVEDP from 7 to 11 mmHg, but no overt signs of HF. [PCr] and forward flux (k_f $\times$ [PCr]) reported, but not k_f alone. [PCr] obtained from PCr/ATP ratio $\times$ biopsy [ATP].
[d] Ye et al. (2001a). Duration 8 weeks. n = 10, 9, 7. LVEDP = 6, 7, 20 mmHg respectively.
[e] Gupta et al. (2011). Duration 7–8 weeks. n = 11, 10.
[f] Xiong et al. (2015). Duration 1- & 8-weeks. n = 8, 22. Data presented in bar graph form only and read using a pixel counter for baseline and 8-weeks.
[g] Murakami et al. (1999a). Duration 6 weeks. n = 9, 13, 6. LCx ligation; LVH animals had a 22% increase in LV-body mass ratio and rise in LVEDP from 6 to 9 mmHg, but no cyanosis and/or ascites; the HF group had a 48% increase in LV-body mass ratio, LVEDP 16 mmHg and cyanosis and/or ascites.
[h] Bottomley et al. (2009). n = 15, 15. Chronic anterior MI, LVEF 30 $\pm$ 9%. In hearts post MI, myocardial k_f and PCr/ATP were unchanged, [PCr] and [ATP] were reduced by 39-44%, and CK flux was reduced by 48%

CK total activity is fixed, and resting ATP delivery rate / CK total activity ratio is increased, then CK-dependent phosphotransfer could become limiting, and this could contribute to transition to failure.

TAN pool

Although there were insufficient values to make between-group comparisons, TAN pool values recorded in sevAS were comparable those from four previous studies in human LV (all in nmol/mg protein):

- Mean (SEM) TAN pool values in peri-operative LV samples taken before, during and after cardioplegia for sevAS (n = 9) were 33 ± 2 (endocardium) and 39 ± 2 (epicardium) (Swain et al., 1982).

- Mean (SEM) [ATP] values in intra-operative transmural LV biopsies were 37.7 ± 3.3 (endocardium) and 36.8 ± 3.3 (epicardium) in 4 patients without LVH (2 MR, 1 tricuspid stenosis, 1 2-vessel CAD) and 25.9 ± 1.7 (endocardium) and 31.5 ± 1.6 (epicardium) in 10 patients with severe AS and no CAD (Peyton et al., 1982).

- Mean (SEM) TAN pool values were 39 ± 3 and 37 ± 4 in NICM (n = 19) and controls (n = 14) respectively (Regitz and Fleck, 1992).

- Mean (SEM) [ATP] values were 38 ± 2 in cold-preserved normal donor hearts (n = 10) and 24.4 ± 1.3 in right ventricle (RV) endomyocardial biopsies from NICM patients undergoing heart transplantation (n = 24) (Starling et al., 1998).

This should reassure us that no meaningful bias was introduced by the post cardioplegia sampling technique in this study.

Late follow-up

This study does not reproduce previous findings of a relative rise in PCr/ATP ratio post AVR in human AS (by 31% (n = 14) (Mahmod et al., 2014) and 15% (n = 9) (Beyerbacht et al., 2001)). This is not implausible given the participants' ages. The follow-up k_f result is original, but arguably underpowered.

Limitations

As these data cannot separate out variation in CK and CS activities due to intrinsic inter-individual variation from variation due to pressure overload-induced transition to failure, these results do not establish the timing of any falls in CK and CS activity

in relation to AS severity or LVEF trajectory. To answer this kind of question would require within-person repeated sampling, which is infeasible given the requirement for LV biopsy. The CK system was not assessed under conditions of acutely increased stress, when it is thought to be most important, as contractile reserve and stress testing are contraindicated in symptomatic severe AS. Nor was CK-independent phosphotransfer through adenylate kinase measured. AK contributes about 10% of phosphotransfer in the normal heart and can increase its contribution in heart failure (up to 21% in dogs), albeit not sufficiently to fully compensate for large changes in the CK system (Dzeja et al., 1999). As k_f reflects a weighted average for all ATP-producing CK activity, one cannot be sure of the differential contribution of normally minor pathways such as ATP-production by glycolysis-coupled MM-CK to the results obtained, but the strength of the correlation between CK and CS activity (see previous chapter) argues for predominantly oxidatively-linked energy transfer.

The mechanism for the fall in CK total activity and CS activity as one moved from NH to sevAS-pEF and sevAS-rEF is still unclear. It is unknown whether LBBB contributed to this fall, whether it solely depressed LVEF, and/or whether it was symptomatic of the transition to HF. I did not measure creatine transporter expression or creatine uptake kinetics, so am unable to say whether this may have contributed to reduced total creatine in those participants where total creatine or CK capacity were reduced. Biopsy size also precluded a polarographic assessment of oxidative capacity. Nor did I assess upstream aspects of metabolism such as fractional substrate oxidation, which would require transmyocardial blood sampling, or myocardial efficiency, which would require invasive quantification of myocardial external work and VO_2.

I did not systematically measure classical markers of pathological hypertrophy (ANP, α-actin, MHC, SERCA2a, Section 1.2), myocardial fibrosis, extracellular volume (ECV), diastolic indices, more sensitive markers of systolic dysfunction (GLS), or serum NT-proBNP. However, groups differed on LVMi and LVEF, and scan

time and biopsy size were at the upper limit of acceptable tolerance. Many patients would not have participated had the scans been longer or not arranged the day before their operations.

Although apparently cleanly separated by LVEF, participants with sevAS-pEF and sevAS-rEF did not represent completely distinct phenotypes, as evidenced by the overlap in AS severity, LVMi, CK and CS activities, total creatine, CK isoforms and estimated CK flux. As already explained, the LVEF cutoff was chosen for its prognostic importance and ease of translation to clinical thinking, but any dichotomization of a continuous variable can reduce the statistical power to find between-group differences (Altman and Royston, 2006). It is possible that there were patients transitioning to failure in the (mostly symptomatic) sevAS-pEF group, which could downwardly bias CK activity values. Had the sevAS-pEF group been filtered to accept only asymptomatic patients or patients with low natriuretic peptide levels, CK activity values may have been adjusted upward. Conversely, the sickest patients with sevAS-rEF could neither be recruited nor biopsied, as they either felt too unwell to consent or were not listed for surgical AVR. This could have exerted upward bias on values observed in sevAS-rEF hearts. For these reasons, the sevAS-rEF hearts here should not be expected to represent an equivalent stage or degree of HF as patients in historical HF studies undergoing heart transplantation, and the sevAS-pEF hearts do not represent an equivalent stage of pathological hypertrophy as historical participants with asymptomatic hypertensive LVH (cf. Smith et al. (2006)). Any differences observed therefore are likely to reflect differences between participants who were at earlier versus later stages of transition to HF.

In clinical practice, participants with reduced LVEF at time of diagnosis of severe AS are more likely to have had prior MI than those with preserved LVEF (31% vs 12% using a cut-off LVEF of 0.50 (Ito et al., 2018)). Whether these findings translate to participants with prior MI or concomitant flow-limiting CAD is unknown; this study

was designed to assess the association of markers of metabolic reserve in participants with or without pressure overload-related failure.

The NH group did not display CK-B relative expression values as low as some historical controls have done, nor MtCK relative expression values as high, and were also older than historical controls with some degree of hypertension. Nevertheless, I would argue they serve well as a non-hypertrophied, normal LVEF control group which underwent similar sample handling.

Biopsies were taken from papillary muscle in participants undergoing MV replacement and from septal LV endocardium in participants undergoing AV replacement or aortic aneurysm repair. Any variance in sampling location is unlikely to have biased the results, as no significant differences were previously seen in median:IQR total CK activity between LV septum (112:101–123), LV subendocardium (111:96–151), LV subepicardium (120:95–157) and papillary muscle (129:103–144), nor in CS activity, in donor hearts (n = 9) (Sylvén et al., 1991). As shown in the previous chapter, sample storage time did not influence the results and all biopsy samples were obtained on cardiopulmonary bypass within 10–15 minutes of establishing cardioplegic arrest. It is unlikely that differences in time from aortic cross-clamp to surgical biopsy differed sufficiently to explain variation in the measured variables.

The estimate of [PCr] was based on literature values of [ATP], as absolute quantification was not completed. Forward flux was derived from estimated [PCr] $\times$ k_f adj, but I also plotted an estimate of flux estimated by total creatine $\times$ k_f adj. This latter estimate makes the assumption that falls in total creatine (i.e. free creatine + PCr) match falls in [PCr]. While not demonstrated in humans, a constant free creatine:PCr ratio was demonstrated in a longitudinal pacing-induced HF model in dogs (Shen et al., 1999). There it was argued that the parallel fall in both free creatine and PCr reflects an attempt by the CK system to maintain its equilibrium position in the face of falling PCr/ATP ratio and TAN pool, so keeping [ADP] low and [ATP]/[ADP] normal.

As the present study also showed correlation between TAN and CK total activity and between total creatine $\times$ k_f and CK total activity (Table 3.2, p. 98, Fig. 3.3, p. 100), I would argue that this second estimate of flux has validity.

Outstanding questions

Outstanding questions include: how to prospectively identify all those who develop greater degrees of 'otherwise unexplained' LVEF decline in the face of pressure overload, what the contribution of reduced metabolic reserve is to this myocardial vulnerability (the vulnerable ventricle hypothesis), and whether (and in whom, and how) metabolic reserve may be compromised upstream of CK.

In summary, these results open the door to developing metabolic imaging techniques as a possible prognostic strategy for identifying those at higher risk of transition to failure (the metabolic biomarker hypothesis), and should stimulate the development of therapeutic strategies based on improving cardiac metabolism to delay transition to failure (the metabolic HF hypothesis). Both are worthy of further investigation.

5 *ATP delivery rates in chronic volume loading by primary mitral regurgitation*

5.1 INTRODUCTION

This chapter aims to investigate

- ATP delivery rates in severe primary MR with preserved systolic function, and
- Whether late after repair of severe primary MR there is normalisation of PCr/ATP.

MR is the most prevalent VHD and the second most commonly intervened upon. At least moderate MR had a prevalence of 6.4% in population studies of adults aged 65-74 (Nkomo et al., 2006) and was recently identified in 5.2% of all echocardiograms performed across 19 European centres (Monteagudo Ruiz et al., 2018). In this latter study, 55% of cases were primary MR. In a UK community population aged >18 and referred for echo for suspected HF, the prevalence of at least moderate MR was 3.1% (Marciniak et al., 2017).

Primary MR is defined as a primary abnormality of the MV apparatus. The commonest cause is myxomatous degeneration of the leaflets leading to MV prolapse,

and ranges over a spectrum from fibroelastic deficiency (thin leaflets, focal prolapse and presentation typically with chordal rupture and flail leaflet causing severe MR) to Barlow's disease (diffusely thickened and redundant leaflet tissue, bileaflet prolapse, and less well defined onset of severe MR). This kind of MR is characterised by excess leaflet motion (Carpentier type II) – nearly all patients recruited in this chapter had this kind of primary MR. Primary MR may also arise in the setting of normal leaflet motion (Carpentier type I) from leaflet perforation or congenital clefts, and in the setting of restricted leaflet motion (Carpentier type IIIa) due to mitral annular calcification, rheumatic disease, drugs, radiation and connective tissue disease.[1] Secondary MR is defined as a disease of the atrium or ventricle, may be caused by atrial MR, NICM and ischaemic cardiomyopathy, and is not discussed further.

A classically understood natural history of isolated primary MR is outlined here. The lesion both volume overloads the LV and reduces LV afterload by allowing ejection into the low pressure left atrium (LA). Sudden increases in LA pressure precipitate acute presentations with pulmonary oedema, but more commonly a compensated minimally symptomatic stage arises, where the LV dilates to maintain forward stroke volume but at the cost of increased LV wall tension and LA size. After months–years, a variable combination of progressive LV enlargement, rise in LVEDP, reduced LV contractility, atrial fibrillation, and pulmonary hypertension develops and patients present with exertional dyspnoea.

Like severe AS, untreated severe primary MR carries a poor prognosis, with well-timed MV repair able to restore most of the life expectancy at risk. Unlike in severe AS, surgical repair is preferred; percutaneous repair is approved only in patients at high surgical risk, and greater surgical expertise is demanded, so feasibility of durable repair must also be considered. Conversion to MV replacement increases late mortality (Enriquez-Sarano et al., 2009; Thourani et al., 2003). Decisions around timing must

[1] Reviewed (El Sabbagh et al., 2018).

balance the risks of late surgery (persistent LV dysfunction, higher mortality) against the risks of early surgery (operative mortality, risks of requiring MV replacement in case of immediate failure of repair, earlier exposure to increased risk of endocarditis, late failure of repair and reintervention for this), and consider patient life expectancy and hospital and surgeon procedural volume (Bolling et al., 2010; Gammie et al., 2007; LaPar et al., 2014).

Current indications for intervention in severe primary MR include symptoms, asymptomatic LV dilation (LVESD $\geq$ 45 mm)[2] or dysfunction (LVEF 0.30–0.60) (all class I), atrial fibrillation or resting pulmonary hypertension, LVESD 40–44 mm with flail leaflet or significant LA dilation ($\geq$ 60 ml/m^2) in sinus rhythm and high likelihood of successful repair (all class IIa) (Baumgartner et al., 2017). Severe LV dysfunction (LVEF $\leq$ 0.30, LVESD > 55 mm) is a relative contra-indication (class IIb) as it predicts poor recovery of contractility after repair. 15-year mortality declines stepwise when comparing repair for class I indications with repair indicated by atrial fibrillation or pulmonary hypertension, and with repair indicated by severe MR with highly likely successful repair (Enriquez-Sarano et al., 2015), indicating that class I indications represent a later stage of disease.

There are several areas where we lack understanding. The first is whether to recommend early repair. Today, early repair refers to repair in the asymptomatic patient without LV dilation or dysfunction. No randomized trials comparing a strategy of early repair versus active surveillance exist, with observational studies supporting both early repair (Enriquez-Sarano et al., 2005; Grigioni et al., 2008; Kang et al., 2009, 2014; Suri et al., 2013) and active surveillance (Zilberszac et al., 2018) strategies. There are also data suggesting that careful surveillance can result in survival comparable to the general population and can delay operation in 55 $\pm$ 6% of patients at 8 years (Rosenhek et al., 2006). Interpretation of these studies is tricky, as participants under

[2] 40 mm in American guidelines (Nishimura et al., 2014; Tribouilloy et al., 2009).

active surveillance ranged from truly asymptomatic to minimally symptomatic, may or may not have had exercise testing, may or may not have had class IIa indications for repair, and had imaging at variable follow-up intervals. Conversely, there was variation in surgical outcomes and rates of repair versus replacement, partly due to variation in surgical skill, but also to variation in repairability and imperfect pre-operative prediction of repairability. There is likely also variation in rates of sending patients with non-severe MR prematurely for repair, as implied by the relatively low interobserver agreement on quantitative parameters of MR severity (see below), and the discordance between echo and cardiac MRI estimation of MR severity (Myerson et al., 2016; Penicka et al., 2018; Uretsky et al., 2015).

A second problem is that the transition to failure in primary MR is poorly defined, so that despite similar preoperative LVEF and surgical approaches, we cannot reliably predict postoperative LV dysfunction. While some fall in LVEF is expected after correction of loading conditions, early postoperative LVEF < 0.50 is not uncommon (even in patients with preoperative LVEF > 0.60), predicts persistent postoperative LV dysfunction, is predicted by pre-operative LVEF and LVESD, and worsens prognosis (Crawford et al., 1990; Enriquez-Sarano et al., 1994b; Matsumura et al., 2003; Quintana et al., 2014; Varghese et al., 2014). Both pre-operative parameters (LVEF < 0.60 and LVESD > 40 mm) also predict persistent late LV dysfunction and survival (Chenot et al., 2009; Enriquez-Sarano et al., 1995, 1994a,b; Ling et al., 1996; Quintana et al., 2014; Schuler et al., 1979; Tribouilloy et al., 2009; Zile et al., 1984), yet do not capture all the risk: 'normal LVEF' (> 0.60) can mask significant histological myofibrillar degeneration (Ahmed et al., 2010), and in 585 patients operated for primary MR without class I or IIa indications for surgery (i.e. very early), 68/585 (12%) had otherwise unexplained early postoperative LVEF < 0.50 (Quintana et al., 2014). For this reason, serial declines in LVEF (above 0.60) or rises in LVESD (below 40 mm) are worrying and favour repair if this is highly feasible (El Sabbagh et al., 2018).

(They may also indicate initation of medical therapy or more frequent surveillance.)

There are several ways to tackle these problems. In summary, these include: more accurate and reproducible versions of current biomarkers (LVEF, LVESD, MR regurgitant volume), unconventional biomarkers of latent LV transition to failure (LA size (Le Tourneau et al., 2010; Rusinaru et al., 2011), treadmill exercise duration (Supino et al., 2007), treadmill exercise capacity (Naji et al., 2014a,b), peak oxygen uptake (Leung et al., 1997; Messika-Zeitoun et al., 2006), post-exercise LVEF increment or LVESVi (Lee et al., 2005; Leung et al., 1996), exercise-induced increase in regurgitant volume by $\geq$ 15 ml or effective regurgitant orifice area (EROA) by $\geq$ 10 mm^2 (Magne et al., 2010a), exercise-induced pulmonary hypertension (Magne et al., 2015, 2010b), resting systolic tissue Doppler velocity (Agricola et al., 2004), BNP (Detaint et al., 2005; Klaar et al., 2011; Magne et al., 2012; Pizarro et al., 2009), LV GLS (Witkowski et al., 2013), exercise LV GLS (Donal et al., 2012; Magne et al., 2014), interstitial fibrosis, and PCr/ATP ratio), longitudinal comparison of biomarker against outcome, and randomized studies of (biomarker-guided) treatment strategies. To this effect, current trials comparing treatment strategies include the UK Early Mitral Surgery Trial and REVERSE-MR (NCT03389542), while a study is underway comparing MRI-derived ECV with post-repair reverse remodelling (Liu et al., 2017).

Despite its inferior assessment of MV anatomy (MR mechanism) compared with echo, and currently limited outcome data, cardiac MRI can make contributions to both current and unconventional biomarkers. The limitations of echo assessment in MR are well known: acoustic window, nonholosystolic, nonhemispheric, eccentric or multiple jets, extrapolation from a single systolic frame (peak regurgitant rate) to mean regurgitant rate, noncircular EROA, need to integrate multiple parameters, poor interobserver agreement on quantitative parameters of MR severity (Biner et al., 2010), and poor interobserver limits of agreement for aortic and mitral stroke volume by 2D pulse-wave transthoracic echo (4.7 $\pm$ 29.1 and 2.9 $\pm$ 19.6 ml respectively) (Thavendi-

ranathan et al., 2012). In comparison, MRI-assessed LV volumes are considered the reference standard (Bellenger et al., 2000; Wood et al., 2014). MRI-assessed regurgitant volume compared well with invasive assessments (Hundley et al., 1995), LVEDVi (Uretsky et al., 2010), and (unlike echo) with post-repair fall in LVEDV (Uretsky et al., 2015), with low inter-observer variability for regurgitant volume (Aplin et al., 2016; Uretsky et al., 2015, 2010) and MR grade (Penicka et al., 2018; Uretsky et al., 2015). Compared with transthoracic echo in 26 participants with (mostly primary) MR, cardiac MRI showed less interobserver variability using MRI measures of LV volumes, LVEF, and regurgitant volume, although for regurgitant volume the difference was not statistically significant (Cawley et al., 2013); in another study of 60 participants with MR (half primary), regurgitant volume was significantly less variable by MRI (Lopez-Mattei et al., 2016).[3] In the largest and most recent study, MRI-assessed MR category (moderate or severe) correlated better with LVEDVi than echo-assessed category, and patients with discordant grading (MRI-moderate/echo-severe or MRI-severe/echo-moderate) had outcomes similar to patients with concordant moderate or severe grading respectively (Penicka et al., 2018). In summary, despite most studies lacking a reference standard for regurgitant volume, MRI probably provides both a more accurate and reproducible quantification.

Echo data relating regurgitant volume in primary MR to all-cause mortality dates from 2005 and is limited to holosystolic MR (Enriquez-Sarano et al., 2005); MRI data is more recent and is not so limited. In 109 patients with asymptomatic moderate or severe primary MR followed for a mean 2.5 ± 1.9 years, MRI-assessed thresholds of regurgitant volume > 55 ml, regurgitant fraction > 40%, LVEDVi > 100 ml/m^2, LVM > 171 g, LVESVi > 36 ml/m^2 and LVEF < 0.65 discriminated those more likely to develop a surgical indication (Myerson et al., 2016). In 258 patients with asymptomatic moderate or severe primary MR, sinus rhythm and LVEF > 0.60, MRI-

[3] For a list of studies comparing CMR and echo using quantitative methods see Uretsky et al. (2018).

assessed MR category (moderate or severe) had less inter-observer variability than echo-based category (10 vs 40%), and MRI-assessed regurgitant volume, LVESVi and MR category independently predicted all-cause mortality (Penicka et al., 2018). MRI-assessed regurgitant volume (the best threshold being $\geq$ 50 ml) offered the best prediction of all-cause mortality or development of a surgical indication over a median 5.0 years, compared with MRI-assessed LVESVi and echo-derived LVESD, regurgitant volume, and EROA. Specificity of MRI-assessed regurgitant volume was improved by adding LVESVi > 35 ml/m^2. While these data are promising, challenges for MRI assessment still include: lack of specific thresholds for severity, concomitant aortic regurgitation, intracardiac shunt or atrial fibrillation, and lack of phase-contrast sequences that track flow at the MV plane (phase-contrast planes are currently fixed during the cardiac cycle).

The arguments for MRI do not just include more consistent assessment of MR severity, prediction of need for surgery or mid-term outcome mortality, or more consistent selection into trials of management strategy – it may also (as I argued for AS) provide mechanistic explanations for cardiac decompensation. Regurgitant volume/LVEDV ratio is larger in primary rather than in secondary MR (Gaasch and Meyer, 2018), indicating more myopathy in secondary MR; longitudinal falls in this ratio could indicate decompensation in primary MR. However, owing to greater variability in assessing severity compared with AS, the field has not addressed whether some ventricles exposed to similar degrees of primary MR develop greater degrees of dilation, and if so, why.[4] Nor do we understand (from observations in instrumented dogs) why the hypertrophic response to a similar stroke work demand is less in MR than in AS, nor why, given similar degrees of hypertrophy, the LV is more likely to exhibit contractile dysfunction in MR than in AS (Carabello et al., 1992). Whether

[4] The hypothesis of disproportionate secondary MR, i.e. a high regurgitant volume/LVEDV ratio, being a predictor of benefit from therapies reducing MR, was recently introduced to explain the discordant benefit observed from mitraclip in the COAPT and MITRA-FR trials (Grayburn et al., 2019).

limited metabolic reserve could be contributing to variability in decompensation is an important question.

There are small studies reporting focal (Han et al., 2008; Van De Heyning et al., 2014) and/or interstitial fibrosis (Bui et al., 2017; Edwards et al., 2014; Pradella et al., 2019) in patients with primary MR, and reports of focal fibrosis in arrhythmic MV prolapse without MR (Basso et al., 2015), but no longitudinal outcome studies. Fibrosis bears no clear relation to degree of MR, suggesting it may be more specific for arrhythmic risk than for latent transition to failure.

There is one prior study of PCr/ATP ratio in primary MR (Conway et al., 1998). This included patients with a range of MR grades, classified severity using colour flow LA jet area, and predated CK k_f measurement. The ratio was reduced compared with controls and correlated inversely and most clearly with echo-assessed LVESD. There are no human or animal studies of CK k_f in volume-overload hypertrophy.

5.2 RESULTS

Participants

I recruited 20 participants with severe primary MR, preserved LV systolic function at clinical echo, and a decision for surgical repair, as per Table 2.1. These participants were used as models of volume overload-induced pathological hypertrophy, with the control group being 20 healthy volunteers. One participant with MR was excluded from analysis for having unexpected systolic impairment at time of MRI (LVEF 45%, LVEDVi 265 ml/m^2, LVESVi 147 ml/m^2, regurgitant volume 108 ml). Another died from chest sepsis pre-operatively but was included in baseline analyses. Thus 18 underwent operative repair. At operation, prolapse affected the anterior mitral valve leaflet in two and the posterior in sixteen; additionally, seven had at least one flail segment and two had deep MV clefts. All underwent MV repair; ten had concomitant tricuspid valve repair based on intraoperative transoesophageal echo. Mean NYHA

class was 2 ± 0.58. Of the three who denied exertional breathlessness, two had flail segments and two had palpitations.

Participant medical histories are listed in Table 5.1. Participants had higher age, heart rate (HR), mean arterial pressure, lower 6 minute walk distances, and were more likely to have hypertension, atrial fibrillation, and be taking ACE-I/ARB, loop diuretic or oral anticoagulant (OAC). RV systolic pressure was assessable in only 6 clinical echo reports, so not quoted here.

LV mass and volumes

As a group, patients with primary MR met criteria for severe MR (even accepting that there are no established criteria specific to MRI, and that MRI-assessed regurgitant volume thresholds should likely be lower than those established for echo). Mean LVEDV was increased by 63 ml (222 vs 160 ml), LVSV by 43 ml (142 vs 99 ml) and RVSV decreased by 20 ml (81 vs 101 ml), resulting in a mean regurgitant volume difference of +63–68 ml, depending on whether this was estimated by LVSV–aortic forward stroke volume (AoForw) or by LVSV–RVSV (Table 5.2, Figures 5.1, 5.2). Regurgitant fraction (regurgitant volume/LVSV) was 42% by both methods. LVMi was increased 22%, LVEDVi 35%, and LVESVi 28%, while LVEF was preserved and RVEF reduced. This indicates significant pathological hypertrophic remodelling, yet not detectable by LVEF or LVESD.

Energetic measures

Mean PCr/ATP ratio was reduced in primary MR (1.56 vs 2.08), but mean CK k_f was not significantly different (Table 5.3, Figure 5.3 Panels A–B). Scatterplotting these measures against regurgitant volume (Figure 5.4), a negative correlation (r = –0.58, p = 1e–4) was observed for PCr/ATP and none for k_f. Removing healthy volunteers from these figures resulted in no significant correlation between PCr/ATP and regurgitant volume (r = –0.21, p = .40, not shown). Scatterplotting PCr/ATP against LVEDVi and

Table 5.1: Participants' medical and drug history (MR)[a]

Parameter	MR	HV
n	19	20
Age (years) ∗	65 (62, 78)	37 (29, 64)
BMI (kg/m^2)	26 (23, 29)	24 (22, 27)
Male (%)	12 (63)	9 (45)
NYHA 1 (%)	3 (16)	
NYHA 2 (%)	13 (68)	
NYHA 3 (%)	3 (16)	
HR (/min) ∗	67 (61, 74)	60 (53, 65)
SBP (mmHg)	133 (19)	123 (18)
DBP (mmHg)	72 (7)	67 (11)
MAP (mmHg) ∗	92 (9)	86 (11)
6mwt (m) ∗	533 (96)	606 (63)
Serum Cr (µmol/l)	85 (18)	
History:		
DM (%)	0 (0)	0 (0)
Hypertension (%) ∗	6 (32)	1 (5)
VTE (%)	0 (0)	0 (0)
TIA/stroke (%)	1 (5)	0 (0)
Smoker (%)	0 (0)	0 (0)
Prior smoker (%)	8 (42)	9 (45)

[a] Counts given as number (%); continuous variables as mean (SD) or median (IQR). Reporting as for Table 4.3.

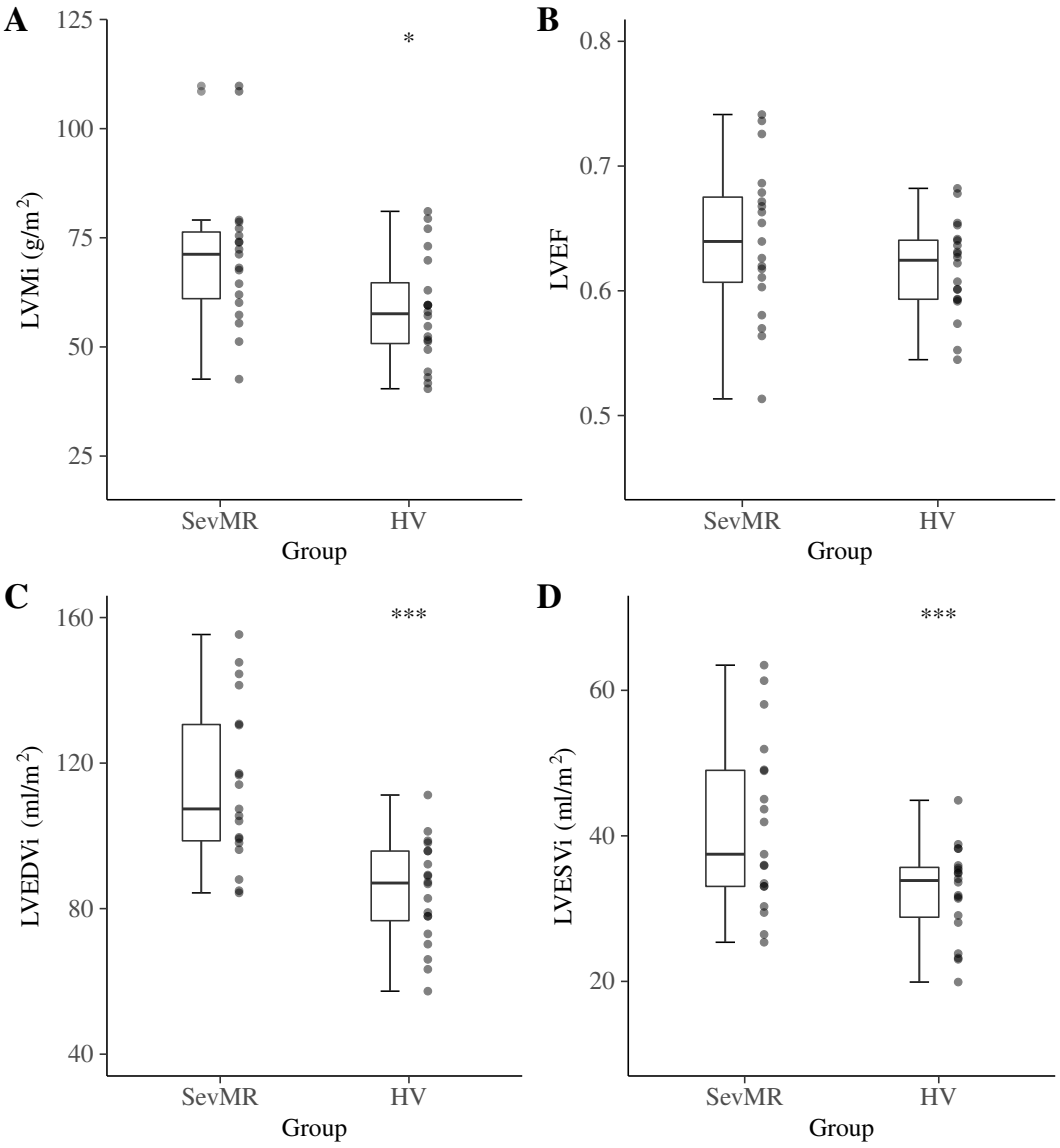


Figure 5.1: LVMi, LVEF, and LV volumes in primary MR and healthy volunteers. Conventions as for Figure 4.1.

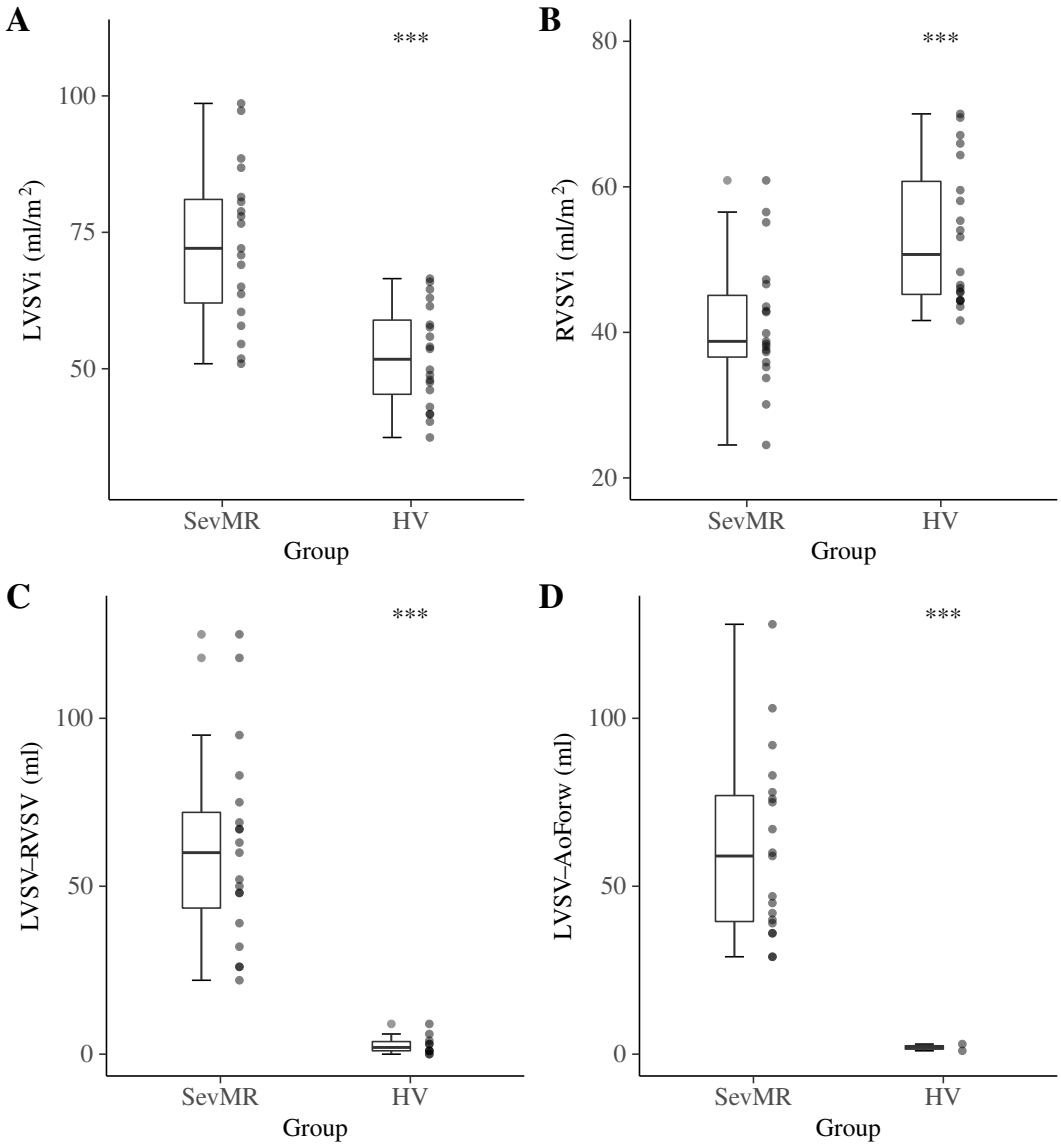


Figure 5.2: LVSVi, RVSVi, and MR regurgitant volume calculated by two methods (LVSV–RVSV and LVSV–Aortic forward flow) in primary MR and healthy volunteers.

Table 5.1: Participants' medical and drug history (MR)[a] (continued)

Parameter	MR	HV
ECG:		
AFib (%) ∗	4 (21)	0 (0)
LBBB (%)	0 (0)	1 (5)
TWI/strain (%)	1 (5)	0 (0)
QRS width (ms) ∗	102 (88, 102)	92 (84, 98)
Drugs:		
Beta-blocker (%)	7 (37)	2 (10)
ACE-I/ARB (%) ∗	9 (47)	1 (5)
MRA (%)	2 (11)	0 (0)
Loop diuretic (%) ∗	8 (42)	0 (0)
Antiplatelet (%)	3 (16)	0 (0)
OAC (%) ∗	4 (21)	0 (0)

[a] Counts given as number (%); continuous variables as mean (SD) or median (IQR). Reporting as for Table 4.3.

LVESVi (Figure 5.5), a negative correlation was observed for LVEDVi (r = –0.4, p = .013). Again, removing healthy volunteers resulted in no significant correlation with LVEDVi (r = –0.10, p = .69, not shown). No significant correlations were observed between PCr/ATP and LVESD (not shown).

Mean forward flux estimated by $k_f \times$ estimated [PCr] was reduced in the MR group (by 34%, two-sided p = .027). There was no significant correlation between this measure and estimated regurgitant volume (r = –0.29, p = .08), nor with LVEDVi (r = –0.06, p = .7). While this likely indicates a fall in resting forward flux in the face of increased wall stress (cavity dilation) and stroke work, this could not be corroborated by biopsy-obtained CK total activity, as only two samples were large enough to assess

Table 5.2: Chamber dimensions by CMR in severe MR[a]

Parameter	MR Mean (95% CI)	HV Mean (95% CI)	Sig.
BSA (m^2)	1.93 (1.80, 2.05)	1.88 (1.77, 1.98)	.53
LVMi (g/m^2) ∗	71.0 (63.0, 79.0)	58.3 (52.5, 64.1)	.011
LVEF (%)	64.1 (61.1, 67.0)	61.8 (60.0, 63.5)	.17
LVEDVi (ml/m^2) ∗	114.0 (103.4, 124.6)	84.7 (78.1, 91.2)	3e–5
LVESVi (ml/m^2) ∗	41.3 (35.7, 46.9)	32.3 (29.4, 35.3)	.006
LVSVi (ml/m^2) ∗	72.8 (65.9, 79.7)	52.3 (48.0, 56.5)	1e–5
LVM/LVEDV (g/ml)	0.62 (0.58, 0.67)	0.69 (0.64, 0.75)	.051
RVEDVi (ml/m^2)[b]	74.0 (60.3, 94.2)	86.5 (73.3, 97.4)	.09
RVESVi (ml/m^2)[b]	31.1 (24.0, 48.5)	34.2 (27.5, 39.5)	.84
RVSVi (ml/m^2)[b] ∗	38.8 (35.9, 46.6)	50.7 (45.0, 62.0)	1e–4
RVEF (%) ∗	54.6 (50.4, 58.8)	61.5 (59.3, 63.7)	.004
LVSV–RVSV (ml) ∗	61.3 (47.3, 75.3)	–2.1 (–4.7, 0.5)	1e–8
LVSV–AoForw (ml) ∗	61.3 (48.1, 74.5)	–6.4 (–10.2, –2.6)	1e–9
(LVSV–RVSV)/LVSV (%) ∗	42.1 (36.1, 48.1)	0.0 (0.0, 0.1)	1e–13
(LVSV–AoForw)/LVSV (%) ∗	42.4 (36.9, 48.0)	0.1 (0.0, 0.1)	4e–15
LVESD-SA-MRI (mm)	38.1 (35.9, 40.3)	36.4 (34.7, 38.0)	.19
LVESD-3ch-MRI (mm)	37.8 (35.2, 40.4)	35.1 (33.0, 37.1)	.09

[a] Mean (95% CI) values for 19 patients with primary MR and 20 healthy volunteers. LVESD-SA and LVESD-3ch, LV end-systolic diameter on short-axis and 3-chamber cine MRI.
[b] Given as median (IQR).

CK total activity and CS activity.[5] In these two samples, values of CK total activity and CK capacity were comparable with NH hearts (Table A.3, p. 240). Also consistent

[5] Fewer LV biopsies were taken in primary MR than in AS, because this is technically more difficult (the scalpel is passed through the MV from the LA, rather than through the LVOT after the AV has been removed).

with there being no impairment of CK capacity, mean total creatine was comparable or increased compared with NH hearts (94.7 (26.2) vs 66.2 (14.5) nmol/mg protein, n = 7 vs 6, two-sided p = .03, Table 4.5, p. 139).[6]

Table 5.3: Baseline energetic measures in MR[a]

Parameter	MR	HV	Sig.
PCr/ATP	1.56 (1.40, 1.72)	2.08 (1.90, 2.26)	6e–5
CK k_f adj (/s)	0.19 (0.15, 0.24)	0.23 (0.18, 0.29)	.24
k_f adj × est [PCr] (μmol/g/s)	1.8 (1.3, 2.4)	2.8 (2.1, 3.4)	.027
Total creatine (nmol/mg protein)[b]	94.7 (70.5, 119.0)		
TAN pool (nmol/mg protein)[c]	81.0 (42.9, 110.0)		
CK total activity (IU/mg protein)[d]	4.71		
CS activity (IU/mg protein)[d]	0.288		

[a] Mean (95% CI) values for 19 patients with MR and 20 healthy volunteers. Two-sided p-values given. Compare with Table A.3, p. 240.
[b] n = 7.
[c] n = 6.
[d] n = 2.

CK isoform expression

This could be assessed in only two samples (see Table A.3 and Section 4.3 for discussion). The MR group had the highest recorded MtCK:total CK and MtCK:CS ratios, but I will not speculate on this further given the low numbers.

Late follow-up after MV repair

14 of 18 returned for repeat PCr/ATP ratio and MRI. (k_f was not repeated.) Reasons for not returning were: pacemaker insertion in two and patient declined in two (one with new-onset rheumatoid arthritis).

[6] TAN pool values (n = 6, median 74 nmol/mg protein, IQR 59–106) were higher than in other biopsied groups, for unclear reasons.

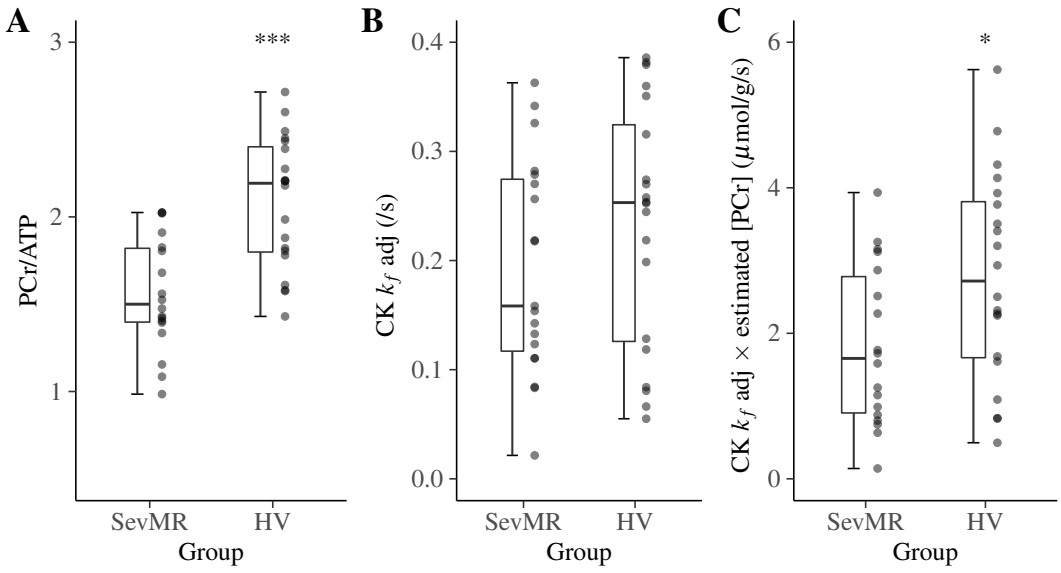


Figure 5.3: (A) PCr/ATP ratio, (B) CK k_f adj, and (C) k_f × estimated [PCr] in primary MR and healthy volunteers.

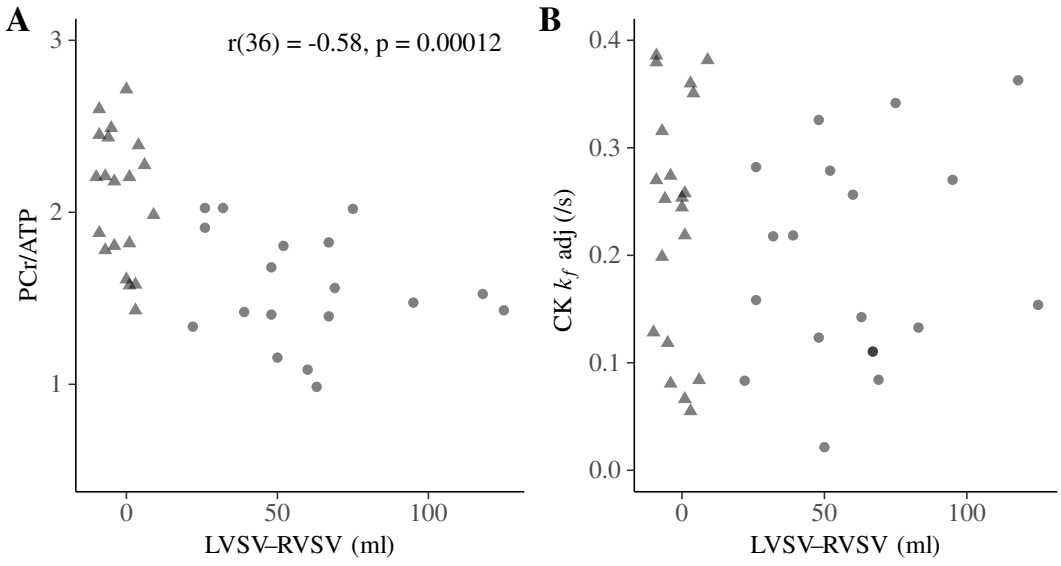


Figure 5.4: Scatter plot of MR regurgitant volume (LVSV–RVSV) against (A) PCr/ATP; (B) CK k_f in primary MR (circles) and healthy volunteers (triangles).

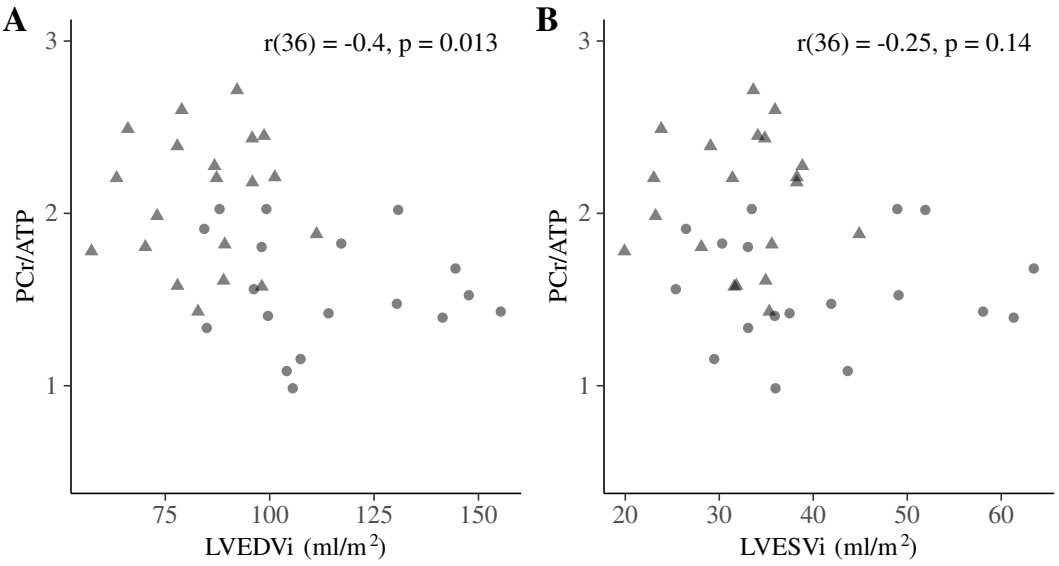


Figure 5.5: Scatter plot of (A) LVEDVi, (B) LVESVi against PCr/ATP ratio in primary MR (circles) and healthy volunteers (triangles).

In the paired dataset, follow-up scans were a median (IQR) 7.0 (6.2, 7.4) months post-op and 7.5 (7.4, 10.0) months post initial scan. Alongside normalisation of estimated regurgitant volume, mean LVMi decreased by 16%, LVEDVi by 36%, and LVESVi by 27%, resulting in a 19% increase in LVM/LVEDV (Table 5.4). In the face of increased afterload, LVEF reduced by 8% (relative) and 4.8% (absolute). There were improvements in RVESVi and RVEF, perhaps reflecting (unmeasured) falls in pulmonary pressures. PCr/ATP increased from 1.55 (0.34) to 1.83 (0.53) (n = 13 as one participant had an excessively noisy pre-op spectrum, one-sided p = .040).

There was no significant difference in 6 minute walk distance (m): mean (SD) 537 (112) from 531 (110) (two-sided p = .59).

5.3 DISCUSSION

In summary, the original findings in this chapter are that in a group of mostly symptomatic patients with severe primary MR listed for MV repair and clinically-judged

Table 5.4: LV energetics and dimensions after MV repair[a]

Parameter	Pre-op	Late f/u	*p*-value
BSA (m^2)	1.89 (0.26)	1.91 (0.26)	.13[b]
PCr/ATP ratio ∗	1.55 (0.34)	1.83 (0.53)	.040
LVMi (g/m^2) ∗	66.1 (10.7)	55.3 (10.0)	5e–4
LVEF (%) ∗	63.9 (5.9)	59.1 (7.7)	.024[b]
LVEDVi (ml/m^2) ∗	111.0 (21.8)	71.2 (12.5)	1e–7
LVESVi (ml/m^2) ∗	40.3 (11.3)	29.5 (9.4)	4e–6
LVSVi (ml/m^2) ∗	70.8 (13.9)	41.7 (7.5)	2e–6
LVM/LVEDV (g/ml) ∗	0.59 (0.56, 0.67)	0.78 (0.71, 0.81)	9e–4[b]
RVEDVi (ml/m^2)	71.7 (60.3, 84.9)	68.5 (58.3, 73.6)	.63[b]
RVESVi (ml/m^2) ∗	30.4 (22.7, 39.2)	27.2 (24.6, 28.6)	.042[b]
RVSVi (ml/m^2)	40.2 (6.4)	42.0 (10.2)	.40[b]
RVEF (%) ∗	54.8 (9.5)	58.7 (6.3)	.042[b]
LVSV–RVSV (ml) ∗	58.6 (29.8)	–0.2 (10.7)	1e–6
LVSV–AoForw (ml) ∗	59.9 (28.7)	–3.3 (8.8)	6e–7

[a] Summary data for 14 patients with primary MR at late follow-up. n = 13 for PCr/ATP ratio. p-values given as one-sided unless otherwise marked. Values given as mean (SD) or median (IQR).
[b] Two-sided p-values given.

'preserved' LVEF, PCr/ATP ratio was significantly reduced compared with healthy volunteers and increased at late follow-up, while CK k_f was no different pre-operatively. As a result, estimated flux ($k_f \times$ est [PCr]) was reduced at baseline.

The findings should be set in context of disease stage. Participants did not undergo 'early repair': 16/19 admitted dyspnoea (although exercise-testing to prove asymptomatic status was not performed), mean 6 minute walk distance was reduced, 4 had atrial fibrillation, and RVEF was reduced. Using previously identified prognostic

thresholds (see Introduction), 12 had LVEDVi > 100 ml/m^2, 12 had LVESVi >35 ml/m^2, 10 had LVEF < 0.65, 10–12 had regurgitant volume $\geq$ 50 ml (depending on method used), 3 had LVM > 171 g, and 7 had LVESD $\geq$ 40 mm (all by MRI). The pre-operative data also extend previous findings of discordance between MRI and echo: although all had echo-assessed severe MR, only 10–12 had regurgitant volume $\geq$ 50 ml by MRI.

The degree of pathological hypertrophy (mean LVMi 71.0 g/m^2) in primary MR, versus 68.0 in modAS and 75.2 in sevAS-pEF, Table 4.4) should also be set in context of the inciting stimulus. In instrumented dogs with chronic severe primary MR or chronic severe AS, matched increases in stroke work (140% of normal) resulted in increases in LV/body weight ratio of 25 and 88% respectively and therefore increased stroke work per gram myocardium more in MR. In a second comparison, matched increases in LV/body weight ratio (125% of normal) resulted in increased stroke work and depressed contractile function[7] in MR relative to AS (Carabello et al., 1992). Thus, relative to AS, one would expect similar stroke work increases to be associated with less hypertrophy in MR, and similar degrees of hypertrophy to be associated with greater degrees of contractile dysfunction in MR. One might also expect greater degrees of energetic impairment, although to my knowledge this study has not been performed (compare Tables 4.5 and 5.3). In this chapter, stroke work, the area within a pressure-volume loop, was not measured invasively (and cannot be accurately estimated from LVSV and MAP because the pressure-volume loop in MR particularly is not rectangular); nor was ejection time measured. Nevertheless, the degree of hypertrophy was similar to that in modAS while LVESVi was increased, suggesting greater systolic dysfunction in MR, in agreement with previous animal work.

[7]Contractile dysfunction was defined as reduced fractional shortening and reduced velocity of circumferential fibre shortening (V_{CF}) relative to end-systolic wall stress, where V_{CF} is (LVEDD–LVESD)/(LVEDD $\times$ ejection time).

The mechanisms underlying greater degrees of systolic dysfunction in primary MR (relative to AS) for similar degrees of LVMi are not well defined, but presumably relate to the trigger in MR (raised end-diastolic wall stress) not recruiting growth signalling to the same extent as other pathways, resulting in earlier exposure to higher degrees of stroke work per gram myocardium. This chapter's results indicate that reduced phosphotransfer reserve – at least at the stage of disease studied – comprises part of the metabolic remodelling process, with potential for reversibility once the lesion is corrected. The post-repair rise in ratio also argues against the difference being largely explained by the patients being older than the healthy volunteers.

I did not replicate previous findings of an inverse correlation between PCr/ATP and LVESD (Conway et al., 1998), but in that study a wider spectrum of disease was included, as indicated by the echo-assessed mean LVMi ranging 104–146–222 g/cm^2 and LVESD ranging 2.92–3.48–4.31 cm across three grades of MR severity.

Part of the heterogeneity in this MR group represents real-world practice, as consecutive patients listed for operation were approached. While all had 'preserved LV systolic function' on echo, there was significant LV dilation and reduced RVEF; metabolic reserve (and by implication contractile reserve) was significantly reduced. The findings do not directly support earlier intervention, as comparison between early versus later intervention strategies was not performed, but do extend previous findings of echo–MRI discordance in MR severity grading and argue against complacency in this patient group.

Outstanding questions include: whether some patients develop greater degrees of dilation than others for similar degrees of regurgitant volume (the vulnerable ventricle hypothesis), whether some patients develop greater degrees of metabolic impairment for similar degrees of regurgitant volume, whether these two groups are in fact the same group (the metabolic HF hypothesis), whether patients listed for 'early repair' (asymptomatic, without LV/RV dilation or dysfunction) display similar degrees of

reduced metabolic reserve as those here, and whether markers of metabolic reserve could predict late persistent LV dysfunction post-repair (the metabolic biomarker hypothesis).

6 ATP delivery rates in acute increases in work and physiological hypertrophy

This chapter aims to investigate

- Whether in physiological hypertrophy ATP delivery rates through CK are normal and unrelated to LV mass.
- Whether CK k_f and ATP delivery rate increase in normal and athletically-remodelled hearts subject to acute increases in work driven by catecholamine stress.

6.1 INTRODUCTION

The athletic heart

MRS offers the opportunity to investigate the reasons for both reduced and increased muscle performance. In recent years there has been increasing interest in the athletically-remodelled heart. The reasons for this include:

1. The increased clinical use of MRI has allowed detection of milder phenotypes of hypertrophic, dilated, arrhythmogenic and noncompaction cardiomyopathy,

such that extents of wall thickening, cavity dilation and/or trabeculation may overlap with those seen in athletic hypertrophy.[1] Answering these diagnostic questions (rightly or wrongly) may disqualify from sport.

2. The athletic heart is 'a pro-arrhythmic heart' but the threshold between physiological and pathological remodelling is unclear, and a threshold for arrhythmic risk may not exist in the conventional sense (Heidbuchel, 2018). Whether some (perhaps more vulnerable) hearts react to excessive degrees of exercise-training by developing focal fibrosis, and how much this increases arrhythmic risk, are scientific but also public health questions, given increased amateur involvement in endurance sport.

3. There is interest in whether muscle metabolism can be manipulated to improve performance further in elite athletes and the military (Cox et al., 2016).

4. As physiological hypertrophic signalling may antagonise pathological hypertrophic signalling and be cardioprotective (see p. 7), understanding how physiological hypertrophy 'works' could provide insights translatable to those with or at risk of heart failure.

Commonly understood, athletic remodelling constitutes morphological and electrical remodelling which varies depending on the type and dose of exercise. Building on my prior outline of mechanisms underlying physiological hypertrophy (p. 5), it is clear that metabolic remodelling also contributes to the athletic heart phenotype. The details of how metabolism permits or activates phenotypic changes in physiological hypertrophy are still unclear, but include metabolite signalling, altered gene expression and coordination of growth pathways.[2] Acute changes in metabolism during exercise must be differentiated from chronic, resting-state adaptations. Most of our current

[1] The phenotype is reviewed elsewhere (Baggish and Wood, 2011; La Gerche et al., 2017, 2009; Sharma et al., 2015).

[2] Reviewed (Gibb and Hill, 2018).

understanding of metabolism in physiological hypertrophy comes from studies of substrate handling in animal models; little is known in humans.

Human studies of myocardial energetics in athletic hypertrophy have found no differences in PCr/ATP at rest (Perseghin et al., 2007; Pluim et al., 1996) or during dobutamine stress (Pluim et al., 1998). One study found moderate correlation between PCr/ATP ratio and maximal work capacity in healthy volunteers (Klug et al., 2007). No study has assessed k_f in physiologic hypertrophy.

CK responds to exercise training in skeletal (Apple and Rogers, 1986; Zoll et al., 2002) and cardiac muscle (Ventura-Clapier et al., 2007). Myocardial CK total activity and % CK-MB increased in response to mixed sprint/endurance exercise training in dogs (Stuewe et al., 2001), swim-training in rats (Rockstein et al., 1981), and running in young mice (Steinhagen-Thiessen and Reznick, 1987), but CK total activity did not increase in endurance-only regimens in dogs (Miller et al., 1989), or in older swimming rats (Chesky et al., 1983) or older running mice (Steinhagen-Thiessen and Reznick, 1987). Therefore the relationship between CK total activity and physiologic hypertrophy is unlikely to be straightforward.

The stressed heart

Why does cardiac CK activity during stress matter? Investigators building on early studies (discussed Section 1.3) showed that contractile activity in hypoxia (Bittl et al., 1987a) and postischaemic recovery, both situations where oxphos is impaired, were linked to mtCK activity (Bittl et al., 1985) and/or forward CK flux (Neubauer et al., 1988). The first reason then is that understanding CK activity over a range of physiological states fundamentally informs our understanding of respiratory control. The candidate controllers for oxphos rate in muscle are the substrates of that reaction ($3\,ADP + 3\,P_i + NADH + H^+ + \frac{1}{2}\,O_2 \longrightarrow 3\,ATP + NAD^+ + H_2O$); under normoxic conditions [ADP], [P_i], and mitochondrial redox state are the key candidates. In

theory, the relation between oxphos rate as a proportion of its maximum (V/V_{max}) and the concentration of each candidate controller observes a Michaelis-Menten hyperbola – $V/V_{max} = 1/(1 + K_m/[ADP])$ – so that kinetic control is exerted when the concentration of the controller is low relative to its K_m (Chance et al., 1985).[3] However, in vivo, the relative contribution of the candidate controllers across the range of oxphos rates ($0 < V/V_{max} < 1$), and the validity of this simple Michaelis-Menten model, remain unknown (Balaban, 1990). At least two steady-state oxphos rates (or workloads) must be studied if we are to understand respiratory control (or separate normal from abnormal). As previously discussed (p. 35), cardiac adenine nucleotides are compartmented, improving the kinetics and thermodynamics of ATP hydrolysis and synthesis, but introducing a dependence on CK kinetics such that free creatine also becomes a feedback regulator of oxphos flux. This complicates the question of the relative contribution of candidate controllers in myocardium, as myocardial O_2 consumption rate (MVO_2) may depend on the ratio $[P_i][Cr][ADP]/[ATP][PCr]$ (Walsh et al., 2001).

Second, abnormal CK reserve may underlie the exaggerated fall in PCr/ATP ratio seen during dobutamine stress in subjects with heart failure or conditions predisposing to heart failure. We know from animal studies that in health, depending on species, exchange between PCr and ATP is 6–12-fold (Bittl and Ingwall, 1985; Kupriyanov et al., 1984; Matthews et al., 1982), 9–18-fold (Perry et al., 1988) or >10-fold (Katz et al., 1989; Ye et al., 2001b) faster than oxidative ATP synthesis rates,[4] and that when heart energy demands increase, oxidative ATP synthesis can increase 4–6 fold, which

[3] There is a trade-off between work rate and energy cost: as the concentrations of ADP or P_i rise, ΔG_{ATP} falls and cytosolic ATPases become thermodynamically limited; similarly if NADH/NAD^+ rises excessively, the mitochondrial ETC cannot accept electrons and substrate oxidation is limited.

[4] This large margin of reserve is referred to by some as indicating that 'the CK system' is 'at equilibrium', i.e. that the CK reaction is sufficiently fast to maintain cytosolic reactants at their equilibrium concentrations (from the MRS-perspective) across a range of workloads. This should not be confused with the contemporary understanding of four CK compartments (p. 37), each with their own equilibrium position. Some authors refer to the equilibrium position of soluble cytosolic CK as a 'quasi-equilibrium', in contrast to that of coupled mtCK or myofibrillar CK, which have extreme, 'unidirectional', equilibrium positions.

may approach resting CK activity, particularly if resting activity is reduced. The mechanism for stress-related falls in PCr/ATP may thus involve a fall in CK reserve flux relative to respiratory flux, yet this has not been demonstrated in humans. Also, an abnormal CK reserve may be easier to detect using stress responsiveness than with resting k_f, as I have already shown that total activity and resting k_f vary substantially.

Third, the experimental data in this area is discordant. The question comes down to the relative importance of the candidate controllers at any given oxphos rate (V/V_{max}). As [Cr][ADP]/[ATP][PCr] depends on the CK equilibrium, the question can be reframed as the relative importance of mitochondrial redox state, [P_i], the CK equilibrium position, and CK velocity. (CK velocity is not limiting in health at rest, but is in postischaemic recovery and may be in HF, so defining its contribution is necessary if we are to separate normal from abnormal physiology.) What is agreed is that at any given workload, forward and reverse CK fluxes are equal, and so are ATP synthesis and ATP hydrolysis fluxes (assuming steady-state) – otherwise [ATP] would change. As workload rises, MVO_2 (ATP synthesis) and ATP hydrolysis rates increase while [ATP] remains constant; alongside this, PCr/Cr ratio and [PCr] generally fall, while [P_i] rises (Bittl and Ingwall, 1985; Kupriyanov et al., 1984). However, each of these changes in isolation is too small to explain the degree of change in MVO_2 (assuming a simple Michaelis-Menten model) and stability of [ATP], and changes in other factors (CK flux, calculated [ADP], mitochondrial redox state and membrane potential, cooperativity factors) need to be invoked. Most of the disagreement (or speculation) is around what happens to these other factors. Studies that find rises in forward CK flux with workload report increases in k_f ([PCr] does not rise) and conclude that CK contributes to coupling ATP hydrolysis rates with oxphos rates; studies that find unresponsive k_f report unchanged CK flux with workload, and conclude that over the workload range studied, rises in [ADP], [P_i], or other factors play a greater role. In the latter case, the CK system is considered to be 'at equilibrium'

(see previous footnote), so that "increases in CK flux are not required to accommodate physiological increases in workload" (Murakami et al., 1999a).

I have summarised previous studies of CK k_f in hearts subject to different workloads in Table 6.1: those in small animals generally found rises in forward CK flux with workload; those in large animals generally did not. The only human study included six subjects, so was arguably underpowered. I have excluded studies in post-ischaemic hearts (Neubauer et al., 1988; Nunnally and Hollis, 1979), because the usual relation between contractile performance and VO_2 becomes confounded by post-ischaemic O_2-wasting.

The above discussion has concentrated on understanding the control of oxphos rate over the range of oxphos rates available. A separate question concerns the control of CK reaction velocity. This is related to substrate concentration, total enzyme activity, isoenzyme localization and pH (see Appendix, p. 229).

6.2 RESULTS

Participants

I recruited 20 healthy volunteers and 20 'athletes', whose hearts were considered likely models of physiological hypertrophy on the basis of >8 hours/week endurance exercise training for $\geq$ 1 year. Most were triathletes, with a minority training solely in cycling or rowing. As no professional athletes were recruited, 'athlete' status was only confirmed after the result of CPET testing, where both indexed peak VO_2 and anaerobic threshold (as a % of peak VO_2) had to be substantially raised.

19 of 20 healthy volunteers and 20 of 20 athletes had dobutamine studies. One control did not receive dobutamine as her resting SBP was 175 mmHg. Results from 17 of 20 athletes were carried forward for analysis: three men were dropped for having indexed peak VO_2 <45 ml/kg (27, 40, 41).

Table 6.1: Prior studies of CK k_f and flux at different workloads (1)

Model, MVO_2 variation	Mean k_f (/s) (-fold response)	Mean CK flux[a] (-fold response to ↑ MVO_2)
Rabbit ex vivo.[b] MVO_2 variation unclear.	0.15, 0.70 (↑ 4.7-fold).	Not given.
Rat ex vivo.[c] MVO_2 ↑ 3.1-fold.	0.27, 0.42, 0.46 (↑ 1.7-fold).	3.4, 4.6, 4.3 (↑ 1.3-fold, p = ns).
Rat ex vivo.[d] MVO_2 ↑ 6.6-fold.	0.37, 0.80 (↑ 2.2-fold).	↑ 1.5-fold.
Rat ex vivo.[e] MVO_2 ↑ 7.8-fold.	0.27, 1.30 (↑ 4.8-fold).	↑ 3.8-fold.
Rat ex vivo.[f] MVO_2 ↑ 1.2-fold.	↑ 2.4-fold.	↑ 2.2-fold.
Rat in vivo.[g] RPP ↑ 2.5-fold.	0.35, 0.50, 1.17 (↑ 3.3-fold).	15.4, 20.5, 30.1 (↑ 2.0-fold).
Rat in vivo.[h] RPP ↓ 33–49%.	↓ 17–71%.	↓ 37–75%.
Rabbit ex vivo, 3.7% mtCK.[i] MVO_2 ↑ 4.2-fold.	0.51, 1.09, 1.06 (↑ 2.1-fold).	9.7, 15.7, 17.9 (↑ 1.8-fold).
Rabbit ex vivo, 9.3% mtCK.[i] MVO_2 ↑ 4.2-fold.	0.68, 0.80, 1.48 (↑ 2.2-fold).	14.7, 22.0, 27.1 (↑ 1.8-fold).

[a] Flux usually in µmol/g dry weight/s but varies. ns, not significant.
[b] KCl arrest, control (Nunnally and Hollis, 1979).
[c] KCl arrest, 70 cm, 140 cm hydrostatic pressure (Matthews et al., 1982).
[d] KCl arrest, high work (Kupriyanov et al., 1984).
[e] KCl arrest, high work (Bittl and Ingwall, 1985).
[f] KCl arrest & variable LV pressure (Bittl and Ingwall, 1986).
[g] 2% halothane, 1% halothane, noradrenaline (Bittl et al., 1987b).
[h] 21, 10 or 8% O_2 (Bittl et al., 1987a).
[i] KCl arrest, empty beating, isovolumic beating (Perry et al., 1988).

Table 6.1: Prior studies of CK k_f and flux at different workloads (2) (continued)

Model, MVO_2 variation	Mean k_f (/s) (-fold response)	Mean CK flux (-fold response to ↑ MVO_2)
Dog in vivo.[a] MVO_2 ↑ 1.9-fold.	No change.	No change.
Pig in vivo.[b] MVO_2 ↑ 2-fold.	No change.	No change.
Sheep in vivo.[c] MVO_2 ↑ 3.3-fold.	No change.	No change.
Mouse ex vivo.[d] RPP 0, 29100, 33000 mmHg/min.	0.24, 0.43, 0.39. (↑ 1.6-fold.)	3.8, 7.8, 6.6. (↑ 1.7-fold.)
Pig in vivo.[e] MVO_2 ↑ 2.1-fold.	No change.	Flux ↓ 30%.
Dog in vivo.[f] MVO_2 ↑ 3.3-fold.	No change.	No change.
Human.[g] RPP ↑ 2-fold.	No change.	No change.
Pig in vivo.[h] RPP ↑ 3.2-fold.	No change.	No change.

[a] Control, rapid pacing (Katz et al., 1989).
[b] Control, noradrenaline infusion (Martin et al., 1989).
[c] Control, adrenaline infusion (Portman and Ning, 1992).
[d] KCl arrest, rapid pacing. (Van Dorsten et al., 1998).
[e] Control, dobutamine infusion (Murakami et al., 1999a).
[f] Control, dobutamine infusion (Ye et al., 2001b).
[g] Control, dobutamine infusion (Weiss et al., 2005).
[h] Control, dobutamine & dopamine infusion (Xiong et al., 2015).

9/19 (47%) controls and 13/17 (76%) athletes were male (p = .07); median age was 35 in both groups. All were in sinus rhythm and had normal ECGs.

LV mass and volumes, diastolic indices and CPET

Athletes had significantly increased LVMi, LV and RV volumes, and LVM/LVEDV ratio compared with controls (Table 6.2, Figures 6.1, 6.2, 6.3). Mean LVEDVi was comparable to the primary MR group (athlete vs sevMR, 106.9 vs 114.0 ml/m^2, Table 5.2 p. 180), while mean LVMi (81.1 vs 71.0 g/m^2) and median RVEDVi (106.4 vs 74.0 ml/m^2) were significantly larger. These comparisons indicate that the intermittent volume-loading stimulus in physiological hypertrophy is not just biventricular, but likely recruits different growth pathways.

When comparing resting diastolic indices by echo, athletes had larger E/A ratios (uncorrected for HR) and lateral MV annular tissue Doppler velocities (Table 6.3). CPET values indicated significant separation in cardiopulmonary fitness between groups (all p-values < 10^{-5}, Table 6.4). Peak indexed VO_2 was 58% higher in athletes, and the anaerobic threshold was raised from 48% to 79% of VO_2 peak. The reader will notice some overlap in peak VO_2: the lowest three values for athletes were in women (Figure 6.4); however these women were competitive at national level and had anaerobic threshold (AT)/VO_2 ratios of 0.78–0.83 so were accepted as highly trained. By comparison, the three highest VO_2 values in controls came from men, who had AT/VO_2 ratios of 0.31–0.40.

Energetic measures at rest and stress

Resting BP was no different between groups (median MAP 82 mmHg in both), but athletes had lower HR, so resting rate-pressure product (RPP) was reduced in athletes by 22% compared with controls (Table 6.5). Dobutamine resulted in comparable RPPs in both groups, such that athletes developed a larger -fold change from rest (3.1 vs. 2.5, p = .001). Larger doses were required to maintain HRs in athletes.

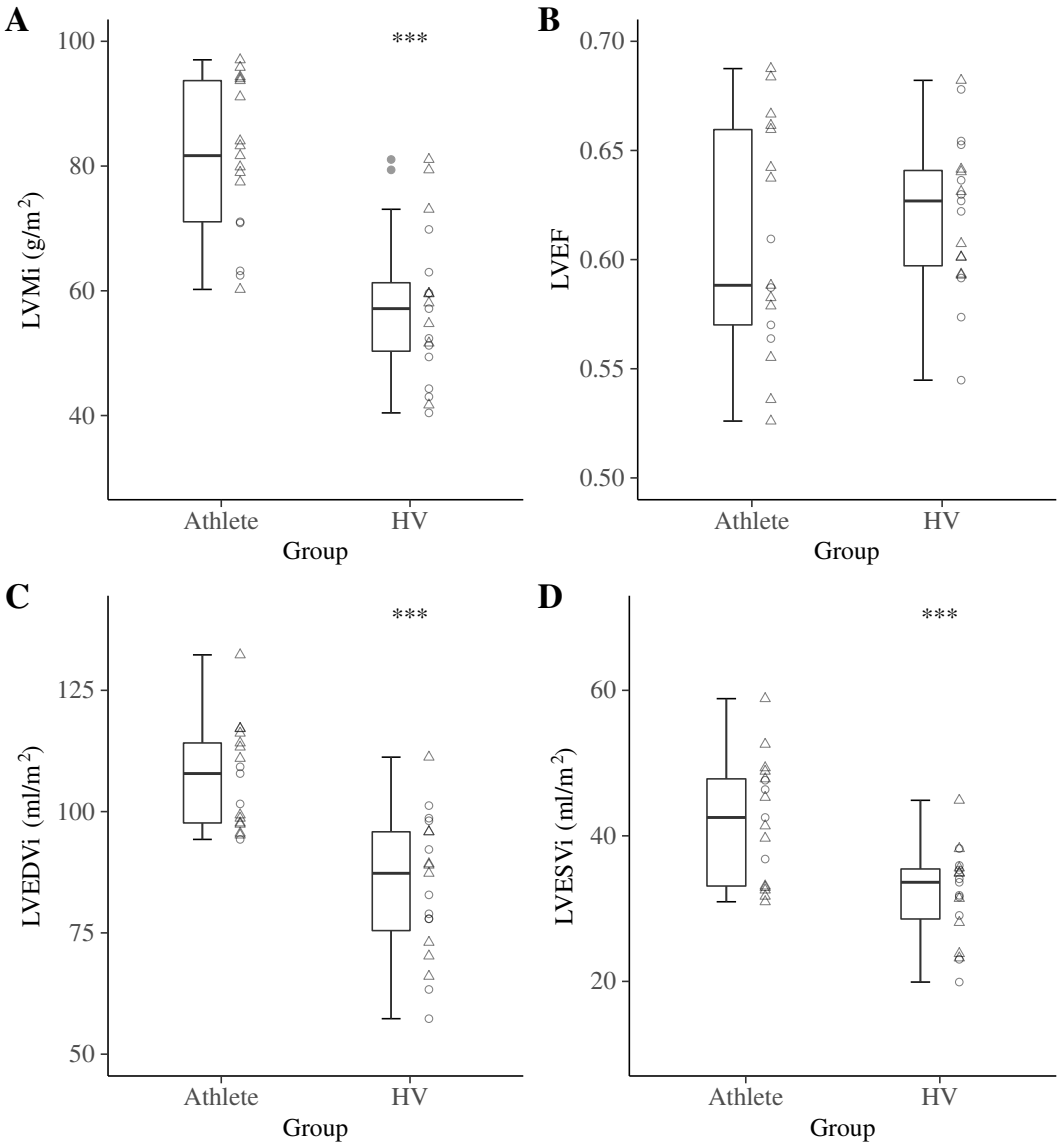


Figure 6.1: LVMi, LVEF, and LV volumes in athletes and controls. *Males shown as triangles, females as circles.*

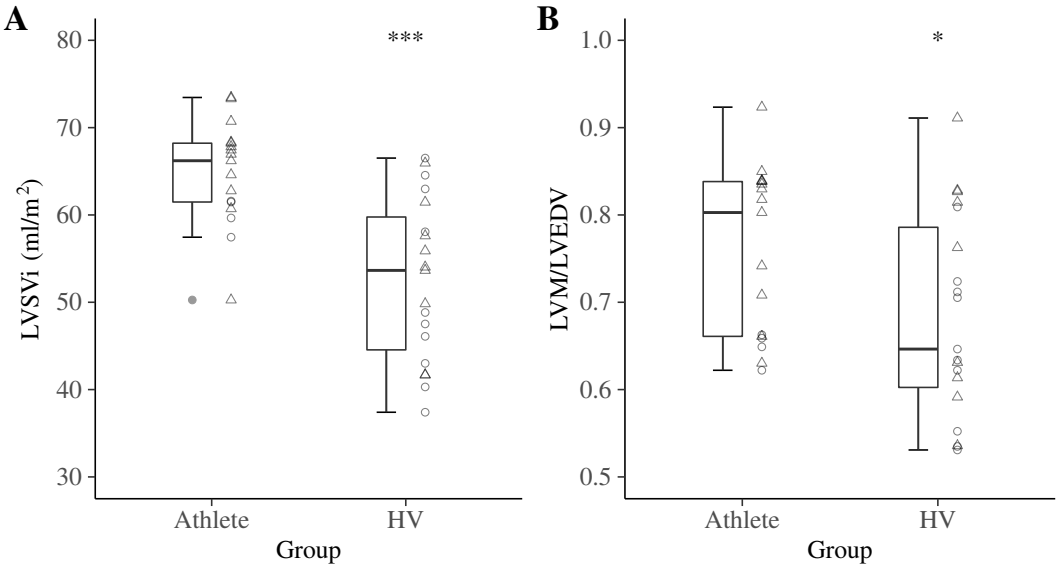


Figure 6.2: LVSVi and LVM/LVEDV ratio in athletes and controls.

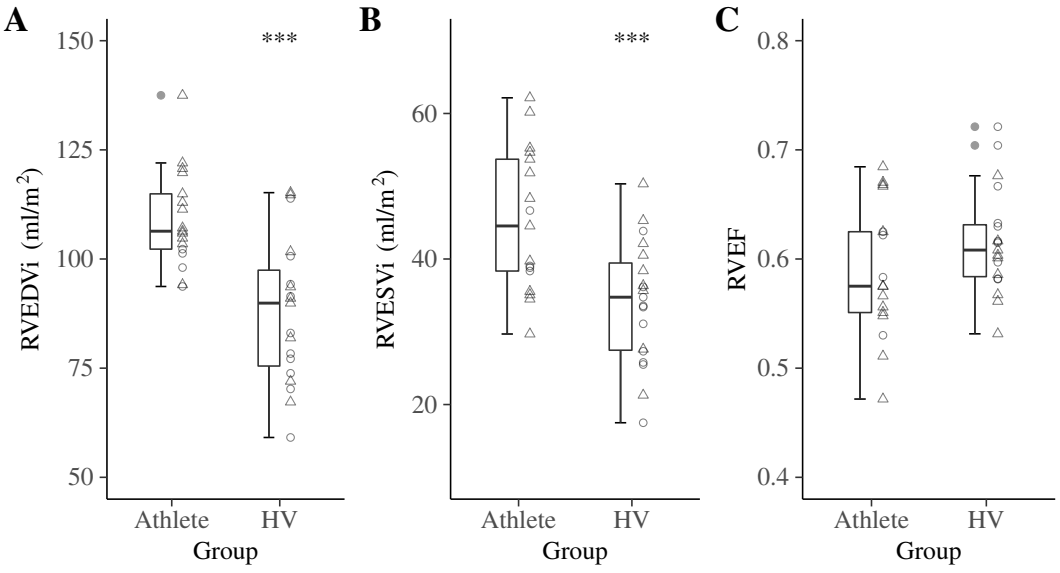


Figure 6.3: RV volumes and RVEF in athletes and controls.

Table 6.2: Chamber dimensions by CMR in controls and athletes[a]

Parameter	Control		Athlete		
	Mean	(95% CI)	Mean	(95% CI)	Sig.
Age (years)[b]	35	(28, 63)	35	(30, 42)	.57
BMI (kg/m^2)	24.5	(22.8, 26.1)	23.5	(22.7, 24.3)	.26
BSA (m^2)	1.89	(1.77, 2.00)	1.96	(1.86, 2.06)	.32
LVMi (g/m^2) $*$	57.3	(51.6, 63.1)	81.1	(74.8, 87.4)	1e–6
LVEF (%)	62.1	(60.4, 63.8)	60.8	(58.1, 63.5)	.39
LVEDVi (ml/m^2) $*$	84.5	(77.6, 91.5)	106.9	(101.5, 112.4)	7e–6
LVESVi (ml/m^2) $*$	32.0	(29.0, 35.0)	42.3	(38.0, 46.5)	3e–4
LVSVi (ml/m^2) $*$	52.5	(48.0, 57.0)	64.8	(61.7, 67.8)	4e–5
LVM/LVEDV (g/ml) $*$	0.68	(0.63, 0.74)	0.76	(0.71, 0.81)	.04
RVEDVi (ml/m^2)[b] $*$	89.9	(73.8, 100.6)	106.4	(102.3, 114.9)	1e–4
RVESVi (ml/m^2) $*$	34.0	(29.9, 38.1)	45.2	(40.1, 50.2)	.001
RVSVi (ml/m^2)[b] $*$	53.1	(45.5, 64.4)	64.4	(60.2, 69.0)	.002
RVEF (%)	61.6	(59.2, 63.9)	59.0	(55.8, 62.1)	.18

[a] Summary data for 19 controls and 17 athletes. All p-values two-sided.
[b] Given as median (IQR).

Resting and stress k_f adj values were not significantly different between groups (Table 6.6, bottom row). There was a significant stress-induced rise in k_f adj in controls, by a median 1.50-fold or +0.13 /s (Table 6.6); in athletes the median rise of 1.15-fold or +0.02/s was not statistically significant (Figure 6.5, Panels A–B).

PCr/γ-ATP ratios were obtainable at rest and stress during the long TR, control-saturation sequences (#4–5, Table 2.3, p. 69) and recorded for two adjacent voxels (-1 and -2, where -1 refers to the voxel where k_f was recorded, and -2 refers to the voxel immediately posterior). These did not indicate stress-induced falls in PCr, which

Table 6.3: Diastolic parameters by echocardiography in controls and athletes[a]

Parameter	Control		Athlete		
	Mean	(95% CI)	Mean	(95% CI)	Sig.
Mitral E (cm/s)	72	(66, 79)	78	(70, 86)	.25
Mitral E decel (ms)[b]	164	(155, 200)	170	(160, 180)	.83
Mitral A (cm/s)[b] $*$	54	(51, 69)	39	(36, 55)	.03
E/A[b] $*$	1.2	(0.9, 1.6)	1.7	(1.6, 2.1)	.004
E' septal (cm/s)	9.7	(8.2, 11.1)	10.4	(9.4, 11.5)	.37
E' lateral (cm/s) $*$	14.3	(12.1, 16.4)	17.2	(15.3, 19.0)	.04
E' average (cm/s)	12.0	(10.2, 13.7)	13.8	(12.5, 15.2)	.09
E/E' septal[b]	7.6	(6.4, 9.4)	7.0	(6.1, 8.3)	.52
E/E' lateral	5.3	(4.8, 5.9)	4.7	(4.1, 5.2)	.08
E/E' average[b]	6.3	(5.4, 7.1)	5.2	(4.9, 6.8)	.13
PVs/PVd	1.2	(1.0, 1.4)	1.0	(0.8, 1.3)	.25

[a] Summary data for 18 controls and 17 athletes. All p-values two-sided.
[b] Given as median (IQR).

would offset the effect of rises in k_f on forward CK flux. Thus estimated forward flux (calculated as before by k_f adj $\times$ estimated [PCr], making the reasonable assumption of constant [ATP]) followed the direction of k_f in both groups (Table 6.6). There were no between-group differences in estimated forward flux at rest or stress, or in the stress–rest difference (p = .39 and .55 for voxels -1 and -2 respectively).

When groups were pooled the median rise in RPP induced by dobutamine was 2.7-fold; k_f adj rose by a median 1.25-fold (IQR 1.03–1.72) or a mean +0.09 (SD 0.14) /s (Figure 6.5 Panel C, Table 6.7). Estimated forward flux rose by 1.0 (95% CI 0.1–1.9) and 0.9 (95% CI 0.2–1.6) μmol/g/s in voxels-1 and -2 respectively.

The relation between k_f^{stress} and k_f^{rest} was plotted for each group separately (Panels

Table 6.4: Cardiopulmonary exercise test results in controls and athletes[a]

Parameter	Control		Athlete	
	Mean	(95% CI)	Mean	(95% CI)
AT absolute VO_2 (l/min) $*$	1.18	(0.97, 1.38)	3.23	(2.78, 3.68)
AT indexed VO_2 (ml/min/kg) $*$	15.7	(13.6, 17.8)	41.3	(37.4, 45.2)
AT VO_2/VO_2 peak (%) $*$	48.0	(43.0, 53.0)	79.4	(75.8, 83.1)
AT WR (W) $*$	90	(72, 109)	259	(231, 287)
VO_2 peak absolute (l/min) $*$	2.45	(2.10, 2.81)	4.05	(3.56, 4.54)
VO_2 peak indexed (ml/min/kg) $*$	33.2	(29.1, 37.2)	52.2	(48.2, 56.3)
VO_2 peak WR (W) $*$	219	(187, 251)	346	(313, 379)

[a] Summary data for 19 controls and 17 athletes. All row-wise comparisons by independent t-test for the null hypothesis (true difference in means is equal to 0) were significant, p-value < 10^{-5}. AT, anaerobic threshold, VO_2, minute oxygen consumption, WR, work rate (Watts).

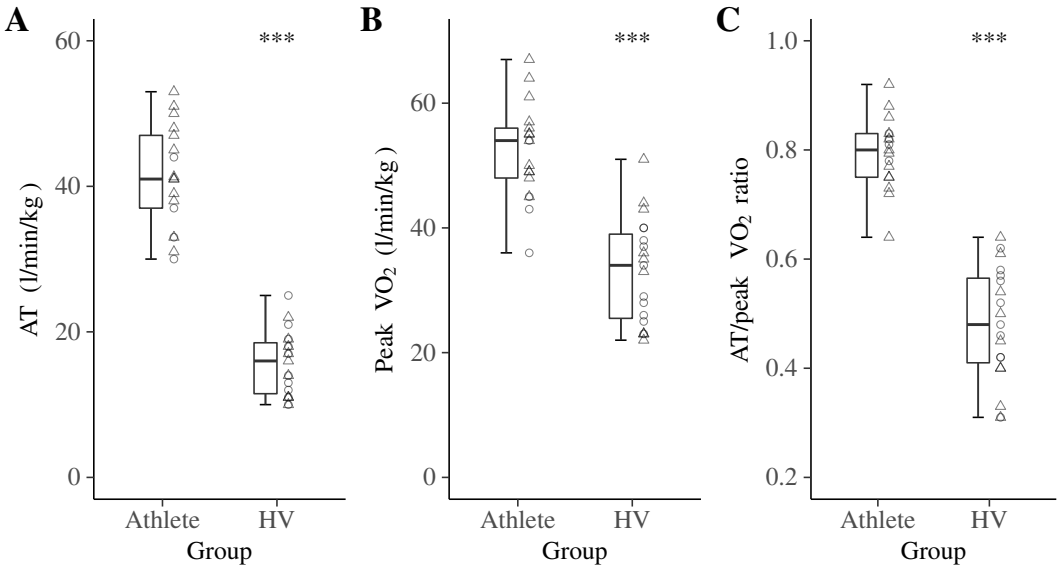


Figure 6.4: Anaerobic threshold (AT), peak VO_2, and AT/peak VO_2 ratio in athletes and controls. *Males shown as triangles, females as circles.*

A–B in Figures 6.5–6.6) and for the pooled groups (Figure 6.5, Panel C, Figure 6.6, Panels C–D). Dashed lines indicating the assumptions of a linear model derived from the data (Table 6.8) were plotted alongside the dotted line $k_f^{stress} = k_f^{rest}$ to visualise the effect of dobutamine. In the pooled group, the model predicted a dobutamine-induced rise in k_f of $0.12 + 0.87 \times k_f^{rest}$ adj /s and accounted for 40% of the variance in k_f^{stress}.[5] Tests of the model intercept indicated that this was greater than 0, while tests of the model slope (i.e. the coefficient for k_f^{rest}) indicated that this was not significantly different from 1.[6,7] In summary, a linear model approach indicated that the main effect of dobutamine was to raise k_f across the range of k_f^{rest}.

There was no correlation between fold-change in k_f during stress and fold-change in RPP during stress. Nor was there correlation between k_f (stress or rest) and LVMi, LV volumes or anaerobic threshold in the pooled group, but in athletes alone there was moderate correlation between k_f^{rest} and LVMi (r = .48, p = .053), k_f^{stress} and LVMi (r = .47, p = .058), and k_f^{rest} and RVEDVi (r = .52, p = .034). These were not backed up by correlations with LVEDVi or anaerobic threshold so are not discussed further.

6.3 DISCUSSION

In summary, k_f^{rest} did not significantly differ in physiological hypertrophy from the non-hypertrophied condition, and dobutamine increased k_f significantly in control hearts but not in physiological hypertrophy, where the group was relatively smaller and the signal less well powered. When the groups were pooled, k_f^{stress} remained greater than k_f^{rest}, and there was no clear influence of sex or anaerobic threshold on

[5] There was no clear effect of sex, anaerobic threshold or fold-change in RPP on k_f^{stress}, but k_f^{rest} had a small effect (larger values predicting smaller responses to dobutamine). None of the measured variables (MRI, echo, CPET, sex) was found to predict the difference between stress and rest k_f.

[6] The null hypothesis, coefficient b = 1 for k_f^{rest}, was tested by comparing $(b-1)/SE$ against quantiles of the t_{n-2} distribution. For controls, athletes and pooled groups these p-values were .54, .72, and .75 respectively.

[7] An alternate approach is to test the null hypothesis $k_f^{stress} - k_f^{rest} = 0$ for all values of k_f^{rest}, i.e. to compare b/SE against quantiles of the t_{n-1} distribution. This approach predicted the relation $k_f^{stress} - k_f^{rest} = 0.12$ (for the intercept $P(t > |t|) = .013$).

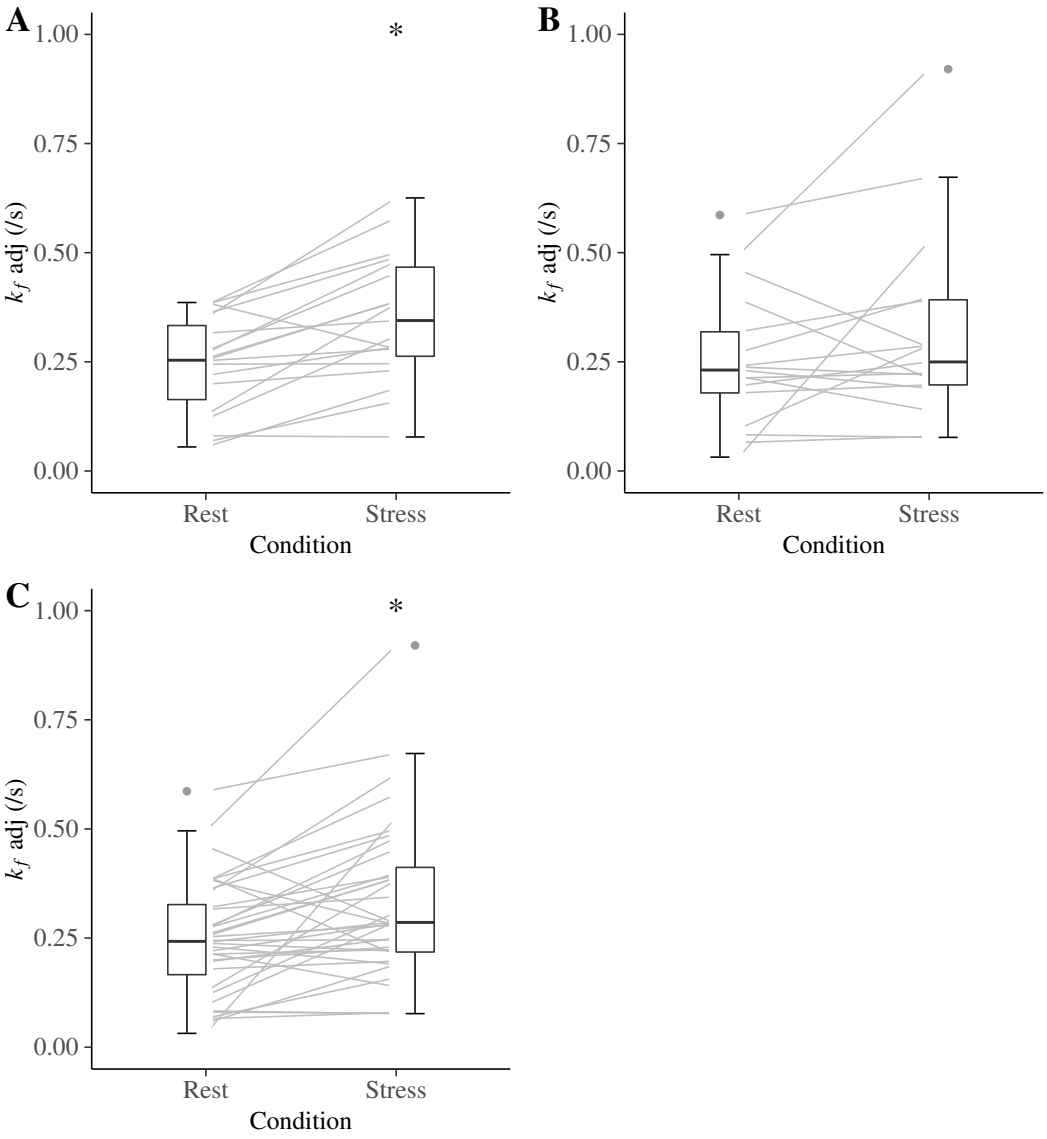


Figure 6.5: Response of k_f to dobutamine stress in (A) controls, (B) athletes, (C) both.

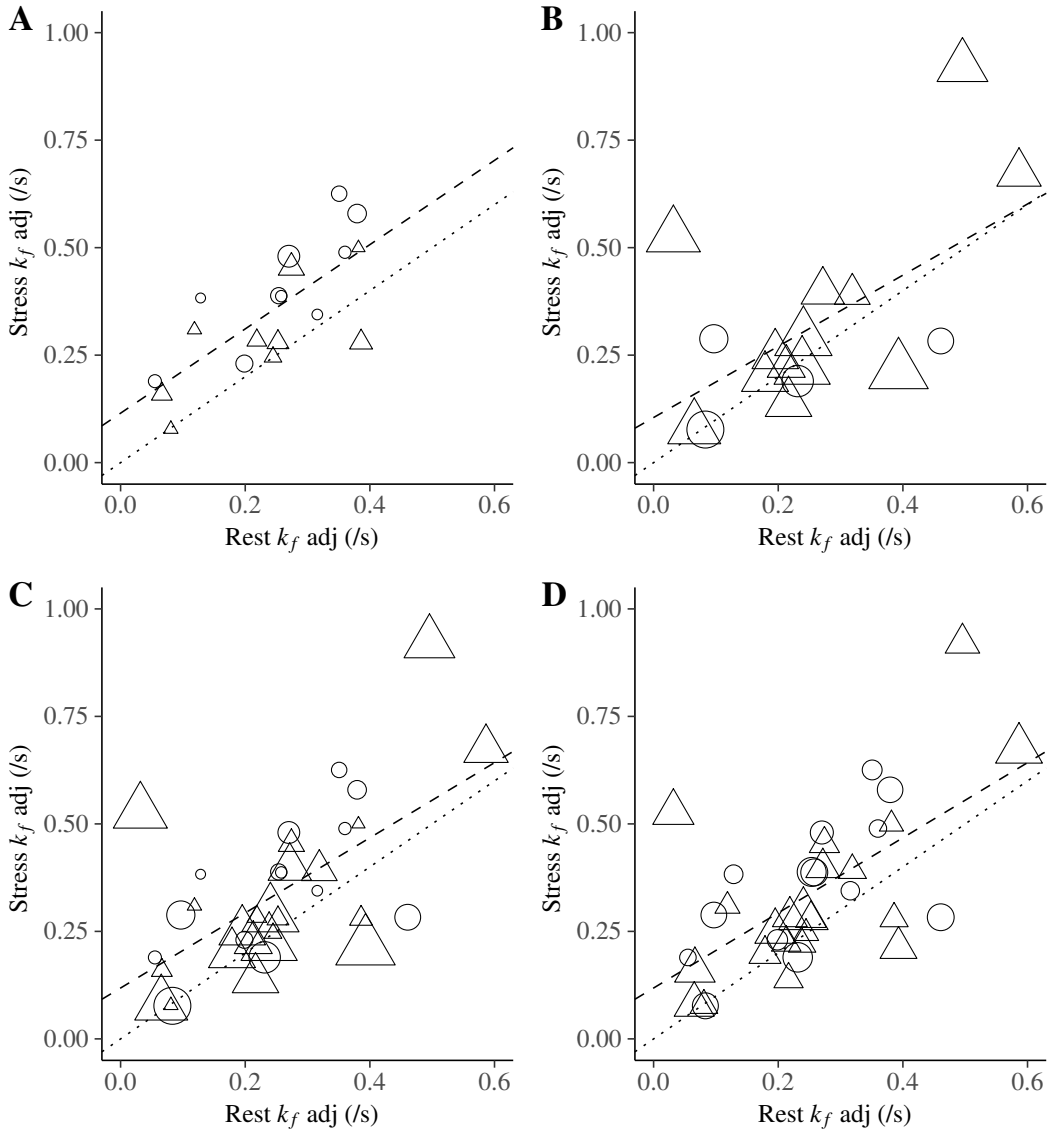


Figure 6.6: Response of k_f to dobutamine stress in (A) controls, (B) athletes, (C–D) both. *Males shown as triangles, females as circles. In (A–C) icon size is proportional to anaerobic threshold across all participants; in (D) icon size is proportional to -fold change in RPP. Dotted lines have intercept (b_0) = 0, slope (b_1) = 1; dashed lines follow the linear model* $k_f^{stress} = b_0 + b_1\ k_f^{rest}$ *(for coefficients see Table 6.8).*

Table 6.5: Effect of dobutamine on haemodynamics in controls and athletes[a]

Group, Parameter	Rest		Stress	
	Mean (95% CI)	Sig.	Mean (95% CI)	Sig.
Control				
HR (/min)	60 (56, 64) ∗	2e–4	114 (110, 118) ∗	.039
SBP (mmHg)[b]	116 (108, 135)	.49	152 (147, 157)	.16
RPP ($\times 10^3$ mmHg/min)[b]	6.96 (6.50, 7.98) ∗	7e–4	17.7 (16.1, 18.5)	.53
Fold-increase in RPP			2.5 (2.3, 2.7) ∗	.001
Athlete				
HR (/min)	48 (44, 52)		108 (102, 113)	
SBP (mmHg)[b]	115 (111, 121)		159 (151, 167)	
RPP ($\times 10^3$ mmHg/min)[b]	5.36 (4.72, 6.22)		16.1 (15.9, 18.9)	
Fold-increase in RPP			3.1 (2.8, 3.4)	

[a] Summary data for 19 controls and 17 athletes. Abbreviations: HR, heart rate, SBP, systolic blood pressure, RPP, rate-pressure product. P-values given as ∗ for comparisons between groups (control, athlete). All paired comparisons between rest and stress: $p < 10^{-5}$.
[b] Given as median (IQR).

the response. PCr/γ-ATP did not change significantly during stress, so forward flux followed the direction of k_f. This is the first evidence that CK k_f does react (and contribute) to oxphos rates in vivo (assuming evenly distributed P/O ratios and H^+-wasting) and informs current understanding about the way energy is handled during high demand situations.

The mechanism underlying any acute rise in CK k_f and forward flux in acutely stressed myocardium remains unclear. As $k_f = k_2$ [ADP] (see Section A.1), k_f may rise if free [ADP] rises. Besides changes in substrate concentrations, acute regulation of CK activity is poorly understood. Post-translational modifications presumably underlie the previous finding in dogs that 30 min after coronary occlusion, CK activity

Table 6.6: Effect of dobutamine on CK system in controls and athletes[a]

Group, Parameter	Rest	Stress	Difference	Sig.[b]
Control				
k_f adj (/s) $*$	0.25	0.34	0.11 (0.10)	2e–4
k_f adj (/s) (IQR)	(0.13, 0.35)	(0.25, 0.48)		
PCr/γ-ATP-1	2.6 (0.7)	2.5 (0.6)		.12
PCr/γ-ATP-2	2.0 (0.6)	1.9 (0.5)		.28
Est flux-1 (μmol/g/s)	3.5 (1.3, 6.0)	4.6 (3.4, 7.5)	1.4 (2.0)	.005
Est flux-2 (μmol/g/s)	2.9 (0.9, 4.4)	3.8 (2.2, 5.5)	1.1 (1.8)	.011
Athlete				
k_f adj (/s) $*$	0.23	0.25	0.02	.19
k_f adj (/s) (IQR)	(0.18, 0.32)	(0.20, 0.39)	(–0.02, 0.09)	
PCr/γ-ATP-1	2.6 (0.6)	2.4 (0.7)		.64
PCr/γ-ATP-2	2.2 (0.5)	2.1 (0.6)		.29
Est flux-1 (μmol/g/s)	3.8 (2.2, 4.6)	3.2 (1.7, 6.2)	0.6 (3.2)	.55
Est flux-2 (μmol/g/s)	2.6 (1.9, 4.7)	2.9 (1.5, 5.2)	0.7 (2.3)	.22
p-value[b]	.78	.27	.057	

[a] Summary data for 19 controls and 17 athletes. Parameters given as median (IQR) or mean (SD). Flux estimated from k_f adj $\times$ est [PCr], where est [PCr] = PCr/ATP $\times$ literature value for [ATP] (Weiss et al., 2005); suffix -1 refers to the voxel-picked for k_f, -2 refers to the voxel one deeper.

[b] All p-values two-sided. Right column shows paired tests by row; bottom row shows unpaired tests on k_f by column.

Table 6.7: Effect of dobutamine on CK system (controls and athletes pooled)[a]

Group, Parameter	Rest	Stress	Difference	Sig.
k_f adj (/s) $*$	0.24	0.29	0.09 (0.14)	3e–4
k_f adj (/s) (IQR)	(0.15, 0.33)	(0.22, 0.43)		
PCr/γ-ATP-1	2.6 (0.7)	2.4 (0.7)		.14
PCr/γ-ATP-2	2.1 (0.6)	2.0 (0.5)		.16
Est flux-1 (μmol/g/s) $*$	3.7 (1.9, 5.1)	4.1 (2.3, 7.4)	1.0 (2.6)	.022
Est flux-2 (μmol/g/s) $*$	2.8 (1.7, 4.4)	3.3 (1.8, 5.4)	0.9 (2.0)	.010

[a] Summary data for 36 participants. Conventions as for Table 6.6.

Table 6.8: Coefficients for linear models (dependent variable: k_f^{stress})

			Unstandardized				
Group	R^2	Parameter	b	SE	β	t	p-value[a]
Controls	.54	(Intercept)	0.12	0.06		2.01	.06
		k_f^{rest} adj	0.98	0.22	0.74	4.51	3e–4
Athletes	.35	(Intercept)	0.10	0.09		1.22	.24
		k_f^{rest} adj	0.83	0.29	0.59	2.84	.01
Pooled	.40	(Intercept)	0.12	0.05		2.31	.03
		k_f^{rest} adj	0.87	0.18	0.63	4.77	3e–5

[a] These two-sided p-values test the null hypothesis that the coefficient b = 0.

in serial LV biopsies increased by 60-70% in the remote viable myocardium (Braasch et al., 1968). The significance of the coupling of CK activity with workload is that falls in CK reserve may not be evident from resting studies (MRS or biopsy) alone. Conversely, a lack of change in flux with workload may be interpreted either as the CK system being 'at equilibrium' (i.e. with plenty of reserve, see Section 6.1) or with other factors more involved: [ADP], [P_i], and CK-independent phosphotransfer.

Experimental discordance in prior studies (Table 6.1) is partly due to experimental challenges: achieving steady-state at two different workloads (particularly in ex vivo experiments) and measuring every candidate, which requires a combination of NMR and biochemical techniques.[8] The same group found CK flux values in the living rat to be 54% of values in the buffer-perfused ex vivo heart despite being at a 28% greater RPP (Bittl et al., 1987b; Bittl and Ingwall, 1985), and speculated that the difference could be due to differences in MVO_2, free [ADP] or efficiency. Other reasons may include the hyperbolic relation between oxphos and forward CK flux,[9] with most physiological variation occuring at the flatter part of the curve, and true inter-species differences, e.g. dogs are less likely than cats to display rises in [P_i]/[PCr] at increasing workloads (Ligeti et al., 1987).[10]

Attempts to link workload and CK flux must also be interpreted bearing in mind that k_f represents a weighted average of all ATP-producing CK activity (p. 44) so contributions come from both free cytosolic and 'functionally coupled' isozymes.

[8] MVO_2 requires arteriovenous O_2 extraction and coronary flow; ATP synthesis requires VO_2 and P:O ratio (usually assumed as 3); [ATP] requires freeze-clamping; [PCr] requires PCr/ATP $\times$ [ATP]; calculated [ADP] requires PCr/ATP, Cr (usually by subtraction of [PCr] from [total creatine]) and K_{eq} (see p. 229 and p. 87); for k_f see p. 61 and 231; for [P_i] see Schmid et al. (2019).

[9] In two species ex vivo (Bittl and Ingwall, 1985; Perry et al., 1988), CK flux (F, ordinate) had a Michaelis-Menten hyperbolic relation with MVO_2 (abscissa): $F = F_{max} \cdot (MVO_2)/(MVO_2 + K_m)$, where K_m is the level of oxygen consumption at which half-maximum flux is observed. Thus over the VO_2 range between intermediate–high work (1.5-fold rise), CK flux only rose in hearts with mtCK > 6% (Perry et al., 1988).

[10] The reader might wonder whether measuring reverse CK flux might help, as increases in oxphos deliver more ATP to mtCK, and increase reverse CK flux (Saks et al., 1975). The problem is that this is only true up to a point, after which the increased ATP supply is transferred to points of use independent of CK by diffusion or by adenine nucleotide 'channeling'; second, k_r is more difficult to measure (see Section 3.1).

Several studies showed greater correlation between CK flux and workload over the difference between KCl-arrest and resting state than between resting state and twice-resting state workload. If CK flux and workload do not correlate over the difference between resting and twice-resting state work, this implies that over this range, flux through the functionally coupled isozymes makes a relatively smaller contribution to total energy use than at workloads below resting state. Second, it implies that as workload rises from resting state, flux through the functionally coupled enzymes makes a relatively smaller contribution to k_f compared with flux through free cytosolic enzymes, i.e. there is a shift in the average CK equilibrium position, so that the apparent position takes more account of the cytosolic compartment.

In this study, it is not clear why smaller responses to dobutamine were shown in athletes compared with controls. Athletes experienced larger relative increases in RPP, albeit from a lower baseline. It would be reasonable to assume that dobutamine provoked a several-fold increase in MVO_2 in both groups, and that both groups' hearts continued to derive >90% of ATP from oxphos across this range. There are several reasons that might explain the difference, but these are speculative. First, it may be that CK reserve and CK total activity is larger in athletes, so that at comparable RPPs, CK flux does not need to increase to accommodate comparable increases in MVO_2. Second, it may be that athletic hearts are more efficient, so that at comparable RPPs, MVO_2 is smaller. Third, athletic hearts may have adaptive increases in CK-independent energy transfer, so that at comparable MVO_2s, adenine nucleotide diffusion or channeling flux is higher. As RPP increased more than k_f increased in this and any animal study showing an increase in k_f during stress, it is clear that CK-independent ATP transfer increases during stress. A fourth reason concerns [ADP]. It may be that the second-order rate constant increases equally in both groups, but that in athletes there is a smaller (or no) increase in [ADP]. An increased sensitivity of respiratory control to [ADP] has been demonstrated in trained rat skeletal muscle

(Dudley et al., 1987; Egan and Zierath, 2013). Fifth, athlete hearts may have slightly higher [PCr], so that to achieve a given CK flux a smaller k_f will suffice. Although this data (and MRS technique (Bakermans et al., 2017)) was underpowered to show a between-group difference of 10% (see PCr/ATP, Table 6.6), this would also reduce the change in k_f at stress. In summary, small contributions from all the above factors could collectively result in the discordant response observed. However, with a given sample size, it is always statistically harder to confirm the absence of a relationship than to find a relationship, so this study can only be considered an early attempt at understanding the relationship between MVO_2 and CK flux in human myocardium.

Several further limitations may be noted. PCr/γ-ATP ratios lacked skeletal muscle and liver saturation bands and blood-correction, so were recorded at two depths and should be considered estimates. Physiologic hypertrophy develops longitudinally (Arbab-Zadeh et al., 2014), and to greater or lesser extents depending on the exercise 'dose' over years. The athletes recruited here had smaller mean LVEDVi and RVEDVi than those of exclusively male competitive athletes (D'Ascenzi et al., 2019), reflecting the lesser 'stage' of physiological hypertrophy studied here and the inclusion of female athletes, who have smaller chamber volumes and VO_2 values (there is no consensus on normalising VO_2 for sex). This chapter's findings do not necessarily apply to the hearts of more remodelled athletes.

7 *Correlation of energy handling with ultrastructure*

This chapter attempts to relate ultrastructure with energetics, and aims to:

- Estimate the distribution of ATP diffusion distances between mitochondrial and sarcomeric compartments using a 3D tomographic model.
- Investigate whether changes in this distribution reflect changes in CK activity such that distances will reduce to compensate for significant falls in CK activity.

7.1 INTRODUCTION

ATP may be delivered to (and ADP removed from) sites of use by two processes: simple diffusion (Jacobus, 1985b) and facilitated diffusion (the CK system) (Meyer et al., 1984) (Figure 1.4). There is disagreement over the relative importance of these processes in cardiac muscle (Greenhaff, 2001). From one extreme one might argue that simple diffusion can replace the work of a nonfunctioning CK system; from the other side, the case for the importance of facilitated diffusion argues that simple diffusion is not so 'simple' if there are effectively restrictions to ADP diffusion in place (Saks et al., 1994; Veksler et al., 1995). Both sides are required to make assumptions to state their case, and common to both sides is the assumption of fixed

diffusion distances.[1] It is this assumption that I will tackle in this chapter.

This is not just an exercise in pedantry: tackling the question of diffusion distance informs the interpretation of reduced CK capacity, as falls in CK flux would be expected to have worse consequences if diffusion distances were large or simple diffusion were limited. Paul Bottomley has documented that (simple) PCr diffusion is not limiting in human skeletal muscle (Gabr et al., 2011) over the inter-mitochondrial distance of 2 μm (Birkedal et al., 2006), but this does not go far enough: first, if simple diffusion really is not limiting, then why should falls in CK flux matter enough to impact mortality (Bottomley et al., 2013b); second, we are interested in ADP diffusion, as this is the CK substrate most observed to be diffusion restricted[2] yet the hardest to study with NMR, and net fluxes at steady-state proceed at the rate of the slowest partner; third, energy transfer (in many respects) works differently in oxidative muscle; fourth, the relevant distance distribution is from myofibril to mitochondrion.

The case for the importance of facilitated diffusion includes several arguments: that the accessibility of cytosolic ADP to mitochondria is much lower in skinned fibres (mitochondria in situ) than in isolated mitochondria, indicating diffusion restriction in vivo (Kay et al., 2000; Saks et al., 2001),[3] that the kinetics of cytosolic, MM-bound and mitochondrial CK can be separated in the ex vivo rat heart, suggesting that the concentrations of CK substrates vary with subcellular localization (Joubert et al., 2002a,b), and that when equal concentration gradients for each metabolite are assumed, the mere presence of a functioning CK system makes simple diffusion far less a contributor to diffusive flux (Jacobus, 1985b; Meyer et al., 1984). Further

[1] Other assumptions include a fixed concentration gradient for each metabolite, as diffusive flux is the product of the diffusive coefficient and the concentration gradient (de Graaf et al., 2000), a well-mixed cytosol (challenged by ^{18}O-labelling experiments demonstrating that the metabolically active pool of ADP increases with frequency of muscle contraction over >10 min (Dzeja et al., 1998)), a known and fixed equilibrium constant for CK (allosteric modulation is poorly understood), and a known and fixed permeability coefficient for ATP/ADP transfer across the outer mitochondrial membrane (Hettling and van Beek, 2011).

[2] Diffusive flux is three orders of magnitude lower for Mg.ADP than for PCr (Jacobus, 1985b).

[3] Reviewed (Ventura-Clapier et al., 2004).

arguments include the tissue-specific expression of CK isoforms, the variation of CK activity and K_m for ADP with athletic training (see Section 6.1 for refs) and HF (see Section 1.3 and Chapter 4), and the mitochondrial adaptations of skeletal and cardiac muscle in CK DKO mice. In DKO cardiac muscle mitochondrial content was unchanged, but sensitivity to external ADP increased, and ultrastructurally:

> Frequent splitting of the myofibrils resulted in formation of thinner myofilament bundles and their deviation from the longitudinal direction ... mitochondria entering the myofibrils at sites of splitting could be observed ... Mitochondria reorganized within myofilaments and tended to decrease diffusion distances, showing that subcellular organization is sensitive to energy deficiency (Kaasik et al., 2001).

This promotion of "direct crosstalk" may underlie the preservation of cardiac function during moderate workloads in DKO hearts.

This chapter therefore aimed to build on the hypothesis that mitochondrial structure remodels to minimise metabolite diffusion distance, and test the hypothesis that mitochondria-myofibril diffusion distances fall to compensate for falls in CK capacity in humans. A study testing the former hypothesis in mouse skeletal muscle was notable for using 3D focussed ion beam scanning electron microscopy (SEM) (15-nm isotropic voxels), allowing an unbiased quantitative approach (Glancy et al., 2015). Similar 3D approaches had not been tested in human or cardiac muscle when this study was started. In this study, each 3D dataset was built using a diamond knife to take serial sections, mandating a larger z-distance. A voxel size of 10–10–100 nm (x–y–z) was used as this still allowed 3–5 sections of the same mitochondrion in the z-direction, and the dataset was interpolated to 20 nm isotropic (see Methods, p. 77).

7.2 RESULTS

14 participants' samples (4 sevAS-pEF, 4 sevAS-rEF, 2 sevMR, 3 NH including 2 mitral stenosis (MS) and 1 LA mass, 1 MS with reduced EF) were sectioned and

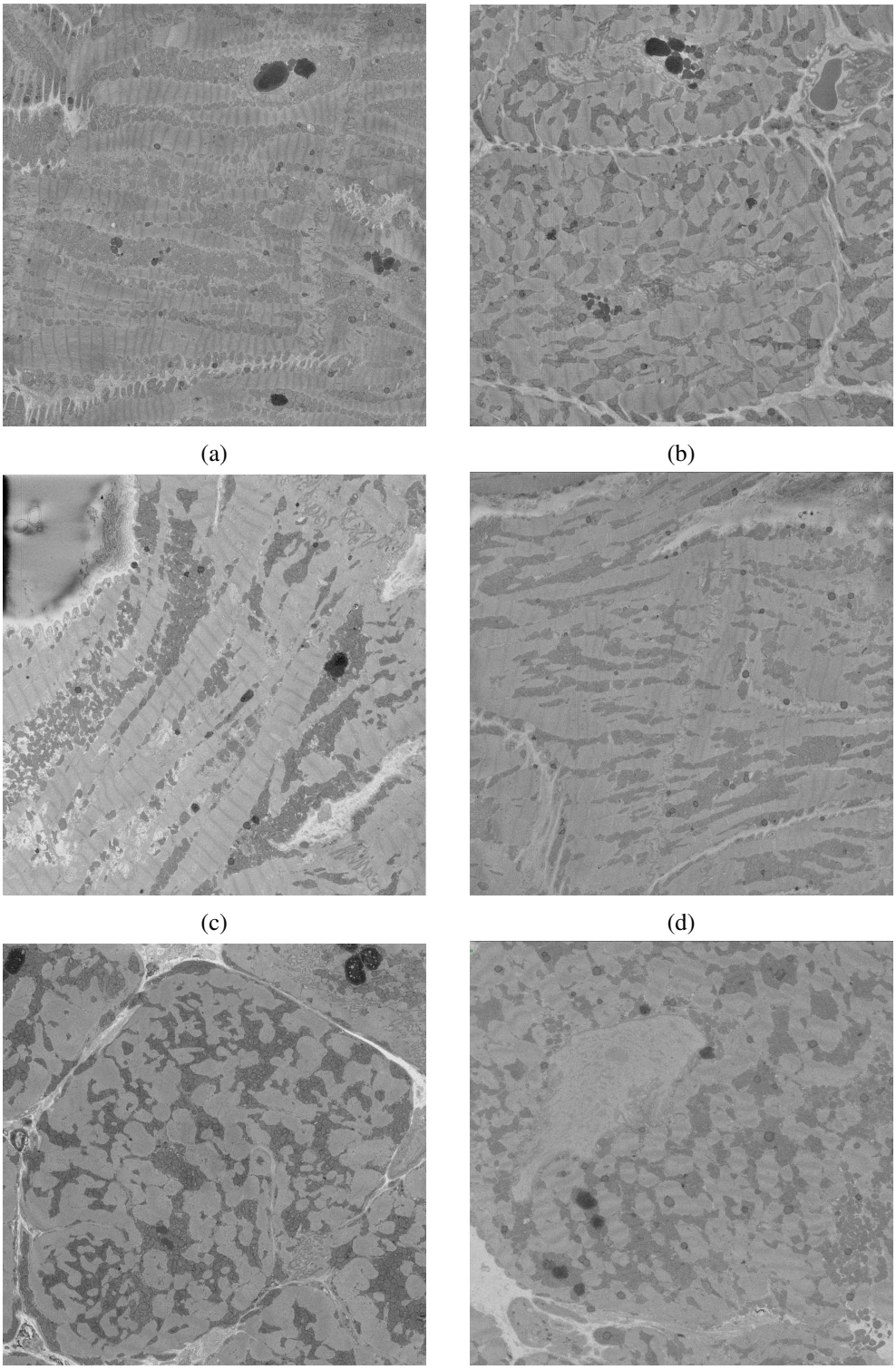
mounted for imaging. 13 were successfully imaged (for screenshots see Figures 7.1a–7.2f), manually contoured, and interpolated. One had to be reimaged because the first block was largely extracellular; in another, two unsuccessful attempts were made to image but were either extracellular or stopped prematurely by the microscope with focus or vacuum difficulties. Interpolation was not revisited, so the results reflect the first 'best effort' given the time contraints. The decision to section was made before results of CK activity were known, so I chose samples from each group.

Once all analyses were complete, 11 samples had paired CK total activity (one sevAS-pEF and one sevMR did not). Two samples (one sevAS-pEF, one MS-rEF) were then excluded after a second look with the TEM found the datasets impossible to analyse fairly: one had holes in the resin (Figure 7.3a) and the other was partially out of focus on SEM, yet on TEM had substantial areas of electron-dense dust-like material which were neither sarcomere nor mitochondrion (Figure 7.3b). These were not present in other TEM datasets.

For the remaining 9 datasets, the distribution of 3D distances was plotted as a histogram and the median distance taken as the summary statistic for that dataset. The mean (SD) number of distances contributing to each histogram was $6.1 \pm 1.2 \times 10^8$, and histograms were all similarly shaped. There was good correlation between median diffusion distance and CK total activity and CK capacity estimated by CK total activity $\times$ total creatine, but not with total creatine (Figure 7.4).

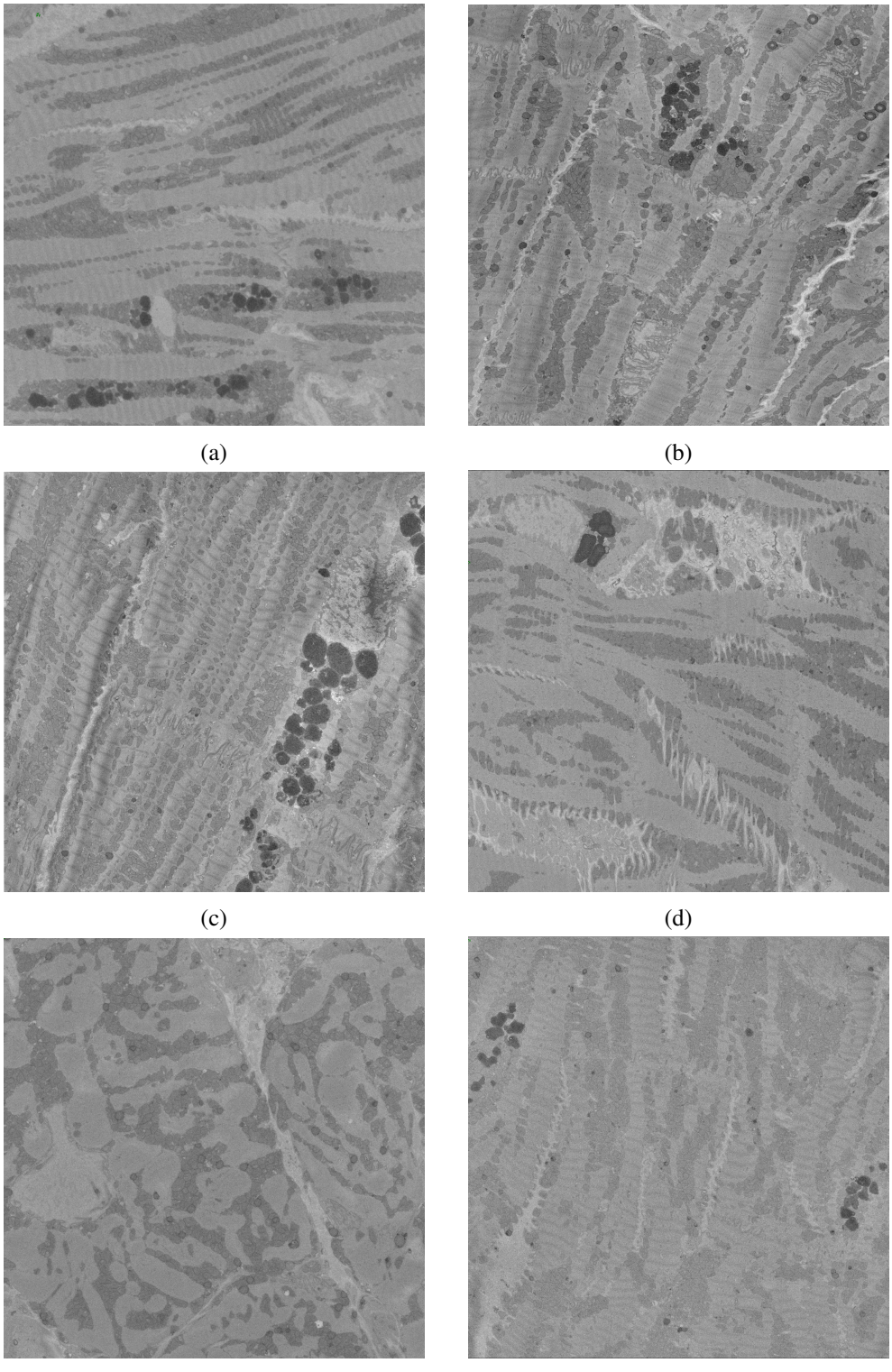
7.3 DISCUSSION

In summary, a 3D tomographic SBEM technique was used to obtain a distribution of 3D distances from each of 13 datasets. There was substantial overlap of distributions between datasets, which were summarised using the median distance. Paired CK total activity and estimated CK capacity correlated with median 3D distance from sarocomere to mitochondrion in the 9 available datasets.



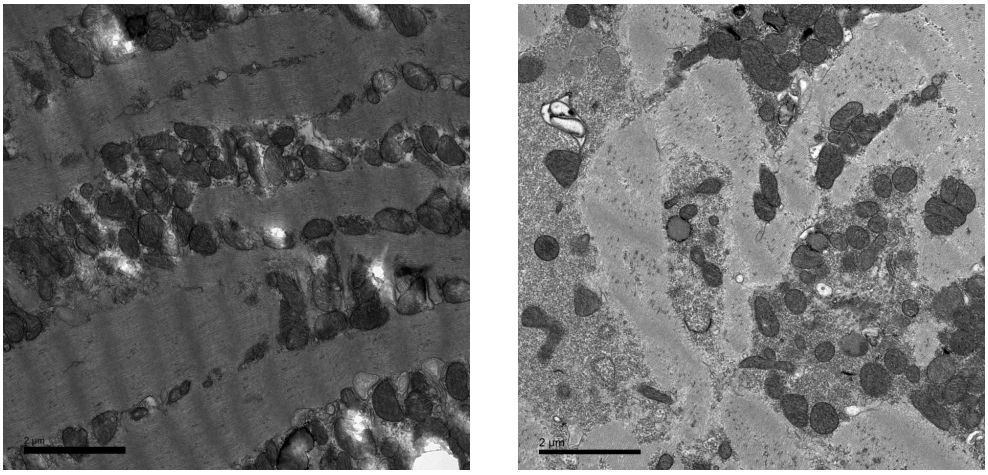
(a) (b) (c) (d) (e) (f)

Figure 7.1: Representative screenshots for SEM datasets (a) _021, (b) _035, (c) _033, (d) _081, (e) _041, and (f) _145. Subfigures (a–d), sevAS-pEF, (e–f), sevAS-rEF.



(a) (b) (c) (d) (e) (f)

Figure 7.2: Representative screenshots for SEM datasets (a) _139, (b) _015, (c) _023, (d) _048, (e) _066, and (f) _092. Subfigures (a), sevAS-rEF, (b–c), sevMR, (d–f), NH.



(a) (b)

Figure 7.3: TEM in (a) (_033) indicated holes in the resin; in (b) (_126) indicated ambiguous regions.

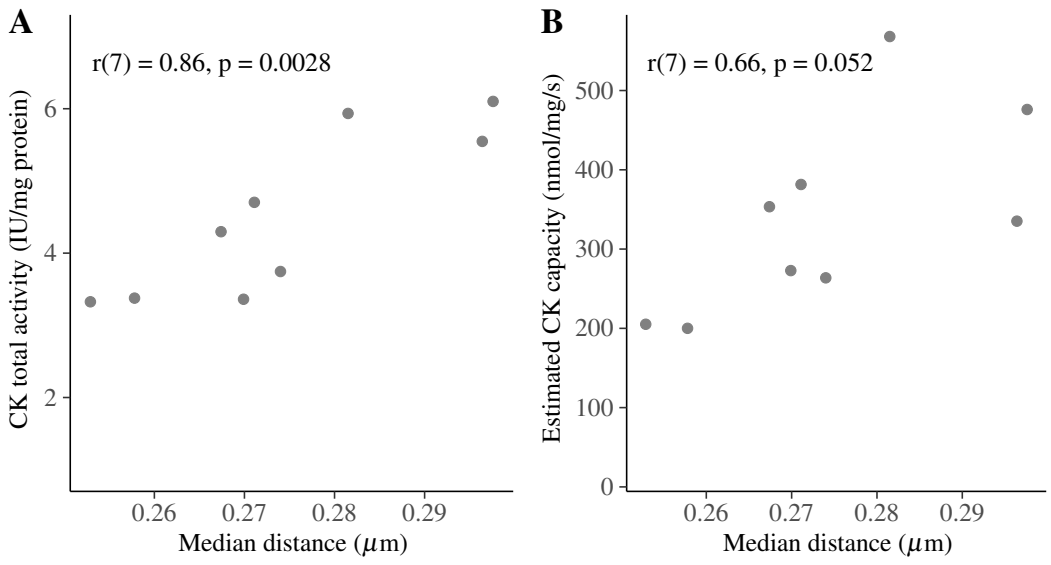


Figure 7.4: Scatterplots of median diffusion distance (A) against CK total activity, (B) against CK capacity estimated by CK total activity $\times$ total creatine.

The results are in agreement with qualitative descriptions of ultrastructural adaptation in CK DKO mice (Kaasik et al., 2001). Unexpectedly however, no differences in mitochondrial ultrastructure (inter-mitochondrial distances) or ADP sensitivity were found in creatine-deficient GAMT KO hearts using quantitative analysis of confocal images (Branovets et al., 2013).[4] As creatine deficiency reduces CK catalytic capacity but not its presence or binding, the discordance between these studies could be explained by the structural role CK plays in the mitochondrial inter-membrane space, and also by differences in genetic background. Unlike prior studies, this study was performed in human myocardium with only physiological variation in CK activity.

Two recent studies extended prior classic TEM studies (Leyton and Sonnenblick, 1969; Maron and Ferrans, 1978; Maron et al., 1975; Sekiguchi, 1974) mainly by providing control hearts. One, in peri-operative $10 \times 1 \times 1$ mm biopsies in humans with normal hearts, sevAS-pEF, or sevAS-rEF (n = 2, 5, 4 respectively), found increased mitochondrial fragmentation, cristae destruction, vacuolar degeneration and swelling, reduced mitochondrial area, and T-tubule dilation in HFpEF, findings which were more pronounced in HFrEF (Chaanine et al., 2019). Expression of markers of mitochondrial biogenesis, dynamics and citrate synthase were unchanged in HFpEF. The results conflated the presence or absence of CAD and did not assess mitochondrial oxidative flux. In contrast, another recent study in explanted end-stage HF or normal donor human hearts found no between-group differences in mitochondrial area or cristae packing by normalised grayscale intensity on TEM (n = 5 vs 6), nor in oxidative capacity in isolated mitochondria for glycolysis-derived or FA-derived substrates, but did find reduced contact and increased distance between mitochondria and lipid droplets (Holzem et al., 2016). The present chapter did not optimise fixation for TEM and did not systematically assess mitochondrial area or cristae packing, although this could be attempted. Although different disease stages were compared, it is difficult to

[4]The same group found no difference in mitochondrial density in CK overexpression (Whittington et al., 2018).

reconcile these divergent ultrastructural findings.

Several assumptions were implicit in this chapter. As distances were calculated from each sarcomeric voxel to the nearest voxel labelled mitochondrion, the assumption was that every mitochondrial border was equally able to supply ATP or receive ADP. Mitochondrial ADP sensitivity could not be assessed with polarography given limited biopsy sizes. In contrast, prior quantitative analyses examined 3D distances between centres of mitochondrial clusters and ignored subsarcolemmal and perinuclear mitochondria (Birkedal et al., 2006; Branovets et al., 2013). The magnification used on SBEM was sufficient to distinguish mitochondria, myofibrils, lipid droplets, lipofuscin granules, intercalated disc, nucleus, sarcolemma, and dilated T-tubules, but insufficient to distinguish small (normal) regions of T-tubules and sarcoplasmic reticulum and intra-mitochondrial cristae. A volume of $40 \times 40 \times 6.1$ µm was contoured and the results generalised for the entire LV, making the assumption of that the sample was representative of a homogenous myocardial pathology. As some samples were not oriented longitudinally, sarcomere lengths could not be used as a check of variable between-sample contracture, but times to fixation were similar. The distributions were assumed to be of the same shape between datasets, but this couldn't be proven mathematically, as they did not fit any one simple distribution. The median was taken as the sparsest useful estimate of diffusion distance, but other parameters such as the size of the right-hand tail may also be important regarding reliance on facilitated diffusion.

There are also some reassuring points. The z-distance between contoured slices was several-fold greater than the largest distances found (Figure 2.15, p. 84), so avoiding the artefact of reduced choice of diffusion direction at either end of the dataset. The magnification chosen was a trade-off between coverage and detail, and was consistent between datasets. Although the linear interpolation will have magnified any errors in segmentation, each mitochondrion was sectioned 2–3 times

when counting alternate slices, no slices were copied and pasted onto any other, I was blinded to CK activities and diffusion distance calculations until contours were complete, and analyses were performed automatically, so any human error should be evenly distributed across all datasets. Analyses were not confounded by sample preparation processes, as the time to fixation was consistently short in all cases and, aside from the samples excluded, no significant artefacts (distortion during dehydration, mitochondrial swelling, knife artefacts, oil spots, knife vibration) marred the volumes contoured (Chandler and Roberson, 2009).

The simplest interpretation of the correlations found is that there is some ultrastructural sensitivity to CK capacity at the level of mitochondrial organisation which might be expected to compensate for reduced CK capacity. However, the between-group overlap was large and there was likely more similarity than difference. We should be cautious about drawing further conclusions as there are other (CK-independent) phosphotransfer mechanisms that were not measured here, and mitochondrial ADP sensitivity (i.e. diffusion limitation) could not be assessed given the limited biopsy sizes.

8 Summary and future directions

In summary, Ch. 1 introduced the challenge of assessing cardiac metabolic phenotype and set ATP delivery and ADP removal as the final common pathway downstream of substrate oxidation and oxphos. Metabolic phenotyping ideally requires assessment of transcriptome, proteome, enzyme activities, metabolome and flux, alongside a clearly defined disease stage. Pathological and physiological hypertrophy were introduced as two processes affecting human hearts, both with molecular signatures involving metabolism, that may be antagonistic at the molecular signalling level. The metabolic starvation hypothesis of heart failure was introduced, which in its soft form states that impaired metabolic reserve may contribute to initiating and/or maintaining contractile dysfunction in HF. To what extent impaired metabolic reserve may be a necessary or sufficient driver of HF, and to what extent it may be merely a symptom of HF, was explored by reviewing animal models of hypertrophy, failure and manipulated metabolism, and human energetic studies to date. This set up two further hypotheses: can an effective biomarker of impaired metabolic reserve be identified in situations where human hearts develop "otherwise unexplained" failure, and can metabolically-targeted therapies be used therapeutically in situations where metabolic reserve is limiting? With these hypotheses in mind, this thesis aimed to assess the phospho-transfer side of the metabolic signature of both kinds of hypertrophy using the best techniques available in human hearts.

Ch. 2 summarised the methods used and developed for this thesis, which concen-

trated on protein expression (CK isoenzymes), enzyme activities (CK, CS), metabolome (total creatine, TAN pool, PCr/ATP ratio), flux (k_f and k_f-based measures) and adenine nucleotide diffusion distance. Disease staging was implicit in the participant groups and MRI-assessed LV volumes and mass. Together these comprise the most systematic attempt at assessing the CK system in human myocardium to date.

Ch. 3 observed strong correlations between CK total activity and CS activity, good correlations with total creatine concentration and CK flux estimated by $k_f \times$ total creatine, and moderate correlations with k_f alone and CK flux estimated by $k_f \times$ estimated [PCr]. There was moderate positive correlation with LVEF and moderate negative correlation with LV volumes and LVMi. CK total activity and CK/CS activity ratio, an index arguably more specific to extra-mitochondrial CK activity, were the only two correlates of CK k_f. The simplest CS-including model that predicted CK total activity better than any one single variable was CS activity + k_f; the simplest CS-excluding models were total creatine + k_f + LVESVi and total creatine + k_f + LVEF. These findings are an important step toward developing a non-invasive biomarker of metabolic reserve.

If future noninvasive estimates of total creatine by ^{1}H-MRS improved sufficiently, a next step would be to validate this noninvasive assessment of metabolic reserve prospectively. At a basic level the established correlations should prompt exploration of factors implicated in pathological hypertrophic signalling that may co-suppress CK activity, CS activity and total creatine, and factors that may co-modulate these variables in the absence of disease. At a clinical level the prognostic relevance of CK activity to survival, and its possible contribution to post-operative non-resolution of symptoms, could be explored in patients with and without ischaemia (so developing the metabolic biomarker hypothesis in human hearts). These strands would then tie in with ongoing efforts to therapeutically augment CK capacity in situations where it is limiting (the metabolic starvation hypothesis of HF).

Ch. 4 developed an argument for the assessment of metabolic reserve as a way of identifying – and explaining – the recently described subset of patients whose ventricles deteriorate sooner in the face of pressure overload (the vulnerable ventricle hypothesis, really a soft form of the metabolic starvation hypothesis of HF). Median CK total activity reduced across the groups (NH > sevAS-pEF > sevAS-rEF), underpinned by stepwise falls in MtCK and CK-MM activities and associated with stepwise falls in CS activity and isoform redistribution toward CK-MM and CK-BB. There were also reducing trends in median CK capacity (CK activity $\times$ total creatine) and ATP delivery through CK (estimated [PCr] $\times$ k_f) (post-hoc pairwise tests not significant). This was despite substantial within-group variation in CK total activity, to which the contribution of intrinsic biological variation is unknown. k_f alone did not discriminate between groups.

Thus enzyme activity and PCr pool size were implicated as the main factors reducing ATP delivery (and CK capacity) in sevAS. Although the observed changes were not prerequisites for sevAS-rEF, they could nevertheless contribute to reduced contractile reserve and transition to failure in AS. Prior to this it was not known whether markers of metabolic reserve associate with (and have explanatory power in) human AS with reduced LVEF. The results identified a possible prognostic strategy (using metabolic imaging techniques to identify those at risk of transition to failure, the metabolic biomarker hypothesis) and a possible therapeutic strategy (of improving cardiac metabolism to delay transition to failure). Both are worthy of further investigation.

The clinical utility of MRI is primary MR differs from that in AS, and is also under development; Ch. 5 developed an argument for the assessment of metabolic reserve in primary MR, again based on the vulnerable ventricle hypothesis. In this group of patients, PCr/ATP ratio was reduced pre-operatively and increased post-operatively; k_f was no different pre-operatively, so estimated [PCr] $\times$ k_f was reduced, implying

reduced flux in the face of increased wall stress and stroke work. Timing was generally not representative of 'early repair', so outstanding questions remain whether metabolic phenotyping could identify more vulnerable ventricles or predict late persistent LV dysfunction post-repair (the metabolic biomarker hypothesis).

Ch. 6 assessed k_f and PCr/γ-ATP in normal and physiologically-hypertrophied hearts at rest and stress. Dobutamine increased k_f in controls but not in athletes; when groups were pooled, k_f^{stress} remained greater than k_f^{rest}. As estimated [PCr] did not change between the conditions, estimated flux matched increases in k_f. This is the first observation in humans that CK k_f does react (and contribute) to oxphos rates in vivo, but sits in the context of discordant animal studies. The discordant response between athletes and controls should be replicated, as multiple mechanisms could underlie this.

Ch. 7 tackled the assumption that diffusion distance is fixed, as this is really a distribution which may modulate the effect of changes in CK capacity. A 3D tomographic model was contoured and interpolated to derive a distribution in 13 datasets; correlation was found with CK total activity but also significant overlap. The next steps would be to quantify the overlap between datasets and use machine learning techniques to train a neural network to segment these and other datasets more fully, in order to establish expected distributions in the presence and absence of hypertrophy. Possible further analysis could relate mitochondrial area to CS activity.

The project had several practical limitations. Patients with prior MI were excluded, so the meaningfulness of k_f in these patients and the contribution of MI to CK kinetics were not assessed. Outside of rejected donor hearts, numbers of nonhypertrophied hearts with normal function available for LV biopsy will always be limited. Similarly, patients with sevAS-rEF, no prior MI and listed for SAVR are limited. Healthy volunteers consented to undergo dobutamine stress as part of recruitment, and could not be age-matched to all of the athlete, sevAS and sevMR groups. For good reasons

several measures were not directly assessed, including measures of pathological hypertrophic signalling, CK post-translational modifications, CrT expression, creatine uptake kinetics, [P_i], [PCr], MVO_2, myocardial pressure-volume area, upstream substrate availability and fractional oxidation rates, oxphos capacity in the presence of different substrates, and CK-independent phosphotransfer systems. Each of these alone would have required major additional technical or participant time investment, or biopsies an order of magnitude larger.

Several design strengths should also be emphasised. Before this project started, k_f in humans had been attempted in only one centre, but never co-assessed with invasive phenotyping. I obtained biopsies from non-ischaemic hearts with or without hypertrophy, and with or without LV dysfunction. This was an important design element to address the contributions of hypertrophy and LV dysfunction, but made recruitment challenging. Longitudinal assessment of k_f was attempted in sevAS-pEF. Finally, the project fortunately predated the low-risk TAVR trials, which will likely reduce the supply of patients for future studies of this kind.

A Appendix

A.1 CK EQUILIBRIUM CONSTANT, RATE EQUATION AND RESERVE

The equilibrium constant of the CK reaction

$$\mathrm{MgADP^- + PCr^{2-} + H^+ \underset{k_{-1}}{\overset{k_1}{\rightleftharpoons}} MgATP^{2-} + Cr}$$

is defined as

$$K_{eq} = \frac{[ATP][creatine]}{[ADP][PCr][H^+]}.$$

$K_{eq}[H^+]$ has been measured in rat skeletal muscle at 38°C, pH 7.0, ionic strength 0.25 and free [Mg^{2+}] 0 and 1 mmol as 37.8 and 166 respectively (Lawson and Veech, 1979; Veech et al., 1979). This in vitro value was found to be 25 times greater than that measured from measured metabolite contents in vivo, and the discordance interpreted as evidence that the free cytosolic [ADP] is 25-fold lower than measured cell [ADP] content owing to extensive binding or segregation. For any given combination of [PCr], [creatine], [ADP] and [ATP], as [Mg^{2+}] rises above [ATP], [$MgADP^{2-}$]/[$MgATP^{-}$] ratio rises (owing to their different stability constants) and the ATP-generating reaction direction becomes favoured (Saks et al., 1975). When zero < [Mg^{2+}] < [ATP], Mg^{2+} is completely bound to ATP and the PCr-generating direction is favoured.

In the absence of oxidative phosphorylation, whose product ATP has an exaggerated influence on CK rates, the rate of the CK reaction may be modelled kinetically as v_1, the rate of the ATP-producing direction, v_{-1}, the rate of the PCr-producing

direction, and v, the net or overall rate in the ATP-producing direction –

$$v_1 = k_1[E \cdot MgADP \cdot PCr]$$
$$v_{-1} = k_{-1}[E \cdot MgATP \cdot Cr]$$
$$v = v_1 - v_{-1}$$

– where $[E \cdot MgADP \cdot PCr]$ is the concentration of the ternary complex enzyme–MgADP–PCr (Kupriyanov et al., 1984; Saks et al., 1975).

This can be written more fully as

$$v_1 = \frac{V^f_{max}[MgADP][PCr]}{K_c K_{id} D}$$
$$v_{-1} = \frac{V^r_{max}[MgATP][Cr]}{K_a K_{ib} D},$$

where

$$D = 1 + \frac{[MgATP]}{K_{ia}} + \frac{[Cr]}{K_{ib}} + \frac{[MgADP]}{K_{ic}} + \frac{[PCr]}{K_{id}} + \frac{[Cr][MgATP]}{K_a K_{ib}} + \frac{[PCr][MgADP]}{K_c K_{id}} + \frac{[Cr][MgADP]}{K_c K_{ib}},$$

V^f_{max} and V^r_{max} are maximal reaction rates in the ATP- and PCr-producing directions respectively, $K_{ia} \ldots K_{id}$ are dissociation constants for the binary enzyme–substrate complexes, and $K_a \ldots K_d$ are dissociation constants for the ternary complexes.

Thus the rate equation predicts reaction velocity to be proportional to enzyme activity and to have a hyperbolic relation with substrate concentration (Bittl et al., 1987c). Animal studies have tended to find that PCr and ATP are present in saturating concentrations relative to their dissociation constants, while Cr and ADP are present in lower concentrations (concentrations that regulate reaction velocity). In vivo enzyme activity may also depend on enzyme localisation: when oxphos is allowed to proceed, reverse CK flux increases (Saks et al., 1975); rabbits with increased mtCK (% of total CK) but equal total CK activity and ages showed increased V^f_{max} (Perry et al., 1988):

this may be because hearts with lower mtCK proportions are less able to regenerate PCr for the ATP-generating reaction.

V^f_{max} may be written as $k_1[E]_0$ and V^r_{max} as $k_{-1}[E]_0$, where $[E]_0$ is the total enzyme concentration. For any given isozyme and reaction direction, there is a bell-curved relation between V_{max} and pH (Hall et al., 1979). The maximal flux in the ATP-producing direction is proportional to $V^f_{max}[MgADP][PCr]$, or $k_1[E]_0[MgADP][PCr]$ (Kupriyanov et al., 1984; Morrison and Cleland, 1966; Van Dorsten et al., 1996). Thus at a given pH, the reaction is second-order with respect to $[MgADP][PCr]$ and flux is given by $k_2[MgADP][PCr]$, where k_2 is a second-order rate constant. From the perspective of magnetisation transfer, the reaction is first-order with respect to $[PCr]$ and flux is given by $k_f[PCr]$, where k_f is a pseudo-first-order rate constant (see next section).

At Mg^{2+} concentrations where overall reaction rate is zero the system is at thermodynamic equilibrium and $V^f_{max} - V^r_{max} = 0$. At equilibrium, the equilibrium constant is related to the reaction rate by

$$\frac{[MgATP][Cr]}{[MgADP][PCr]} = \frac{V^f_{max}K_aK_{ib}}{V^r_{max}K_cK_{id}} = K_{eq}.$$

With fixed substrate concentrations, as Mg^{2+} concentrations fall, [MgADP]/[MgATP] falls, the reaction shifts left from equilibrium and the free energy change

$$\Delta G = -RT\ln K_{eq} + RT\ln\frac{[MgADP][PCr]}{[MgATP][Cr]}$$

is negative if PCr is synthesized, until a new equilibrium is found.

A.2 BASIC PRINCIPLES UNDERLYING NMR MAGNETISATION TRANSFER EXPERIMENTS

Magnetisation transfer experiments are a specialised kind of NMR observation which can measure the rate of chemical reactions.[1] In the simplest cases, the system under

[1] Reviewed elsewhere (Alger and Shulman, 1984; Bottomley, 2016; Brindle and Radda, 1985; Gadian, 1995; Ingwall, 1982; Kemp and Brindle, 2012; Meyer et al., 1982; Valkovič et al., 2017).

study is at steady state, such that the concentrations of reacting moieties remain constant for the duration of the observation. A label, in this case a non-equilibrium nuclear spin magnetisation, is introduced selectively onto a reacting moiety. If the chemical exchange is rapid enough, the label can be observed to flow to other moieties before it is relaxed by the T_1 mechanism. By observing this flow, the rate constants for chemical exchange may be determined. These rate constants are unusual as they are unidirectional and first-order, even though the underlying reaction may not be. This will be developed below.

Two broad classes of magnetisation transfer experiment include the steady state experiment, where the label is continuously introduced and the observation is taken after the system comes to a new steady state, and the temporal experiment, where the label is introduced transiently and the observation includes the time course of its flow to other moieties.

In magnetisation transfer experiments we are interested in measuring the bulk longitudinal magnetisation, M, assignable to a reactant or product. When placed in a static magnetic field, B_0, the individual nuclei, which each have a spin angular momentum, align along the field in either low-energy α or higher energy β states, with the population distribution given by the Boltzmann distribution. At equilibrium, the bulk longitudinal magnetisation is the vector sum of these states, or the net population excess in α spins, which is very slightly greater than zero. M therefore has magnitude (proportional to the number of nuclei contributing) and direction – it is a vector. For M to become measureable it must be perturbed away from its equilibrium direction by an applied magnetic field, B_1. The signal thereby generated has an intensity proportional to the amplitude of M.

In the simplest case of chemical exchange between two sites, A and B:

$$\mathrm{A} \underset{k_B}{\overset{k_A}{\rightleftharpoons}} \mathrm{B},$$

the rates of appearance of A and B are

$$V_A = -k_A(A) + k_B(B) \tag{A.1}$$

$$V_B = k_A(A) - k_B(B), \tag{A.2}$$

where k_A and k_B are unidirectional first-order rate constants and (A) and (B) are quantities of A and B. If the underlying reaction is not first order with respect to either reactant the rate constants become apparent first-order, or pseudo-first-order. In the case of a steady state experiment, $V_A = V_B = 0$. In the case of an equilibrium steady state, neither A nor B react with other moieties, while in the case of a non-equilibrium steady state, A and/or B may react with other moieties.

Assuming that A and B are NMR-visible, that their resonances are distinct from each other,[2] and that nuclear spin states do not change when nuclei are exchanged in chemical reactions, similar expressions may be written for the rates of appearance of α and β spins at A and B:

$$V_{A\alpha} = -k_A(A_\alpha) + k_B(B_\alpha) \tag{A.3}$$

$$V_{A\beta} = -k_A(A_\beta) + k_B(B_\beta) \tag{A.4}$$

$$V_{B\alpha} = k_A(A_\alpha) - k_B(B_\alpha) \tag{A.5}$$

$$V_{B\beta} = k_A(A_\beta) - k_B(B_\beta). \tag{A.6}$$

As magnetisation at A, M_A, is proportional to $A_\alpha - A_\beta$, the rate of appearance of magnetisation at A assuming no diminution by T_1 is given by $V_{A\alpha} - V_{A\beta}$, and similarly for B:

$$\frac{dM_A}{dt} = -k_A M_A + k_B M_B \tag{A.7}$$

$$\frac{dM_B}{dt} = k_A M_A - k_B M_B. \tag{A.8}$$

[2] This requires sufficiently narrow line-widths, sufficiently large chemical shifts, and for the exchange rate to be in the slow exchange limit.

If the T_1 mechanism is accounted for, then these become:

$$\frac{dM_A}{dt} = R_1^A(M_A^0 - M_A) - k_A M_A + k_B M_B \tag{A.9}$$

$$\frac{dM_B}{dt} = R_1^B(M_B^0 - M_B) + k_A M_A - k_B M_B, \tag{A.10}$$

where M_A^0 and M_B^0 are the equilibrium magnetisations at A and B respectively (before introduction of the nuclear label) and R_1^A and R_1^B are the $\frac{1}{T_1}$'s at A and B in the absence of chemical exchange. (It is assumed that the T_1 of the magnetisation of any enzyme-bound intermediate is much longer than that of A or B.)

In the case of the two site steady state magnetisation transfer experiment where the introducing label has the effect of, say, saturating only the B resonance (i.e. setting $B_\alpha - B_\beta = 0$, where before, $B_\alpha - B_\beta > 0$), the chemical reaction carries the excess of β spins at site B to site A, so that A appears to become saturated (M_A diminishes by an amount $\Delta M_A = M_A^0 - M_A$). At the same time the T_1 mechanism is restoring M_A toward its equilibrium amplitude (i.e. restoring the Boltzmann distribution of spin states). Once these two opposing effects on M_A equal each other a new equilibrium is established. The equations may thus be solved for k_A by measuring M_A^0 before introducing the label, introducing the label, then once the new equilibrium is achieved, by measuring M_A and T_1^A and setting $M_B = 0$; $\frac{dM_A}{dt} = 0$. The important point here is that saturating B results in the term k_B dropping out and the equation becoming solvable for k_A. (The T_1 at A once the new equilibrium is achieved may not equal the T_1 beforehand, so once the new equilibrium is achieved the measured T_1 is called T_1'.)

The relationship between the fractional change in resonance intensity at A, $\Delta M_A/M_A^0$, and k_A/R_A is plotted (Figure A.1). If $k_A \gg R_A$, then the fractional change approaches 1, and if $k_A \ll R_A$, no change in M_A is observed. The experiment is therefore only helpful for solving for k_A when $0.1 < k_A/R_A < 10$.

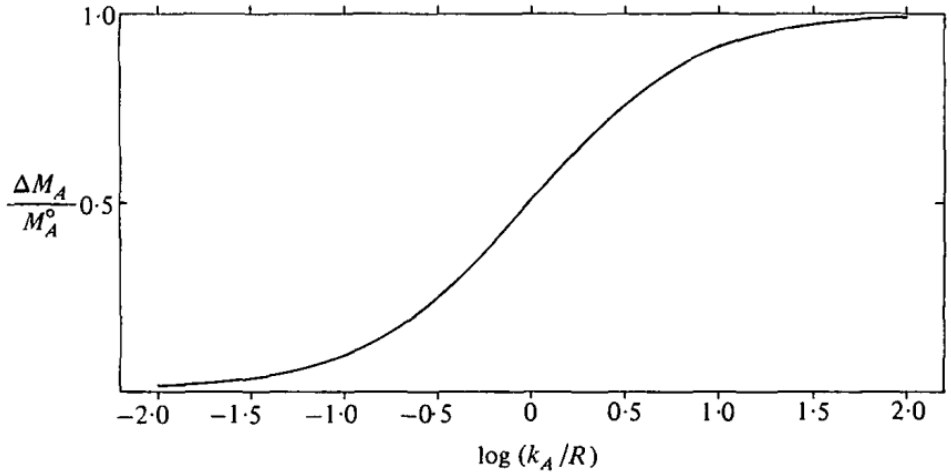


Figure A.1: The relationship between the fractional change in resonance intensity at A, $\Delta M_A/M_A^0$, and k_A/R_A, from Alger and Shulman (1984).

A.3 CORRELATES OF CK/CS ACTIVITY RATIO

Please see Table A.1 and Figure A.2.

Table A.1: Correlates of CK/CS activity ratio[a]

Parameter	n	r[b]	p-value[b]	rho[c]	p-value[c]
CK total activity (IU/mg protein)	.62	47	3e–6	.53	1e–4
CK k_f (/s)	.51	37	.001	.39	.017
k_f × est [PCr] (μmol/g/s)	.47	35	.005	.45	.006
k_f × total creatine (nmol/mg/s)	.52	37	.001	.40	.014
LVESVi (ml/m^2)	–.30	46	.041	–.25	ns
LVEF (%)	.29	46	.049	.23	ns

[a] Only those correlates meeting p $\leq$ .05 are included. ns, not significant.
[b] Pearson r correlation coefficient.
[c] Spearman rho correlation coefficient.

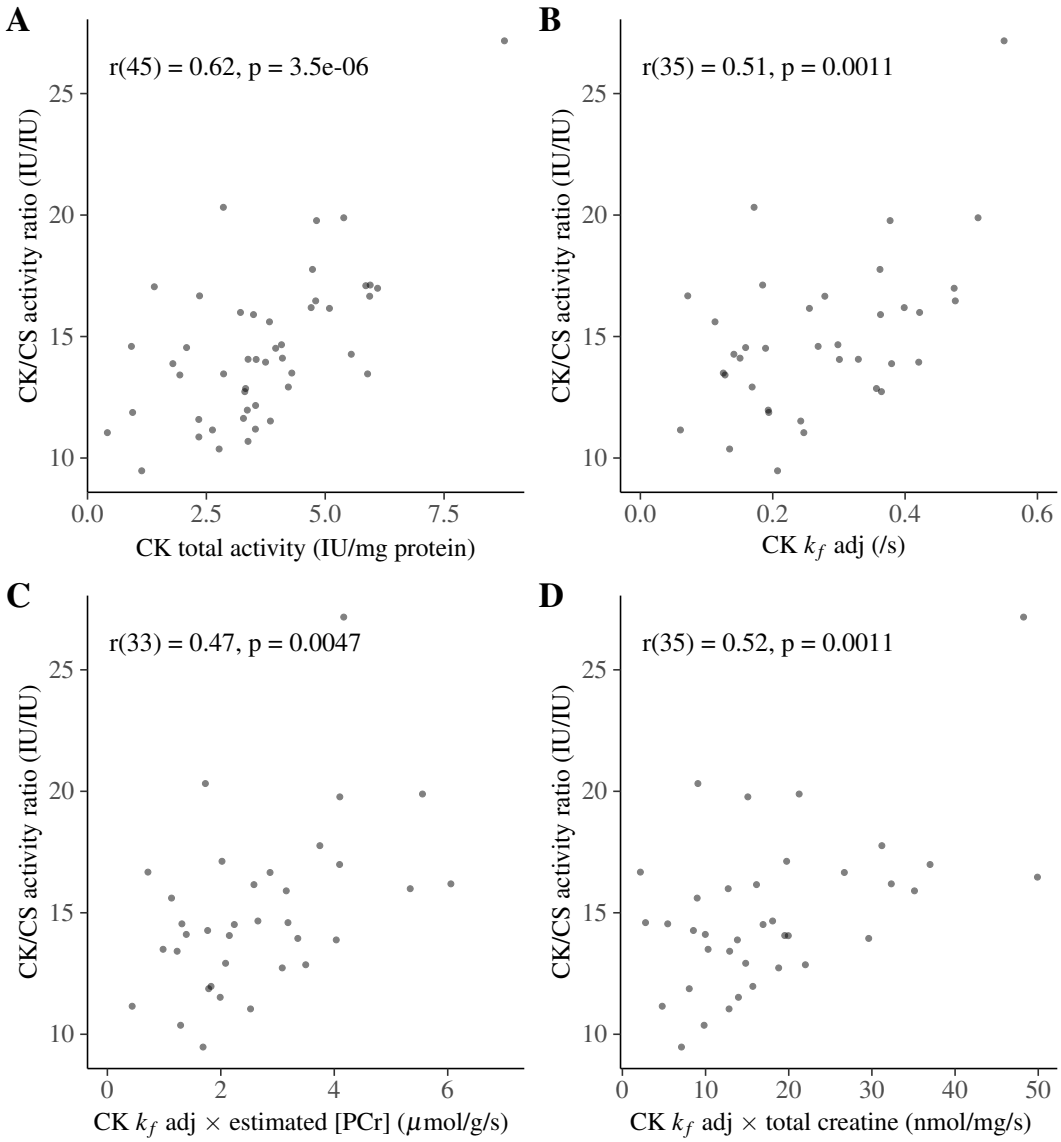


Figure A.2: Scatter plots for (A) CK total activity, (B) CK k_f, (C) CK flux estimated by k_f × estimated [PCr], and (D) CK flux estimated by total creatine × k_f against CK/CS activity ratio. (Note that total creatine was not significantly correlated with CK/CS activity ratio. Compare Figure 3.3, p. 100.)

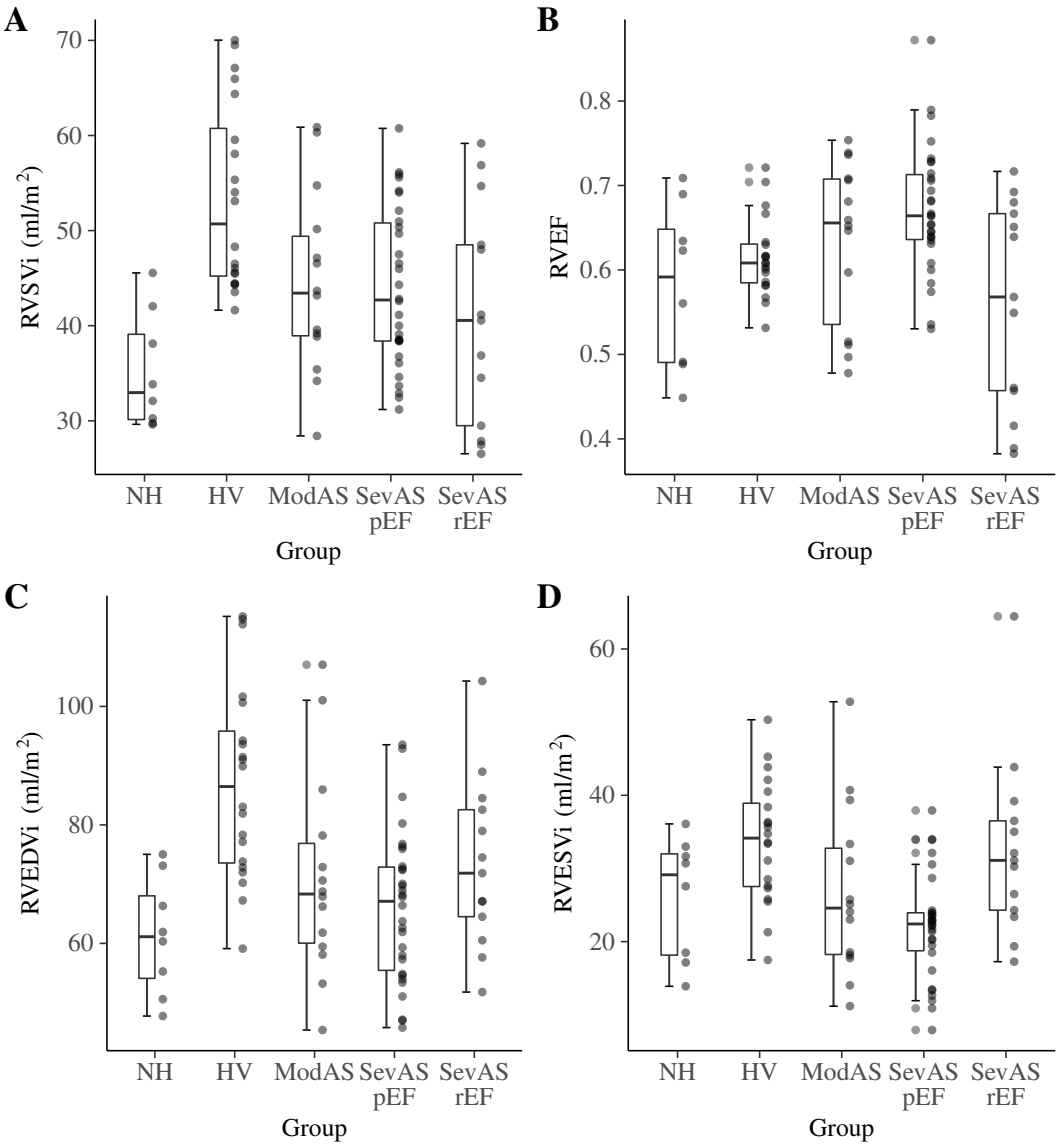


Figure A.3: RVSVi, RVEF, and RV volumes in two control and three AS groups.

A.4 RV DIMENSIONS IN AS COHORTS

Please see Table A.2 and Figure A.3.

Table A.2: RV Chamber dimensions by CMR in AS[a]

Parameter	NH	HV	ModAS	SevAS-pEF	SevAS-rEF	MS-rEF
n =	8	20	14	30	13	2
BSA (m^2)	1.66 (1.56, 1.85)	1.82 (1.70, 2.07)	1.97 (1.87, 2.04)	1.94 (1.82, 2.12)	2.00 (1.85, 2.17)	1.76
RVEF (%)	58.1 (49.9, 66.3)	61.5 (59.3, 63.7)	63.4 (57.8, 69.1)	67.1 (64.4, 69.9)	55.9 (48.4, 63.4)	42.7
RVEDVi (ml/m^2)	61.3 (53.0, 69.6)	87.1 (79.4, 94.8)	71.2 (61.2, 81.2)	66.0 (61.3, 70.7)	73.4 (64.7, 82.1)	55.0
RVESVi (ml/m^2)	26.1 (19.1, 33.1)	33.7 (29.8, 37.7)	26.8 (20.1, 33.5)	22.0 (19.3, 24.7)	32.6 (25.1, 40.0)	31.6
RVSVi (ml/m^2)	35.2 (30.1, 40.2)	53.4 (48.8, 57.9)	44.4 (38.9, 50.0)	44.0 (40.9, 47.2)	40.9 (33.9, 47.9)	23.7

[a] Mean (95% CI) values given, except for BSA (median (IQR)).

A.5 CK ISOFORMS IN SEVERE MR

Please see Table A.3.

Table A.3: CK isoform activities (expanded from Tables 4.5 and 4.6)

Parameter	NH	SevAS-pEF	SevAS-rEF	MS-rEF	MR
n (isoform activities) =	6	26	9	2	2
CK total activity (IU/mg protein) ∗†	5.47 (4.70, 5.89)	3.54 (2.86, 4.30)∗	3.11 (1.14, 3.75)∗†	2.08	4.71
CS activity (IU/mg protein) ∗†	0.325 (0.271, 0.389)	0.280 (0.215, 0.316)∗	0.226 (0.120, 0.269)∗†	0.141	0.288
Estimated CK capacity †	353 (224, 381)	222 (171, 321)	155 (39, 273)	68	453
Total creatine (nmol/mg protein)	66.2 (14.5)	63.3 (25.6)	55.9 (25.6)	35.8	94.7 (26.2)
MtCK (IU/mg protein) ∗†	0.83 (0.71, 1.08)	0.62 (0.48, 0.81)∗	0.49 (0.15, 0.61)∗†	0.33	0.95
CK-MM (IU/mg protein) ∗†	2.87 (2.67, 3.06)	2.17 (1.79, 2.54)∗	1.56 (0.74, 2.21)∗†	1.42	2.68
CK-MB (IU/mg protein) ∗†	1.47 (1.24, 1.58)	0.66 (0.48, 0.81)∗	0.61 (0.23, 0.76)∗	0.28	0.88
CK-BB (IU/mg protein)	0.14 (0.09, 0.22)	0.14 (0.08, 0.26)	0.12 (0.06, 0.13)	0.05	0.21
MtCK (% of total CK)	16.4 (15.1, 17.7)	16.8 (15.5, 18.6)	15.3 (13.2, 17.9)	16.1	19.2
CK-MM (% of total CK)	54.1 (52.0, 56.7)	59.8 (54.9, 62.9)	58.9 (54.6, 60.7)	64.7	57.6
CK-MB (% of total CK)	25.8 (23.6, 28.4)	18.7 (15.3, 21.6)	20.0 (18.0, 22.7)	16.3	19.1
CK-BB (% of total CK)	3.0 (2.0, 3.9)	4.1 (1.8, 6.3)	4.5 (3.8, 5.5)∗	2.9	4.2
MtCK (% of CS activity, IU/IU)	2.54 (0.49)	2.60 (0.68)	2.13 (0.77)	2.24	3.14

[a] Median (IQR) or mean (SD) values are given. Conventions as for Table 4.5, p. 139.

Bibliography

Abel, E. D. and Doenst, T. (2011). Mitochondrial adaptations to physiological vs. pathological cardiac hypertrophy. *Cardiovasc Res*, 90(2):234–242.

Abraham, M. R., Bottomley, P. A., Dimaano, V. L., Pinheiro, A., Steinberg, A., Traill, T. A., Abraham, T. P., and Weiss, R. G. (2013). Creatine kinase adenosine triphosphate and phosphocreatine energy supply in a single kindred of patients with hypertrophic cardiomyopathy. *American Journal of Cardiology*, 112(6):861–866.

Abraham, M. R., Selivanov, V. A., Hodgson, D. M., Pucar, D., Zingman, L. V., Wieringa, B., Dzeja, P. P., Alekseev, A. E., and Terzic, A. (2002). Coupling of Cell Energetics with Membrane Metabolic Sensing: Integrative Signaling Through Creatine Kinase Phosphotransfer Disrupted By M-Ck Gene Knock-Out. *J Biol Chem*, 277(27):24427–24434.

Adams, D. H., Popma, J. J., Reardon, M. J., Yakubov, S. J., Coselli, J. S., Deeb, G. M., Gleason, T. G., Buchbinder, M., Hermiller, J., Kleiman, N. S., Chetcuti, S., Heiser, J., Merhi, W., Zorn, G., Tadros, P., Robinson, N., Petrossian, G., Hughes, G. C., Harrison, J. K., Conte, J., Maini, B., Mumtaz, M., Chenoweth, S., and Oh, J. K. (2014). Transcatheter Aortic-Valve Replacement with a Self-Expanding Prosthesis. *New England Journal of Medicine*, 370(19):1790–1798.

Agricola, E., Oppizzi, M., Maisano, F., De Bonis, M., Schinkel, A. F., Torracca, L., Margonato, A., Melisurgo, G., and Alfieri, O. (2004). Echocardiographic classification of chronic ischemic mitral regurgitation caused by restricted motion according to tethering pattern. *European Journal of Echocardiography*, 5(5):326–334.

Ahmed, M. I., Gladden, J. D., Litovsky, S. H., Lloyd, S. G., Gupta, H., Inusah, S., Denney, T., Powell, P., McGiffin, D. C., and Dell'Italia, L. J. (2010). Increased Oxidative Stress and Cardiomyocyte Myofibrillar Degeneration in Patients With Chronic Isolated Mitral Regurgitation and Ejection Fraction >60%. *Journal of the American College of Cardiology*, 55(7):671–679.

Aitman, T. J., Glazier, A. M., Wallace, C. A., Cooper, L. D., Norsworthy, P. J., Wahid, F. N., Al-Majali, K. M., Trembling, P. M., Mann, C. J., Shoulders, C. C., Graf, D., Lezin, E. S., Kurtz, T. W., Kren, V., Pravenec, M., Ibrahimi, A., Abumrad, N. A.,

Stanton, L. W., and Scott, J. (1999). Identification of Cd36 (Fat) as an insulin-resistance gene causing defective fatty acid and glucose metabolism in hypertensive rats. *Nat Genet*, 21(1):76–83.

Akhter, S. A., Luttrell, L. M., Rockman, H. A., Iaccarino, G., Lefkowitz, R. J., and Koch, W. J. (1998). Targeting the receptor-G(q) interface to inhibit in vivo pressure overload myocardial hypertrophy. *Science*, 280(5363):574–577.

Akki, A., Su, J., Yano, T., Gupta, A., Wang, Y., Leppo, M. K., Chacko, V. P., Steenbergen, C., and Weiss, R. G. (2012). Creatine kinase overexpression improves ATP kinetics and contractile function in postischemic myocardium. *Am J Physiol Heart Circ Physiol*, 303(7):H844–H852.

Aksentijević, D., McAndrew, D. J., Karlstädt, A., Zervou, S., Sebag-Montefiore, L., Cross, R., Douglas, G., Regitz-Zagrosek, V., Lopaschuk, G. D., Neubauer, S., and Lygate, C. A. (2014). Cardiac dysfunction and peri-weaning mortality in malonyl-coenzyme A decarboxylase (MCD) knockout mice as a consequence of restricting substrate plasticity. *J Mol Cell Cardiol*, 75:76–87.

Al-Azizi, K., Hamandi, M., and Mack, M. (2019). Clinical trials of transcatheter aortic valve replacement. *Heart (British Cardiac Society)*, 105(Suppl 2):s6–s9.

Alaynick, W. A., Kondo, R. P., Xie, W., He, W., Dufour, C. R., Downes, M., Jonker, J. W., Giles, W., Naviaux, R. K., Giguère, V., and Evans, R. M. (2007). ERRγ Directs and Maintains the Transition to Oxidative Metabolism in the Postnatal Heart. *Cell Metab*, 6(1):13–24.

Alger, T. R. and Shulman, R. G. (1984). NMR Studies of Enzymatic Rates in vitro and in Vivo by Magnetization Transfer. *Quarterly Reviews of Biophysics*, 17(1):83–124.

Allard, M. F., Schonekess, B. O., Henning, S. L., English, D. R., and Lopaschuk, G. D. (1994). Contribution of oxidative metabolism and glycolysis to ATP production in hypertrophied hearts. *Am J Physiol Heart Circ Physiol*, 267(2):H742–H750.

Altman, D. G. and Royston, P. (2006). Statistics Notes: The cost of dichotomising continuous variables. *BMJ : British Medical Journal*, 332(7549):1080.

Amorim, P. A., Nguyen, T. D., Shingu, Y., Schwarzer, M., Mohr, F. W., Schrepper, A., and Doenst, T. (2010). Myocardial infarction in rats causes partial impairment in insulin response associated with reduced fatty acid oxidation and mitochondrial gene expression. *J Thorac Cardiov Sur*, 140(5):1160–1167.

Aplin, M., Kyhl, K., Bjerre, J., Ihlemann, N., Greenwood, J. P., Plein, S., Uddin, A., Tønder, N., Høst, N. B., Ahlström, M. G., Hove, J., Hassager, C., Iversen, K., Vejlstrup, N. G., and Lav Madsen, P. (2016). Cardiac remodelling and function with primary mitral valve insufficiency studied by magnetic resonance imaging. *European Heart Journal - Cardiovascular Imaging*, 17(8):863–870.

Apple, F. S. and Rogers, M. A. (1986). Mitochondrial creatine kinase activity alterations in skeletal muscle during long-distance running. *Journal of Applied Physiology*, 61(2):482.

Arbab-Zadeh, A., Perhonen, M., Howden, E., Peshock, R. M., Zhang, R., Adams-Huet, B., Haykowsky, M. J., and Levine, B. D. (2014). Cardiac Remodeling in Response to 1 Year of Intensive Endurance Training. *Circulation*, 130(24):2152–2161.

Atkinson, D. E. (1968). Energy charge of the adenylate pool as a regulatory parameter. Interaction with feedback modifiers. *Biochemistry-US*, 7(11):4030–4034.

Aubert, G., Martin, O. J., Horton, J. L., Lai, L., Vega, R. B., Leone, T. C., Koves, T., Gardell, S. J., Krüger, M., Hoppel, C. L., Lewandowski, E. D., Crawford, P. A., Muoio, D. M., and Kelly, D. P. (2016). The Failing Heart Relies on Ketone Bodies as a Fuel. *Circulation*, 133(8):698–705.

Aubert, G., Vega, R. B., and Kelly, D. P. (2013). Perturbations in the gene regulatory pathways controlling mitochondrial energy production in the failing heart. *Biochimica Et Biophysica Acta-Mol Cell Research*, 1833(4):840–847.

Augustus, A. S., Buchanan, J., Park, T.-S., Hirata, K., Noh, H.-l., Sun, J., Homma, S., D'armiento, J., Abel, E. D., and Goldberg, I. J. (2006). Loss of Lipoprotein Lipase-derived Fatty Acids Leads to Increased Cardiac Glucose Metabolism and Heart Dysfunction. *J Biol Chem*, 281(13):8716–8723.

Aurigemma, G. P., Silver, K. H., Priest, M. A., and Gaasch, W. H. (1995). Geometric changes allow normal ejection fraction despite depressed myocardial shortening in hypertensive left ventricular hypertrophy. *Journal of the American College of Cardiology*, 26(1):195–202.

Azevedo, C. F., Nigri, M., Higuchi, M. L., Pomerantzeff, P. M., Spina, G. S., Sampaio, R. O., Tarasoutchi, F., Grinberg, M., and Rochitte, C. E. (2010). Prognostic Significance of Myocardial Fibrosis Quantification by Histopathology and Magnetic Resonance Imaging in Patients With Severe Aortic Valve Disease. *Journal of the American College of Cardiology*, 56(4):278–287.

Bache, R. J., Zhang, J., Murakami, Y., Zhang, Y., Cho, Y. K., Merkle, H., Gong, G., From, A. H. L., and Ugurbil, K. (1999). Myocardial oxygenation at high workstates in hearts with left ventricular hypertrophy. *Cardiovasc Res*, 42(3):616–626.

Bache, R. J., Zhang, J., Path, G., Merkle, H., Hendrich, K., From, A. H., and Ugurbil, K. (1994). High-energy phosphate responses to tachycardia and inotropic stimulation in left ventricular hypertrophy. *Am J Physiol Heart Circ Physiol*, 266(5):H1959–H1970.

Backs, J., Backs, T., Neef, S., Kreusser, M. M., Lehmann, L. H., Patrick, D. M., Grueter, C. E., Qi, X., Richardson, J. A., Hill, J. A., Katus, H. A., Bassel-Duby,

R., Maier, L. S., and Olson, E. N. (2009). The delta isoform of CaM kinase II is required for pathological cardiac hypertrophy and remodeling after pressure overload. *Proceedings of the National Academy of Sciences*, 106(7):2342–2347.

Baggish, A. L. and Wood, M. J. (2011). Athlete's Heart and Cardiovascular Care of the Athlete. *Circulation*, 123(23):2723–2735.

Baicu, C. F., Zile, M. R., Aurigemma, G. P., and Gaasch, W. H. (2005). Left ventricular systolic performance, function, and contractility in patients with diastolic heart failure. *Circulation*, 111(18):2306–2312.

Bakermans, A. J., Bazil, J. N., Nederveen, A. J., Strijkers, G. J., Boekholdt, S. M., Beard, D. A., and Jeneson, J. A. (2017). Human cardiac 31P-MR spectroscopy at 3 tesla cannot detect failing myocardial energy homeostasis during exercise. *Frontiers in Physiology*, 8(Nov):939.

Balaban, R. S. (1984). The application of nuclear magnetic resonance to the study of cellular physiology. *The American journal of physiology*, 246(1 Pt 1):C10–9.

Balaban, R. S. (1990). Regulation of oxidative phosphorylation in the mammalian cell. *Am J Physiol*, 258(3):C377–C389.

Balaban, R. S., Kantor, H. L., Katz, L. A., and Briggs, R. W. (1986). Relation between Work and Phosphate Metabolite in the in Vivo Paced Mammalian Heart. *Science*, 232(4754):1121–1123.

Balschi, J. A., Shen, H., Madden, M. C., Hai, J. O., Bradley, Jr, E. L., and Wolkowicz, P. E. (1997). Model Systems for Modulating the Free Energy of ATP Hydrolysis in Normoxically Perfused Rat Hearts. *Journal of Molecular and Cellular Cardiology*, 29(11):3123–3133.

Barclay, C. J. (2008). Getting energy to where it is required is a problem in the failing heart. *J Physiol*, 586(21):5037–5038.

Barger, P. M., Brandt, J. M., Leone, T. C., Weinheimer, C. J., and Kelly, D. P. (2000). Deactivation of peroxisome proliferator-activated receptor-α during cardiac hypertrophic growth. *J Clin Invest*, 105(12):1723–1730.

Barger, P. M. and Kelly, D. P. (2000). PPAR Signaling in the Control of Cardiac Energy Metabolism. *Trends Cardiovas Med*, 10(6):238–245.

Barish, G. D., Narkar, V. A., and Evans, R. M. (2006). PPARδ: a dagger in the heart of the metabolic syndrome. *J Clin Invest*, 116(3):590–597.

Baron, S. J., Arnold, S. V., Herrmann, H. C., Holmes Jr, D. R., Szeto, W. Y., Allen, K. B., Chhatriwalla, A. K., Vemulapali, S., O'Brien, S., Dai, D., and Cohen, D. J. (2016). Impact of Ejection Fraction and Aortic Valve Gradient on Outcomes of Transcatheter Aortic Valve Replacement. *Journal of the American College of Cardiology*, 67(20):2349–2358.

Barone-Rochette, G., Piérard, S., De Meester de Ravenstein, C., Seldrum, S., Melchior, J., Maes, F., Pouleur, A.-C., Vancraeynest, D., Pasquet, A., Vanoverschelde, J.-L., and Gerber, B. L. (2014). Prognostic Significance of LGE by CMR in Aortic Stenosis Patients Undergoing Valve Replacement. *Journal of the American College of Cardiology*, 64(2):144–154.

Basso, C., Perazzolo Marra, M., Rizzo, S., De Lazzari, M., Giorgi, B., Cipriani, A., Frigo, A. C., Rigato, I., Migliore, F., Pilichou, K., Bertaglia, E., Cacciavillani, L., Bauce, B., Corrado, D., Thiene, G., and Iliceto, S. (2015). Arrhythmic Mitral Valve Prolapse and Sudden Cardiac Death. *Circulation*, 132(7):556–566.

Baumgartner, H., Hung, J., Bermejo, J., Chambers, J. B., Edvardsen, T., Goldstein, S., Lancellotti, P., LeFevre, M., Miller Jr, F., and Otto, C. M. (2017). Recommendations on the Echocardiographic Assessment of Aortic Valve Stenosis: A Focused Update from the European Association of Cardiovascular Imaging and the American Society of Echocardiography. *Journal of the American Society of Echocardiography*, 30(4):372–392.

Baumgartner, H., Hung, J., Bermejo, J., Chambers, J. B., Evangelista, A., Griffin, B. P., Iung, B., Otto, C. M., Pellikka, P. A., and Quiñones, M. (2009). Echocardiographic Assessment of Valve Stenosis: EAE/ASE Recommendations for Clinical Practice. *Journal of the American Society of Echocardiography*, 22(1):1–23.

Bedi, K. C., Snyder, N. W., Brandimarto, J., Aziz, M., Mesaros, C., Worth, A. J., Wang, L. L., Javaheri, A., Blair, I. A., Margulies, K. B., and Rame, J. E. (2016). Evidence for Intramyocardial Disruption of Lipid Metabolism and Increased Myocardial Ketone Utilization in Advanced Human Heart Failure. *Circulation*, 133(8):706–716.

Beisvag, V., Kemi, O. J., Arbo, I., Loennechen, J. P., Wisløff, U., Langaas, M., Sandvik, A. K., and Ellingsen, Ø. (2009). Pathological and physiological hypertrophies are regulated by distinct gene programs. *European Journal of Cardiovascular Prevention and Rehabilitation*, 16(6):690–697.

Belevich, I., Joensuu, M., Kumar, D., Vihinen, H., and Jokitalo, E. (2016). Microscopy Image Browser: A Platform for Segmentation and Analysis of Multidimensional Datasets. *Plos Biology*, 14(1):e1002340.

Bellenger, N. G., Burgess, M. I., Ray, S. G., Lahiri, A., Coats, A. J., Cleland, J. G., and Pennell, D. J. (2000). Comparison of left ventricular ejection fraction and volumes in heart failure by echocardiography, radionuclide ventriculography and cardiovascular magnetic resonance; are they interchangeable? *European Heart Journal*, 21(16):1387–1396.

Ben Cheikh, R., Guendouz, A., and Moravec, J. (1994). Control of oxidative metabolism in volume-overloaded rat hearts: effects of different lipid substrates. *Am J Physiol Heart Circ Physiol*, 266(5):H2090–H2097.

Bendz, R., Ström, S., and Olin, C. (1980). CK-MB in serum and in heart and skeletal muscles in patients subjected to mitral valve replacement. *European journal of cardiology*, 12(1):25–39.

Bergeron, R., Ren, J. M., Cadman, K. S., Moore, I. K., Perret, P., Pypaert, M., Young, L. H., Semenkovich, C. F., and Shulman, G. I. (2001). Chronic activation of AMP kinase results in NRF-1 activation and mitochondrial biogenesis. *Am J Physiol-Endoc M*, 281(6):E1340–E1346.

Bernardo, B. C., Ooi, J. Y. Y., Weeks, K. L., Patterson, N. L., and McMullen, J. R. (2018). Understanding Key Mechanisms of Exercise-Induced Cardiac Protection to Mitigate Disease: Current Knowledge and Emerging Concepts. *Physiological Reviews*, 98(1):419–475.

Bernardo, B. C., Weeks, K. L., Pretorius, L., and McMullen, J. R. (2010). Molecular distinction between physiological and pathological cardiac hypertrophy: Experimental findings and therapeutic strategies. *Pharmacology & Therapeutics*, 128(1):191–227.

Bersell, K., Arab, S., Haring, B., and Kühn, B. (2009). Neuregulin1/ErbB4 Signaling Induces Cardiomyocyte Proliferation and Repair of Heart Injury. *Cell*, 138(2):257–270.

Bessman, S. P. and Fonyo, A. (1966). The possible role of the mitochondrial bound creatine kinase in regulation of mitochondrial respiration. *Biochemical and Biophysical Research Communications*, 22(5):597–602.

Bessman, S. P. and Geiger, P. J. (1981). Transport of energy in muscle: the phosphorylcreatine shuttle. *Science*, 211(4481):448–452.

Bessman, S. P., Yang, W. C., Geiger, P. J., and Erickson-Viitanen, S. (1980). Intimate coupling of creatine phosphokinase and myofibrillar adenosinetriphosphatase. *Biochemical and Biophysical Research Communications*, 96(3):1414–1420.

Beyerbacht, H. P., Lamb, H. J., van der Laarse, A., Vliegen, H. W., Leujes, F., Hazekamp, M. G., de Roos, A., and van der Wall, E. E. (2001). Aortic Valve Replacement in Patients with Aortic Valve Stenosis Improves Myocardial Metabolism and Diastolic Function. *Radiology*, 219(3):637–643.

Bezzerides, V. J., Platt, C., Lerchenmüller, C., Paruchuri, K., Oh, N. L., Xiao, C., Cao, Y., Mann, N., Spiegelman, B. M., and Rosenzweig, A. (2016). CITED4 induces physiologic hypertrophy and promotes functional recovery after ischemic injury. *JCI Insight*, 1(9):e85904.

Biner, S., Rafique, A., Rafii, F., Tolstrup, K., Noorani, O., Shiota, T., Gurudevan, S., and Siegel, R. J. (2010). Reproducibility of Proximal Isovelocity Surface Area, Vena Contracta, and Regurgitant Jet Area for Assessment of Mitral Regurgitation Severity. *JACC: Cardiovascular Imaging*, 3(3):235–243.

Birkedal, R., Shiels, H. A., and Vendelin, M. (2006). Three-dimensional mitochondrial arrangement in ventricular myocytes: from chaos to order. *American Journal of Physiology-Cell Physiology*, 291(6):C1148–C1158.

Bisognano, J. D., Weinberger, H. D., Bohlmeyer, T. J., Pende, A., Raynolds, M. V., Sastravaha, A., Roden, R., Asano, K., Blaxall, B. C., Wu, S. C., Communal, C., Singh, K., Colucci, W., Bristow, M. R., and Port, D. J. (2000). Myocardial-directed overexpression of the human β1-adrenergic receptor in transgenic mice. *Journal of Molecular and Cellular Cardiology*, 32(5):817–830.

Bittl, J. A., Balschi, J. A., and Ingwall, J. S. (1987a). Contractile failure and high-energy phosphate turnover during hypoxia: 31P-NMR surface coil studies in living rat. *Circ Res*, 60(6):871–878.

Bittl, J. A., Balschi, J. A., and Ingwall, J. S. (1987b). Effects of norepinephrine infusion on myocardial high-energy phosphate content and turnover in the living rat. *J Clin Invest*, 79(6):1852–1859.

Bittl, J. A., DeLayre, J., and Ingwall, J. S. (1987c). Rate equation for creatine kinase predicts the in vivo reaction velocity: phosphorus-31 NMR surface coil studies in brain, heart, and skeletal muscle of the living rat. *Biochemistry-US*, 26(19):6083–6090.

Bittl, J. A. and Ingwall, J. S. (1985). Reaction rates of creatine kinase and ATP synthesis in the isolated rat heart. A 31P NMR magnetization transfer study. *J Biol Chem*, 260(6):3512–3517.

Bittl, J. A. and Ingwall, J. S. (1986). The energetics of myocardial stretch. Creatine kinase flux and oxygen consumption in the noncontracting rat heart. *Circ Res*, 58(3):378–383.

Bittl, J. A., Weisfeldt, M. L., and Jacobus, W. E. (1985). Creatine kinase of heart mitochondria. The progressive loss of enzyme activity during in vivo ischemia and its correlation to depressed myocardial function. *Journal of Biological Chemistry*, 260(1):208–214.

Blum, H. E., Deus, B., and Gerok, W. (1983). Mitochondrial Creatine Kinase from Human Heart Muscle: Purification and Characterization of the Crystallized Isoenzyme. *The Journal of Biochemistry*, 94(4):1247–1257.

Boehm, E., Ventura-Clapier, R., Mateo, P., Lechène, P., and Veksler, V. (2000). Glycolysis supports calcium uptake by the sarcoplasmic reticulum in skinned ventricular fibres of mice deficient in mitochondrial and cytosolic creatine kinase. *J Mol Cell Cardiol*, 32(6):891–902.

Bogner, W., Chmelik, M., Schmid, A. I., Moser, E., Trattnig, S., and Gruber, S. (2009). Assessment of 31P relaxation times in the human calf muscle: A comparison between 3 T and 7 T in vivo. *Magnetic resonance in medicine*, 62(3):574–582.

Bohbot, Y., de Meester de Ravenstein, C., Chadha, G., Rusinaru, D., Belkhir, K., Trouillet, C., Pasquet, A., Marechaux, S., Vanoverschelde, J.-L., and Tribouilloy, C. (2019). Relationship Between Left Ventricular Ejection Fraction and Mortality in Asymptomatic and Minimally Symptomatic Patients With Severe Aortic Stenosis. *JACC: Cardiovascular Imaging*, 12(1):38–48.

Bolling, S. F., Li, S., O'Brien, S. M., Brennan, J. M., Prager, R. L., and Gammie, J. S. (2010). Predictors of Mitral Valve Repair: Clinical and Surgeon Factors. *The Annals of thoracic surgery*, 90(6):1904–1912.

Boström, P., Mann, N., Wu, J., Quintero, P. A., Plovie, E. R., Panáková, D., Gupta, R. K., Xiao, C., MacRae, C. A., Rosenzweig, A., and Spiegelman, B. M. (2010). C/EBPβ controls exercise-induced cardiac growth and protects against pathological cardiac remodeling. *Cell*, 143(7):1072–1083.

Bottomley, P. A. (2016). Measuring Biochemical Reaction Rates In Vivo with Magnetization Transfer. *eMagRes*, 5:843–858.

Bottomley, P. A., Ouwerkerk, R., Lee, R. F., and Weiss, R. G. (2002). Four-angle saturation transfer (FAST) method for measuring creatine kinase reaction rates in vivo. *Magnetic resonance in medicine*, 47(5):850–863.

Bottomley, P. A., Panjrath, G. S., Lai, S., Hirsch, G. A., Wu, K., Najjar, S. S., Steinberg, A., Gerstenblith, G., and Weiss, R. G. (2013a). Metabolic Rates of ATP Transfer Through Creatine Kinase (CK Flux) Predict Clinical Heart Failure Events and Death. *Sci Transl Med*, 5(215):215re3–215re3.

Bottomley, P. A., Panjrath, G. S., Lai, S., Hirsch, G. A., Wu, K., Najjar, S. S., Steinberg, A., Gerstenblith, G., and Weiss, R. G. (2013b). Metabolic Rates of ATP Transfer Through Creatine Kinase (CK Flux) Predict Clinical Heart Failure Events and Death. *Sci Transl Med*, 5(215):215re3–215re3.

Bottomley, P. A. and Weiss, R. G. (1998). Non-invasive magnetic-resonance detection of creatine depletion in non-viable infarcted myocardium. *Lancet*, 351(9104):714–718.

Bottomley, P. A. and Weiss, R. G. (2001). Noninvasive Localized MR Quantification of Creatine Kinase Metabolites in Normal and Infarcted Canine Myocardium. *Radiology*, 219(2):411–418.

Bottomley, P. A., Wu, K. C., Gerstenblith, G., Schulman, S. P., Steinberg, A., and Weiss, R. G. (2009). Reduced Myocardial Creatine Kinase Flux in Human Myocardial Infarction: An In Vivo Phosphorus Magnetic Resonance Spectroscopy Study. *Circulation*, 119(14):1918–1924.

Boudina, S., Bugger, H., Sena, S., O'Neill, B. T., Zaha, V. G., Ilkun, O., Wright, J. J., Mazumder, P. K., Palfreyman, E., Tidwell, T. J., Theobald, H., Khalimonchuk,

O., Wayment, B., Sheng, X., Rodnick, K. J., Centini, R., Chen, D., Litwin, S. E., Weimer, B. E., and Abel, E. D. (2009). Contribution of Impaired Myocardial Insulin Signaling to Mitochondrial Dysfunction and Oxidative Stress in the Heart. *Circulation*, 119(9):1272–1283.

Braasch, W., Gudbjarnason, S., Puri, P. S., Ravens, K. G., and Bing, R. J. (1968). Early changes in energy metabolism in the myocardium following acute coronary artery occlusion in anesthetized dogs. *Circulation Research*, 23(3):429–438.

Branovets, J., Sepp, M., Kotlyarova, S., Jepihhina, N., Sokolova, N., Aksentijevic, D., Lygate, C. A., Neubauer, S., Vendelin, M., and Birkedal, R. (2013). Unchanged mitochondrial organization and compartmentation of high-energy phosphates in creatine-deficient GAMT-/- mouse hearts. *Am J Physiol Heart Circ Physiol*, 305(4):H506–20.

Brindle, K. M. and Radda, G. K. (1985). Measurements of exchange in the reaction catalysed by creatine kinase using 14C and 15N isotope labels and the NMR technique of saturation transfer. *Biochimica et Biophysica Acta (BBA) - Protein Structure and Molecular Enzymology*, 829(2):188–201.

Bristow, M. R. (2000). β-Adrenergic Receptor Blockade in Chronic Heart Failure. *Circulation*, 101(5):558–569.

Brogan, W. C., Grayburn, P. A., Lange, R. A., and Hillis, L. D. (1993). Prognosis after valve replacement in patients with severe aortic stenosis and a low transvalvular pressure gradient. *Journal of the American College of Cardiology*, 21(7):1657–1660.

Brown, T. R., Gadian, D. G., Garlick, P. B., Radda, G. K., Seeley, P. J., and Styles, P. (1978). Creatine kinase activities in skeletal and cardiac muscle measured by saturation transfer NMR. *Frontiers of Biological Energetics*, 2:1341–1349.

Bui, A. H., Roujol, S., Foppa, M., Kissinger, K. V., Goddu, B., Hauser, T. H., Zimetbaum, P. J., Ngo, L. H., Manning, W. J., Nezafat, R., and Delling, F. N. (2017). Diffuse myocardial fibrosis in patients with mitral valve prolapse and ventricular arrhythmia. *Heart*, 103(3):204–209.

Burkart, E. M., Sambandam, N., Han, X., Gross, R. W., Courtois, M., Gierasch, C. M., Shoghi, K., Welch, M. J., and Kelly, D. P. (2007). Nuclear receptors PPARβ/δ and PPARα direct distinct metabolic regulatory programs in the mouse heart. *J Clin Invest*, 117(12):3930–3939.

Burkhoff, D., Weiss, R. G., Schulman, S. P., Kalil-Filho, R., Wannenburg, T., and Gerstenblith, G. (1991). Influence of metabolic substrate on rat heart function and metabolism at different coronary flows. *Am J Physiol Heart Circ Physiol*, 261(3):H741–H750.

Bygrave, F. L. and Lehninger, A. L. (1967). The affinity of mitochondrial oxidative phosphorylation mechanisms for phosphate and adenosine diphosphate. *Proceedings of the National Academy of Sciences of the United States of America*, 57(5):1409–1415.

Cahill, T. J., Chen, M., Hayashida, K., Latib, A., Modine, T., Piazza, N., Redwood, S., Søndergaard, L., and Prendergast, B. D. (2018). Transcatheter aortic valve implantation: current status and future perspectives. *European Heart Journal*, pages ehy244–ehy244.

Cain, D. and Davies, R. (1962). Breakdown of adenosine triphosphate during a single contraction of working muscle. *Biochemical and Biophysical Research Communications*, 8(5):361–366.

Cain, D. F., Infante, A. A., and Davies, R. E. (1962). Chemistry of muscle contraction: Adenosine triphosphate and phosphorylcreatine as energy supplies for single contractions of working muscle. *Nature*, 196(4851):214–217.

Calvert, J. W., Condit, M. E., Aragón, J. P., Nicholson, C. K., Moody, B. F., Hood, R. L., Sindler, A. L., Gundewar, S., Seals, D. R., Barouch, L. A., and Lefer, D. J. (2011). Exercise protects against myocardial ischemia-reperfusion injury via stimulation of β3-adrenergic receptors and increased nitric oxide signaling: Role of nitrite and nitrosothiols. *Circulation Research*, 108(12):1448–1458.

Capoulade, R., Le Ven, F., Clavel, M.-A., Dumesnil, J. G., Dahou, A., Thébault, C., Arsenault, M., O'Connor, K., Bédard, É., Beaudoin, J., Sénéchal, M., Bernier, M., and Pibarot, P. (2016). Echocardiographic predictors of outcomes in adults with aortic stenosis. *Heart*, 102(12):934–942.

Carabello, B. A. (2002). Evolution of the study of left ventricular function: Everything old is new again. *Circulation*, 105(23):2701–2703.

Carabello, B. A., Green, L. H., Grossman, W., Cohn, L. H., Koster, J. K., and Collins, J. J. (1980). Hemodynamic determinants of prognosis of aortic valve replacement in critical aortic stenosis and advanced congestive heart failure. *Circulation*, 62(1):42–48.

Carabello, B. A., Zile, M. R., Tanaka, R., and Cooper, G. (1992). Left ventricular hypertrophy due to volume overload versus pressure overload. *The American journal of physiology*, 263(4 Pt 2):H1137–44.

Carvajal, K., Zarrinpashneh, E., Szarszoi, O., Joubert, F., Athea, Y., Mateo, P., Gillet, B., Vaulont, S., Viollet, B., Bigard, X., Bertrand, L., Ventura-Clapier, R., and Hoerter, J. A. (2007). Dual cardiac contractile effects of the α2-AMPK deletion in low-flow ischemia and reperfusion. *Am J Physiol Heart Circ Physiol*, 292(6):H3136–H3147.

Cawley, P. J., Hamilton-Craig, C., Owens, D. S., Krieger, E. V., Strugnell, W. E., Mitsumori, L., D'Jang, C. L., Schwaegler, R. G., Nguyen, K. Q., Nguyen, B., Maki, J. H., and Otto, C. M. (2013). Prospective Comparison of Valve Regurgitation Quantitation by Cardiac Magnetic Resonance Imaging and Transthoracic Echocardiography. *Circulation: Cardiovascular Imaging*, 6(1):48.

Cha, Y.-M., Dzeja, P. P., Redfield, M. M., Shen, W. K., and Terzic, A. (2006). Bioenergetic protection of failing atrial and ventricular myocardium by vasopeptidase inhibitor omapatrilat. *American Journal of Physiology-Heart and Circulatory Physiology*, 290(4):H1686–H1692.

Chaanine, A. H., Joyce, L. D., Stulak, J. M., Maltais, S., Joyce, D. L., Dearani, J. A., Klaus, K., Nair, K. S., Hajjar, R. J., and Redfield, M. M. (2019). Mitochondrial Morphology, Dynamics, and Function in Human Pressure Overload or Ischemic Heart Disease With Preserved or Reduced Ejection Fraction. *Circulation: Heart Failure*, 12(2).

Chance, B., Leigh, J. S., Clark, B. J., Maris, J., Kent, J., Nioka, S., and Smith, D. (1985). Control of oxidative metabolism and oxygen delivery in human skeletal muscle: A steady-state analysis of the work/energy cost transfer function. *Proceedings of the National Academy of Sciences of the United States of America*, 82(24):8384–8388.

Chance, B., Leigh, J. S., Kent, J., Mccully, K., Nioka, S., Clarkii, B. J., Maris, J. M., and Graham, T. (1986). Multiple controls of oxidative metabolism in living tissues as studied by phosphorus magnetic resonance. *PNAS*, 83(December):9458–9462.

Chance, B. and Williams, G. R. (1955). Respiratory enzymes in oxidative phosphorylation: III. The steady state. *The J Biol Chem*, 217(1):409–427.

Chandler, D. E. and Roberson, R. W. (2009). *Bioimaging: current concepts in light and electron microscopy*. Jones & Bartlett Publishers, Sudbury, Massachussetts.

Cheng, L., Ding, G., Qin, Q., Huang, Y., Lewis, W., He, N., Evans, R. M., Schneider, M. D., Brako, F. A., Xiao, Y., Chen, Y. E., and Yang, Q. (2004). Cardiomyocyte-restricted peroxisome proliferator-activated receptor-[delta] deletion perturbs myocardial fatty acid oxidation and leads to cardiomyopathy. *Nat Med*, 10(11):1245–1250.

Chenot, F., Montant, P., Vancraeynest, D., Pasquet, A., Gerber, B., Noirhomme, P. H., Khoury, G. E., and Vanoverschelde, J.-L. (2009). Long-term clinical outcome of mitral valve repair in asymptomatic severe mitral regurgitation. *European Journal of Cardio-Thoracic Surgery*, 36(3):539–545.

Chesky, J. A., LaFollette, S., Travis, M., and Fortado, C. (1983). Effect of physical training on myocardial enzyme activities in aging rats. *Journal of Applied Physiology*, 55(4):1349–1353.

Chevli, R. and Fitch, C. D. (1979). β-Guanidinopropionate and phosphorylated β-guanidinopropionate as substrates for creatine kinase. *Biochemical Medicine*, 21(2):162–167.

Chin, C. W. L., Everett, R. J., Kwiecinski, J., Vesey, A. T., Yeung, E., Esson, G., Jenkins, W., Koo, M., Mirsadraee, S., White, A. C., Japp, A. G., Prasad, S. K., Semple, S., Newby, D. E., and Dweck, M. R. (2017). Myocardial Fibrosis and Cardiac Decompensation in Aortic Stenosis. *JACC: Cardiovascular Imaging*, 10(11):1320–1333.

Christe, M. E. and Rodgers, R. L. (1994). Altered glucose and fatty acid oxidation in hearts of the spontaneously hypertensive rat. *J Mol Cell Cardiol*, 26(10):1371–1375.

Clarke, W. T. (2016). *Human Cardiac Magnetic Resonance Spectroscopy*. PhD thesis, University of Oxford.

Clarke, W. T., Peterzan, M. A., Rayner, J. J., Sayeed, R. A., Petrou, M., Krasopoulos, G., Lake, H. A., Raman, B., Watson, W. D., Cox, P., Hundertmark, M. J., Apps, A. P., Lygate, C. A., Neubauer, S., Rider, O. J., and Rodgers, C. T. (2019). Localized rest and stress human cardiac creatine kinase reaction kinetics at 3 T. *NMR in Biomedicine*, 32(6):e4085.

Clarke, W. T., Robson, M. D., Neubauer, S., and Rodgers, C. T. (2017). Creatine kinase rate constant in the human heart measured with 3D-localization at 7 tesla. *Magnetic resonance in medicine*, 78(1):20–32.

Clavel, M.-A., Berthelot-Richer, M., Le Ven, F., Capoulade, R., Dahou, A., Dumesnil, J. G., Mathieu, P., and Pibarot, P. (2015). Impact of Classic and Paradoxical Low Flow on Survival After Aortic Valve Replacement for Severe Aortic Stenosis. *J Am Coll Cardiol*, 65(7):645–653.

Colomer, J. M., Mao, L., Rockman, H. A., and Means, A. R. (2003). Pressure Overload Selectively Up-Regulates Ca 2+ /Calmodulin-Dependent Protein Kinase II in Vivo. *Molecular Endocrinology*, 17(2):183–192.

Connolly, H. M., Oh, J. K., Schaff, H. V., Roger, V. L., Osborn, S. L., Hodge, D. O., and Tajik, A. J. (2000). Severe Aortic Stenosis With Low Transvalvular Gradient and Severe Left Ventricular Dysfunction: Result of Aortic Valve Replacement in 52 Patients. *Circulation*, 101(16):1940–1946.

Conway, M. A., Allis, J., Ouwerkerk, R., Niioka, T., Rajagopalan, B., and Radda, G. K. (1991). Detection of low phosphocreatine to ATP ratio in failing hypertrophied human myocardium by 31P magnetic resonance spectroscopy. *Lancet*, 338(8773):973–976.

Conway, M. A., Bottomley, P. A., Ouwerkerk, R., Radda, G. K., and Rajagopalan, B. (1998). Mitral Regurgitation: Impaired Systolic Function, Eccentric Hypertrophy, and Increased Severity Are Linked to Lower Phosphocreatine/ATP Ratios in Humans. *Circulation*, 97(17):1716–1723.

Cooney, G. J., Taegtmeyer, H., and Newsholme, E. A. (1981). Tricarboxylic acid cycle flux and enzyme activities in the isolated working rat heart. *Biochem J*, 200(3):701–703.

Cordero-Reyes, A. M., Gupte, A. A., Youker, K. A., Loebe, M., Hsueh, W. A., Torre-Amione, G., Taegtmeyer, H., and Hamilton, D. J. (2014). Freshly isolated mitochondria from failing human hearts exhibit preserved respiratory function. *J Mol Cell Cardiol*, 68:98–105.

Cotter, D. G., Schugar, R. C., and Crawford, P. A. (2013). Ketone body metabolism and cardiovascular disease. *American Journal of Physiology - Heart and Circulatory Physiology*, 304(8):H1060.

Cox, P. J., Kirk, T., Ashmore, T., Willerton, K., Evans, R., Smith, A., Murray, A. J., Stubbs, B., West, J., McLure, S. W., King, M. T., Dodd, M. S., Holloway, C., Neubauer, S., Drawer, S., Veech, R. L., Griffin, J. L., and Clarke, K. (2016). Nutritional Ketosis Alters Fuel Preference and Thereby Endurance Performance in Athletes. *Cell Metabolism*, 24(2):256–268.

Crawford, M. H., Souchek, J., Oprian, C. A., Miller, D. C., Rahimtoola, S., Giacomini, J. C., Sethi, G., and Hammermeister, K. E. (1990). Determinants of survival and left ventricular performance after mitral valve replacement. Department of Veterans Affairs Cooperative Study on Valvular Heart Disease. *Circulation*, 81(4):1173–1181.

Crawford, P. A. (2018). Refueling the Failing Heart. *JACC: Basic to Translational Science*, 3(5):588–590.

Crawford, P. A. and Schaffer, J. E. (2013). Metabolic stress in the myocardium: Adaptations of gene expression. *J Mol Cell Cardiol*, 55:130–138.

Crawley, M. J. (2015). *Statistics: An introduction using R*. John Wiley & Sons, Ltd, Chichester, UK, 2nd edition.

Cribier, A., Eltchaninoff, H., Bash, A., Borenstein, N., Tron, C., Bauer, F., Derumeaux, G., Anselme, F., Laborde, F., and Leon, M. B. (2002). Percutaneous Transcatheter Implantation of an Aortic Valve Prosthesis for Calcific Aortic Stenosis: First Human Case Description. *Circulation*, 106(24):3006–3008.

Crozatier, B., Badoual, T., Boehm, E., Ennezat, P.-V., Guenoun, T., Su, J., Veksler, V., Hittinger, L., and Ventura-Clapier, R. (2002). Role of creatine kinase in cardiac excitation-contraction coupling: studies in creatine kinase-deficient mice. *FASEB J*, 16(7):653–660.

D 'Angelo, D. D., Sakata, Y., Lorenz, J. N., Boivin, G. P., Walsh, R. A., Liggett, S. B., and Dorn Ii, G. W. (1997). Transgenic Gαq overexpression induces cardiac contractile failure in mice. *Medical Sciences*, 94(15):8121–8126.

Dahl, J. S. and Carter-Storch, R. (2019). First-Phase Ejection Fraction: The FEV1 of the Heart? *JACC: Cardiovascular Imaging*, 12(1):64–66.

Dahl, J. S., Eleid, M. F., Michelena, H. I., Scott, C. G., Suri, R. M., Schaff, H. V., and Pellikka, P. A. (2015). Effect of Left Ventricular Ejection Fraction on Postoperative Outcome in Patients With Severe Aortic Stenosis Undergoing Aortic Valve Replacement. *Circulation: Cardiovascular Imaging*, 8(4).

D'Ascenzi, F., Anselmi, F., Piu, P., Fiorentini, C., Carbone, S. F., Volterrani, L., Focardi, M., Bonifazi, M., and Mondillo, S. (2019). Cardiac Magnetic Resonance Normal Reference Values of Biventricular Size and Function in Male Athlete's Heart. *JACC: Cardiovascular Imaging*, 12(9):1755–1765.

Dávila-Román, V. G., Vedala, G., Herrero, P., de las Fuentes, L., Rogers, J. G., Kelly, D. P., and Gropler, R. J. (2002). Altered myocardial fatty acid and glucose metabolism in idiopathic dilated cardiomyopathy. *J Am Coll Cardiol*, 40(2):271–277.

Davuluri, S. P., Hird, F. J., and McLean, R. M. (1981). A re-appraisal of the function and synthesis of phosphoarginine and phosphocreatine in muscle. *Comparative Biochemistry and Physiology – Part B: Comparative Biochemistry*, 69(3):329–336.

Dayan, V., Vignolo, G., Magne, J., Clavel, M.-A., Mohty, D., and Pibarot, P. (2015). Outcome and Impact of Aortic Valve Replacement in Patients With Preserved LVEF and Low-Gradient Aortic Stenosis. *Journal of the American College of Cardiology*, 66(23):2594–2603.

de Graaf, R. A., van Kranenburg, A., and Nicolay, K. (2000). In Vivo 31P-NMR Diffusion Spectroscopy of ATP and Phosphocreatine in Rat Skeletal Muscle. *Biophysical Journal*, 78(4):1657–1664.

de Groof, A. J. C., Fransen, J. A. M., Errington, R. J., Willems, P. H. G. M., Wieringa, B., and Koopman, W. J. H. (2002). The Creatine Kinase System Is Essential for Optimal Refill of the Sarcoplasmic Reticulum Ca2+ Store in Skeletal Muscle. *J Biol Chem*, 277(7):5275–5284.

de las Fuentes, L., Herrero, P., Peterson, L. R., Kelly, D. P., Gropler, R. J., and Dávila-Román, V. G. (2003). Myocardial Fatty Acid Metabolism: Independent Predictor of Left Ventricular Mass in Hypertensive Heart Disease. *Hypertension*, 41(1):83–87.

de las Fuentes, L., Soto, P. F., Cupps, B. P., Pasque, M. K., Herrero, P., Gropler, R. J., Waggoner, A. D., and Dávila-Román, V. G. (2006). Hypertensive left ventricular hypertrophy is associated with abnormal myocardial fatty acid metabolism and myocardial efficiency. *J Nucl Cardiol*, 13(3):369–377.

De Sousa, E., Veksler, V., Minajeva, A., Kaasik, A., Mateo, P., Mayoux, E., Hoerter, J., Bigard, X., Serrurier, B., and Ventura-Clapier, R. (1999). Subcellular Creatine Kinase Alterations: Implications in Heart Failure. *Circ Res*, 85(1):68–76.

de Waard, M. C., van Haperen, R., Soullié, T., Tempel, D., de Crom, R., and Duncker, D. J. (2010). Beneficial effects of exercise training after myocardial infarction require full eNOS expression. *Journal of Molecular and Cellular Cardiology*, 48(6):1041–1049.

DeBosch, B., Treskov, I., Lupu, T. S., Weinheimer, C., Kovacs, A., Courtois, M., and Muslin, A. J. (2006). Akt1 is required for physiological cardiac growth. *Circulation*, 113(17):2097–2104.

Deeb, G. M., Reardon, M. J., Chetcuti, S., Patel, H. J., Grossman, P. M., Yakubov, S. J., Kleiman, N. S., Coselli, J. S., Gleason, T. G., Lee, J. S., Hermiller, J. B., Heiser, J., Merhi, W., Zorn, G. L., Tadros, P., Robinson, N., Petrossian, G., Hughes, G. C., Harrison, J. K., Maini, B., Mumtaz, M., Conte, J., Resar, J., Aharonian, V., Pfeffer, T., Oh, J. K., Qiao, H., Adams, D. H., and Popma, J. J. (2016). 3-Year Outcomes in High-Risk Patients Who Underwent Surgical or Transcatheter Aortic Valve Replacement. *Journal of the American College of Cardiology*, 67(22):2565–2574.

Degens, H., de Brouwer, K. F. J., Gilde, A. J., Lindhout, M., Willemsen, P. H. M., Janssen, B. J., van der Vusse, G. J., and van Bilsen, M. (2006). Cardiac fatty acid metabolism is preserved in the compensated hypertrophic rat heart. *Basic Res Cardiol*, 101(1):17–26.

Detaint, D., Messika-Zeitoun, D., Avierinos, J.-F., Scott, C., Chen, H., Burnett, J. C., and Enriquez-Sarano, M. (2005). B-Type Natriuretic Peptide in Organic Mitral Regurgitation. *Circulation*, 111(18):2391–2397.

Ding, B., Peterzan, M. A., Mozes, F. E., Lake, H. A., Lygate, C. A., Sayeed, R. A., Petrou, M., Krasopoulos, G., Rider, O. J., Valkovic, L., and Rodgers, C. T. (2019). Cardiac creatine quantified by cycled water-suppressed 1H-MRS at 3T. In *ISMRM*, Montreal, QC, Canada.

Dodd, M. S., Ball, D. R., Schroeder, M. A., Le Page, L. M., Atherton, H. J., Heather, L. C., Seymour, A.-M., Ashrafian, H., Watkins, H., Clarke, K., and Tyler, D. J. (2012). In vivo alterations in cardiac metabolism and function in the spontaneously hypertensive rat heart. *Cardiovasc Res*, 95(1):69–76.

Doenst, T., Goodwin, G. W., Cedars, A. M., Wang, M., Stepkowski, S., and Taegtmeyer, H. (2001). Load-induced changes in vivo alter substrate fluxes and insulin responsiveness of rat heart in vitro. *Metabolism*, 50(9):1083–1090.

Doenst, T., Pytel, G., Schrepper, A., Amorim, P., Färber, G., Shingu, Y., Mohr, F. W., and Schwarzer, M. (2010). Decreased rates of substrate oxidation ex vivo predict the onset of heart failure and contractile dysfunction in rats with pressure overload. *Cardiovasc Res*, 86(3):461–470.

Donal, E., Mascle, S., Brunet, A., Thebault, C., Corbineau, H., Laurent, M., Leguerrier, A., and Mabo, P. (2012). Prediction of left ventricular ejection fraction 6 months after surgical correction of organic mitral regurgitation: the value of exercise echocardiography and deformation imaging. *European Heart Journal - Cardiovascular Imaging*, 13(11):922–930.

Dörner, A., Schulze, K., Rauch, U., and Schultheiss, H. P. (1997). Adenine nucleotide translocator in dilated cardiomyopathy: Pathophysiological alterations in expression and function. *Mol Cell Biochem*, 174(1):261–269.

Drazner, M. H. (2011). The Progression of Hypertensive Heart Disease. *Circulation*, 123(3):327–334.

Dudley, G. A., Tullson, P. C., and Terjung, R. L. (1987). Influence of mitochondrial content on the sensitivity of respiratory control. *Journal of Biological Chemistry*, 262(19):9109–9114.

Dufour, C. R., Wilson, B. J., Huss, J. M., Kelly, D. P., Alaynick, W. A., Downes, M., Evans, R. M., Blanchette, M., and Giguère, V. (2007). Genome-wide Orchestration of Cardiac Functions by the Orphan Nuclear Receptors ERRα and γ. *Cell Metab*, 5(5):345–356.

Dumesnil, J. G. and Shoucri, R. M. (1991). Quantitative relationships between left ventricular ejection and wall thickening and geometry. *Journal of Applied Physiology*, 70(1):48–54.

Duncan, J. G., Bharadwaj, K. G., Fong, J. L., Mitra, R., Sambandam, N., Courtois, M. R., Lavine, K. J., Goldberg, I. J., and Kelly, D. P. (2010). Rescue of Cardiomyopathy in Peroxisome Proliferator-Activated Receptor-α Transgenic Mice by Deletion of Lipoprotein Lipase Identifies Sources of Cardiac Lipids and Peroxisome Proliferator-Activated Receptor-α Activators. *Circulation*, 121(3):426–435.

D'Uva, G., Aharonov, A., Lauriola, M., Kain, D., Yahalom-Ronen, Y., Carvalho, S., Weisinger, K., Bassat, E., Rajchman, D., Yifa, O., Lysenko, M., Konfino, T., Hegesh, J., Brenner, O., Neeman, M., Yarden, Y., Leor, J., Sarig, R., Harvey, R. P., and Tzahor, E. (2015). ERBB2 triggers mammalian heart regeneration by promoting cardiomyocyte dedifferentiation and proliferation. *Nature Cell Biology*, 17(5):627–638.

Dweck, M. R., Joshi, S., Murigu, T., Alpendurada, F., Jabbour, A., Melina, G., Banya, W., Gulati, A., Roussin, I., Raza, S., Prasad, N. A., Wage, R., Quarto, C., Angeloni, E., Refice, S., Sheppard, M., Cook, S. A., Kilner, P. J., Pennell, D. J., Newby, D. E., Mohiaddin, R. H., Pepper, J., and Prasad, S. K. (2011). Midwall Fibrosis Is an Independent Predictor of Mortality in Patients With Aortic Stenosis. *Journal of the American College of Cardiology*, 58(12):1271–1279.

Dzeja, P. P., Hoyer, K., Tian, R., Zhang, S., Nemutlu, E., Spindler, M., and Ingwall, J. S. (2011). Rearrangement of energetic and substrate utilization networks compensate for chronic myocardial creatine kinase deficiency. *The J Physiol*, 589(21):5193–5211.

Dzeja, P. P. and Terzic, A. (2003). Phosphotransfer networks and cellular energetics. *J Exp Biol*, 206(12):2039–2047.

Dzeja, P. P., Vitkevicius, K. T., Redfield, M. M., Burnett, J. C., and Terzic, A. (1999). Adenylate Kinase-Catalyzed Phosphotransfer in the Myocardium: Increased Contribution in Heart Failure. *Circ Res*, 84(10):1137–1143.

Dzeja, P. P., Zeleznikar, R. J., and Goldberg, N. D. (1998). Adenylate kinase: Kinetic behavior in intact cells indicates it is integral to multiple cellular processes. *Molecular and Cellular Biochemistry*, 184(1-2):169–182.

Edwards, N. C., Moody, W. E., Yuan, M., Weale, P., Neal, D., Townend, J. N., and Steeds, R. P. (2014). Quantification of Left Ventricular Interstitial Fibrosis in Asymptomatic Chronic Primary Degenerative Mitral Regurgitation. *Circulation: Cardiovascular Imaging*, 7(6):946–953.

Egan, B. and Zierath, J. R. (2013). Exercise metabolism and the molecular regulation of skeletal muscle adaptation. *Cell Metabolism*, 17(2):162–184.

el Alaoui-Talibi, Z., Landormy, S., Loireau, A., and Moravec, J. (1992). Fatty acid oxidation and mechanical performance of volume-overloaded rat hearts. *Am J Physiol Heart Circ Physiol*, 262(4):H1068–H1074.

El Sabbagh, A., Reddy, Y. N., and Nishimura, R. A. (2018). Mitral Valve Regurgitation in the Contemporary Era: Insights Into Diagnosis, Management, and Future Directions. *JACC: Cardiovascular Imaging*, 11(4):628–643.

El-Sharkawy, A.-M., Schär, M., Ouwerkerk, R., Weiss, R. G., and Bottomley, P. A. (2009). Quantitative cardiac 31P spectroscopy at 3 Tesla using adiabatic pulses. *Magnetic resonance in medicine*, 61(4):785–795.

Engelhardt, S., Hein, L., Wiesmann, F., and Lohse, M. J. (1999). Progressive hypertrophy and heart failure in beta1-adrenergic receptor transgenic mice. *Proceedings of the National Academy of Sciences*, 96(12):7059–7064.

Engelhardt, W. A. and Ljubimowa, M. N. (1939). Myosine and adenosinetriphosphatase. *Nature*, 144(3650):668–669.

Enriquez-Sarano, M., Akins, C. W., and Vahanian, A. (2009). Mitral regurgitation. *Lancet*, 373(9672):1382–1394.

Enriquez-Sarano, M., Avierinos, J.-F., Messika-Zeitoun, D., Detaint, D., Capps, M., Nkomo, V., Scott, C., Schaff, H. V., and Tajik, A. J. (2005). Quantitative Determinants of the Outcome of Asymptomatic Mitral Regurgitation. *New England Journal of Medicine*, 352(9):875–883.

Enriquez-Sarano, M., Schaff, H. V., Orszulak, T. A., Bailey, K. R., Tajik, A. J., and Frye, R. L. (1995). Congestive Heart Failure After Surgical Correction of Mitral Regurgitation. *Circulation*, 92(9):2496.

Enriquez-Sarano, M., Suri, R. M., Clavel, M.-A., Mantovani, F., Michelena, H. I., Pislaru, S., Mahoney, D. W., and Schaff, H. V. (2015). Is there an outcome penalty linked to guideline-based indications for valvular surgery? Early and long-term analysis of patients with organic mitral regurgitation. *The Journal of Thoracic and Cardiovascular Surgery*, 150(1):50–58.

Enriquez-Sarano, M., Tajik, A. J., Schaff, H. V., Orszulak, T. A., Bailey, K. R., and Frye, R. L. (1994a). Echocardiographic prediction of survival after surgical correction of organic mitral regurgitation. *Circulation*, 90(2):830–837.

Enriquez-Sarano, M., Tajik, A. J., Schaff, H. V., Orszulak, T. A., McGoon, M. D., Bailey, K. R., and Frye, R. L. (1994b). Echocardiographic prediction of left ventricular function after correction of mitral regurgitation: Results and clinical implications. *Journal of the American College of Cardiology*, 24(6):1536–1543.

Esterhammer, R., Klug, G., Wolf, C., Mayr, A., Reinstadler, S., Feistritzer, H.-J., Metzler, B., and Schocke, M. F. H. (2014). Cardiac High-Energy Phosphate Metabolism Alters with Age as Studied in 196 Healthy Males with the Help of 31-Phosphorus 2-Dimensional Chemical Shift Imaging. *PLoS ONE*, 9(6):e97368.

Faller, K. M., Atzler, D., McAndrew, D. J., Zervou, S., Whittington, H. J., Simon, J. N., Aksentijevic, D., Ten Hove, M., Choe, C. U., Isbrandt, D., Casadei, B., Schneider, J. E., Neubauer, S., and Lygate, C. A. (2018). Impaired cardiac contractile function in arginine:glycine amidinotransferase knockout mice devoid of creatine is rescued by homoarginine but not creatine. *Cardiovascular Research*, 114(3):417–430.

Feinstein, M. B. (1962). Effects of Experimental Congestive Heart Failure, Ouabain, and Asphyxia on the High-Energy Phosphate and Creatine Content of the Guinea Pig Heart. *Circ Res*, 10(3):333–346.

Fernandes, T., Baraúna, V. G., Negrão, C. E., Phillips, M. I., and Oliveira, E. M. (2015). Aerobic exercise training promotes physiological cardiac remodeling involving a set of microRNAs. *American journal of physiology. Heart and circulatory physiology*, 309(4):H543–52.

Ferrannini, E., Mark, M., and Mayoux, E. (2016). CV Protection in the EMPA-REG OUTCOME Trial: A 'Thrifty Substrate' Hypothesis. *Diabetes Care*, 39(7):1108–1114.

Fillmore, N. and Lopaschuk, G. D. (2013). Targeting mitochondrial oxidative metabolism as an approach to treat heart failure. *BBA-Mol Cell Res*, 1833(4):857–865.

Fillmore, N., Mori, J., and Lopaschuk, G. D. (2014). Mitochondrial fatty acid oxidation alterations in heart failure, ischaemic heart disease and diabetic cardiomyopathy. *British Journal of Pharmacology*, 171(8):2080–2090.

Finck, B. N., Han, X., Courtois, M., Aimond, F., Nerbonne, J. M., Kovacs, A., Gross, R. W., and Kelly, D. P. (2003). A critical role for PPARα-mediated lipotoxicity in the pathogenesis of diabetic cardiomyopathy: Modulation by dietary fat content. *Proceedings of the National Academy of Sciences of the United States of America*, 100(3):1226–1231.

Finck, B. N., Lehman, J. J., Leone, T. C., Welch, M. J., Bennett, M. J., Kovacs, A., Han, X., Gross, R. W., Kozak, R., Lopaschuk, G. D., and Kelly, D. P. (2002). The cardiac phenotype induced by PPARα overexpression mimics that caused by diabetes mellitus. *J Clin Invest*, 109(1):121–130.

Fiske, C. H. and Subbarow, Y. (1927). The nature of the "inorganic phosphate" in voluntary muscle. *Science*, 65(1686):401–403.

Fiske, C. H. and Subbarow, Y. (1928). The isolation and function of phosphocreatine. *Science*, 67(1728):169–170.

Fontanet, H. L., Trask, R. V., Haas, R. C., Strauss, A. W., Abendschein, D. R., and Billadello, J. J. (1991). Regulation of expression of M, B, and mitochondrial creatine kinase mRNAs in the left ventricle after pressure overload in rats. *Circ Res*, 68(4):1007–1012.

Fossel, E. T. and Hoefeler, H. (1987). Complete inhibition of creatine kinase in isolated perfused rat hearts. *American Journal of Physiology - Endocrinology and Metabolism*, 252(1):E124–E129.

Fossel, E. T., Morgan, H. E., and Ingwall, J. S. (1980). Measurement of changes in high-energy phosphates in the cardiac cycle using gated 31P nuclear magnetic renonance. *Proceedings of the National Academy of Sciences of the United States of America*, 77(6):3654–8.

Friehs, I., Moran, A. M., Stamm, C., Colan, S. D., Takeuchi, K., Cao-Danh, H., Rader, C. M., McGowan, F. X., and del Nido, P. J. (1999). Impaired Glucose Transporter Activity in Pressure-Overload Hypertrophy Is an Early Indicator of Progression to Failure. *Circulation*, 100(suppl 2):II–187–Ii–193.

From, A. H. L., Zimmer, S. D., Michurski, S. P., Mohanakrishnan, P., Ulstad, V. K., Thoma, W. J., and Ugurbil, K. (1990). Regulation of the oxidative phosphorylation rate in the intact cell. *Biochemistry-US*, 29(15):3731–3743.

Gaasch, W. H. and Meyer, T. E. (2018). Secondary mitral regurgitation (part 1): volumetric quantification and analysis. *Heart*, 104:634–638.

Gabr, R. E., El-Sharkawy, A.-M. M., Schär, M., Weiss, R. G., and Bottomley, P. A. (2011). High-energy phosphate transfer in human muscle: diffusion of phosphocreatine. *Am J Physiol*, 301(1):C234–C241.

Gadian, D. G. (1995). *NMR and its Applications to Living Systems*. Oxford University Press, 2nd edition.

Gadian, D. G., Dawson, M. J., and Wilkie, D. R. (1977). Contraction and recovery of living muscles studied by 31p nuclear magnetic resonance. *The Journal of Physiology*, 267(3):703–735.

Galderisi, M., Cosyns, B., Edvardsen, T., Cardim, N., Delgado, V., Di Salvo, G., Donal, E., Sade, L. E., Ernande, L., Garbi, M., Grapsa, J., Hagendorff, A., Kamp, O., Magne, J., Santoro, C., Stefanidis, A., Lancellotti, P., Popescu, B., Habib, G., Flachskampf, F. A., Gerber, B., Gimelli, A., and Haugaa, K. (2017). Standardization of adult transthoracic echocardiography reporting in agreement with recent chamber quantification, diastolic function, and heart valve disease recommendations: An expert consensus document of the European Association of Cardiovascular Imag. *European Heart Journal Cardiovascular Imaging*, 18(12):1301–1310.

Galli, E., Lancellotti, P., Sengupta, P. P., and Donal, E. (2014). LV Mechanics in Mitral and Aortic Valve Diseases: Value of Functional Assessment Beyond Ejection Fraction. *JACC: Cardiovascular Imaging*, 7(11):1151–1166.

Gammie, J. S., O'Brien, S. M., Griffith, B. P., Ferguson, T. B., and Peterson, E. D. (2007). Influence of Hospital Procedural Volume on Care Process and Mortality for Patients Undergoing Elective Surgery for Mitral Regurgitation. *Circulation*, 115(7):881.

Ganau, A., Devereux, R. B., Roman, M. J., de Simone, G., Pickering, T. G., Saba, P. S., Vargiu, P., Simongini, I., and Laragh, J. H. (1992). Patterns of left ventricular hypertrophy and geometric remodeling in essential hypertension. *J Am Coll Cardiol*, 19(7):1550–1558.

Gandy, S. J., Lambert, M., Belch, J., Cavin, I., Crowe, E., Littleford, R., MacFarlane, J. A., Matthew, S. Z., Martin, P., Nicholas, R. S., Struthers, A., Sullivan, F., Waugh, S. A., White, R. D., Weir-McCall, J. R., and Houston, J. G. (2016). 3T MRI investigation of cardiac left ventricular structure and function in a UK population: The tayside screening for the prevention of cardiac events (TASCFORCE) study. *Journal of Magnetic Resonance Imaging*, 44(5):1186–1196.

Garlick, P. B., Radda, G. K., Seeley, P. J., and Chance, B. (1977). Phosphorus NMR studies on perfused heart. *Biochemical and Biophysical Research Communications*, 74(3):1256–1262.

Garnier, A., Zoll, J., Fortin, D., N'Guessan, B., Lefebvre, F., Geny, B., Mettauer, B., Veksler, V., and Ventura-Clapier, R. (2009). Control by Circulating Factors of Mitochondrial Function and Transcription Cascade in Heart Failure: A Role for Endothelin-1 and Angiotensin II. *Circ-Heart Fail*, 2(4):342–350.

Gavina, C., Falcão-Pires, I., Pinho, P., Manso, M.-C., Gonçalves, A., Rocha-Gonçalves, F., and Leite-Moreira, A. (2016). Relevance of residual left ventricular hypertrophy after surgery for isolated aortic stenosis. *European Journal of Cardio-Thoracic Surgery*, 49(3):952–959.

Gelman, A. (2008). Scaling regression inputs by dividing by two standard deviations. *Statistics in Medicine*, 27(15):2865–2873.

Généreux, P., Stone, G. W., O'Gara, P. T., Marquis-Gravel, G., Redfors, B., Giustino, G., Pibarot, P., Bax, J. J., Bonow, R. O., and Leon, M. B. (2016). Natural History, Diagnostic Approaches, and Therapeutic Strategies for Patients With Asymptomatic Severe Aortic Stenosis. *Journal of the American College of Cardiology*, 67(19):2263–2288.

Gibb, A. A., Epstein, P. N., Uchida, S., Zheng, Y., McNally, L. A., Obal, D., Katragadda, K., Trainor, P., Conklin, D. J., Brittian, K. R., Tseng, M. T., Wang, J., Jones, S. P., Bhatnagar, A., and Hill, B. G. (2017). Exercise-Induced Changes in Glucose Metabolism Promote Physiological Cardiac Growth. *Circulation*, 136(22):2144–2157.

Gibb, A. A. and Hill, B. G. (2018). Metabolic Coordination of Physiological and Pathological Cardiac Remodeling. *Circulation Research*, 123(1):107–128.

Gibbs, C. (1985). The cytoplasmic phosphorylation potential: Its possible role in the control of myocardial respiration and cardiac contractility. *J Mol Cell Cardiol*, 17(8):727–731.

Gilde, A. J., van der Lee, K. A. J. M., Willemsen, P. H. M., Chinetti, G., van der Leij, F. R., van der Vusse, G. J., Staels, B., and van Bilsen, M. (2003). Peroxisome Proliferator-Activated Receptor (PPAR) α and PPARβ/δ, but not PPARγ, Modulate the Expression of Genes Involved in Cardiac Lipid Metabolism. *Circ Res*, 92(5):518–524.

Glancy, B. and Balaban, R. S. (2012). Role of Mitochondrial Ca2+ in the Regulation of Cellular Energetics. *Biochemistry-US*, 51(14):2959–2973.

Glancy, B., Hartnell, L. M., Malide, D., Yu, Z.-X., Combs, C. A., Connelly, P. S., Subramaniam, S., and Balaban, R. S. (2015). Mitochondrial reticulum for cellular energy distribution in muscle. *Nature*, 523(7562):617–620.

Gleason, T. G., Reardon, M. J., Popma, J. J., Deeb, G. M., Yakubov, S. J., Lee, J. S., Kleiman, N. S., Chetcuti, S., Hermiller, J. B., Heiser, J., Merhi, W., Zorn, G. L.,

Tadros, P., Robinson, N., Petrossian, G., Hughes, G. C., Harrison, J. K., Conte, J. V., Mumtaz, M., Oh, J. K., Huang, J., and Adams, D. H. (2018). 5-Year Outcomes of Self-Expanding Transcatheter Versus Surgical Aortic Valve Replacement in High-Risk Patients. *Journal of the American College of Cardiology*, 72(22):2687–2696.

Goldberg, J. B., DeSimone, J. P., Kramer, R. S., DiScipio, A. W., Russo, L., Dacey, L. J., Leavitt, B. J., Helm, R. E., Baribeau, Y. R., Sardella, G., Clough, R. A., Surgenor, S. D., Sorensen, M. J., Ross, C. S., Olmstead, E. M., MacKenzie, T. A., Malenka, D. J., and Likosky, D. S. (2013). Impact of preoperative left ventricular ejection fraction on long-term survival after aortic valve replacement for aortic stenosis. *Circulation: Cardiovascular Quality and Outcomes*, 6(1):35–41.

Goodpaster, B. H. and Sparks, L. M. (2017). Metabolic Flexibility in Health and Disease. *Cell Metabolism*, 25(5):1027–1036.

Grayburn, P. A., Sannino, A., and Packer, M. (2019). Proportionate and Disproportionate Functional Mitral Regurgitation. *JACC: Cardiovascular Imaging*, 12(2):353–362.

Greenhaff, P. L. (2001). The creatine-phosphocreatine system: there's more than one song in its repertoire. *The Journal of Physiology*, 537(3):657–657.

Grigioni, F., Tribouilloy, C., Avierinos, J. F., Barbieri, A., Ferlito, M., Trojette, F., Tafanelli, L., Branzi, A., Szymanski, C., Habib, G., Modena, M. G., and Enriquez-Sarano, M. (2008). Outcomes in Mitral Regurgitation Due to Flail Leaflets: A Multicenter European Study. *JACC: Cardiovascular Imaging*, 1(2):133–141.

Grossman, W., Jones, D., and McLaurin, L. P. (1975). Wall stress and patterns of hypertrophy in the human left ventricle. *J Clin Invest*, 56(1):56–64.

Gudbjarnason, S., Mathes, P., and Ravens, K. G. (1970). Functional compartmentation of ATP and creatine phosphate in heart muscle. *Journal of Molecular and Cellular Cardiology*, 1(3):325–339.

Gupta, A., Akki, A., Wang, Y., Leppo, M. K., Chacko, V. P., Foster, D. B., Caceres, V., Shi, S., Kirk, J. A., and Su, J. (2012). Creatine kinase-mediated improvement of function in failing mouse hearts provides causal evidence the failing heart is energy starved. *J Clin Invest*, 122(1):291–302.

Gupta, A., Chacko, V. P., Schär, M., Akki, A., and Weiss, R. G. (2011). Impaired ATP kinetics in failing in vivo mouse heart. *Circulation: Cardiovascular Imaging*, 4(1):42–50.

Gupta, A., Rohlfsen, C., Leppo, M. K., Chacko, V. P., Wang, Y., Steenbergen, C., and Weiss, R. G. (2013). Creatine Kinase-Overexpression Improves Myocardial Energetics, Contractile Dysfunction and Survival in Murine Doxorubicin Cardiotoxicity. *PLoS One*, 8(10).

Gupte, A. A., Hamilton, D. J., Cordero-Reyes, A. M., Youker, K. A., Yin, Z., Estep, J. D., Stevens, R. D., Wenner, B., Ilkayeva, O., Loebe, M., Peterson, L. E., Lyon, C. J., Wong, S. T. C., Newgard, C. B., Torre-Amione, G., Taegtmeyer, H., and Hsueh, W. A. (2014). Mechanical Unloading Promotes Myocardial Energy Recovery in Human Heart Failure. *Circ-Cardiovasc Gene*, 7(3):266–276.

Gustafson, L. A. and Van Beek, J. H. G. M. (2002). Activation time of myocardial oxidative phosphorylation in creatine kinase and adenylate kinase knockout mice. *American Journal of Physiology - Heart and Circulatory Physiology*, 282(6):H2259–H2264.

Gwinn, D. M., Shackelford, D. B., Egan, D. F., Mihaylova, M. M., Mery, A., Vasquez, D. S., Turk, B. E., and Shaw, R. J. (2008). AMPK Phosphorylation of Raptor Mediates a Metabolic Checkpoint. *Mol Cell*, 30(2):214–226.

Hachicha, Z., Dumesnil, J. G., Bogaty, P., and Pibarot, P. (2007). Paradoxical Low-Flow, Low-Gradient Severe Aortic Stenosis Despite Preserved Ejection Fraction Is Associated With Higher Afterload and Reduced Survival. *Circulation*, 115(22):2856–2864.

Hagemann, D., Bohlender, J., Hoch, B., Kraus, E. G., and Karczewski, P. (2001). Expression of Ca2+/calmodulin-dependent protein kinase II δ-subunit isoforms in rats with hypertensive cardiac hypertrophy. *Molecular and Cellular Biochemistry*, 220(1-2):69–76.

Hajri, T., Ibrahimi, A., Coburn, C. T., Knapp, F. F., Kurtz, T., Pravenec, M., and Abumrad, N. A. (2001). Defective Fatty Acid Uptake in the Spontaneously Hypertensive Rat Is a Primary Determinant of Altered Glucose Metabolism, Hyperinsulinemia, and Myocardial Hypertrophy. *J Biol Chem*, 276(26):23661–23666.

Hall, N., DeLuca, M., and Addis, P. (1979). Mitochondrial Creatine Kinase. Physical and Kinetic Properties of the Purified Enzyme from Beef Heart. *Biochemistry*, 18(9):1745–1751.

Hamman, B. L., Bittl, J. A., Jacobus, W. E., Allen, P. D., Spencer, R. S., Tian, R., and Ingwall, J. S. (1995). Inhibition of the creatine kinase reaction decreases the contractile reserve of isolated rat hearts. *American Journal of Physiology - Heart and Circulatory Physiology*, 269(3 38-3):H1030–H1036.

Han, J.-C., Taberner, A. J., Tran, K., Goo, S., Nickerson, D. P., Nash, M. P., Nielsen, P. M. F., Crampin, E. J., and Loiselle, D. S. (2012). Comparison of the Gibbs and Suga formulations of cardiac energetics: the demise of "isoefficiency". *Journal of Applied Physiology*, 113(7):996–1003.

Han, Y., Peters, D. C., Salton, C. J., Bzymek, D., Nezafat, R., Goddu, B., Kissinger, K. V., Zimetbaum, P. J., Manning, W. J., and Yeon, S. B. (2008). Cardiovascular Magnetic Resonance Characterization of Mitral Valve Prolapse. *JACC: Cardiovascular Imaging*, 1(3):294–303.

Haq, S., Choukroun, G., Lim, H., Tymitz, K. M., del Monte, F., Gwathmey, J., Grazette, L., Michael, A., Hajjar, R., and Force, T. (2001). Differential activation of signal transduction pathways in human hearts with hypertrophy versus advanced heart failure. *Circulation*, 103(5):670–677.

Haralambie, G. and Uy, J. (1980). Enzyme activities of human myocardium: Creatine kinase and hexose phosphate isomerase. *Clinical Cardiology*, 3(3):192–196.

Hardie, D. G. (1992). Regulation of fatty acid and cholesterol metabolism by the AMP-activated protein kinase. *Biochimica et Biophysica Acta (BBA)/Lipids and Lipid Metabolism*, 1123(3):231–238.

Hardie, D. G. (2014). AMPK - Sensing Energy while Talking to Other Signaling Pathways. *Cell Metab*, 20(6):939–952.

Harrison, G. J., Van Wijhe, M. H., De Groot, B., Dijk, F. J., Gustafson, L. A., and Van Beek, J. H. (2003). Glycolytic buffering affects cardiac bioenergetic signaling and contractile reserve similar to creatine kinase. *American Journal of Physiology - Heart and Circulatory Physiology*, 285(2):H883–H890.

Hawley, S., Ross, F., Gowans, G., Tibarewal, P., Leslie, N., and Hardie, D. G. (2014). Phosphorylation by Akt within the ST loop of AMPK-α1 down-regulates its activation in tumour cells. *Biochem J*, 459(2):275–287.

He, L., Kim, T., Long, Q., Liu, J., Wang, P., Zhou, Y., Ding, Y., Prasain, J., Wood, P. A., and Yang, Q. (2012). Carnitine Palmitoyltransferase-1b (CPT1b) Deficiency Aggravates Pressure-Overload-Induced Cardiac Hypertrophy due to Lipotoxicity. *Circulation*, 126(14):1705–1716.

Heather, L. C., Cole, M. A., Lygate, C. A., Evans, R. D., Stuckey, D. J., Murray, A. J., Neubauer, S., and Clarke, K. (2006). Fatty acid transporter levels and palmitate oxidation rate correlate with ejection fraction in the infarcted rat heart. *Cardiovasc Res*, 72(3):430–437.

Heidbuchel, H. (2018). The athlete's heart is a proarrhythmic heart, and what that means for clinical decision making. *EP Europace*, 20(9):1401–1411.

Henkel, D. M., Malouf, J. F., Connolly, H. M., Michelena, H. I., Sarano, M. E., Schaff, H. V., Scott, C. G., and Pellikka, P. A. (2012). Asymptomatic left ventricular systolic dysfunction in patients with severe aortic stenosis: Characteristics and outcomes. *Journal of the American College of Cardiology*, 60(22):2325–2329.

Hermiller, J. B., Yakubov, S. J., Reardon, M. J., Deeb, G. M., Adams, D. H., Afilalo, J., Huang, J., and Popma, J. J. (2016). Predicting Early and Late Mortality After Transcatheter Aortic Valve Replacement. *Journal of the American College of Cardiology*, 68(4):343–352.

Herrmann, H. C., Pibarot, P., Hueter, I., Gertz, Z. M., Stewart, W. J., Kapadia, S., Tuczu, E. M., Babaliaros, V., Thourani, V., and Szeto, W. Y. (2013). Predictors of mortality and outcomes of therapy in low flow severe aortic stenosis: a PARTNER trial analysis. *Circulation*, 127:2316–2326.

Herrmann, S., Störk, S., Niemann, M., Lange, V., Strotmann, J. M., Frantz, S., Beer, M., Gattenlöhner, S., Voelker, W., Ertl, G., and Weidemann, F. (2011). Low-Gradient Aortic Valve Stenosis: Myocardial Fibrosis and Its Influence on Function and Outcome. *Journal of the American College of Cardiology*, 58(4):402–412.

Hettling, H. and van Beek, J. H. (2011). Analyzing the Functional Properties of the Creatine Kinase System with Multiscale 'Sloppy' Modeling. *PLoS Computational Biology*, 7(8):e1002130.

Hill, A. V. (1932). The revolution in muscle physiology. *Physiological Reviews*, 12(1):56–67.

Hoch, B., Meyer, R., Hetzer, R., Krause, E. G., and Karczewski, P. (1999). Identification and expression of δ-isoforms of the multifunctional Ca2+/calmodulin-dependent protein kinase in failing and nonfailing human myocardium. *Circulation Research*, 84(6):713–721.

Hochachka, P. W., Clark, C. M., Holden, J. E., Stanley, C., Ugurbil, K., and Menon, R. S. (1996). 31P magnetic resonance spectroscopy of the Sherpa heart: A phosphocreatine/adenosine triphosphate signature of metabolic defense against hypobaric hypoxia. *Proceedings of the National Academy of Sciences of the United States of America*, 93(3):1215–1220.

Hohorst, H. J., Reim, M., and Bartels, H. (1962). Studies on the creatine kinase equilibrium in muscle and the significance of ATP and ADP levels. *Biochemical and Biophysical Research Communications*, 7(2):142–146.

Hollingsworth, K. G., Blamire, A. M., Keavney, B. D., and MacGowan, G. A. (2012). Left ventricular torsion, energetics, and diastolic function in normal human aging. *Am J Physiol Heart Circ Physiol*, 302(4):H885–H892.

Hollis, D. P., Nunnally, R. L., Taylor IV, G. J., Weisfeldt, M. L., and Jacobus, W. E. (1978). Phosphorus nuclear magnetic resonance studies of heart physiology. *Journal of Magnetic Resonance (1969)*, 29(2):319–330.

Holzem, K. M., Vinnakota, K. C., Ravikumar, V. K., Madden, E. J., Ewald, G. A., Dikranian, K., Beard, D. A., and Efimov, I. R. (2016). Mitochondrial structure and function are not different between nonfailing donor and end-stage failing human hearts. *FASEB J*, 30(8):2698–2707.

Horn, M., Remkes, H., Strömer, H., Dienesch, C., and Neubauer, S. (2001). Chronic Phosphocreatine Depletion by the Creatine Analogue β-Guanidinopropionate Is

Associated With Increased Mortality and Loss of ATP in Rats After Myocardial Infarction. *Circulation*, 104(15):1844–1849.

Hoult, D. I., Busby, S. J. W., Gadian, D. G., Radda, G. K., Richards, R. E., and Seeley, P. J. (1974). Observation of tissue metabolites using 31P nuclear magnetic resonance. *Nature*, 252(5481):285–287.

How, O.-J., Aasum, E., Kunnathu, S., Severson, D. L., Myhre, E. S. P., and Larsen, T. S. (2005). Influence of substrate supply on cardiac efficiency, as measured by pressure-volume analysis in ex vivo mouse hearts. *Am J Physiol Heart Circ Physiol*, 288(6):H2979–H2985.

Hu, Q., Wang, X., Lee, J., Mansoor, A., Liu, J., Zeng, L., Swingen, C., Zhang, G., Feygin, J., Ochiai, K., Bransford, T. L., From, A. H. L., Bache, R. J., and Zhang, J. (2006). Profound bioenergetic abnormalities in peri-infarct myocardial regions. *Am J Physiol Heart Circ Physiol*, 291(2):H648–H657.

Hu, X. L., Xu, X., Lu, Z. B., Zhang, P., Fassett, J., Zhang, Y., Xin, Y., Hall, J. L., Viollet, B., Bache, R. J., Huang, Y. M., and Chen, Y. J. (2011). AMP Activated Protein Kinase-alpha 2 Regulates Expression of Estrogen-Related Receptor-alpha, a Metabolic Transcription Factor Related to Heart Failure Development. *Hypertension*, 58(4):696–U376.

Hügel, S., Horn, M., de Groot, M., Remkes, H., Dienesch, C., Hu, K., Ertl, G., and Neubauer, S. (1999). Effects of ACE inhibition and β-receptor blockade on energy metabolism in rats postmyocardial infarction. *Am J Physiol Heart Circ Physiol*, 277(6):H2167–H2175.

Hundley, W. G., Li, H. F., Hillis, L. D., Meshack, B. M., Lange, R. A., Willard, J. E., Landau, C., and Peshock, R. M. (1995). Quantitation of cardiac output with velocity-encoded, phase-difference magnetic resonance imaging. *Am J Cardiol*, 75(17):1250–1255.

Huss, J. M., Garbacz, W. G., and Xie, W. (2015). Constitutive activities of estrogen-related receptors: Transcriptional regulation of metabolism by the ERR pathways in health and disease. *BBA-Mol Basis Dis*, 1852(9):1912–1927.

Huss, J. M., Imahashi, K.-i., Dufour, C. R., Weinheimer, C. J., Courtois, M., Kovacs, A., Giguère, V., Murphy, E., and Kelly, D. P. (2007). The Nuclear Receptor ERRα Is Required for the Bioenergetic and Functional Adaptation to Cardiac Pressure Overload. *Cell Metab*, 6(1):25–37.

Huss, J. M. and Kelly, D. P. (2004). Nuclear Receptor Signaling and Cardiac Energetics. *Circ Res*, 95(6):568–578.

Iemitsu, M., Miyauchi, T., Maeda, S., Sakai, S., Fujii, N., Miyazaki, H., Kakinuma, Y., Matsuda, M., and Yamaguchi, I. (2003). Cardiac Hypertrophy by Hypertension

and Exercise Training Exhibits Different Gene Expression of Enzymes in Energy Metabolism. *Hypertension Research*, 26(10):829–837.

Iemitsu, M., Miyauchi, T., Maeda, S., Sakai, S., Kobayashi, T., Fujii, N., Miyazaki, H., Matsuda, M., and Yamaguchi, I. (2001). Physiological and pathological cardiac hypertrophy induce different molecular phenotypes in the rat. *American J Physiol-Regulatory, Integrative and Comparative Physiology*, 281(6):R2029–R2036.

Ingwall, J. S. (1982). Phosphorus nuclear magnetic resonance spectroscopy of cardiac and skeletal muscles. *Am J Physiol Heart Circ Physiol*, 242(5):H729–H744.

Ingwall, J. S. (1984). The hypertrophied myocardium accumulates the MB-creatine kinase isozyme. *Eur Heart J*, 5(suppl F):129–139.

Ingwall, J. S. (1993). Is Cardiac Failure a Consequence of Decreased Energy Reserve? *Circulation*, 87(Suppl 7):VII58–VII62.

Ingwall, J. S. (2002). *ATP and the Heart*. Springer Science & Business Media New York.

Ingwall, J. S. (2009). Energy metabolism in heart failure and remodelling. *Cardiovasc Res*, 81(3):412–419.

Ingwall, J. S., Atkinson, D. E., Clarke, K., and Fetters, J. K. (1990). Energetic correlates of cardiac failure: Changes in the creatine kinase system in the failing myocardium. *Eur Heart J*, 11(suppl B):108–115.

Ingwall, J. S., Kramer, M. F., Fifer, M. A., Lorell, B. H., Shemin, R., Grossman, W., and Allen, P. D. (1985). The Creatine Kinase System in Normal and Diseased Human Myocardium. *New Engl J Med*, 313(17):1050–1054.

Ingwall, J. S. and Weiss, R. G. (2004). Is the Failing Heart Energy Starved?: On Using Chemical Energy to Support Cardiac Function. *Circ Res*, 95(2):135–145.

Ito, S., Miranda, W. R., Nkomo, V. T., Connolly, H. M., Pislaru, S. V., Greason, K. L., Pellikka, P. A., Lewis, B. R., and Oh, J. K. (2018). Reduced Left Ventricular Ejection Fraction in Patients With Aortic Stenosis. *Journal of the American College of Cardiology*, 71(12):1313–1321.

Iung, B., Baron, G., Butchart, E. G., Delahaye, F., Gohlke-Bärwolf, C., Levang, O. W., Tornos, P., Vanoverschelde, J.-L., Vermeer, F., Boersma, E., Ravaud, P., and Vahanian, A. (2003). A prospective survey of patients with valvular heart disease in Europe: The Euro Heart Survey on Valvular Heart Disease. *European Heart Journal*, 24(13):1231–1243.

Iwase, M., Bishop, S. P., Uechi, M., Vatner, D. E., Shannon, R. P., Kudej, R. K., Wight, D. C., Wagner, T. E., Ishikawa, Y., Homcy, C. J., and Vatner, S. F. (1996). Adverse effects of chronic endogenous sympathetic drive induced by cardiac Gsα overexpression. *Circulation Research*, 78(4):517–524.

Iyengar, M. R. (1984). Creatine kinase as an intracellular regulator. *Journal of Muscle Research and Cell Motility*, 5(5):527–534.

Jacobs, H., Heldt, H., and Klingenberg, M. (1964). High activity of creatine kinase in mitochondria from muscle and brain and evidence for a separate mitochondrial isoenzyme of creatine kinase. *Biochemical and Biophysical Research Communications*, 16(6):516–521.

Jacobus, W. E. (1985a). Respiratory control and the integration of heart high-energy phosphate metabolism by mitochondrial creatine kinase. *Annual Review of Physiology*, 47(1):707–725.

Jacobus, W. E. (1985b). Theoretical support for the heart phosphocreatine energy transport shuttle based on the intracellular diffusion limited mobility of ADP. *Biochem Bioph Res Co*, 133(3):1035–1041.

Jacobus, W. E. and Lehninger, A. L. (1973). Creatine kinase of rat heart mitochondria: coupling of creatine phosphorylation to electron transport. *Journal of Biological Chemistry*, 248(13):4803–4810.

Jacobus, W. E., Taylor IV, G. J., Hollis, D. P., and Nunnally, R. L. (1977). Phosphorus nuclear magnetic resonance of perfused working rat hearts. *Nature*, 265(5596):756–758.

Jakovljevic, D. G., Papakonstantinou, L., Blamire, A. M., MacGowan, G. A., Taylor, R., Hollingsworth, K. G., and Trenell, M. I. (2015). Effect of Physical Activity on Age-Related Changes in Cardiac Function and Performance in Women. *Circulation: Cardiovascular Imaging*, 8(1).

Joubert, F., Hoerter, J. A., and Mazet, J.-L. (2001). Discrimination of Cardiac Subcellular Creatine Kinase Fluxes by NMR Spectroscopy: A New Method of Analysis. *Biophysical Journal*, 81(6):2995–3004.

Joubert, F., Hoerter, J. A., and Mazet, J. L. (2002a). Modeling the energy transfer pathways. Creatine kinase activities and heterogeneous distribution of ADP in the perfused heart. *Molecular Biology Reports*, 29(1-2):177–182.

Joubert, F., Mazet, J.-L., Mateo, P., and Hoerter, J. A. (2002b). 31P NMR detection of subcellular creatine kinase fluxes in the perfused rat heart contractility modifies energy transfer pathways. *J Biol Chem*, 277(21):18469–18476.

Joubert, F., Wilding, J. R., Fortin, D., Domergue-Dupont, V., Novotova, M., Ventura-Clapier, R., and Veksler, V. (2008). Local energetic regulation of sarcoplasmic and myosin ATPase is differently impaired in rats with heart failure. *J Physiol*, 586(21):5181–5192.

Kaasik, A., Veksler, V., Boehm, E., Novotova, M., Minajeva, A., and Ventura-Clapier, R. (2001). Energetic Crosstalk Between Organelles: Architectural Integration of Energy Production and Utilization. *Circ Res*, 89(2):153–159.

Kaasik, A., Veksler, V., Boehm, E., Novotova, M., and Ventura-Clapier, R. (2003). From energy store to energy flux: a study in creatine kinase-deficient fast skeletal muscle. *FASEB J*, 17(6):708–710.

Kagaya, Y., Kanno, Y., Takeyama, D., Ishide, N., Maruyama, Y., Takahashi, T., Ido, T., and Takishima, T. (1990). Effects of long-term pressure overload on regional myocardial glucose and free fatty acid uptake in rats. A quantitative autoradiographic study. *Circulation*, 81(4):1353–1361.

Kalsi, K. K., Smolenski, R. T., Pritchard, R. D., Khaghani, A., Seymour, A. M. L., and Yacoub, M. H. (1999). Energetics and function of the failing human heart with dilated or hypertrophic cardiomyopathy. *European J Clin Invest*, 29(6):469–477.

Kang, D.-H., Kim, J. H., Rim, J. H., Kim, M.-J., Yun, S.-C., Song, J.-M., Song, H., Choi, K.-J., Song, J.-K., and Lee, J.-W. (2009). Comparison of Early Surgery Versus Conventional Treatment in Asymptomatic Severe Mitral Regurgitation. *Circulation*, 119(6):797.

Kang, D.-H., Park, S.-J., Sun, B. J., Cho, E. J., Kim, D.-H., Yun, S.-C., Song, J.-M., Park, S. W., Chung, C.-H., Song, J.-K., Lee, J.-W., and Park, P.-W. (2014). Early Surgery Versus Conventional Treatment for Asymptomatic Severe Mitral Regurgitation: A Propensity Analysis. *Journal of the American College of Cardiology*, 63(22):2398–2407.

Kapadia, S. R., Leon, M. B., Makkar, R. R., Tuzcu, E. M., Svensson, L. G., Kodali, S., Webb, J. G., Mack, M. J., Douglas, P. S., Thourani, V. H., Babaliaros, V. C., Herrmann, H. C., Szeto, W. Y., Pichard, A. D., Williams, M. R., Fontana, G. P., Miller, D. C., Anderson, W. N., Smith, C. R., Akin, J. J., and Davidson, M. J. (2015). 5-year outcomes of transcatheter aortic valve replacement compared with standard treatment for patients with inoperable aortic stenosis (PARTNER 1): a randomised controlled trial. *The Lancet*, 385(9986):2485–2491.

Kapelko, V. I., Kupriyanov, V. V., Novikova, N. A., Lakomkin, V. L., Steinschneider, A. Y., Severina, M. Y., Veksler, V. I., and Saks, V. A. (1988). The cardiac contractile failure induced by chronic creatine and phosphocreatine deficiency. *J Mol Cell Cardiol*, 20(6):465–479.

Kapelko, V. I., Lakomkin, V. L., Korchazhkina, O. V., and Pisarenko, O. I. (1996). Cardiac pump function of the isolated rat heart at two modes of energy deprivation and effect of adrenergic stimulation. *Molecular and Cellular Biochemistry*, 163-164(1):131–136.

Kappel, B. A., Lehrke, M., Schütt, K., Artati, A., Adamski, J., Lebherz, C., and Marx, N. (2017). Effect of Empagliflozin on the Metabolic Signature of Patients With Type 2 Diabetes Mellitus and Cardiovascular Disease. *Circulation*, 136(10):969–972.

Kappetein, A. P., Head, S. J., Généreux, P., Piazza, N., van Mieghem, N. M., Blackstone, E. H., Brott, T. G., Cohen, D. J., Cutlip, D. E., van Es, G.-A., Hahn, R. T., Kirtane, A. J., Krucoff, M. W., Kodali, S., Mack, M. J., Mehran, R., Rodés-Cabau, J., Vranckx, P., Webb, J. G., Windecker, S., Serruys, P. W., and Leon, M. B. (2012). Updated Standardized Endpoint Definitions for Transcatheter Aortic Valve Implantation: The Valve Academic Research Consortium-2 Consensus Document. *Journal of the American College of Cardiology*, 60(15):1438–1454.

Kassiotis, C., Rajabi, M., and Taegtmeyer, H. (2008). Metabolic Reserve of the Heart: The Forgotten Link Between Contraction and Coronary Flow. *Prog Cardiovasc Dis*, 51(1):74–88.

Kato, T., Niizuma, S., Inuzuka, Y., Kawashima, T., Okuda, J., Tamaki, Y., Iwanaga, Y., Narazaki, M., Matsuda, T., Soga, T., Kita, T., Kimura, T., and Shioi, T. (2010). Analysis of Metabolic Remodeling in Compensated Left Ventricular Hypertrophy and Heart Failure. *Circ-Heart Fail*, 3(3):420–430.

Katz, L. A., Swain, J. A., Portman, M. A., and Balaban, R. S. (1989). Relation between phosphate metabolites and oxygen consumption of heart in vivo. *Am J Physiol Heart Circ Physiol*, 256(1):H265–H274.

Kawel-Boehm, N., Maceira, A., Valsangiacomo-Buechel, E. R., Vogel-Claussen, J., Turkbey, E. B., Williams, R., Plein, S., Tee, M., Eng, J., and Bluemke, D. A. (2015). Normal values for cardiovascular magnetic resonance in adults and children. *Journal of Cardiovascular Magnetic Resonance*, 17(1):29.

Kay, L., Nicolay, K., Wieringa, B., Saks, V., and Wallimann, T. (2000). Direct Evidence for the Control of Mitochondrial Respiration by Mitochondrial Creatine Kinase in Oxidative Muscle Cells in Situ. *J Biol Chem*, 275(10):6937–6944.

Kemi, O. J., Høydal, M. A., Haram, P. M., Garnier, A., Fortin, D., Ventura-Clapier, R., and Ellingsen, Ø. (2007). Exercise training restores aerobic capacity and energy transfer systems in heart failure treated with losartan. *Cardiovasc Res*, 76(1):91–99.

Kemp, G. J. and Brindle, K. M. (2012). What do magnetic resonance-based measurements of Pi→ATP flux tell us about skeletal muscle metabolism? *Diabetes*, 61(8):1927–1934.

Khan, R. S., Lin, Y., Hu, Y., Son, N.-H., Bharadwaj, K. G., Palacios, C., Chokshi, A., Ji, R., Yu, S., Homma, S., Schulze, P. C., Tian, R., and Goldberg, I. J. (2013). Rescue of heart lipoprotein lipase-knockout mice confirms a role for triglyceride in optimal heart metabolism and function. *Am J Physiol-Endoc M*, 305(11):E1339–E1347.

Kienesberger, P. C., Pulinilkunnil, T., Sung, M. M. Y., Nagendran, J., Haemmerle, G., Kershaw, E. E., Young, M. E., Light, P. E., Oudit, G. Y., Zechner, R., and Dyck, J. R. B. (2012). Myocardial ATGL Overexpression Decreases the Reliance on Fatty Acid Oxidation and Protects against Pressure Overload-Induced Cardiac Dysfunction. *Mol Cell Biol*, 32(4):740–750.

Kim, J., Wende, A. R., Sena, S., Theobald, H. A., Soto, J., Sloan, C., Wayment, B. E., Litwin, S. E., Holzenberger, M., LeRoith, D., and Abel, E. D. (2008). Insulin-Like Growth Factor I Receptor Signaling Is Required for Exercise-Induced Cardiac Hypertrophy. *Molecular Endocrinology*, 22(11):2531–2543.

Kirchhefer, U., Schmitz, W., Scholz, H., and Neumann, J. (1999). Activity of cAMP-dependent protein kinase and Ca2+/calmodulin- dependent protein kinase in failing and nonfailing human hearts. *Cardiovascular Research*, 42(1):254–261.

Klaar, U., Gabriel, H., Bergler-Klein, J., Pernicka, E., Heger, M., Mascherbauer, J., Rosenhek, R., Binder, T., Maurer, G., and Baumgartner, H. (2011). Prognostic value of serial B-type natriuretic peptide measurement in asymptomatic organic mitral regurgitation. *European Journal of Heart Failure*, 13(2):163–169.

Klug, G., Zwick, R., Frick, M., Wolf, C., Schocke, M., Conci, E., Jaschke, W., Pachinger, O., and Metzler, B. (2007). Impact of Exercise Capacity on Myocardial High-Energy Phosphate Metabolism. *International Journal of Sports Medicine*, 28(8):667–672.

Knaapen, P., Germans, T., Knuuti, J., Paulus, W. J., Dijkmans, P. A., Allaart, C. P., Lammertsma, A. A., and Visser, F. C. (2007). Myocardial Energetics and Efficiency: Current Status of the Noninvasive Approach. *Circulation*, 115(7):918–927.

Kobayashi, K. and Neely, J. R. (1979). Control of maximum rates of glycolysis in rat cardiac muscle. *Circulation Research*, 44(2):166–175.

Kohlhaas, M. and Maack, C. (2013). Calcium release microdomains and mitochondria. *Cardiovasc Res*, 98(2):259–268.

Kolwicz, S. C. (2018). An "Exercise" in Cardiac Metabolism. *Frontiers in Cardiovascular Medicine*, 5.

Kolwicz, S. C., Olson, D. P., Marney, L. C., Garcia-Menendez, L., Synovec, R. E., and Tian, R. (2012). Cardiac-Specific Deletion of Acetyl CoA Carboxylase 2 Prevents Metabolic Remodeling During Pressure-Overload Hypertrophy. *Circ Res*, 111(6):728–738.

Kong, S. W., Bodyak, N., Yue, P., Liu, Z., Brown, J., Izumo, S., and Kang, P. M. (2005). Genetic expression profiles during physiological and pathological cardiac hypertrophy and heart failure in rats. *Physiol Genomics*, 21(1):34–42.

Koretsky, A. P., Wang, S., Klein, M. P., James, T. L., and Weiner, M. W. (1986). 31P NMR saturation transfer measurements of phosphorus exchange reactions in rat heart and kidney in situ. *Biochemistry*, 25(1):77–84.

Korvald, C., Elvenes, O. P., and Myrmel, T. (2000). Myocardial substrate metabolism influences left ventricular energetics in vivo. *Am J Physiol Heart Circ Physiol*, 278(4):H1345–H1351.

Koziris, L. P., Hickson, R. C., Chatterton Jr., R. T., Groseth, R. T., Christie, J. M., Goldflies, D. G., and Unterman, T. G. (1999). Serum levels of total and free IGF-I and IGFBP-3 are increased and maintained in long-term training. *Journal of Applied Physiology*, 86(4):1436–1442.

Kuby, S. A., Noda, L., and Lardy, H. A. (1954). Adenosinetriphosphate-creatine transphosphorylase I. Isolation of the crystalline enzyme from rabbit muscle. *Journal of Biological Chemistry*, 209(1):191–201.

Kupriyanov, V. V., Seppet, E. K., Emelin, I. V., and Saks, V. A. (1980). Phosphocreatine production coupled to the glycolytic reactions in the cytosol of cardiac cells. *Biochimica et Biophysica Acta - Bioenergetics*, 592(2):197–210.

Kupriyanov, V. V., Steinschneider, A. Y., Ruuge, E. K., Kapel'ko, V. I., Zueva, M. Y., Lakomkin, V. L., Smirnov, V. N., and Saks, V. A. (1984). Regulation of energy flux through the creatine kinase reaction in vitro and in perfused rat heart. *BBA-Mol Cell Res*, 805(4):319–331.

Kuum, M., Kaasik, A., Joubert, F., Ventura-Clapier, R., and Veksler, V. (2009). Energetic state is a strong regulator of sarcoplasmic reticulum Ca2+ loss in cardiac muscle: different efficiencies of different energy sources. *Cardiovasc Res*, 83(1):89–96.

La Gerche, A., Rakhit, D. J., and Claessen, G. (2017). Exercise and the right ventricle: a potential Achilles' heel. *Cardiovascular Research*, 113(12):1499–1508.

La Gerche, A., Taylor, A. J., and Prior, D. L. (2009). Athlete's Heart: The Potential for Multimodality Imaging to Address the Critical Remaining Questions. *JACC: Cardiovascular Imaging*, 2(3):350–363.

Labarthe, F., Khairallah, M., Bouchard, B., Stanley, W. C., and Des Rosiers, C. (2005). Fatty acid oxidation and its impact on response of spontaneously hypertensive rat hearts to an adrenergic stress: benefits of a medium-chain fatty acid. *Am J Physiol Heart Circ Physiol*, 288(3):H1425–H1436.

Lai, L., Leone, T. C., Keller, M. P., Martin, O. J., Broman, A. T., Nigro, J., Kapoor, K., Koves, T. R., Stevens, R., Ilkayeva, O. R., Vega, R. B., Attie, A. D., Muoio, D. M., and Kelly, D. P. (2014). Energy Metabolic Reprogramming in the Hypertrophied and Early Stage Failing Heart: A Multisystems Approach. *Circ-Heart Fail*, 7(6):1022–1031.

Lamb, H. J., Beyerbacht, H. P., van der Laarse, A., Stoel, B. C., Doornbos, J., van der Wall, E. E., and de Roos, A. (1999). Diastolic Dysfunction in Hypertensive Heart Disease Is Associated With Altered Myocardial Metabolism. *Circulation*, 99(17):2261–2267.

Lancellotti, P., Magne, J., Dulgheru, R., Clavel, M. A., Donal, E., Vannan, M. A., Chambers, J., Rosenhek, R., Habib, G., Lloyd, G., Nistri, S., Garbi, M., Marchetta, S., Fattouch, K., Coisne, A., Montaigne, D., Modine, T., Davin, L., Gach, O., Radermecker, M., Liu, S., Gillam, L., Rossi, A., Galli, E., Ilardi, F., Tastet, L., Capoulade, R., Zilberszac, R., Vollema, E. M., Delgado, V., Cosyns, B., Lafitte, S., Bernard, A., Pierard, L. A., Bax, J. J., Pibarot, P., and Oury, C. (2018). Outcomes of Patients with Asymptomatic Aortic Stenosis Followed Up in Heart Valve Clinics. *JAMA Cardiology*, 3(11):1060–1068.

Lancellotti, P., Rosenhek, R., Pibarot, P., Iung, B., Otto, C. M., Tornos, P., Donal, E., Prendergast, B., Magne, J., La Canna, G., Piérard, L. A., and Maurer, G. (2013). ESC Working Group on Valvular Heart Disease Position Paper - heart valve clinics: organization, structure, and experiences. *European Heart Journal*, 34(21):1597–1606.

Lang, R. M., Badano, L. P., Mor-Avi, V., Afilalo, J., Armstrong, A., Ernande, L., Flachskampf, F. A., Foster, E., Goldstein, S. A., Kuznetsova, T., Lancellotti, P., Muraru, D., Picard, M. H., Rietzschel, E. R., Rudski, L., Spencer, K. T., Tsang, W., and Voigt, J.-U. (2015). Recommendations for Cardiac Chamber Quantification by Echocardiography in Adults: An Update from the American Society of Echocardiography and the European Association of Cardiovascular Imaging. *Journal of the American Society of Echocardiography*, 28(1):1–39.e14.

Lang, R. M., Bierig, M., Devereux, R. B., Flachskampf, F. A., Foster, E., Pellikka, P. A., Picard, M. H., Roman, M. J., Seward, J., Shanewise, J. S., Solomon, S. D., Spencer, K. T., St John Sutton, M., and Stewart, W. J. (2005). Recommendations for Chamber Quantification: A Report from the American Society of Echocardiography's Guidelines and Standards Committee and the Chamber Quantification Writing Group, Developed in Conjunction with the European Association of Echocardiograph. *Journal of the American Society of Echocardiography*, 18(12):1440–1463.

LaPar, D. J., Ailawadi, G., Isbell, J. M., Crosby, I. K., Kern, J. A., Rich, J. B., Speir, A. M., and Kron, I. L. (2014). Mitral valve repair rates correlate with surgeon and institutional experience. *The Journal of Thoracic and Cardiovascular Surgery*, 148(3):995–1004.

Larsen, S., Nielsen, J., Hansen, C. N., Nielsen, L. B., Wibrand, F., Stride, N., Schroder, H. D., Boushel, R., Helge, J. W., Dela, F., and Hey-Mogensen, M. (2012). Biomarkers of mitochondrial content in skeletal muscle of healthy young human subjects. *The Journal of Physiology*, 590(14):3349–3360.

Laser, A., Neubauer, S., Tian, R., Hu, K., Gaudron, P., Ingwall, J. S., and Ertl, G. (1996). Long-term beta-blocker treatment prevents chronic creatine kinase and lactate dehydrogenase system changes in rat hearts after myocardial infarction. *J Am Coll Cardiol*, 27(2):487–493.

Lawson, J. W. and Veech, R. L. (1979). Effects of pH and free Mg2+ on the Keq of the creatine kinase reaction and other phosphate hydrolyses and phosphate transfer reactions. *Journal of Biological Chemistry*, 254(14):6528–6537.

Le Tourneau, T., Messika-Zeitoun, D., Russo, A., Detaint, D., Topilsky, Y., Mahoney, D. W., Suri, R., and Enriquez-Sarano, M. (2010). Impact of Left Atrial Volume on Clinical Outcome in Organic Mitral Regurgitation. *Journal of the American College of Cardiology*, 56(7):570–578.

Le Ven, F., Freeman, M., Webb, J., Clavel, M.-A., Wheeler, M., Dumont, É., Thompson, C., De Larochellière, R., Moss, R., Doyle, D., Ribeiro, H. B., Urena, M., Nombela-Franco, L., Rodés-Cabau, J., and Pibarot, P. (2013). Impact of Low Flow on the Outcome of High-Risk Patients Undergoing Transcatheter Aortic Valve Replacement. *Journal of the American College of Cardiology*, 62(9):782–788.

Lee, R., Haluska, B., Leung, D. Y., Case, C., Mundy, J., and Marwick, T. H. (2005). Functional and prognostic implications of left ventricular contractile reserve in patients with asymptomatic severe mitral regurgitation. *Heart*, 91(11):1407–1412.

Lehman, J. J., Boudina, S., Banke, N. H., Sambandam, N., Han, X., Young, D. M., Leone, T. C., Gross, R. W., Lewandowski, E. D., Abel, E. D., and Kelly, D. P. (2008). The transcriptional coactivator PGC-1α is essential for maximal and efficient cardiac mitochondrial fatty acid oxidation and lipid homeostasis. *Am J Physiol Heart Circ Physiol*, 295(1):H185–H196.

Lehman, J. J. and Kelly, D. P. (2002). Transcriptional activation of energy metabolic switches in the developing and hypertrophied heart. *Clin Exp Pharmacol P*, 29(4):339–345.

Lehmann, H. (1935). Über die enzymatische Synthese der Kreatinphosphorsäure durch Umesterung der Phosphobrenztraubensäure. *Biochemische Zeitschrift*, 281:271–291.

Lei, B., Lionetti, V., Young, M. E., Chandler, M. P., d' Agostino, C., Kang, E., Altarejos, M., Matsuo, K., Hintze, T. H., Stanley, W. C., and Recchia, F. A. (2004). Paradoxical downregulation of the glucose oxidation pathway despite enhanced flux in severe heart failure. *J Mol Cell Cardiol*, 36(4):567–576.

Leon, M. B., Smith, C. R., Mack, M., Miller, D. C., Moses, J. W., Svensson, L. G., Tuzcu, E. M., Webb, J. G., Fontana, G. P., Makkar, R. R., Brown, D. L., Block, P. C., Guyton, R. A., Pichard, A. D., Bavaria, J. E., Herrmann, H. C., Douglas, P. S., Petersen, J. L., Akin, J. J., Anderson, W. N., Wang, D., and Pocock, S. (2010).

Transcatheter Aortic-Valve Implantation for Aortic Stenosis in Patients Who Cannot Undergo Surgery. *New England Journal of Medicine*, 363(17):1597–1607.

Leon, M. B., Smith, C. R., Mack, M. J., Makkar, R. R., Svensson, L. G., Kodali, S. K., Thourani, V. H., Tuzcu, E. M., Miller, D. C., Herrmann, H. C., Doshi, D., Cohen, D. J., Pichard, A. D., Kapadia, S., Dewey, T., Babaliaros, V., Szeto, W. Y., Williams, M. R., Kereiakes, D., Zajarias, A., Greason, K. L., Whisenant, B. K., Hodson, R. W., Moses, J. W., Trento, A., Brown, D. L., Fearon, W. F., Pibarot, P., Hahn, R. T., Jaber, W. A., Anderson, W. N., Alu, M. C., and Webb, J. G. (2016). Transcatheter or Surgical Aortic-Valve Replacement in Intermediate-Risk Patients. *New England Journal of Medicine*, 374(17):1609–1620.

Leung, D. Y., Griffin, B. P., Snader, C. E., Luthern, L., Thomas, J. D., and Marwick, T. H. (1997). Determinants of Functional Capacity in Chronic Mitral Regurgitation Unassociated With Coronary Artery Disease or Left Ventricular Dysfunction. *The American Journal of Cardiology*, 79(7):914–920.

Leung, D. Y., Griffin, B. P., Stewart, W. J., Cosgrove, D. M., Thomas, J. D., and Marwick, T. H. (1996). Left ventricular function after valve repair for chronic mitral regurgitation: Predictive value of preoperative assessment of contractile reserve by exercise echocardiography. *Journal of the American College of Cardiology*, 28(5):1198–1205.

Lewandowski, E. D., O'Donnell, J. M., Scholz, T. D., Sorokina, N., and Buttrick, P. M. (2007). Recruitment of NADH shuttling in pressure-overloaded and hypertrophic rat hearts. *Am J Physiol*, 292(5):C1880–C1886.

Leyton, R. A. and Sonnenblick, E. H. (1969). The ultrastructure of the failing heart. *The American journal of the medical sciences*, 258(5):301–327.

Liao, R., Jain, M., Cui, L., D'Agostino, J., Aiello, F., Luptak, I., Ngoy, S., Mortensen, R. M., and Tian, R. (2002). Cardiac-Specific Overexpression of GLUT1 Prevents the Development of Heart Failure Attributable to Pressure Overload in Mice. *Circulation*, 106(16):2125–2131.

Liao, R., Nascimben, L., Friedrich, J., Gwathmey, J. K., and Ingwall, J. S. (1996). Decreased Energy Reserve in an Animal Model of Dilated Cardiomyopathy: Relationship to Contractile Performance. *Circ Res*, 78(5):893–902.

Ligeti, L., Osbakken, M. D., Clark, B. J., Schnall, M., Bolinger, L., Subramanian, H., Leigh, J. S., and Chance, B. (1987). Cardiac transfer function relating energy metabolism to workload in different species as studied with 31P NMR. *Magnetic Resonance in Medicine*, 4(2):112–119.

Lin, J., Wu, H., Tarr, P. T., Zhang, C. Y., Wu, Z., Boss, O., Michael, L. F., Puigserver, P., Isotani, E., Olson, E. N., Lowell, B. B., Bassel-Duby, R., and Spiegelman, B. M. (2002). Transcriptional co-activator PGC-1α drives the formation of slow-twitch muscle fibres. *Nature*, 418(6899):797–801.

Ling, L. H., Enriquez-Sarano, M., Seward, J. B., Tajik, A. J., Schaff, H. V., Bailey, K. R., and Frye, R. L. (1996). Clinical Outcome of Mitral Regurgitation Due to Flail Leaflet. *New England Journal of Medicine*, 335(19):1417–1423.

Liu, B., Edwards, N. C., Neal, D. A. H., Weston, C., Nash, G., Nikolaidis, N., Barker, T., Patel, R., Bhabra, M., and Steeds, R. P. (2017). A prospective study examining the role of myocardial Fibrosis in outcome following mitral valve repair IN DEgenerative mitral Regurgitation: rationale and design of the mitral FINDER study. *BMC Cardiovascular Disorders*, 17(1):282.

Liu, J., Wang, C., Murakami, Y., Gong, G., Ishibashi, Y., Prody, C., Ochiai, K., Bache, R. J., Godinot, C., and Zhang, J. (2001). Mitochondrial ATPase and high-energy phosphates in failing hearts. *Am J Physiol Heart Circ Physiol*, 281(3):H1319–H1326.

Liu, X., Xiao, J., Zhu, H., Wei, X., Platt, C., Damilano, F., Xiao, C., Bezzerides, V., Boström, P., Che, L., Zhang, C., Spiegelman, B. M., and Rosenzweig, A. (2015). MiR-222 is necessary for exercise-induced cardiac growth and protects against pathological cardiac remodeling. *Cell Metabolism*, 21(4):584–595.

Lohman, K. (1931). Darstellung der adenylprophosphorsäure aus muskulatur. *Biochemische Zeitschrift*, 191:106.

Lopaschuk, G. and Verma, S. (2016). Empagliflozin's Fuel Hypothesis: Not so Soon. *Cell Metabolism*, 24(2):200–202.

Lopaschuk, G. D. (2017). Metabolic Modulators in Heart Disease: Past, Present, and Future. *Canadian Journal of Cardiology*, 33(7):838–849.

Lopaschuk, G. D., Ussher, J. R., Folmes, C. D. L., Jaswal, J. S., and Stanley, W. C. (2010). Myocardial Fatty Acid Metabolism in Health and Disease. *Physiol Rev*, 90(1):207–258.

Lopez-Mattei, J. C., Ibrahim, H., Shaikh, K. A., Little, S. H., Shah, D. J., Maragiannis, D., and Zoghbi, W. A. (2016). Comparative Assessment of Mitral Regurgitation Severity by Transthoracic Echocardiography and Cardiac Magnetic Resonance Using an Integrative and Quantitative Approach. *Am J Cardiol*, 117(2):264–270.

Luptak, I., Balschi, J. A., Xing, Y., Leone, T. C., Kelly, D. P., and Tian, R. (2005). Decreased Contractile and Metabolic Reserve in Peroxisome Proliferator-Activated Receptor-α-Null Hearts Can Be Rescued by Increasing Glucose Transport and Utilization. *Circulation*, 112(15):2339–2346.

Lydell, C. P., Chan, A., Wambolt, R. B., Sambandam, N., Parsons, H., Bondy, G. P., Rodrigues, B., Popov, K. M., Harris, R. A., Brownsey, R. W., and Allard, M. F. (2002). Pyruvate dehydrogenase and the regulation of glucose oxidation in hypertrophied rat hearts. *Cardiovasc Res*, 53(4):841–851.

Lygate, C. A., Aksentijevic, D., Dawson, D., ten Hove, M., Phillips, D., de Bono, J. P., Medway, D. J., Sebag-Montefiore, L., Hunyor, I., Channon, K. M., Clarke, K., Zervou, S., Watkins, H., Balaban, R. S., and Neubauer, S. (2013). Living Without Creatine: Unchanged Exercise Capacity and Response to Chronic Myocardial Infarction in Creatine-Deficient Mice. *Circ Res*, 112(6):945–955.

Lygate, C. A., Bohl, S., Ten Hove, M., Faller, K. M., Ostrowski, P. J., Zervou, S., Medway, D. J., Aksentijevic, D., Sebag-Montefiore, L., Wallis, J., Clarke, K., Watkins, H., Schneider, J. E., and Neubauer, S. (2012a). Moderate elevation of intracellular creatine by targeting the creatine transporter protects mice from acute myocardial infarction. *Cardiovascular Research*, 96(3):466–475.

Lygate, C. A., Fischer, A., Sebag-Montefiore, L., Wallis, J., ten Hove, M., and Neubauer, S. (2007). The creatine kinase energy transport system in the failing mouse heart. *J Mol Cell Cardiol*, 42(6):1129–1136.

Lygate, C. A., Hunyor, I., Medway, D., de Bono, J. P., Dawson, D., Wallis, J., Sebag-Montefiore, L., and Neubauer, S. (2009). Cardiac phenotype of mitochondrial creatine kinase knockout mice is modified on a pure C57BL/6 genetic background. *J Mol Cell Cardiol*, 46(1):93–99.

Lygate, C. A., Medway, D. J., Ostrowski, P. J., Aksentijevic, D., Sebag-Montefiore, L., Hunyor, I., Zervou, S., Schneider, J. E., and Neubauer, S. (2012b). Chronic creatine kinase deficiency eventually leads to congestive heart failure, but severity is dependent on genetic background, gender and age. *Basic Res Cardiol*, 107(5):1–11.

Lygate, C. A. and Neubauer, S. (2014). The Myocardial Creatine Kinase System in the Normal, Ischaemic and Failing Heart. In Lopaschuk, D. G. and Dhalla, S. N., editors, *Cardiac Energy Metabolism in Health and Disease*, pages 155–168. Springer New York, New York, NY.

Maack, C., Lehrke, M., Backs, J., Heinzel, F. R., Hulot, J. S., Marx, N., Paulus, W. J., Rossignol, P., Taegtmeyer, H., Bauersachs, J., Bayes-Genis, A., Brutsaert, D., Bugger, H., Clarke, K., Cosentino, F., De Keulenaer, G., Cas, A. D., González, A., Huelsmann, M., Iaccarino, G., Lunde, I. G., Lyon, A. R., Pollesello, P., Rena, G., Riksen, N. P., Rosano, G., Staels, B., Van Laake, L. W., Wanner, C., Farmakis, D., Filippatos, G., Ruschitzka, F., Seferovic, P., De Boer, R. A., and Heymans, S. (2018). Heart failure and diabetes: Metabolic alterations and therapeutic interventions: A state-of-The-Art review from the Translational Research Committee of the Heart Failure Association-European Society of Cardiology. *European Heart Journal*, 39(48):4243–4254.

Mack, M. J., Leon, M. B., Smith, C. R., Miller, D. C., Moses, J. W., Tuzcu, E. M., Webb, J. G., Douglas, P. S., Anderson, W. N., Blackstone, E. H., Kodali, S. K., Makkar, R. R., Fontana, G. P., Kapadia, S., Bavaria, J., Hahn, R. T., Thourani, V. H., Babaliaros, V., Pichard, A., Herrmann, H. C., Brown, D. L., Williams, M., Davidson,

M. J., Svensson, L. G., and Akin, J. (2015). 5-year outcomes of transcatheter aortic valve replacement or surgical aortic valve replacement for high surgical risk patients with aortic stenosis (PARTNER 1): a randomised controlled trial. *The Lancet*, 385(9986):2477–2484.

Mack, M. J., Leon, M. B., Thourani, V. H., Makkar, R., Kodali, S. K., Russo, M., Kapadia, S. R., Malaisrie, S. C., Cohen, D. J., Pibarot, P., Leipsic, J., Hahn, R. T., Blanke, P., Williams, M. R., McCabe, J. M., Brown, D. L., Babaliaros, V., Goldman, S., Szeto, W. Y., Genereux, P., Pershad, A., Pocock, S. J., Alu, M. C., Webb, J. G., and Smith, C. R. (2019). Transcatheter Aortic-Valve Replacement with a Balloon-Expandable Valve in Low-Risk Patients. *New England Journal of Medicine*, 380(18):1695–1705.

Magne, J., Cosyns, B., Popescu, B. A., Carstensen, H. G., Dahl, J., Desai, M. Y., Kearney, L., Lancellotti, P., Marwick, T. H., Sato, K., Takeuchi, M., Zito, C., Casalta, A. C., Mohty, D., Piérard, L., Habib, G., and Donal, E. (2019). Distribution and Prognostic Significance of Left Ventricular Global Longitudinal Strain in Asymptomatic Significant Aortic Stenosis: An Individual Participant Data Meta-Analysis. *JACC: Cardiovascular Imaging*, 12(1):84–92.

Magne, J., Donal, E., Mahjoub, H., Miltner, B., Dulgheru, R., Thebault, C., Pierard, L. A., Pibarot, P., and Lancellotti, P. (2015). Impact of exercise pulmonary hypertension on postoperative outcome in primary mitral regurgitation. *Heart*, 101(5):391–396.

Magne, J., Lancellotti, P., and Piérard, L. A. (2010a). Exercise-Induced Changes in Degenerative Mitral Regurgitation. *Journal of the American College of Cardiology*, 56(4):300–309.

Magne, J., Lancellotti, P., and Piérard, L. A. (2010b). Exercise Pulmonary Hypertension in Asymptomatic Degenerative Mitral Regurgitation. *Circulation*, 122(1):33–41.

Magne, J., Mahjoub, H., Dulgheru, R., Pibarot, P., Pierard, L. A., and Lancellotti, P. (2014). Left ventricular contractile reserve in asymptomatic primary mitral regurgitation. *European Heart Journal*, 35(24):1608–1616.

Magne, J., Mahjoub, H., Pierard, L. A., Connor, K., Pirlet, C., Pibarot, P., and Lancellotti, P. (2012). Prognostic importance of brain natriuretic peptide and left ventricular longitudinal function in asymptomatic degenerative mitral regurgitation. *Heart*, 98(7):584.

Mahmod, M., Francis, J. M., Pal, N., Lewis, A., Dass, S., De Silva, R., Petrou, M., Sayeed, R., Westaby, S., Robson, M. D., Ashrafian, H., Neubauer, S., and Karamitsos, T. D. (2014). Myocardial perfusion and oxygenation are impaired during stress in severe aortic stenosis and correlate with impaired energetics and subclinical left ventricular dysfunction. *J Cardiovasc Magn R*, 16(1):29.

Maillet, M., Van Berlo, J. H., and Molkentin, J. D. (2013). Molecular basis of physiological heart growth: Fundamental concepts and new players. *Nature Reviews Molecular Cell Biology*, 14(1):38–48.

Mallet, R. T., Olivencia-Yurvati, A. H., and Bünger, R. (2017). Pyruvate enhancement of cardiac performance: Cellular mechanisms and clinical application. *Experimental Biology and Medicine*, 0:1–13.

Marciniak, A., Glover, K., and Sharma, R. (2017). Cohort profile: prevalence of valvular heart disease in community patients with suspected heart failure in UK. *BMJ open*, 7(1):e012240.

Maron, B. J. and Ferrans, V. J. (1978). Ultrastructural features of hypertrophied human ventricular myocardium. *Progress in cardiovascular diseases*, 21(3):207–238.

Maron, B. J., Ferrans, V. J., and Roberts, W. C. (1975). Ultrastructural features of degenerated cardiac muscle cells in patients with cardiac hypertrophy. *The American journal of pathology*, 79(3):387–434.

Martin, J. F., Guth, B. D., Griffey, R. H., and Hoekenga, D. E. (1989). Myocardial creatine kinase exchange rates and 31P NMR relaxation rates in intact pigs. *Magnetic resonance in medicine*, 11(1):64–72.

Martín, M. A., Gómez, M. A., Guillén, F., Börnstein, B., Campos, Y., Rubio, J. C., de la Calzada, C. S., and Arenas, J. (2000). Myocardial carnitine and carnitine palmitoyltransferase deficiencies in patients with severe heart failure. *BBA-Mol Basis Dis*, 1502(3):330–336.

Masoud, W. G. T., Ussher, J. R., Wang, W., Jaswal, J. S., Wagg, C. S., Dyck, J. R., Lygate, C. A., Neubauer, S., Clanachan, A. S., and Lopaschuk, G. D. (2014). Failing mouse hearts utilize energy inefficiently and benefit from improved coupling of glycolysis and glucose oxidation. *Cardiovasc Res*, 101(1):30–38.

Massie, B. M., Schaefer, S., Garcia, J., McKirnan, M. D., Schwartz, G. G., Wisneski, J. A., Weiner, M. W., and White, F. C. (1995). Myocardial High-Energy Phosphate and Substrate Metabolism in Swine With Moderate Left Ventricular Hypertrophy. *Circulation*, 91(6):1814–1823.

Matlib, M. A., Rembert, J. C., Millard, R. W., Ashraf, M., Rouslin, W., Asano, G., Greenfield, J. C., and Schwartz, A. (1983). Mitochondrial function in canine experimental cardiac hypertrophy. *Journal of Molecular and Cellular Cardiology*, 15(4):221–232.

Matsumura, T., Ohtaki, E., Tanaka, K., Misu, K., Tobaru, T., Asano, R., Nagayama, M., Kitahara, K., Umemura, J., Sumiyoshi, T., Kasegawa, H., and Hosoda, S. (2003). Echocardiographic prediction of left ventricular dysfunction after mitral valve repair for mitral regurgitation as an indicator to decide the optimal timing of repair. *Journal of the American College of Cardiology*, 42(3):458–463.

Matthews, P. M., Bland, J. L., Gadian, D. G., and Radda, G. K. (1981). The steady-state rate of ATP synthesis in the perfused rat heart measured by 31P NMR saturation transfer. *Biochem Bioph Res Co*, 103(3):1052–1059.

Matthews, P. M., Bland, J. L., Gadian, D. G., and Radda, G. K. (1982). A 31P-NMR saturation transfer study of the regulation of creatine kinase in the rat heart. *BBA-Mol Cell Res*, 721(3):312–320.

McKee, P. A., Castelli, W. P., McNamara, P. M., and Kannel, W. B. (1971). The Natural History of Congestive Heart Failure: The Framingham Study. *New England Journal of Medicine*, 285(26):1441–1446.

McMullen, J. R., Amirahmadi, F., Woodcock, E. A., Schinke-Braun, M., Bouwman, R. D., Hewitt, K. A., Mollica, J. P., Zhang, L., Zhang, Y., Shioi, T., Buerger, A., Izumo, S., Jay, P. Y., and Jennings, G. L. (2007). Protective effects of exercise and phosphoinositide 3-kinase(p110alpha) signaling in dilated and hypertrophic cardiomyopathy. *Proceedings of the National Academy of Sciences of the United States of America*, 104(2):612–617.

McMullen, J. R., Shioi, T., Huang, W. Y., Zhang, L., Tarnavski, O., Bisping, E., Schinke, M., Kong, S., Sherwood, M. C., Brown, J., Riggi, L., Kang, P. M., and Izumo, S. (2004). The Insulin-like Growth Factor 1 Receptor Induces Physiological Heart Growth via the Phosphoinositide 3-Kinase(p110α) Pathway. *Journal of Biological Chemistry*, 279(6):4782–4793.

McMullen, J. R., Shioi, T., Zhang, L., Tarnavski, O., Sherwood, M. C., Kang, P. M., and Izumo, S. (2003). Phosphoinositide 3-kinase(p110alpha) plays a critical role for the induction of physiological, but not pathological, cardiac hypertrophy. *Proceedings of the National Academy of Sciences*, 100(21):12355–12360.

Mende, U., Kagen, A., Cohen, A., Aramburu, J., Schoen, F. J., and Neer, E. J. (1998). Transient cardiac expression of constitutively active Gαq leads to hypertrophy and dilated cardiomyopathy by calcineurin-dependent and independent pathways. *Proceedings of the National Academy of Sciences*, 95(23):13893–13898.

Messika-Zeitoun, D., Johnson, B. D., Nkomo, V., Avierinos, J.-F., Allison, T. G., Scott, C., Tajik, A. J., and Enriquez-Sarano, M. (2006). Cardiopulmonary Exercise Testing Determination of Functional Capacity in Mitral Regurgitation: Physiologic and Outcome Implications. *Journal of the American College of Cardiology*, 47(12):2521–2527.

Meyer, R. A., Kuchmerick, M. J., and Brown, T. R. (1982). Application of 31P-NMR spectroscopy study of striated muscle metabolism. *Americal Journal of Physiology*, 242(1):C1–C11.

Meyer, R. A., Sweeney, H. L., and Kushmerick, M. J. (1984). A simple analysis of the "phosphocreatine shuttle". *The American journal of physiology*, 246(5 Pt 1):C365–C377.

Mihaljevic, T., Nowicki, E. R., Rajeswaran, J., Blackstone, E. H., Lagazzi, L., Thomas, J., Lytle, B. W., and Cosgrove, D. M. (2008). Survival after valve replacement for aortic stenosis: Implications for decision making. *The Journal of thoracic and cardiovascular surgery*, 135(6):1270–1279.e12.

Miller, T. D., Rogers, P. J., Bauer, B. A., O'Brien, J. F., Squires, R. W., Bailey, K. R., and Bove, A. A. (1989). Does exercise training alter myocardial creatine kinase MB isoenzyme content? *Medicine and science in sports and exercise*, 21(4):437–440.

Mizuno, Y., Harada, E., Nakagawa, H., Morikawa, Y., Shono, M., Kugimiya, F., Yoshimura, M., and Yasue, H. (2017). The diabetic heart utilizes ketone bodies as an energy source. *Metabolism: Clinical and Experimental*, 77:65–72.

Mjøs, O. D. (1971). Effect of free fatty acids on myocardial function and oxygen consumption in intact dogs. *J Clin Invest*, 50(7):1386.

Moe, G. W., Marin-Garcia, J., Konig, A., Goldenthal, M., Lu, X., and Feng, Q. (2004). In vivo TNF-α inhibition ameliorates cardiac mitochondrial dysfunction, oxidative stress, and apoptosis in experimental heart failure. *Am J Physiol Heart Circ Physiol*, 287(4):H1813–H1820.

Molkentin, J. D., Lu, J.-R., Antos, C. L., Markham, B., Richardson, J., Robbins, J., Grant, S. R., and Olson, E. N. (1998). A Calcineurin-Dependent Transcriptional Pathway for Cardiac Hypertrophy. *Cell*, 93(2):215–228.

Momken, I., Lechêne, P., Koulmann, N., Fortin, D., Mateo, P., Doan, B. T., Hoerter, J., Bigard, X., Veksler, V., and Ventura-Clapier, R. (2005). Impaired voluntary running capacity of creatine kinase-deficient mice. *The J Physiol*, 565(3):951–964.

Monin, J.-L., Quéré, J.-P., Monchi, M., Petit, H., Baleynaud, S., Chauvel, C., Pop, C., Ohlmann, P., Lelguen, C., Dehant, P., Tribouilloy, C., and Guéret, P. (2003). Low-Gradient Aortic Stenosis: Operative Risk Stratification and Predictors for Long-Term Outcome: A Multicenter Study Using Dobutamine Stress Hemodynamics. *Circulation*, 108(3):319–324.

Monteagudo Ruiz, J. M., Galderisi, M., Buonauro, A., Badano, L., Aruta, P., Swaans, M. J., Sanchis, L., Saraste, A., Monaghan, M., Theodoropoulos, K. C., Papitsas, M., Liel-Cohen, N., Kobal, S., Bervar, M., Berlot, B., Filippatos, G., Ikonomidis, I., Katsanos, S., Tanner, F. C., Cassani, D., Faletra, F. F., Leo, L. A., Martinez, A., Matabuena, J., Grande-Trillo, A., Alonso-Rodriguez, D., Mesa, D., Gonzalez-Alujas, T., Sitges, M., Carrasco-Chinchilla, F., Li, C. H., Fernandez-Golfin, C., and Zamorano, J. L. (2018). Overview of mitral regurgitation in Europe: results from the European Registry of mitral regurgitation (EuMiClip). *European Heart Journal - Cardiovascular Imaging*, 19(5):503–507.

Mootha, V. K., Arai, A. E., and Balaban, R. S. (1997). Maximum oxidative phosphorylation capacity of the mammalian heart. *Am J Physiol Heart Circ Physiol*, 272(2):H769–H775.

Morrison, J. F. and Cleland, W. W. (1966). Isotope Exchange Studies of the Mechanism of the Reaction Catalyzed by Adenosine Triphosphate: Creatine Phosphotransferase. *J Biol Chem*, 241(3):673–683.

Mudaliar, S., Alloju, S., and Henry, R. R. (2016). Can a Shift in Fuel Energetics Explain the Beneficial Cardiorenal Outcomes in the EMPA-REG OUTCOME Study? A Unifying Hypothesis. *Diabetes Care*, 39(7):1115–22.

Mudd, J. O. and Kass, D. A. (2008). Tackling heart failure in the twenty-first century. *Nature*, 451(7181):919–928.

Muoio, D. M. (2014). Metabolic inflexibility: When mitochondrial indecision leads to metabolic gridlock. *Cell*, 159(6):1253–1262.

Murakami, Y., Zhang, J., Eijgelshoven, M. H. J., Chen, W., Carlyle, W. C., Zhang, Y., Gong, G., and Bache, R. J. (1999a). Myocardial creatine kinase kinetics in hearts with postinfarction left ventricular remodeling. *Am J Physiol Heart Circ Physiol*, 276(3):H892–H900.

Murakami, Y., Zhang, Y., Cho, Y. K., Mansoor, A. M., Chung, J. K., Chu, C., Francis, G., Ugurbil, K., Bache, R. J., From, A. H. L., Jerosch-Herold, M., Wilke, N., and Zhang, J. (1999b). Myocardial Oxygenation During High Work States in Hearts With Postinfarction Remodeling. *Circulation*, 99(7):942–948.

Murray, A. J., Lygate, C. A., Cole, M. A., Carr, C. A., Radda, G. K., Neubauer, S., and Clarke, K. (2006). Insulin resistance, abnormal energy metabolism and increased ischemic damage in the chronically infarcted rat heart. *Cardiovasc Res*, 71(1):149–157.

Musa, T. A., Treibel, T. A., Vassiliou, V. S., Captur, G., Singh, A., Chin, C., Dobson, L. E., Pica, S., Loudon, M., Malley, T., Rigolli, M., Foley, J. R., Bijsterveld, P., Law, G. R., Dweck, M. R., Myerson, S. G., McCann, G. P., Prasad, S. K., Moon, J. C., and Greenwood, J. P. (2018). Myocardial scar and mortality in severe aortic stenosis: Data from the BSCMR Valve Consortium. *Circulation*, 138(18):1935–1947.

Myerson, S. G., D'Arcy, J., Christiansen, J. P., Dobson, L. E., Mohiaddin, R., Francis, J. M., Prendergast, B., Greenwood, J. P., Karamitsos, T. D., and Neubauer, S. (2016). Determination of Clinical Outcome in Mitral Regurgitation With Cardiovascular Magnetic Resonance Quantification. *Circulation*, 133(23):2287–2296.

Naga Prasad, S. V., Barak, L. S., Rapacciuolo, A., Caron, M. G., and Rockman, H. A. (2001). Agonist-dependent recruitment of phosphoinositide 3-kinase to the membrane by β-adrenergic receptor kinase 1. *Journal of Biological Chemistry*, 276(22):18953–18959.

Nahrendorf, M., Spindler, M., Hu, K., Bauer, L., Ritter, O., Nordbeck, P., Quaschning, T., Hiller, K.-H., Wallis, J., Ertl, G., Bauer, W. R., and Neubauer, S. (2005). Creatine

kinase knockout mice show left ventricular hypertrophy and dilatation, but unaltered remodeling post-myocardial infarction. *Cardiovasc Res*, 65(2):419–427.

Nahrendorf, M., Streif, J. U., Hiller, K.-H., Hu, K., Nordbeck, P., Ritter, O., Sosnovik, D., Bauer, L., Neubauer, S., Jakob, P. M., Ertl, G., Spindler, M., and Bauer, W. R. (2006). Multimodal functional cardiac MRI in creatine kinase-deficient mice reveals subtle abnormalities in myocardial perfusion and mechanics. *Am J Physiol Heart Circ Physiol*, 290(6):H2516–H2521.

Naji, P., Griffin, B. P., Asfahan, F., Barr, T., Rodriguez, L. L., Grimm, R., Agarwal, S., Stewart, W. J., Mihaljevic, T., Gillinov, A. M., and Desai, M. Y. (2014a). Predictors of Long-Term Outcomes in Patients With Significant Myxomatous Mitral Regurgitation Undergoing Exercise Echocardiography. *Circulation*, 129(12):1310–1319.

Naji, P., Griffin, B. P., Barr, T., Asfahan, F., Gillinov, A. M., Grimm, R. A., Rodriguez, L. L., Mihaljevic, T., Stewart, W. J., and Desai, M. Y. (2014b). Importance of exercise capacity in predicting outcomes and determining optimal timing of surgery in significant primary mitral regurgitation. *Journal of the American Heart Association*, 3(5).

Nakae, I., Mitsunami, K., Matsuo, S., Inubushi, T., Morikawa, S., Tsutamoto, T., Koh, T., and Horie, M. (2005). Myocardial Creatine Concentration in Various Nonischemic Heart Diseases Assessed by 1H Magnetic Resonance Spectroscopy. *Circulation Journal*, 69(6):711–716.

Nakae, I., Mitsunami, K., Matsuo, S., Matsumoto, T., Morikawa, S., Inubushi, T., Koh, T., and Horie, M. (2004a). Assessment of myocardial creatine concentration in dysfunctional human heart by proton magnetic resonance spectroscopy. *Magnetic Resonance in Medical Sciences*, 3(1):19–25.

Nakae, I., Mitsunami, K., Omura, T., Yabe, T., Tsutamoto, T., Matsuo, S., Takahashi, M., Morikawa, S., Inubushi, T., Nakamura, Y., Kinoshita, M., and Horie, M. (2003). Proton magnetic resonance spectroscopy can detect creatine depletion associated with the progression of heart failure in cardiomyopathy. *J Am Coll Cardiol*, 42(9):1587–1593.

Nakae, I., Mitsunami, K., Yabe, T., Inubushi, T., Morikawa, S., Matsuo, S., Koh, T., and Horie, M. (2004b). Detection of metabolic abnormality in asynergic regions of ischemic human myocardium using 31P and 1H magnetic resonance spectroscopy. *J Cardiovasc Magn R*, 6(3):685–696.

Nakamura, M. and Sadoshima, J. (2018). Mechanisms of physiological and pathological cardiac hypertrophy. *Nature Reviews Cardiology*, 15:387–407.

Narkar, V. A., Downes, M., Yu, R. T., Embler, E., Wang, Y. X., Banayo, E., Mihaylova, M. M., Nelson, M. C., Zou, Y., Juguilon, H., Kang, H., Shaw, R. J., and Evans, R. M. (2008). AMPK and PPARδ Agonists Are Exercise Mimetics. *Cell*, 134(3):405–415.

Nascimben, L., Friedrich, J., Liao, R., Pauletto, P., Pessina, A. C., and Ingwall, J. S. (1995). Enalapril Treatment Increases Cardiac Performance and Energy Reserve Via the Creatine Kinase Reaction in Myocardium of Syrian Myopathic Hamsters With Advanced Heart Failure. *Circulation*, 91(6):1824–1833.

Nascimben, L., Ingwall, J. S., Lorell, B. H., Pinz, I., Schultz, V., Tornheim, K., and Tian, R. (2004). Mechanisms for Increased Glycolysis in the Hypertrophied Rat Heart. *Hypertension*, 44(5):662–667.

Nascimben, L., Ingwall, J. S., Pauletto, P., Friedrich, J., Gwathmey, J. K., Saks, V., Pessina, A. C., and Allen, P. D. (1996). Creatine Kinase System in Failing and Nonfailing Human Myocardium. *Circulation*, 94(8):1894–1901.

Nashef, S. A., Roques, F., Michel, P., Gauducheau, E., Lemeshow, S., and Salamon, R. (1999). European system for cardiac operative risk evaluation (EuroSCORE). *European Journal of Cardio-thoracic Surgery*, 16(1):9–13.

Nashef, S. A. M., Roques, F., Sharples, L. D., Nilsson, J., Smith, C., Goldstone, A. R., and Lockowandt, U. (2012). Euroscore II. *European Journal of Cardio-thoracic Surgery*, 41(4):734–745.

Nathania, M., Hollingsworth, K. G., Bates, M., Eggett, C., Trenell, M. I., Velicki, L., Seferovic, P. M., MacGowan, G. A., Turnbull, D. M., and Jakovljevic, D. G. (2018). Impact of age on the association between cardiac high-energy phosphate metabolism and cardiac power in women. *Heart (British Cardiac Society)*, 104(2):111–118.

Neely, J. R. and Morgan, H. E. (1974). Relationship Between Carbohydrate and Lipid Metabolism and the Energy Balance of Heart Muscle. *Annual Review of Physiology*, 36(1):413–459.

Neglia, D., De Caterina, A., Marraccini, P., Natali, A., Ciardetti, M., Vecoli, C., Gastaldelli, A., Ciociaro, D., Pellegrini, P., Testa, R., Menichetti, L., L'Abbate, A., Stanley, W. C., and Recchia, F. A. (2007). Impaired myocardial metabolic reserve and substrate selection flexibility during stress in patients with idiopathic dilated cardiomyopathy. *Am J Physiol Heart Circ Physiol*, 293(6):H3270–H3278.

Neri Serneri, G. G., Boddi, M., Modesti, P. A., Cecioni, I., Coppo, M., Padeletti, L., Michelucci, A., Colella, A., and Galanti, G. (2001). Increased cardiac sympathetic activity and insulin-like growth factor-I formation are associated with physiological hypertrophy in athletes. *Circulation Research*, 89(11):977–982.

Neubauer, S. (2007). The Failing Heart - An Engine Out of Fuel. *New Engl J Med*, 356(11):1140–1151.

Neubauer, S., Frank, M., Hu, K., Remkes, H., Laser, A., Horn, M., Ertl, G., and Lohse, M. J. (1998). Changes of Creatine Kinase Gene Expression in Rat Heart Post-Myocardial Infarction. *J Mol Cell Cardiol*, 30(4):803–810.

Neubauer, S., Hamman, B. L., Perry, S. B., Bittl, J. A., and Ingwall, J. S. (1988). Velocity of the creatine kinase reaction decreases in postischemic myocardium: a 31P-NMR magnetization transfer study of the isolated ferret heart. *Circ Res*, 63(1):1–15.

Neubauer, S., Horn, M., Cramer, M., Harre, K., Newell, J. B., Peters, W., Pabst, T., Ertl, G., Hahn, D., Ingwall, J. S., and Kochsiek, K. (1997a). Myocardial Phosphocreatine-to-ATP Ratio Is a Predictor of Mortality in Patients With Dilated Cardiomyopathy. *Circulation*, 96(7):2190–2196.

Neubauer, S., Horn, M., Naumann, A., Tian, R., Hu, K., Laser, M., Friedrich, J., Gaudron, P., Schnackerz, K., and Ingwall, J. S. (1995). Impairment of energy metabolism in intact residual myocardium of rat hearts with chronic myocardial infarction. *J Clin Invest*, 95(3):1092–1100.

Neubauer, S., Horn, M., Pabst, T., Harre, K., Strömer, H., Bertsch, G., Sandstede, J., Ertl, G., Hahn, D., and Kochsiek, K. (1997b). Cardiac high-energy phosphate metabolism in patients with aortic valve disease assessed by 31P-magnetic resonance spectroscopy. *J Invest Med*, 45(8):453–462.

Neubauer, S., Hu, K., Horn, M., Remkes, H., Hoffmann, K. D., Schmidt, C., Schmidt, T. J., Schnackerz, K., and Ertl, G. (1999a). Functional and Energetic Consequences of Chronic Myocardial Creatine Depletion by β -Guanidinopropionate in Perfused Hearts and in Intact Rats. *J Mol Cell Cardiol*, 31(10):1845–1855.

Neubauer, S., Krahe, T., Schindler, R., Horn, M., Hillenbrand, H., Entzeroth, C., Mader, H., Kromer, E. P., Riegger, G. A., and Lackner, K. (1992). 31P magnetic resonance spectroscopy in dilated cardiomyopathy and coronary artery disease. Altered cardiac high-energy phosphate metabolism in heart failure. *Circulation*, 86(6):1810–1818.

Neubauer, S., Remkes, H., Spindler, M., Horn, M., Wiesmann, F., Prestle, J., Walzel, B., Ertl, G., Hasenfuss, G., and Wallimann, T. (1999b). Downregulation of the Na+-Creatine Cotransporter in Failing Human Myocardium and in Experimental Heart Failure. *Circulation*, 100(18):1847–1850.

Nikolaidis, L. A., Poornima, I., Parikh, P., Magovern, M., Shen, Y.-T., and Shannon, R. P. (2006). The Effects of Combined Versus Selective Adrenergic Blockade on Left Ventricular and Systemic Hemodynamics, Myocardial Substrate Preference, and Regional Perfusion in Conscious Dogs With Dilated Cardiomyopathy. *J Am Coll Cardiol*, 47(9):1871–1881.

Nikolaidis, L. A., Sturzu, A., Stolarski, C., Elahi, D., Shen, Y.-T., and Shannon, R. P. (2004). The development of myocardial insulin resistance in conscious dogs with advanced dilated cardiomyopathy. *Cardiovasc Res*, 61(2):297–306.

Ning, X.-H., Zhang, J., Liu, J., Ye, Y., Chen, S.-H., From, A. H. L., Bache, R. J., and Portman, M. A. (2000). Signaling and expression for mitochondrial membrane proteins during left ventricular remodeling and contractile failure after myocardial infarction. *J Am Coll Cardiol*, 36(1):282–287.

Nishimura, R. A., Otto, C. M., Bonow, R. O., Carabello, B. A., Erwin Iii, J. P., Guyton, R. A., O'Gara, P. T., Ruiz, C. E., Skubas, N. J., Sorajja, P., Sundt Iii, T. M., and Thomas, J. D. (2014). 2014 AHA/ACC Guideline for the Management of Patients With Valvular Heart Disease: Executive Summary: A Report of the American College of Cardiology/American Heart Association Task Force on Practice Guidelines. *J Am Coll Cardiol*, 63(22):2438–2488.

Nkomo, V. T., Gardin, J. M., Skelton, T. N., Gottdiener, J. S., Scott, C. G., and Enriquez-Sarano, M. (2006). Burden of valvular heart diseases: a population-based study. *The Lancet*, 368(9540):1005–1011.

Nunnally, R. L. and Hollis, D. P. (1979). Adenosine triphosphate compartmentation in living hearts: a phosphorus nuclear magnetic resonance saturation transfer study. *Biochemistry-US*, 18(16):3642–3646.

O'Brien, S. M., Feng, L., He, X., Xian, Y., Jacobs, J. P., Badhwar, V., Kurlansky, P. A., Furnary, A. P., Cleveland, J. C., Lobdell, K. W., Vassileva, C., Wyler von Ballmoos, M. C., Thourani, V. H., Rankin, J. S., Edgerton, J. R., D'Agostino, R. S., Desai, N. D., Edwards, F. H., and Shahian, D. M. (2018). The Society of Thoracic Surgeons 2018 Adult Cardiac Surgery Risk Models: Part 2 - Statistical Methods and Results. *Annals of Thoracic Surgery*, 105(5):1419–1428.

O'Brien, S. M., Shahian, D. M., Filardo, G., Ferraris, V. A., Haan, C. K., Rich, J. B., Normand, S.-L. T., DeLong, E. R., Shewan, C. M., Dokholyan, R. S., Peterson, E. D., Edwards, F. H., and Anderson, R. P. (2009). The Society of Thoracic Surgeons 2008 Cardiac Surgery Risk Models: Part 2 - Isolated Valve Surgery. *The Annals of thoracic surgery*, 88(1):S23–S42.

O'Donnell, J. M., Fields, A. D., Sorokina, N., and Lewandowski, E. D. (2008). The absence of endogenous lipid oxidation in early stage heart failure exposes limits in lipid storage and turnover. *J Mol Cell Cardiol*, 44(2):315–322.

Oliveira, S. M., Zhang, Y. H., Solis, R. S., Isackson, H., Bellahcene, M., Yavari, A., Pinter, K., Davies, J. K., Ge, Y., Ashrafian, H., Walker, J. W., Carling, D., Watkins, H., Casadei, B., and Redwood, C. (2012). AMP-Activated protein kinase phosphorylates cardiac troponin i and alters contractility of murine ventricular myocytes. *Circ Res*, 110(9):1192–1201.

Oliver, I. T. (1955). A spectrophotometric method for the determination of creative phosphokinase and myokinase. *Biochemical Journal*, 61(1):116–122.

O'Neill, B. T., Kim, J., Wende, A. R., Theobald, H. A., Tuinei, J., Buchanan, J., Guo, A., Zaha, V. G., Davis, D. K., Schell, J. C., Boudina, S., Wayment, B., Litwin, S. E., Shioi, T., Izumo, S., Birnbaum, M. J., and Abel, E. D. (2007). A Conserved Role for Phosphatidylinositol 3-Kinase but Not Akt Signaling in Mitochondrial Adaptations that Accompany Physiological Cardiac Hypertrophy. *Cell Metab*, 6(4):294–306.

Osbakken, M., Douglas, P. S., Ivanics, T., Zhang, D., and Winkle, T. V. (1992). Creatine kinase kinetics studied by phosphorus-31 nuclear magnetic resonance in a canine model of chronic hypertension-induced cardiac hypertrophy. *J Am Coll Cardiol*, 19(1):223–228.

Osorio, J. C., Stanley, W. C., Linke, A., Castellari, M., Diep, Q. N., Panchal, A. R., Hintze, T. H., Lopaschuk, G. D., and Recchia, F. A. (2002). Impaired Myocardial Fatty Acid Oxidation and Reduced Protein Expression of Retinoid X Receptor-α in Pacing-Induced Heart Failure. *Circulation*, 106(5):606–612.

O'Toole, J. D., Geiser, E. A., Reddy, P. S., Curtiss, E. I., and Landfair, R. M. (1978). Effect of preoperative ejection fraction on survival and hemodynamic improvement following aortic valve replacement. *Circulation*, 58(6):1175–1184.

Oudman, I., Clark, J. F., and Brewster, L. M. (2013). The Effect of the Creatine Analogue Beta-guanidinopropionic Acid on Energy Metabolism: A Systematic Review. *PLoS One*, 8(1):e52879.

Park, S. J., Zhang, J., Ye, Y., Ormaza, S., Liang, P., Bank, A. J., Miller, L. W., and Bache, R. J. (2002). Myocardial creatine kinase expression after left ventricular assist device support. *J Am Coll Cardiol*, 39(11):1773–1779.

Park, S.-Y., Gifford, J. R., Andtbacka, R. H. I., Trinity, J. D., Hyngstrom, J. R., Garten, R. S., Diakos, N. A., Ives, S. J., Dela, F., Larsen, S., Drakos, S., and Richardson, R. S. (2014). Cardiac, skeletal, and smooth muscle mitochondrial respiration: are all mitochondria created equal? *AJP: Heart and Circulatory Physiology*, 307(3):H346–H352.

Patel, V. B., Zhabyeyev, P., Chen, X., Wang, F., Paul, M., Fan, D., McLean, B. A., Basu, R., Zhang, P., Shah, S., Dawson, J. F., Pyle, W. G., Hazra, M., Kassiri, Z., Hazra, S., Vanhaesebroeck, B., McCulloch, C. A., and Oudit, G. Y. (2018). PI3Kalpha-regulated gelsolin activity is a critical determinant of cardiac cytoskeletal remodeling and heart disease. *Nature communications*, 9(1):5390.

Paternostro, G., Clarke, K., Heath, J., Seymour, A.-M. L., and Radda, G. K. (1995). Decreased GLUT-4 mRNA content and insulin-sensitive deoxyglucose uptake show insulin resistance in the hypertensive rat heart. *Cardiovasc Res*, 30(2):205–211.

Pellikka, P. A., Nishimura, R. A., Bailey, K. R., and Tajik, A. J. (1990). The natural history of adults with asymptomatic, hemodynamically significant aortic stenosis. *Journal of the American College of Cardiology*, 15(5):1012–1017.

Pellikka, P. A., She, L., Holly, T. A., Lin, G., Varadarajan, P., Pai, R. G., Bonow, R. O., Pohost, G. M., Panza, J. A., Berman, D. S., Prior, D. L., Asch, F. M., Borges-Neto, S., Grayburn, P., Al-Khalidi, H. R., Miszalski-Jamka, K., Desvigne-Nickens, P., Lee, K. L., Velazquez, E. J., and Oh, J. K. (2018). Variability in Ejection Fraction Measured By Echocardiography, Gated Single-Photon Emission Computed Tomography, and Cardiac Magnetic Resonance in Patients With Coronary Artery Disease and Left Ventricular Dysfunction. *JAMA Network Open*, 1(4):e181456.

Penicka, M., Vecera, J., Mirica, D. C., Kotrc, M., Kockova, R., and Van Camp, G. (2018). Prognostic Implications of Magnetic Resonance-Derived Quantification in Asymptomatic Patients With Organic Mitral Regurgitation: Comparison With Doppler Echocardiography-Derived Integrative Approach. *Circulation*, 137(13):1349–1360.

Perrino, C., Naga Prasad, S. V., Mao, L., Noma, T., Yan, Z., Kim, H. S., Smithies, O., and Rockman, H. A. (2006). Intermittent pressure overload triggers hypertrophy-independent cardiac dysfunction and vascular rarefaction. *Journal of Clinical Investigation*, 116(6):1547–1560.

Perrino, C., Schroder, J. N., Lima, B., Villamizar, N., Nienaber, J. J., Milano, C. A., and Prasad, S. V. (2007). Dynamic regulation of phosphoinositide 3-kinase-γ activity and β-Adrenergic receptor trafficking in end-stage human heart failure. *Circulation*, 116(22):2571–2579.

Perry, S. B., McAuliffe, J., Balschi, J. A., Hickey, P. R., and Ingwall, J. S. (1988). Velocity of the creatine kinase reaction in the neonatal rabbit heart: role of mitochondrial creatine kinase. *Biochemistry-US*, 27(6):2165–2172.

Perseghin, G., De Cobelli, F., Esposito, A., Lattuada, G., Terruzzi, I., La Torre, A., Belloni, E., Canu, T., Scifo, P., Del Maschio, A., Luzi, L., and Alberti, G. (2007). Effect of the sporting discipline on the right and left ventricular morphology and function of elite male track runners: A magnetic resonance imaging and phosphorus 31 spectroscopy study. *American Heart Journal*, 154(5):937–942.

Peterzan, M. A., Lygate, C. A., Neubauer, S., and Rider, O. J. (2017). Metabolic remodeling in hypertrophied and failing myocardium: a review. *American Journal of Physiology-Heart and Circulatory Physiology*, 313(3):H597–H616.

Peyton, R. B., Jones, R. N., Attarian, D., Sink, J. D., Van Trigt, P., Currie, W. D., and Wechsler, A. S. (1982). Depressed high-energy phosphate content in hypertrophied ventricles of animal and man: the biologic basis for increased sensitivity to ischemic injury. *Annals of Surgery*, 196(3):278–284.

Pibarot, P. and Dumesnil, J. G. (2012). Low-Flow, Low-Gradient Aortic Stenosis With Normal and Depressed Left Ventricular Ejection Fraction. *J Am Coll Cardiol*, 60(19):1845–1853.

Pizarro, R., Bazzino, O. O., Oberti, P. F., Falconi, M., Achilli, F., Arias, A., Krauss, J. G., and Cagide, A. M. (2009). Prospective Validation of the Prognostic Usefulness of Brain Natriuretic Peptide in Asymptomatic Patients With Chronic Severe Mitral Regurgitation. *Journal of the American College of Cardiology*, 54(12):1099–1106.

Planavila, A., Laguna, J. C., and Vázquez-Carrera, M. (2005a). Nuclear factor-κB activation leads to down-regulation of fatty acid oxidation during cardiac hypertrophy. *J Biol Chem*, 280(17):17464–17471.

Planavila, A., Rodríguez-Calvo, R., Jové, M., Michalik, L., Wahli, W., Laguna, J. C., and Vázquez-Carrera, M. (2005b). Peroxisome proliferator-activated receptor β/δ activation inhibits hypertrophy in neonatal rat cardiomyocytes. *Cardiovasc Res*, 65(4):832–841.

Platt, C., Houstis, N., and Rosenzweig, A. (2015). Using Exercise to Measure and Modify Cardiac Function. *Cell Metabolism*, 21(2):227–236.

Pluim, B. M., Chin, J. C., De Roos, A., Doornbos, J., Siebelink, H.-M. J., Van der Laarse, A., Vliegen, H. W., Lamerichs, R. M. J. N., Bruschke, A. V. G., and Van der Wall, E. E. (1996). Cardiac anatomy, function and metabolism in elite cyclists assessed by magnetic resonance imaging and spectroscopy. *European Heart Journal*, 17(8):1271–1278.

Pluim, B. M., Lamb, H. J., Kayser, H. W. M., Leujes, F., Beyerbacht, H. P., Zwinderman, A. H., van der Laarse, A., Vliegen, H. W., de Roos, A., and van der Wall, E. E. (1998). Functional and Metabolic Evaluation of the Athlete's Heart By Magnetic Resonance Imaging and Dobutamine Stress Magnetic Resonance Spectroscopy. *Circulation*, 97(7):666–672.

Pool, P. E., Covell, J. W., Chidsey, C. A., and Braunwald, E. (1966). Myocardial high energy phosphate stores in acutely induced hypoxic heart failure. *Circulation Research*, 19(2):221–229.

Popma, J. J., Adams, D. H., Reardon, M. J., Yakubov, S. J., Kleiman, N. S., Heimansohn, D., Hermiller, J., Hughes, G. C., Harrison, J. K., Coselli, J., Diez, J., Kafi, A., Schreiber, T., Gleason, T. G., Conte, J., Buchbinder, M., Deeb, G. M., Carabello, B., Serruys, P. W., Chenoweth, S., and Oh, J. K. (2014). Transcatheter Aortic Valve Replacement Using a Self-Expanding Bioprosthesis in Patients With Severe Aortic Stenosis at Extreme Risk for Surgery. *Journal of the American College of Cardiology*, 63(19):1972–1981.

Popma, J. J., Deeb, G. M., Yakubov, S. J., Mumtaz, M., Gada, H., O'Hair, D., Bajwa, T., Heiser, J. C., Merhi, W., Kleiman, N. S., Askew, J., Sorajja, P., Rovin, J., Chetcuti, S. J., Adams, D. H., Teirstein, P. S., Zorn, G. L., Forrest, J. K., Tchétché, D., Resar, J., Walton, A., Piazza, N., Ramlawi, B., Robinson, N., Petrossian, G., Gleason, T. G., Oh, J. K., Boulware, M. J., Qiao, H., Mugglin, A. S., and Reardon,

M. J. (2019). Transcatheter Aortic-Valve Replacement with a Self-Expanding Valve in Low-Risk Patients. *New England Journal of Medicine*, 380(18):1706–1715.

Portman, M. A. and Ning, X. H. (1992). Maturational changes in respiratory control through creatine kinase in heart in vivo. *Am J Physiol*, 263(2):C453–C460.

Pound, K. M., Sorokina, N., Ballal, K., Berkich, D. A., Fasano, M., Lanoue, K. F., Taegtmeyer, H., O'Donnell, J. M., and Lewandowski, E. D. (2009). Substrate-enzyme competition attenuates upregulated anaplerotic flux through malic enzyme in hypertrophied rat heart and restores triacylglyceride content: Attenuating upregulated anaplerosis in hypertrophy. *Circ Res*, 104(6):805–812.

Power, A. S. C., Pham, T., Loiselle, D. S., Crossman, D. H., Ward, M.-L., and Hickey, A. J. (2016). Impaired ADP channeling to mitochondria and elevated reactive oxygen species in hypertensive hearts. *Am J Physiol Heart Circ Physiol*, 310(11):H1649–H1657.

Pradella, S., Grazzini, G., Brandani, M., Calistri, L., Nardi, C., Mori, F., Miele, V., and Colagrande, S. (2019). Cardiac magnetic resonance in patients with mitral valve prolapse: Focus on late gadolinium enhancement and T1 mapping. *European Radiology*, 29(3):1546–1554.

Pucar, D., Dzeja, P. P., Bast, P., Juranic, N., Macura, S., and Terzic, A. (2001). Cellular Energetics in the Preconditioned State: protective role for phosphotransfer reactions captured by 18O-assisted 31P NMR. *J Biol Chem*, 276(48):44812–44819.

Puigserver, P., Wu, Z., Park, C. W., Graves, R., Wright, M., and Spiegelman, B. M. (1998). A Cold-Inducible Coactivator of Nuclear Receptors Linked to Adaptive Thermogenesis. *Cell*, 92(6):829–839.

Pulinilkunnil, T., Kienesberger, P. C., Nagendran, J., Sharma, N., Young, M. E., and Dyck, J. R. B. (2014). Cardiac-specific adipose triglyceride lipase overexpression protects from cardiac steatosis and dilated cardiomyopathy following diet-induced obesity. *Int J Obes*, 38(2):205–215.

Purvis, L. A. B., Clarke, W. T., Biasiolli, L., Valkovic, L., Robson, M. D., and Rodgers, C. T. (2017). OXSA: An open-source magnetic resonance spectroscopy analysis toolbox in MATLAB. *PLoS One*, 12(9):e0185356.

Quintana, E., Suri, R. M., Thalji, N. M., Daly, R. C., Dearani, J. A., Burkhart, H. M., Li, Z., Enriquez-Sarano, M., and Schaff, H. V. (2014). Left ventricular dysfunction after mitral valve repair - The fallacy of "normal" preoperative myocardial function. *Journal of Thoracic and Cardiovascular Surgery*, 148(6):2752–2762.

R Core Team (2018). R: A Language and Environment for Statistical Computing.

Rainer, P. P. and Kass, D. A. (2016). Old dog, new tricks: Novel cardiac targets and stress regulation by protein kinase G. *Cardiovascular Research*, 111(2):154–162.

Razeghi, P., Young, M. E., Abbasi, S., and Taegtmeyer, H. (2001a). Hypoxia in Vivo Decreases Peroxisome Proliferator-Activated Receptor α-Regulated Gene Expression in Rat Heart. *Biochem Bioph Res Co*, 287(1):5–10.

Razeghi, P., Young, M. E., Alcorn, J. L., Moravec, C. S., Frazier, O. H., and Taegtmeyer, H. (2001b). Metabolic Gene Expression in Fetal and Failing Human Heart. *Circulation*, 104(24):2923–2931.

Reardon, M. J., Van Mieghem, N. M., Popma, J. J., Kleiman, N. S., Søndergaard, L., Mumtaz, M., Adams, D. H., Deeb, G. M., Maini, B., Gada, H., Chetcuti, S., Gleason, T., Heiser, J., Lange, R., Merhi, W., Oh, J. K., Olsen, P. S., Piazza, N., Williams, M., Windecker, S., Yakubov, S. J., Grube, E., Makkar, R., Lee, J. S., Conte, J., Vang, E., Nguyen, H., Chang, Y., Mugglin, A. S., Serruys, P. W. J. C., and Kappetein, A. P. (2017). Surgical or Transcatheter Aortic-Valve Replacement in Intermediate-Risk Patients. *New England Journal of Medicine*, 376(14):1321–1331.

Recchia, F. A., McConnell, P. I., Bernstein, R. D., Vogel, T. R., Xu, X., and Hintze, T. H. (1998). Reduced Nitric Oxide Production and Altered Myocardial Metabolism During the Decompensation of Pacing-Induced Heart Failure in the Conscious Dog. *Circ Res*, 83(10):969–979.

Regitz, V. and Fleck, E. (1992). Myocardial adenine nucleotide concentrations and myocardial norepinephrine content in patients with heart failure secondary to idiopathic dilated or ischemic cardiomyopathy. *Am J Cardiol*, 69(19):1574–1580.

Revis, N. W. and Cameron, A. J. V. (1979). Metabolism of lipids in experimental hypertrophic hearts of rabbits. *Metabolism*, 28(6):601–613.

Riehle, C., Wende, A. R., Zhu, Y., Oliveira, K. J., Pereira, R. O., Jaishy, B. P., Bevins, J., Valdez, S., Noh, J., Kim, B. J., Moreira, A. B., Weatherford, E. T., Manivel, R., Rawlings, T. A., Rech, M., White, M. F., and Abel, E. D. (2014). Insulin Receptor Substrates Are Essential for the Bioenergetic and Hypertrophic Response of the Heart to Exercise Training. *Mol Cell Biol*, 34(18):3450–3460.

Rimbaud, S., Sanchez, H., Garnier, A., Fortin, D., Bigard, X., Veksler, V., and Ventura-Clapier, R. (2009). Stimulus specific changes of energy metabolism in hypertrophied heart. *J Mol Cell Cardiol*, 46(6):952–959.

Ritterhoff, J. and Tian, R. (2017). Metabolism in cardiomyopathy: every substrate matters. *Cardiovasc Res*, 113(4):411–421.

Rockstein, M., Lopez, T., and Chesky, J. A. (1981). Effects of exercise on the biochemical aging of mammalian myocardium. II. Creatine phosphokinase. *Mechanisms of Ageing and Development*, 16(4):379–383.

Rodgers, C. T., Clarke, W. T., Snyder, C., Vaughan, J. T., Neubauer, S., and Robson, M. D. (2014). Human cardiac 31P magnetic resonance spectroscopy at 7 tesla. *Magnetic resonance in medicine*, 72(2):304–315.

Rogers, T., Koifman, E., Patel, N., Gai, J., Torguson, R., Corso, P., and Waksman, R. (2017). Society of Thoracic Surgeons Score Variance Results in Risk Reclassification of Patients Undergoing Transcatheter Aortic Valve Replacement. *JAMA Cardiology*, 2(4):455.

Roman, B. B., Wieringa, B., and Koretsky, A. P. (1997). Functional Equivalence of Creatine Kinase Isoforms in Mouse Skeletal Muscle. *Journal of Biological Chemistry*, 272(28):17790–17794.

Roques, F., Nashef, S. A. M., Michel, P., Gauducheau, E., De Vincentiis, C., Baudet, E., Cortina, J., David, M., Faichney, A., and Gavrielle, F. (1999). Risk factors and outcome in European cardiac surgery: analysis of the EuroSCORE multinational database of 19030 patients. *European Journal of Cardio-thoracic Surgery*, 15(6):816–823.

Rosalki, S. B. (1967). An improved procedure for serum creatine phosphokinase determination. *Journal of Laboratory and Clinical Medicine*, 69(4):696–705.

Rosenblatt-Velin, N., Montessuit, C., Papageorgiou, I., Terrand, J., and Lerch, R. (2001). Postinfarction heart failure in rats is associated with upregulation of GLUT-1 and downregulation of genes of fatty acid metabolism. *Cardiovasc Res*, 52(3):407–416.

Rosenhek, R., Rader, F., Klaar, U., Gabriel, H., Krejc, M., Kalbeck, D., Schemper, M., Maurer, G., and Baumgartner, H. (2006). Outcome of Watchful Waiting in Asymptomatic Severe Mitral Regurgitation. *Circulation*, 113(18):2238.

Rowe, G. C., Jiang, A., and Arany, Z. (2010). PGC-1 Coactivators in Cardiac Development and Disease. *Circ Res*, 107(7):825–838.

Rusinaru, D., Bohbot, Y., Ringle, A., Maréchaux, S., Diouf, M., and Tribouilloy, C. (2018). Impact of low stroke volume on mortality in patients with severe aortic stenosis and preserved left ventricular ejection fraction. *European Heart Journal*, pages ehy123–ehy123.

Rusinaru, D., Tribouilloy, C., Grigioni, F., Avierinos, J. F., Suri, R. M., Barbieri, A., Szymanski, C., Ferlito, M., Michelena, H., Tafanelli, L., Bursi, F., Mezghani, S., Branzi, A., Habib, G., Modena, M. G., and Enriquez-Sarano, M. (2011). Left Atrial Size Is a Potent Predictor of Mortality in Mitral Regurgitation Due to Flail Leaflets. *Circulation: Cardiovascular Imaging*, 4(5):473–481.

Sack, M. N., Rader, T. A., Park, S., Bastin, J., McCune, S. A., and Kelly, D. P. (1996). Fatty Acid Oxidation Enzyme Gene Expression Is Downregulated in the Failing Heart. *Circulation*, 94(11):2837–2842.

Saito, T., Fukuzawa, J., Osaki, J., Sakuragi, H., Yao, N., Haneda, T., Fujino, T., Wakamiya, N., Kikuchi, K., and Hasebe, N. (2003). Roles of calcineurin and

calcium/calmodulin-dependent protein kinase II in pressure overload-induced cardiac hypertrophy. *Journal of Molecular and Cellular Cardiology*, 35(9):1153–1160.

Saks, V., Dzeja, P., Schlattner, U., Vendelin, M., Terzic, A., and Wallimann, T. (2006). Cardiac system bioenergetics: metabolic basis of the Frank-Starling law. *J Physiol*, 571(2):253–273.

Saks, V., Kuznetsov, A. V., Gonzalez-Granillo, M., Tepp, K., Timohhina, N., Karu-Varikmaa, M., Kaambre, T., Santos, P. D., Boucher, F., and Guzun, R. (2012). Intracellular Energetic Units regulate metabolism in cardiac cells. *J Mol Cell Cardiol*, 52(2):419–436.

Saks, V. A., Belikova, Y. O., Kuznetsov, A. V., Khuchua, Z. A., Branishte, T. H., Semenovsky, M. L., and Naumov, V. G. (1991). Phosphocreatine pathway for energy transport: ADP diffusion and cardiomyopathy. *Am J Physiol Heart Circ Physiol*, 261(4):30–38.

Saks, V. A., Chernousova, G. B., Gukovsky, D. E., Smirnov, V. N., and Chazov, E. I. (1975). Studies of Energy Transport in Heart Cells: Mitochondrial Isoenzyme of Creatine Phosphokinase: Kinetic Properties and Regulatory Action of Mg2+ Ions. *European Journal of Biochemistry*, 57(1):273–290.

Saks, V. A., Kaambre, T., Sikk, P., Eimre, M., Orlova, E., Paju, K., Piirsoo, A., Appaix, F., Kay, L., Regitz-Zagrosek, V., Fleck, E., and Seppet, E. (2001). Intracellular energetic units in red muscle cells. *Biochemical Journal*, 356(2):643–657.

Saks, V. A., Khuchua, Z. A., Vasilyeva, E. V., Belikova, O. Y., and Kuznetsov, A. V. (1994). Metabolic compartmentation and substrate channelling in muscle cells. *Mol Cell Biochem*, 133(1):155–192.

Saks, V. A., Kupriyanov, V. V., Elizarova, G. V., and Jacobus, W. E. (1980). Studies of energy transport in heart cells. The importance of creatine kinase localization for the coupling of mitochondrial phosphorylcreatine production to oxidative phosphorylation. *J Biol Chem*, 255(2):755–763.

Saks, V. A., Ventura-Clapier, R., Huchua, Z. A., Preobrazhensky, A. N., and Emelin, I. V. (1984). Creatine kinase in regulation of heart function and metabolism. I. Further evidence for compartmentation of adenine nucleotides in cardiac myofibrillar and sarcolemmal coupled ATPase-creatine kinase systems. *BBA-Mol Cell Res*, 803(4):254–264.

Saupe, K. W., Spindler, M., Hopkins, J. C. A., Shen, W., and Ingwall, J. S. (2000). Kinetic, Thermodynamic, and Developmental Consequences of Deleting Creatine Kinase Isoenzymes from the Heart: Reaction kinetics of the creatine kinase isoenzymes in the intact heart. *J Biol Chem*, 275(26):19742–19746.

Saupe, K. W., Spindler, M., Tian, R., and Ingwall, J. S. (1998). Impaired Cardiac Energetics in Mice Lacking Muscle-Specific Isoenzymes of Creatine Kinase. *Circ Res*, 82(8):898–907.

Schär, M., El-Sharkawy, A. M. M., Weiss, R. G., and Bottomley, P. A. (2010). Triple repetition time saturation transfer (TRiST) 31P spectroscopy for measuring human creatine kinase reaction kinetics. *Magnetic Resonance in Medicine*, 63(6):1493–1501.

Schar, M., Gabr, R. E., El-Sharkawy, A.-M. M., Steinberg, A., Bottomley, P. A., and Weiss, R. G. (2015). Two repetition time saturation transfer (TwiST) with spill-over correction to measure creatine kinase reaction rates in human hearts. *J Cardiovasc Magn R*, 17(1):70.

Scheinowitz, M., Kessler-Icekson, G., Freimann, S., Zimmermann, R., Schaper, W., Golomb, E., Savion, N., and Eldar, M. (2003). Short- and long-term swimming exercise training increases myocardial insulin-like growth factor-I gene expression. *Growth Hormone and IGF Research*, 13(1):19–25.

Schlattner, U., Tokarska-Schlattner, M., and Wallimann, T. (2006). Mitochondrial creatine kinase in human health and disease. *BBA-Mol Basis Dis*, 1762(2):164–180.

Schmid, A. I., Apps, A. P., Valkovic, L., Tunnicliffe, E., Clarke, W. T., Peterzan, M. A., Neubauer, S., Rider, O. J., and Rodgers, C. T. (2019). Human cardiac pH and Pi concentration during dobutamine stress measured by 7T 31P-MRS. In *ISMRM*, Montreal, QC, Canada.

Schmidt, A., Marescau, B., Boehm, E. A., Jan Renema, W. K., Peco, R., Das, A., Steinfeld, R., Chan, S., Wallis, J., Davidoff, M., Ullrich, K., Waldschütz, R., Heerschap, A., De Deyn, P. P., Neubauer, S., and Isbrandt, D. (2004). Severely altered guanidino compound levels, disturbed body weight homeostasis and impaired fertility in a mouse model of guanidinoacetate N-methyltrasferase (GAMT) deficiency. *Human Molecular Genetics*, 13(9):905–921.

Schocke, M. F., Metzler, B., Wolf, C., Steinboeck, P., Kremser, C., Pachinger, O., Jaschke, W., and Lukas, P. (2003). Impact of aging on cardiac high-energy phosphate metabolism determined by phosphorus-31 2-dimensional chemical shift imaging (31P 2D CSI). *Magnetic Resonance Imaging*, 21(5):553–559.

Scholte, H. R. (1973). On the triple localization of creatine kinase in heart and skeletal muscle cells of the rat: Evidence for the existence of myofibrillar and mitochondrial isoenzymes. *BBA - Bioenergetics*, 305(2):413–427.

Schönekess, B. O., Allard, M. F., and Lopaschuk, G. D. (1995). Propionyl l-Carnitine Improvement of Hypertrophied Heart Function Is Accompanied by an Increase in Carbohydrate Oxidation. *Circ Res*, 77(4):726–734.

Schroeder, M. A., Atherton, H. J., Dodd, M. S., Lee, P., Cochlin, L. E., Radda, G. K., Clarke, K., and Tyler, D. J. (2012). The Cycling of Acetyl-Coenzyme A Through Acetylcarnitine Buffers Cardiac Substrate Supply: A Hyperpolarized 13C Magnetic Resonance Study. *Circ-Cardiovasc Imag*, 5(2):201–209.

Schugar, R. C., Moll, A. R., André d'Avignon, D., Weinheimer, C. J., Kovacs, A., and Crawford, P. A. (2014). Cardiomyocyte-specific deficiency of ketone body metabolism promotes accelerated pathological remodeling. *Mol Metab*, 3(7):754–769.

Schuler, G., Peterson, K. L., Johnson, A., Francis, G., Dennish, G., Utley, J., Daily, P. O., Ashburn, W., and Ross, J. (1979). Temporal response of left ventricular performance to mitral valve surgery. *Circulation*, 59(6):1218–1231.

Sebastiani, M., Giordano, C., Nediani, C., Travaglini, C., Borchi, E., Zani, M., Feccia, M., Mancini, M., Petrozza, V., Cossarizza, A., Gallo, P., Taylor, R. W., and D'Amati, G. (2007). Induction of Mitochondrial Biogenesis Is a Maladaptive Mechanism in Mitochondrial Cardiomyopathies. *J Am Coll Cardiol*, 50(14):1362–1369.

Sekiguchi, M. (1974). Electron microscopical observations of the myocardium in patients with idiopathic cardiomyopathy using endomyocardial biopsy. *Journal of Molecular and Cellular Cardiology*, 6(2):111–122.

Seraydarian, M. W. and Abbott, B. C. (1976). The role of the creatine-phosphorylcreatine system in muscle. *Journal of molecular and cellular cardiology*, 8(10):741–746.

Seraydarian, M. W., Abbott, B. C., and Williams, E. B. (1961). Studies on the frog's sartorius at different stages of activity. *BBA - Biochimica et Biophysica Acta*, 46(2):355–363.

Seraydarian, M. W. and Artaza, L. (1976). Regulation of energy metabolism by creatine in cardiac and skeletal muscle cells in culture. *Journal of Molecular and Cellular Cardiology*, 8(9):669–676.

Seraydarian, M. W., Artaza, L., and Abbott, B. C. (1974). Creatine and the control of energy metabolism in cardiac and skeletal muscle cells in culture. *Journal of Molecular and Cellular Cardiology*, 6(5):405–413.

Seraydarian, M. W., Sato, E., and Harary, I. (1970). In vitro studies of beating heart cells in culture XIII. The effect of 1-fluoro-2,4-dinitrobenzene. *Archives of Biochemistry and Biophysics*, 138(1):233–238.

Seraydarian, M. W., Sato, E., Savageau, M., and Harary, I. (1969). In vitro studies of beating heart cells in culture XII. The utilization of ATP and phosphocreatine in oligomycin and 2-deoxyglucose inhibited cells. *BBA - Bioenergetics*, 180(2):264–270.

Seymour, A.-M. L., Giles, L., Ball, V., Miller, J. J., Clarke, K., Carr, C. A., and Tyler, D. J. (2015). In vivo assessment of cardiac metabolism and function in the abdominal aortic banding model of compensated cardiac hypertrophy. *Cardiovasc Res*, 106(2):249–260.

Sharma, S., Merghani, A., and Mont, L. (2015). Exercise and the heart: the good, the bad, and the ugly. *European Heart Journal*, 36(23):1445–1453.

Shen, W., Asai, K., Uechi, M., Mathier, M. A., Shannon, R. P., Vatner, S. F., and Ingwall, J. S. (1999). Progressive Loss of Myocardial ATP Due to a Loss of Total Purines During the Development of Heart Failure in Dogs: A Compensatory Role for the Parallel Loss of Creatine. *Circulation*, 100(20):2113–2118.

Shen, W., Spindler, M., Higgins, M. A., Jin, N., Gill, R. M., Bloem, L. J., Ryan, T. P., and Ingwall, J. S. (2005). The fall in creatine levels and creatine kinase isozyme changes in the failing heart are reversible: Complex post-transcriptional regulation of the components of the CK system. *J Mol Cell Cardiol*, 39(3):537–544.

Shen, W., Vatner, D. E., Vatner, S. F., and Ingwall, J. S. (2010). Progressive loss of creatine maintains a near normal Delta G_ATP in transgenic mouse hearts with cardiomyopathy caused by overexpressing Gsα. *J Mol Cell Cardiol*, 48(4):591–599.

Shimizu, I. and Minamino, T. (2016). Physiological and pathological cardiac hypertrophy. *Journal of Molecular and Cellular Cardiology*, 97:245–262.

Shoubridge, E. A., Jeffry, F. M. H., Keogh, J. M., Radda, G. K., and Seymour, A. M. L. (1985). Creatine kinase kinetics, ATP turnover, and cardiac performance in hearts depleted of creatine with the substrate analogue β-guanidinopropionic acid. *BBA-Mol Cell Res*, 847(1):25–32.

Sihag, S., Cresci, S., Li, A. Y., Sucharov, C. C., and Lehman, J. J. (2009). PGC-1 alpha and ERR alpha target gene downregulation is a signature of the failing human heart. *J Mol Cell Cardiol*, 46(2):201–212.

Simonsen, S. and Kjekshus, J. K. (1978). The effect of free fatty acids on myocardial oxygen consumption during atrial pacing and catecholamine infusion in man. *Circulation*, 58(3):484–491.

Siontis, G. C., Praz, F., Pilgrim, T., Mavridis, D., Verma, S., Salanti, G., Søndergaard, L., Jüni, P., and Windecker, S. (2016). Transcatheter aortic valve implantation vs. surgical aortic valve replacement for treatment of severe aortic stenosis: A meta-analysis of randomized trials. *European Heart Journal*, 37(47):3503–3512a.

Smith, C. R., Leon, M. B., Mack, M. J., Miller, D. C., Moses, J. W., Svensson, L. G., Tuzcu, E. M., Webb, J. G., Fontana, G. P., Makkar, R. R., Williams, M., Dewey, T., Kapadia, S., Babaliaros, V., Thourani, V. H., Corso, P., Pichard, A. D., Bavaria, J. E., Herrmann, H. C., Akin, J. J., Anderson, W. N., Wang, D., and Pocock, S. J.

(2011). Transcatheter versus Surgical Aortic-Valve Replacement in High-Risk Patients. *New England Journal of Medicine*, 364(23):2187–2198.

Smith, C. S., Bottomley, P. A., Schulman, S. P., Gerstenblith, G., and Weiss, R. G. (2006). Altered Creatine Kinase Adenosine Triphosphate Kinetics in Failing Hypertrophied Human Myocardium. *Circulation*, 114(11):1151–1158.

Smith, S. H., Kramer, M. F., Reis, I., Bishop, S. P., and Ingwall, J. S. (1990). Regional changes in creatine kinase and myocyte size in hypertensive and nonhypertensive cardiac hypertrophy. *Circ Res*, 67(6):1334–1344.

Sorokina, N., O'Donnell, J. M., McKinney, R. D., Pound, K. M., Woldegiorgis, G., LaNoue, K. F., Ballal, K., Taegtmeyer, H., Buttrick, P. M., and Lewandowski, E. D. (2007). Recruitment of Compensatory Pathways to Sustain Oxidative Flux With Reduced Carnitine Palmitoyltransferase I Activity Characterizes Inefficiency in Energy Metabolism in Hypertrophied Hearts. *Circulation*, 115(15):2033–2041.

Speer, O., Neukomm, L. J., Murphy, R. M., Zanolla, E., Schlattner, U., Henry, H., Snow, R. J., and Wallimann, T. (2004). Creatine transporters: A reappraisal. *Molecular and Cellular Biochemistry*, 256(1/2):407–424.

Spindler, M., Niebler, R., Remkes, H., Horn, M., Lanz, T., and Neubauer, S. (2002). Mitochondrial creatine kinase is critically necessary for normal myocardial high-energy phosphate metabolism. *Am J Physiol Heart Circ Physiol*, 283(2):H680–H687.

Stanley, W. C., Recchia, F. A., and Lopaschuk, G. D. (2005). Myocardial substrate metabolism in the normal and failing heart. *Physiol Rev*, 85(3):1093–1129.

Starling, R. C., Hammer, D. F., and Altschuld, R. A. (1998). Human myocardial ATP content and in vivo contractile function. *Mol Cell Biochem*, 180(1):171–177.

Steeghs, K., Benders, A., Oerlemans, F., De Haan, A., Heerschap, A., Ruitenbeek, W., Jost, C., Van Deursen, J., Perryman, B., and Pette, D. (1997a). Altered Ca 2+ responses in muscles with combined mitochondrial and cytosolic creatine kinase deficiencies. *Cell*, 89(1):93–103.

Steeghs, K., Heerschap, A., De Haan, A., Ruitenbeek, W., Oerlemans, F., Van Deursen, J., Perryman, B., Pette, D., Brückwilder, M., Koudijs, J., Paul, J., and Wieringa, B. (1997b). Use of gene targeting for compromising energy homeostasis in neuromuscular tissues: The role of sarcomeric mitochondrial creatine kinase. *Journal of Neuroscience Methods*, 71(1):29–41.

Steeghs, K., Oerlemans, F., De Haan, A., Heerschap, A., Verdoodt, L., De Bie, M., Ruitenbeek, W., Benders, A., Jost, C., and Van Deursen, J. (1998). Cytoarchitectural and metabolic adaptations in muscles with mitochondrial and cytosolic creatine kinase deficiencies. *Mol Cell Biochem*, 184:183–194.

Steenbergen, C., Deleeuw, G., and Williamson, J. R. (1978). Analysis of control of glycolysis in ischemic hearts having heterogeneous zones of anoxia. *Journal of Molecular and Cellular Cardiology*, 10(7):635–639.

Steinhagen-Thiessen, E. and Reznick, A. Z. (1987). Effect of Short- and Long-Term Endurance Training on Creatine Phosphokinase Activity in Skeletal and Cardiac Muscles of CW-1 and C57BL Mice. *Gerontology*, 33(1):14–18.

Stride, N., Larsen, S., Hey-Mogensen, M., Sander, K., Lund, J. T., Gustafsson, F., Køber, L., and Dela, F. (2013). Decreased mitochondrial oxidative phosphorylation capacity in the human heart with left ventricular systolic dysfunction. *Eur J Heart Fail*, 15(2):150–157.

Strøm, C. C., Aplin, M., Ploug, T., Christoffersen, T. E., Langfort, J., Viese, M., Galbo, H., Haunsø, S., and Sheikh, S. P. (2005). Expression profiling reveals differences in metabolic gene expression between exercise-induced cardiac effects and maladaptive cardiac hypertrophy. *FEBS Journal*, 272(11):2684–2695.

Stuewe, S. R., Gwirtz, P. A., and Mallet, R. T. (2001). Exercise training increases creatine kinase capacity in canine myocardium. *Medicine and Science in Sports and Exercise*, 33(1):92–98.

Suga, H. (1990). Ventricular energetics. *Physiol Rev*, 70(2):247–277.

Summermatter, S., Shui, G., Maag, D., Santos, G., Wenk, M. R., and Handschin, C. (2013). PGC-1α improves glucose homeostasis in skeletal muscle in an activity-dependent manner. *Diabetes*, 62(1):85–95.

Supino, P. G., Borer, J. S., Schuleri, K., Gupta, A., Hochreiter, C., Kligfield, P., Herrold, E. M., and Preibisz, J. J. (2007). Prognostic Value of Exercise Tolerance Testing in Asymptomatic Chronic Nonischemic Mitral Regurgitation. *Am J Cardiol*, 100(8):1274–1281.

Suri, R. M., Vanoverschelde, J., Grigioni, F., and al., E. (2013). Association between early surgical intervention vs watchful waiting and outcomes for mitral regurgitation due to flail mitral valve leaflets. *JAMA*, 310(6):609–616.

Swain, J. L., Sabina, R. L., Peyton, R. B., Jones, R. N., Wechsler, A. S., and Holmes, E. W. (1982). Derangements in myocardial purine and pyrimidine nucleotide metabolism in patients with coronary artery disease and left ventricular hypertrophy. *Proceedings of the National Academy of Sciences of the United States of America*, 79(2 I):655–659.

Sylvén, C., Jansson, E., and Böök, K. (1988). Key enzymes of myocardial energy metabolism in patients with valvular heart disease: relation to left ventricular function. *Acta physiologica Scandinavica*, 132(3):267–270.

Sylvén, C., Jansson, E., and Olin, C. (1983). Human myocardial and skeletal muscle enzyme activities: creatine kinase and its isozyme MB as related to citrate synthase and muscle fibre types. *Clinical Physiology*, 3(5):461–468.

Sylvén, C., Lin, L., Jansson, E., Sotonyi, P., Fu, L.-X., Waagstein, F., Hjalmarsson, Å., Marcus, C., and Brönnegård, M. (1993). Ventricular adenine nucleotide translocator mRNA is upregulated in dilated cardiomyopathy. *Cardiovasc Res*, 27(7):1295–1299.

Sylvén, C., Lin, L., Kallner, A., Sotonyi, P., Somogyi, E., and Jansson, E. (1991). Dynamics of creatine kinase shuttle enzymes in the human heart. *European J Clin Invest*, 21(3):350–354.

Szasz, G. and Gruber, W. (1978). Creatine kinase in serum: 4. Differences in substrate affinity among the isoenzymes. *Clinical Chemistry*, 24(2):245–249.

Szasz, G., Gruber, W., and Bernt, E. (1976). Creatine kinase in serum: 1. Determination of optimum reaction conditions. *Clinical Chemistry*, 22(5):650–656.

Szasz, G., Waldenstrom, J., and Gruber, W. (1979). Creatine kinase in serum: 6. Inhibition by endogenous polyvalent cations, and effect of chelators on the activity and stability of some assay components. *Clinical Chemistry*, 25(3):446–452.

Taegtmeyer, H., Golfman, L., Sharma, S., Razeghi, P., and Van Arsdall, M. (2004). Linking Gene Expression to Function: Metabolic Flexibility in the Normal and Diseased Heart. *Ann NY Acad Sci*, 1015(1):202–213.

Taegtmeyer, H. and Overturf, M. L. (1988). Effects of moderate hypertension on cardiac function and metabolism in the rabbit. *Hypertension*, 11(5):416–426.

Taegtmeyer, H., Roberts, A. F. C., and Raine, A. E. G. (1985). Energy metabolism in reperfused heart muscle: Metabolic correlates to return of function. *J Am Coll Cardiol*, 6(4):864–870.

Taegtmeyer, H., Young, M. E., Lopaschuk, G. D., Abel, E. D., Brunengraber, H., Darley-Usmar, V., Des Rosiers, C., Gerszten, R., Glatz, J. F., Griffin, J. L., Gropler, R. J., Holzhuetter, H.-G., Kizer, J. R., Lewandowski, E. D., Malloy, C. R., Neubauer, S., Peterson, L. R., Portman, M. A., Recchia, F. A., Van Eyk, J. E., and Wang, T. J. (2016). Assessing Cardiac Metabolism: A Scientific Statement From the American Heart Association. *Circ Res*, 118(10):1659–1701.

Takimoto, E., Koitabashi, N., Hsu, S., Ketner, E. A., Zhang, M., Nagayama, T., Bedja, D., Gabrielson, K. L., Blanton, R., Siderovski, D. P., Mendelsohn, M. E., and Kass, D. A. (2009). Regulator of G protein signaling 2 mediates cardiac compensation to pressure overload and antihypertrophic effects of PDE5 inhibition in mice. *Journal of Clinical Investigation*, 119(2):408–420.

Taniguchi, T., Morimoto, T., Shiomi, H., Ando, K., Kanamori, N., Murata, K., Kitai, T., Kadota, K., Izumi, C., Nakatsuma, K., Sasa, T., Watanabe, H., Kuwabara, Y., Makiyama, T., Ono, K., Shizuta, S., Kato, T., Saito, N., Minatoya, K., Kimura, T., Kimura, T., Taniguchi, T., Shiomi, H., Saito, N., Imai, M., Tazaki, J., Toyota, T., Higami, H., Kawaji, T., Ando, K., Shirai, S., Kourai, K., Arita, T., Miura, S., Yamaji, K., Aoyama, T., Kanamori, N., Onodera, T., Murata, K., Furukawa, Y., Kitai, T., Kim, K., Kadota, K., Kawase, Y., Iwasaki, K., Miyawaki, H., Misao, A., Kuwayama, A., Ohya, M., Shimada, T., Amano, H., Nakagawa, Y., Izumi, C., Miyake, M., Amano, M., Takahashi, Y., Yoshikawa, Y., Nishimura, S., Kuroda, M., Shirotani, M., Mitsuoka, H., Miki, S., Mizoguchi, T., Kato, M., Yokomatsu, T., Kushiyama, A., Yaku, H., Watanabe, T., Miyazaki, S., Hirano, Y., Matsuda, M., Matsuda, S., Sugioka, S., Inada, T., Nagao, K., Takahashi, N., Fukuchi, K., Murakami, T., Mabuchi, H., Takeda, T., Sakaguchi, T., Maeda, K., Yamaji, M., Maenaka, M., Tadano, Y., Sakamoto, H., Takeuchi, Y., Motooka, M., Nishikawa, R., Eizawa, H., Yamane, K., Kawato, M., Kinoshita, M., Aida, K., Tamura, T., Toyofuku, M., Takahashi, K., Ko, E., Akao, M., Ishii, M., Masunaga, N., Ogawa, H., Iguchi, M., Unoki, T., Takabayashi, K., Hamatani, Y., Yamashita, Y., Inoko, M., Minamino-Muta, E., Kato, T., Himura, Y., Ikeda, T., Ishii, K., Komasa, A., Sato, Y., Hotta, K., Tsuji, S., Hiraoka, Y., Higashitani, N., Kouchi, I., Kato, Y., Ikeguchi, S., Inuzuka, Y., Nishio, S., Seki, J., Shinoda, E., Yamada, M., Kawamoto, A., Maeda, C., Konishi, T., Jinnai, T., Sogabe, K., Tachiiri, M., Matsumura, Y., Ota, C., Kitaguchi, S., Morikami, Y., Sakata, R., Minakata, K., Minatoya, K., Hanyu, M., Yamazaki, F., Koyama, T., Komiya, T., Yamanaka, K., Nishiwaki, N., Nakajima, H., Ohnaka, M., Osada, H., Meshii, K., Saga, T., Onoe, M., Nakayama, S., Sakaguchi, G., Iwakura, A., Shiraga, K., Ueyama, K., Fujiwara, K., Fukumoto, A., Park, M., Nishizawa, J., and Kitano, M. (2018). Prognostic Impact of Left Ventricular Ejection Fraction in Patients With Severe Aortic Stenosis. *JACC: Cardiovascular Interventions*, 11(2):145–157.

ten Hove, M., Chan, S., Lygate, C., Monfared, M., Boehm, E., Hulbert, K., Watkins, H., Clarke, K., and Neubauer, S. (2005). Mechanisms of creatine depletion in chronically failing rat heart. *J Mol Cell Cardiol*, 38(2):309–313.

Ten Hove, M., Lygate, C. A., Fischer, A., Schneider, J. E., Sang, A. E., Hulbert, K., Sebag-Montefiore, L., Watkins, H., Clarke, K., Isbrandt, D., Wallis, J., and Neubauer, S. (2005). Reduced inotropic reserve and increased susceptibility to cardiac ischemia/reperfusion injury in phosphocreatine-deficient guanidinoacetate-N- methyltransferase-knockout mice. *Circulation*, 111(19):2477–2485.

ten Hove, M., Makinen, K., Sebag-Montefiore, L., Hunyor, I., Fischer, A., Wallis, J., Isbrandt, D., Lygate, C., and Neubauer, S. (2008). Creatine uptake in mouse hearts with genetically altered creatine levels. *J Mol Cell Cardiol*, 45(3):453–459.

Thavendiranathan, P., Liu, S., Datta, S., Walls, M., Nitinunu, A., Van Houten, T., Tomson, N. A., Vidmar, L., Georgescu, B., Wang, Y., Srinivasan, S., De Michelis,

N., Raman, S. V., Ryan, T., and Vannan, M. A. (2012). Automated Quantification of Mitral Inflow and Aortic Outflow Stroke Volumes by Three-Dimensional Real-Time Volume Color-Flow Doppler Transthoracic Echocardiography: Comparison with Pulsed-Wave Doppler and Cardiac Magnetic Resonance Imaging. *Journal of the American Society of Echocardiography*, 25(1):56–65.

Thourani, V. H., Kodali, S., Makkar, R. R., Herrmann, H. C., Williams, M., Babaliaros, V., Smalling, R., Lim, S., Malaisrie, S. C., Kapadia, S., Szeto, W. Y., Greason, K. L., Kereiakes, D., Ailawadi, G., Whisenant, B. K., Devireddy, C., Leipsic, J., Hahn, R. T., Pibarot, P., Weissman, N. J., Jaber, W. A., Cohen, D. J., Suri, R., Tuzcu, E. M., Svensson, L. G., Webb, J. G., Moses, J. W., Mack, M. J., Miller, D. C., Smith, C. R., Alu, M. C., Parvataneni, R., D'Agostino, R. B., and Leon, M. B. (2016). Transcatheter aortic valve replacement versus surgical valve replacement in intermediate-risk patients: a propensity score analysis. *The Lancet*, 387(10034):2218–2225.

Thourani, V. H., Weintraub, W. S., Guyton, R. A., Jones, E. L., Williams, W. H., Elkabbani, S., and Craver, J. M. (2003). Outcomes and Long-Term Survival for Patients Undergoing Mitral Valve Repair Versus Replacement. *Circulation*, 108(3):298.

Thyregod, H. G. H., Ihlemann, N., Jørgensen, T. H., Nissen, H., Kjeldsen, B. J., Petursson, P., Chang, Y., Franzen, O. W., Engstrøm, T., Clemmensen, P., Hansen, P. B., Andersen, L. W., Steinbruüchel, D. A., Olsen, P. S., and Søndergaard, L. (2019). Five-Year Clinical and Echocardiographic Outcomes From the NOTION Randomized Clinical Trial in Patients at Lower Surgical Risk. *Circulation*, 139(24):2714–2723.

Thyregod, H. G. H., Steinbrüchel, D. A., Ihlemann, N., Nissen, H., Kjeldsen, B. J., Petursson, P., Chang, Y., Franzen, O. W., Engstrøm, T., Clemmensen, P., Hansen, P. B., Andersen, L. W., Olsen, P. S., and Søndergaard, L. (2015). Transcatheter Versus Surgical Aortic Valve Replacement in Patients With Severe Aortic Valve Stenosis: 1-Year Results From the All-Comers NOTION Randomized Clinical Trial. *Journal of the American College of Cardiology*, 65(20):2184–2194.

Tian, R., Christe, M. E., Spindler, M., Hopkins, J. C., Halow, J. M., Camacho, S. A., and Ingwall, J. S. (1997a). Role of MgADP in the development of diastolic dysfunction in the intact beating rat heart. *J Clin Invest*, 99(4):745–751.

Tian, R., Halow, J. M., Meyer, M., Dillmann, W. H., Figueredo, V. M., Ingwall, J. S., and Camacho, S. A. (1998). Thermodynamic limitation for Ca2+ handling contributes to decreased contractile reserve in rat hearts. *Am J Physiol Heart Circ Physiol*, 275(6):H2064–H2071.

Tian, R. and Ingwall, J. S. (1996). Energetic basis for reduced contractile reserve in isolated rat hearts. *Am J Physiol Heart Circ Physiol*, 270(4):H1207–H1216.

Tian, R., Musi, N., D'Agostino, J., Hirshman, M. F., and Goodyear, L. J. (2001). Increased Adenosine Monophosphate-Activated Protein Kinase Activity in Rat Hearts With Pressure-Overload Hypertrophy. *Circulation*, 104(14):1664–1669.

Tian, R., Nascimben, L., Ingwall, J. S., and Lorell, B. H. (1997b). Failure to maintain a low ADP concentration impairs diastolic function in hypertrophied rat hearts. *Circulation*, 96(4):1313–1319.

Tian, R., Nascimben, L., Kaddurah-Daouk, R., and Ingwall, J. S. (1996). Depletion of Energy Reserve via the Creatine Kinase Reaction During the Evolution of Heart Failure in Cardiomyopathic Hamsters. *J Mol Cell Cardiol*, 28(4):755–765.

Treibel, T. A., Kozor, R., Schofield, R., Benedetti, G., Fontana, M., Bhuva, A. N., Sheikh, A., López, B., González, A., Manisty, C., Lloyd, G., Kellman, P., Díez, J., and Moon, J. C. (2018). Reverse Myocardial Remodeling Following Valve Replacement in Patients With Aortic Stenosis. *Journal of the American College of Cardiology*, 71(8):860–871.

Tribouilloy, C., Grigioni, F., Avierinos, J. F., Barbieri, A., Rusinaru, D., Szymanski, C., Ferlito, M., Tafanelli, L., Bursi, F., Trojette, F., Branzi, A., Habib, G., Modena, M. G., and Enriquez-Sarano, M. (2009). Survival Implication of Left Ventricular End-Systolic Diameter in Mitral Regurgitation Due to Flail Leaflets: A Long-Term Follow-Up Multicenter Study. *Journal of the American College of Cardiology*, 54(21):1961–1968.

Tsujita, Y., Muraski, J., Shiraishi, I., Kato, T., Kajstura, J., Anversa, P., and Sussman, M. A. (2006). Nuclear targeting of Akt antagonizes aspects of cardiomyocyte hypertrophy. *Proceedings of the National Academy of Sciences*, 103(32):11946–11951.

Turner, D. C., Wallimann, T., and Eppenberger, H. M. (1973). A protein that binds specifically to the M-line of skeletal muscle is identified as the muscle form of creatine kinase. *Proceedings of the National Academy of Sciences of the United States of America*, 70(3):702–5.

Tuunanen, H., Engblom, E., Naum, A., Någren, K., Hesse, B., Airaksinen, K. E. J., Nuutila, P., Iozzo, P., Ukkonen, H., Opie, L. H., and Knuuti, J. (2006a). Free Fatty Acid Depletion Acutely Decreases Cardiac Work and Efficiency in Cardiomyopathic Heart Failure. *Circulation*, 114(20):2130–2137.

Tuunanen, H., Engblom, E., Naum, A., Scheinin, M., Någren, K., Airaksinen, J., Nuutila, P., Iozzo, P., Ukkonen, H., and Knuuti, J. (2006b). Decreased Myocardial Free Fatty Acid Uptake in Patients With Idiopathic Dilated Cardiomyopathy: Evidence of Relationship With Insulin Resistance and Left Ventricular Dysfunction. *J Card Fail*, 12(8):644–652.

Tyler, D. J., Hudsmith, L. E., Clarke, K., Neubauer, S., and Robson, M. D. (2008). A comparison of cardiac 31P MRS at 1.5 and 3 T. *NMR in biomedicine*, 21(8):793–798.

Ugurbil, K. (1985a). Magnetization transfer measurements of creatine kinase and ATPase rates in intact hearts. *Circulation*, 72(5 Pt 2):IV94–6.

Ugurbil, K. (1985b). Magnetization-transfer measurements of individual rate constants in the presence of multiple reactions. *Journal of Magnetic Resonance (1969)*, 64(2):207–219.

Ugurbil, K., Petein, M., Maidan, R., Michurski, S., and From, A. H. L. (1986). Measurement of an individual rate constant in the presence of multiple exchanges: application to myocardial creatine kinase reaction. *Biochemistry-US*, 25(1):100–107.

Unverferth, D. V., Lee, S. W., and Wallick, E. T. (1988). Human myocardial adenosine triphosphatase activities in health and heart failure. *Am Heart J*, 115(1):139–146.

Urdal, P., Urdal, K., and Stromme, J. H. (1983). Cytoplasmic creatine kinase isoenzyme quantitated in tissue specimens obtained at surgery. *Clinical Chemistry*, 29(2):310–313.

Uretsky, S., Argulian, E., Narula, J., and Wolff, S. D. (2018). Use of Cardiac Magnetic Resonance Imaging in Assessing Mitral Regurgitation: Current Evidence. *Journal of the American College of Cardiology*, 71(5):547–563.

Uretsky, S., Gillam, L., Lang, R., Chaudhry, F. A., Argulian, E., Supariwala, A., Gurram, S., Jain, K., Subero, M., Jang, J. J., Cohen, R., and Wolff, S. D. (2015). Discordance Between Echocardiography and MRI in the Assessment of Mitral Regurgitation Severity: A Prospective Multicenter Trial. *Journal of the American College of Cardiology*, 65(11):1078–1088.

Uretsky, S., Supariwala, A., Nidadovolu, P., Khokhar, S. S., Comeau, C., Shubayev, O., Campanile, F., and Wolff, S. D. (2010). Quantification of left ventricular remodeling in response to isolated aortic or mitral regurgitation. *Journal of Cardiovascular Magnetic Resonance*, 12(1):32.

Valkovič, L., Chmelík, M., and Krššák, M. (2017). In-vivo 31P-MRS of skeletal muscle and liver: A way for non-invasive assessment of their metabolism. *Analytical Biochemistry*, 529:193–215.

Van De Heyning, C. M., Magne, J., Piérard, L. A., Bruyère, P.-J., Davin, L., De Maeyer, C., Paelinck, B. P., Vrints, C. J., and Lancellotti, P. (2014). Late gadolinium enhancement CMR in primary mitral regurgitation. *European Journal of Clinical Investigation*, 44(9):840–847.

van Deursen, J., Heerschap, A., Oerlemans, F., Rultenbeek, W., Jap, P., ter Laak, H., and Wieringa, B. (1993). Skeletal muscles of mice deficient in muscle creatine kinase lack burst activity. *Cell*, 74(4):621–631.

Van Dorsten, F. A., Furter, R., Bijkerk, M., Wallimann, T., and Nicolay, K. (1996). The in vitro kinetics of mitochondrial and cytosolic creatine kinase determined by saturation transfer 31P-NMR. *Biochimica et Biophysica Acta - Bioenergetics*, 1274(1-2):59–66.

Van Dorsten, F. A., Nederhoff, M. G. J., Nicolay, K., and Van Echteld, C. J. A. (1998). 31P NMR studies of creatine kinase flux in M-creatine kinase-deficient mouse heart. *Am J Physiol Heart Circ Physiol*, 275(4):H1191–H1199.

Varghese, R., Itagaki, S., Anyanwu, A. C., Milla, F., and Adams, D. H. (2014). Predicting early left ventricular dysfunction after mitral valve reconstruction: The effect of atrial fibrillation and pulmonary hypertension. *Journal of Thoracic and Cardiovascular Surgery*, 148(2):422–427.

Vassiliou, V. S., Perperoglou, A., Raphael, C. E., Joshi, S., Malley, T., Everett, R., Halliday, B., Pennell, D. J., Dweck, M. R., and Prasad, S. K. (2017). Midwall Fibrosis and 5-Year Outcome in Moderate and Severe Aortic Stenosis. *Journal of the American College of Cardiology*, 69(13):1755–1756.

Vatner, D. E. and Ingwall, J. S. (1984). Effects of Moderate Pressure Overload Cardiac Hypertrophy on The Distribution of Creatine Kinase Isozymes. *Experimental Biology and Medicine*, 175(1):5–9.

Veech, R. L., Lawson, J. W., Cornell, N. W., and Krebs, H. A. (1979). Cytosolic phosphorylation potential. *Journal of Biological Chemistry*, 254(14):6538–6547.

Vega, R. B., Konhilas, J. P., Kelly, D. P., and Leinwand, L. A. (2017). Molecular Mechanisms Underlying Cardiac Adaptation to Exercise. *Cell Metabolism*, 25(5):1012–1026.

Veksler, V. I., Kuznetsov, A. V., Anflous, K., Mateo, P., Van Deursen, J., Wieringa, B., and Ventura-Clapier, R. (1995). Muscle creatine kinase-deficient mice: II. Cardiac and skeletal muscles exhibit tissue-specific adaptation of the mitochondrial function. *J Biol Chem*, 270(34):19921–19929.

Vendelin, M., Hoerter, J. A., Mateo, P., Soboll, S., Gillet, B., and Mazet, J.-L. (2010). Modulation of Energy Transfer Pathways between Mitochondria and Myofibrils by Changes in Performance of Perfused Heart. *J Biol Chem*, 285(48):37240–37250.

Ventura-Clapier, R., Garnier, A., Veksler, V., and Joubert, F. (2011). Bioenergetics of the failing heart. *BBA-Mol Cell Res*, 1813(7):1360–1372.

Ventura-Clapier, R., Kaasik, A., and Veksler, V. (2004). Structural and functional adaptations of striated muscles to CK deficiency. *Mol Cell Biochem*, 256-257(1-2):29–41.

Ventura-Clapier, R., Mettauer, B., and Bigard, X. (2007). Beneficial effects of endurance training on cardiac and skeletal muscle energy metabolism in heart failure. *Cardiovasc Res*, 73(1):10–18.

Vianna, C. R., Huntgeburth, M., Coppari, R., Choi, C. S., Lin, J., Krauss, S., Barbatelli, G., Tzameli, I., Kim, Y.-B., Cinti, S., Shulman, G. I., Spiegelman, B., and Lowell, B. B. (2006). Hypomorphic mutation of PGC-1β causes mitochondrial dysfunction and liver insulin resistance. *Cell Metab*, 4(6):453–464.

Wallimann, T., Wyss, M., Brdiczka, D., Nicolay, K., and Eppenberger, H. M. (1992). Intracellular compartmentation, structure and function of creatine kinase isoenzymes in tissues with high and fluctuating energy demands: the 'phosphocreatine circuit' for cellular energy homeostasis. *Biochemical Journal*, 281(1):21–40.

Walsh, B., Tonkonogi, M., Soderlund, K., Hultman, E., Saks, V., and Sahlin, K. (2001). The role of phosphorylcreatine and creatine in the regulation of mitochondrial respiration in human skeletal muscle. *The Journal of Physiology*, 537(3):971–978.

Walther, T., Tschöpe, C., Sterner-Kock, A., Westermann, D., Heringer-Walther, S., Riad, A., Nikolic, A., Wang, Y., Ebermann, L., Siems, W.-E., Bader, M., Shakibaei, M., Schultheiss, H.-P., and Dörner, A. (2007). Accelerated Mitochondrial Adenosine Diphosphate/Adenosine Triphosphate Transport Improves Hypertension-Induced Heart Disease. *Circulation*, 115(3):333–344.

Wang, T., McDonald, C., Petrenko, N. B., Leblanc, M., Wang, T., Giguere, V., Evans, R. M., Patel, V. V., and Pei, L. M. (2015). Estrogen-Related Receptor alpha (ERR alpha) and ERR gamma Are Essential Coordinators of Cardiac Metabolism and Function. *Mol Cell Biol*, 35(7):1281–1298.

Wang, Y. X., Zhang, C. L., Yu, R. T., Cho, H. K., Nelson, M. C., Bayuga-Ocampo, C. R., Ham, J., Kang, H., and Evans, R. M. (2004). Regulation of muscle fiber type and running endurance by PPARδ. *PLoS Biology*, 2(10):e294.

Waring, C. D., Vicinanza, C., Papalamprou, A., Smith, A. J., Purushothaman, S., Goldspink, D. F., Nadal-Ginard, B., Torella, D., and Ellison, G. M. (2014). The adult heart responds to increased workload with physiologic hypertrophy, cardiac stem cell activation, and new myocyte formation. *European Heart Journal*, 35(39):2722–2731.

Weeks, K. L., Gao, X., Du, X. J., Boey, E. J., Matsumoto, A., Bernardo, B. C., Kiriazis, H., Cemerlang, N., Tan, J. W., Tham, Y. K., Franke, T. F., Qian, H., Bogoyevitch, M. A., Woodcock, E. A., Febbraio, M. A., Gregorevic, P., and McMullen, J. R.

(2012). Phosphoinositide 3-Kinase p110α Is a Master Regulator of Exercise-Induced Cardioprotection and PI3K Gene Therapy Rescues Cardiac Dysfunction. *Circulation: Heart Failure*, 5(4):523–534.

Weidemann, F., Herrmann, S., Störk, S., Niemann, M., Frantz, S., Lange, V., Beer, M., Gattenlöhner, S., Voelker, W., Ertl, G., and Strotmann, J. M. (2009). Impact of Myocardial Fibrosis in Patients With Symptomatic Severe Aortic Stenosis. *Circulation*, 120(7):577–584.

Weiss, R. G., Gerstenblith, G., and Bottomley, P. A. (2005). ATP flux through creatine kinase in the normal, stressed, and failing human heart. *Proceedings of the National Academy of Sciences of the United States of America*, 102(3):808–813.

Wettschureck, N., Rütten, H., Zywietz, A., Gehring, D., Wilkie, T. M., Chen, J., Chien, K. R., and Offermanns, S. (2001). Absence of pressure overload induced myocardial hypertrophy after conditional inactivation of Gαq/Gα11in cardiomyocytes. *Nature Medicine*, 7(11):1236–1240.

Whittington, H. J., McAndrew, D. J., Cross, R. L., Neubauer, S., and Lygate, C. A. (2016). Protective effect of creatine elevation against ischaemia reperfusion injury is retained in the presence of co-morbidities and during cardioplegia. *PLoS One*, 11(1).

Whittington, H. J., Ostrowski, P. J., McAndrew, D. J., Cao, F., Shaw, A., Eykyn, T. R., Lake, H. A., Tyler, J., Schneider, J. E., Neubauer, S., Zervou, S., and Lygate, C. A. (2018). Over-expression of mitochondrial creatine kinase in the murine heart improves functional recovery and protects against injury following ischaemia-reperfusion. *Cardiovascular Research*, 114(6):858–869.

Wilkins, B. J., Dai, Y. S., Bueno, O. F., Parsons, S. A., Xu, J., Plank, D. M., Jones, F., Kimball, T. R., and Molkentin, J. D. (2004). Calcineurin/NFAT Coupling Participates in Pathological, but not Physiological, Cardiac Hypertrophy. *Circulation Research*, 94(1):110–118.

Wilson, M. G., Ellison, G. M., and Cable, N. T. (2015). Basic science behind the cardiovascular benefits of exercise. *Heart*, 101(10):758–765.

Witkowski, T. G., Thomas, J. D., Debonnaire, P. J. M. R., Delgado, V., Hoke, U., Ewe, S. H., Versteegh, M. I. M., Holman, E. R., Schalij, M. J., Bax, J. J., Klautz, R. J. M., and Marsan, N. A. (2013). Global longitudinal strain predicts left ventricular dysfunction after mitral valve repair. *European Heart Journal - Cardiovascular Imaging*, 14(1):69–76.

Witteles, R. M. and Fowler, M. B. (2008). Insulin-Resistant Cardiomyopathy: Clinical Evidence, Mechanisms, and Treatment Options. *J Am Coll Cardiol*, 51(2):93–102.

Wong, P.-P. and Smith, A. (1976). Biochemical differences between the MB and MM isoenzymes of creatine kinase. *Clinica Chimica Acta*, 68(2):147–158.

Wood, P. W., Choy, J. B., Nanda, N. C., and Becher, H. (2014). Left Ventricular Ejection Fraction and Volumes: It Depends on the Imaging Method. *Echocardiography*, 31(1):87–100.

World Medical Association (2013). World Medical Association Declaration of Helsinki. *JAMA*, 310(20):2191–4.

Wyss, M. and Kaddurah-Daouk, R. (2000). Creatine and Creatinine Metabolism. *Physiological reviews*, 80(3):1107.

Xiong, Q., Zhang, P., Guo, J., Swingen, C., Jang, A., and Zhang, J. (2015). Myocardial ATP hydrolysis rates in vivo: a porcine model of pressure overload-induced hypertrophy. *Am J Physiol Heart Circ Physiol*, 309(3):H450–H458.

Yan, J., Young, M. E., Cui, L., Lopaschuk, G. D., Liao, R., and Tian, R. (2009). Increased Glucose Uptake and Oxidation in Mouse Hearts Prevent High Fatty Acid Oxidation but Cause Cardiac Dysfunction in Diet-Induced Obesity. *Circulation*, 119(21):2818–2828.

Yang, J., Sambandam, N., Han, X., Gross, R. W., Courtois, M., Kovacs, A., Febbraio, M., Finck, B. N., and Kelly, D. P. (2007). CD36 Deficiency Rescues Lipotoxic Cardiomyopathy. *Circ Res*, 100(8):1208–1217.

Yang, W. C., Geiger, P. J., Bessman, S. P., and Borrebaek, B. (1977). Formation of creatine phosphate from creatine and 32P-labelled ATP by isolated rabbit heart mitochondria. *Biochemical and Biophysical Research Communications*, 76(3):882–887.

Ye, Y., Gong, G., Ochiai, K., Liu, J., and Zhang, J. (2001a). High-Energy phosphate metabolism and creatine kinase in failing hearts a new porcine model. *Circulation*, 103(11):1570–1576.

Ye, Y., Wang, C., Zhang, J., Cho, Y. K., Gong, G., Murakami, Y., and Bache, R. J. (2001b). Myocardial creatine kinase kinetics and isoform expression in hearts with severe LV hypertrophy. *Am J Physiol Heart Circ Physiol*, 281(1):H376–H386.

Young, M. E., Laws, F. A., Goodwin, G. W., and Taegtmeyer, H. (2001). Reactivation of peroxisome proliferator-activated receptor α is associated with contractile dysfunction in hypertrophied rat heart. *J Biol Chem*, 276(48):44390–44395.

Zaha, V. G. and Young, L. H. (2012). AMP-activated protein kinase regulation and biological actions in the heart. *Circ Res*, 111(6):800–814.

Zahler, R., Bittl, J. A., and Ingwall, J. S. (1987). Analysis of compartmentation of ATP in skeletal and cardiac muscle using 31P nuclear magnetic resonance saturation transfer. *Biophysical Journal*, 51(6):883–893.

Zeleznikar, R. J. and Goldberg, N. D. (1991). Kinetics and compartmentation of energy metabolism in intact skeletal muscle determined from 18O labeling of metabolite phosphoryls. *Journal of Biological Chemistry*, 266(23):15110–15119.

Zervou, S., Ray, T., Sahgal, N., Sebag-Montefiore, L., Cross, R., Medway, D. J., Ostrowski, P. J., Neubauer, S., and Lygate, C. A. (2013). A role for thioredoxin-interacting protein (Txnip) in cellular creatine homeostasis. *Am J Physiol-Endoc M*, 305(2):E263–E270.

Zervou, S., Whittington, H. J., Ostrowski, P. J., Cao, F., Tyler, J., Lake, H. A., Neubauer, S., and Lygate, C. A. (2017). Increasing creatine kinase activity protects against hypoxia / reoxygenation injury but not against anthracycline toxicity in vitro. *PLoS One*, 12(8):e0182994.

Zervou, S., Whittington, H. J., Russell, A. J., and Lygate, C. A. (2016). Augmentation of Creatine in the Heart. *Mini Reviews in Medicinal Chemistry*, 16(1):19–28.

Zhang, J. (2002). Myocardial Energetics In Cardiac Hypertrophy. *Clin Exp Pharmacol P*, 29(4):351–359.

Zhang, J., Duncker, D. J., Ya, X., Zhang, Y., Pavek, T., Wei, H., Merkle, H., Ugurbil, K., From, A. H. L., and Bache, R. J. (1995). Effect of Left Ventricular Hypertrophy Secondary to Chronic Pressure Overload on Transmural Myocardial 2-Deoxyglucose Uptake: A 31P NMR Spectroscopic Study. *Circulation*, 92(5):1274–1283.

Zhang, J., Murakami, Y., Zhang, Y., Cho, Y. K., Ye, Y., Gong, G., Bache, R. J., Ugurbil, K., and From, A. H. L. (1999). Oxygen delivery does not limit cardiac performance during high work states. *Am J Physiol Heart Circ Physiol*, 277(1):H50–H57.

Zhang, L., Jaswal, J. S., Ussher, J. R., Sankaralingam, S., Wagg, C., Zaugg, M., and Lopaschuk, G. D. (2013). Cardiac Insulin-Resistance and Decreased Mitochondrial Energy Production Precede the Development of Systolic Heart Failure After Pressure-Overload Hypertrophy. *Circ-Heart Fail*, 6(5):1039–1048.

Zhang, R., Khoo, M. S., Wu, Y., Yang, Y., Grueter, C. E., Ni, G., Price, E. E., Thiel, W., Guatimosim, S., Song, L. S., Madu, E. C., Shah, A. N., Vishnivetskaya, T. A., Atkinson, J. B., Gurevich, V. V., Salama, G., Lederer, W. J., Colbran, R. J., and Anderson, M. E. (2005). Calmodulin kinase II inhibition protects against structural heart disease. *Nature Medicine*, 11(4):409–417.

Zhang, T., Maier, L. S., Dalton, N. D., Miyamoto, S., Ross, J., Bers, D. M., and Brown, J. H. (2003). The δc isoform of CaMKII is activated in cardiac hypertrophy and induces dilated cardiomyopathy and heart failure. *Circulation Research*, 92(8):912–919.

Zilberszac, R., Heinze, G., Binder, T., Laufer, G., Gabriel, H., and Rosenhek, R. (2018). Long-Term Outcome of Active Surveillance in Severe But Asymptomatic Primary Mitral Regurgitation. *JACC: Cardiovascular Imaging*, 11(9):1213–1221.

Zile, M. R., Gaasch, W. H., Carroll, J. D., and Levine, H. J. (1984). Chronic mitral regurgitation: Predictive value of preoperative echocardiographic indexes of left ventricular function and wall stress. *Journal of the American College of Cardiology*, 3(2):235–242.

Zinman, B., Wanner, C., Lachin, J. M., Fitchett, D., Bluhmki, E., Hantel, S., Mattheus, M., Devins, T., Johansen, O. E., Woerle, H. J., Broedl, U. C., and Inzucchi, S. E. (2015). Empagliflozin, cardiovascular outcomes, and mortality in type 2 diabetes. *New England Journal of Medicine*, 373(22):2117–2128.

Zoll, J., Sanchez, H., N'Guessan, B., Ribera, F., Lampert, E., Bigard, X., Serrurier, B., Fortin, D., Geny, B., Veksler, V., Ventura-Clapier, R., and Mettauer, B. (2002). Physical activity changes the regulation of mitochondrial respiration in human skeletal muscle. *The Journal of Physiology*, 543(1):191–200.

Zweier, J. L., Jacobus, W. E., Korecky, B., and Brandejs-Barry, Y. (1991). Bioenergetic consequences of cardiac phosphocreatine depletion induced by creatine analogue feeding. *J Biol Chem*, 266(30):20296–20304.